THE PETROLOGY, GEOCHEMISTRY AND MINERALOGY OF SOME ALUMINIUM SILICATE-BEARING ROCKS FROM CO. DONEGAL AUREOLES, EIRE

by

MOHAMMED HANAFY EL-NAGGAR

Thesis submitted in accordance with the requirements of the University of Liverpool for the degree of Doctor in Philosophy

August, 1968

ABSTRACT

This work is concerned with the study of the aluminium silicate-bearing rocks in 5 aureoles bordering the Donegal granites, namely, Fanad aureole, Northern aureole of Ardara Pluton, Barnesmore aureole, Thorr aureole and enclaves and the Main Donegal Granite aureole. The way in which the different forms of aluminium silicates occur in these aureoles, i. e. in different zones or intercalated bands, provides an ideal situation to study the factors affecting the formation of one form rather than another. The fact that andalusite is widely present whereas kyanite is restricted to certain areas or even certain bands, imposes a reconsideration of putting the burden of the development of a particular aluminium silicate polymorph solely on the temperature and pressure of metamorphism. The outcome of this study in the form of petrological, chemical and modal data, makes possible the assessment of other factors, if there were any, affecting the development of a particular aluminium silicate polymorph.

The present thesis is divided into three parts:-

PART ONE deals with the fluorescent X-ray spectroscopy as a means of silicate analysis. In the First Chapter of this part, the X-ray spectrochemical analysis of pelitic rocks by a limited compositional range technique is considered. A simple direct pelletization method for the analysis of SiO_2, TiO_2, Al_2O_3, Fe_2O_3 (total), MnO, MgO, CaO, K_2O, Na_2O, P_2O_5 in pelitic rocks carrying abundant biotite and muscovite is described. The reliability of the technique used is investigated at length and the method of analysis described is as good or better than existing published methods using more complex equipment, sample preparation and/or correction

techniques. The limited compositional range used allows direct determination of the composition.

In the Second Chapter, a technique for the fluorescent X-ray spectrographic micro-analysis of silicate minerals is described. The method utilizes 5-8 milligrammes of silicate minerals (biotite and garnet) and the sample preparation is simple and straightforward. The powdered mineral is directly pelletized using cellulose backing and the sample is masked with a lead mask. The precision and accuracy of the determination of SiO_2, TiO_2, Al_2O_3, Fe_2O_3 (total), MnO, MgO, CaO, K_2O, are investigated and proved to be high.

PART TWO of the thesis is a resume of the earlier work done on the aluminium silicate polymorphs. The published data on the temperature and pressure of formation of these minerals are compiled and the arguments and criticisms of the different works are summarized.

PART THREE deals with the aluminium silicate bearing rocks in the contact aureoles studied. The First Chapter of this part deals with the petrology of these rocks, their spatial arrangement in relation to the granites as well as the textural characteristics of the aluminium silicate minerals. In Ardara aureole, a kyanite zone is established and in both Ardara and the Main Donegal granite aureoles, garnet, kyanite, staurolite, andalusite and fibrolite are shown to be aureole minerals. The sequence of crystallisation is an early fibrolite, followed by garnet, then staurolite-kyanite and finally feldspar and andalusite.

In the Second Chapter, the results of the chemical and modal analyses for 80 rocks as well as 21 coexisting biotites from the different aureoles are presented. For this analysis, a rectangular

rock specimen is used. Two parallel slices are cut from both ends and the part in between these two slices is used for the chemical analysis. By this technique, it is hoped that the correlation between the chemistry of the rock and its modal composition is a meaningful one. The analytical results show, among other things, that there is a distinct correlation between the composition of the rock and its coexisting biotite. Phase diagrams of the 80 rocks show that kyanite occurs only in rocks of high M/FM values whereas andalusite occurs in most rocks regardless of their M/FM ratios. Also there is no chemical distinction between andalusite-bearing and sillimanite-bearing rocks. When the 80 rocks are plotted on the same AFM or AKFM diagram, they show a distinct grouping into kyanite-bearing rocks near the M corner and kyanite-free rocks near the F corner. Kyanite development is shown to be dependent on the M/FM of the rock rather than on the spatial arrangement of the rock relative to the granite contact. Consequently, the aluminium silicate-bearing rocks studied are divided into 2 groups of different M/FM ratios, namely:-

kyanite-bearing rocks $\pm$ andalusite $\pm$ staurolite $\pm$ fibrolite.

kyanite-free rocks $\pm$ andalusite and/or sillimanite and/or fibrolite $\pm$ staurolite

It is concluded at the end of this work that the regional chlorite-muscovite $\pm$ biotite rocks evolved to their present mineralogy through two series of reactions:

1. A relatively earlier reaction producing any of the following assemblages depending on the M/FM ratio of the rock:

High M/FM	:	kyanite-biotite-muscovite $\pm$ garnet
Intermediate M/FM	:	kyanite-biotite-muscovite-staurolite $\pm$ garnet
Low M/FM	:	biotite-muscovite $\pm$ staurolite $\pm$ garnet

2. A relatively later reaction irrespective of the M/FM ratio of the rock producing andalusite and/or sillimanite depending on the nearness of the rock to the granite.

The two reactions are concurrent with no time gap in between.

It is also concluded that whereas kyanite production depends on the M/FM ratio of the rock, andalusite development is thought to be due to changes in physical conditions (i. e. an increase in T or a decrease in P). Coarse sillimanite develops only in rocks very close to the granite contact, hence a high temperature is the controlling factor for its development.

ACKNOWLEDGEMENTS

The writer is grateful to Professor W. S. Pitcher for his guidance in the field, his critical discussions and encouragement.

My deepest gratitude is due to Dr. M. P. Atherton for his sincere supervision, invaluable guidance, helpful criticisms and continuous encouragement during the progress of the work and the preparation of this thesis.

The writer is also indebted to Mr. M. S. Brotherton for his help in the wet chemical analysis, Mr. J. Lynch for his draughting assistance, Mr. M. Rizk of the Department of Numerical Analysis who helped in the computer programming and Mr. M. Edmunds and Dr. J. Mather for making available the rock specimens and analytical data used in the calibration of X-ray fluorescence. Thanks are also due to Dr. N. Rast and Dr. D. Flinn for discussions during the work.

The work was financially supported by a grant from the U. A. R. Government, to which the author is grateful.

CONTENTS

Page

PART ONE

FLUORESCENT X-RAY SPECTROSCOPY - A MEANS OF SILICATE ANALYSIS

CHAPTER ONE FLUORESCENT X-RAY SPECTROGRAPHIC ANALYSIS OF SILICATE ROCKS

I. INTRODUCTION 1

II. SAMPLE PREPARATION - PELLETIZATION 5

III. STANDARD USED - EXTERNAL STANDARD 7

IV. EQUIPMENT 8

V. GONIOMETER SETTING 10

VI. INSTRUMENTAL CONDITIONS - PULSE HEIGHT ANALYSIS 10

A. Choice of Counter Voltage, Base Line and Channel Width 11
B. Elimination of Line Interference 14
C. Background and Peak/Background Ratio 15
D. Conditions used in Analysis 16

VII. RELIABILITY OF THE METHOD USED 19

A. Sources of Errors 19
B. Machine Reproducibility - Long and Short Term Variations 22
C. Effect of Grain Size and Pelletization on Reproducibility 26
D. The Effect of Grain Size on Intensity 31
E. Errors due to Crushing 35

VIII. ANALYTICAL DATA 36

A. Chemical Composition of Rock GL-10 used as a Standard 39
B. Results 42

Page

(i) Silica 43
(ii) Titanium oxide 50
(iii) Aluminium oxide 54
(iv) Total iron as Fe_2O_3 55
(v) Manganese oxide 61
(vi) Calcium oxide 64
(vii) Magnesium oxide 69
(viii) Potassium oxide 75
(ix) Sodium oxide 79
(x) Phosphorus oxide 81

C. An Algol KDF9 Computer Programme for Calculation 87
D. A Check on the Calibration Method 87
E. Mica Effect 88

IX. SUMMARY AND DISCUSSION OF THE RELIABILITY OF X-RAY SPECTROGRAPHIC ANALYSIS 90

A. Factors Affecting the Precision 90
B. Factors Affecting the Accuracy 94
C. Interelement or Matrix Effect 95

CHAPTER TWO FLUORESCENT X-RAY SPECTROGRAPHIC MICRO-ANALYSIS OF SILICATE MINERALS

I. INTRODUCTION 106

II. GENERAL CONSIDERATIONS 107

III. PREVIOUS WORK 107

IV. PRELIMINARY WORK 110

V. THE ANALYSIS OF 5-8 MILLIGRAMS OF SILICATE MINERALS 113

A. Sample Preparation 113
B. Sample Presentation to the X-Ray Spectrograph 115
C. Instrumental Conditions 116
D. Calibration 117

Page

E. The Background and its Effect on Calibration 117
F. Precision of the Method 118
G. Analytical Data and the Accuracy of the Method 123

(i) Silica 123
(ii) Aluminium oxide 125
(iii) Titanium oxide 127
(iv) Total iron as Fe_2O_3
(v) Manganese oxide 131
(vi) Calcium oxide 133
(vii) Magnesium oxide 133
(viii) Potassium oxide 135

PART TWO

A REVIEW OF THE ALUMINIUM SILICATE POLYMORPHS 139

PART THREE

THE ALUMINIUM SILICATES-BEARING ROCKS IN THE CONTACT AUREOLES OF COUNTY DONEGAL GRANITE

INTRODUCTION 149

CHAPTER ONE PETROLOGY

I. THE WESTERN FANAD GRANODIORITE AUREOLE 150
II. THE AUREOLE AND ENCLAVES OF THORR GRANODIORITE 155
III. THE BARNESMORE GRANITE AUREOLE 158

Page

IV. THE NORTHERN AUREOLE OF ARDARA PLUTON 160

A. Introduction and Synopsis of Previous Work 160
B. Description of the Aureole 163

1. The kyanite-bearing andalusite schist 164
2. The kyanite-free andalusite schist 167
3. The coarse sillimanite hornfels 168

C. Comments and Conclusions 169

V. THE AUREOLE OF THE MAIN DONEGAL GRANITE PROPER 174

A. Introduction and Previous Work 174
B. Description of the Aluminium Silicate Bearing Rocks in the Aureole 177

1. Fintown area 178
2. Glenaboghil schists 181
3. Lough Reelan area 183
4. Glenkeo kyanite schists 184
5. Lackagh Bridge schists 185
6. Owennagreeve river area 186

C. Conclusions 186

CHAPTER TWO FLUORESCENT X-RAY AND MODAL ANALYSES

I. METHOD OF ROCK ANALYSES 189

II. METHOD OF BIOTITE ANALYSIS 190

III. CONSTRUCTION OF THE PHASE DIAGRAMS 190

IV. RESULTS 192

A. Chemical and Modal Analyses of the Aureole Rocks 193

1. Fanad aureole 193
2. Ardara aureole 200
3. Barnesmore aureole 206
4. Thorr granodiorite aureole and enclaves 208
5. The aureole of the Main Donegal granite 212

Page

B. Values of Phase Diagrams 222

1. Fanad aureole 222
2. Ardara aureole 226
3. Barnesmore aureole 229
4. Thorr granodiorite aureole and enclaves 230
5. The aureole of the Main Donegal granite 232

C. X-ray Fluorescent Partial Analysis of Biotites 237

V. COMMENTS ON THE ANALYTICAL RESULTS 241

A. Individual Aureoles 241
B. The Relationship between the Biotite Composition and its Host Rock 243
C. The Relationship between the Type of Aluminium Silicate and the Composition of its Host Rock in all Aureoles 243
D. The Phase Diagrams 244
E. Main Conclusions 247

VI. DISCUSSION 248

A. The Earlier or First Reaction 250

1. Kyanite ($\pm$ staurolite)-bearing aureoles 250
2. Kyanite-free aureoles 254
3. Comments on the earlier or first reaction 254
(i) The status of staurolite 254
(ii) The presence of absence of garnet 258

B. The Later or Second Reaction 259

C. Fibrolite vs. Coarse Sillimanite 259

VII. CONCLUSIONS 262

REFERENCES 268

APPENDIX I 285

APPENDIX II 286

APPENDIX III 287

APPENDIX IV 290

LIST OF FIGURES

Figure		Follows page
1	Pulse height analysis	13
2	Pulse height analysis	16
3	Effect of grain size on X-ray intensity	34
4 (a)	Calibration graph for SiO_2 in rocks	53
(b)	Calibration graph for TiO_2 in rocks	53
5 (a)	Calibration graph for Al_2O_3 in rocks	60
(b)	Calibration g raph for Fe_2O_3 in rocks	60
6 (a)	Calibration graph for MnO in rocks	68
(b)	Calibration graph for CaO in rocks	68
7 (a)	Calibration graph for MgO in rocks	78
(b)	Calibration graph for K_2O in rocks	78
8 (a)	Calibration graph for Na_2O in rocks	86
(b)	Calibration graph for P_2O_5 in rocks	86
9	Intensity ratio vs. results of chemical and X-ray analyses	99
10	Intensity ratio vs. results of chemical and X-ray analyses	101
11	Intensity ratio vs. results of chemical and X-ray analyses	104
12	Intensity ratio vs. results of chemical and X-ray analyses	104
13 (a)	Calibration graph for SiO_2 in biotites	126
(b)	Calibration graph for Al_2O_3 in biotites	126

Figure		Follows page
14 (a)	Calibration graph for TiO_2 in biotites	128
(b)	Calibration graph for Fe_2O_3 in garnets	128
15 (a)	Calibration graph for Fe_2O_3 in biotites	130
(b)	Calibration graph for Fe_2O_3 in biotites	130
16 (a)	Calibration graph for MnO in garnets	134
(b)	Calibration graph for CaO in garnets	134
17 (a)	Calibration g raph for MgO in biotites	136
(b)	Calibration graph for MgO in garnets	136
18	Calibration g raph for K_2O in biotites	138
19	Kyanite-andalusite-sillimanite triple point	146
20	Geological sketch map of Donegal Granites	149
21	Geological sketch map of the western part of Donegal showing the distribution of metamorphic minerals	149
22	Geological sketch map of Fanad aureole	154
23	Geological sketch map of the northern aureole of Ardara	173
24	Diagramatic map of the Main Donegal Granite	177
25	M/FM ratios in rocks and their coexisting biotites	243
26 (a)	AKF phase diagram of Fanad aureole	247
(b)	AFM phase diagram of Fanad aureole	247
27 (a)	AKF phase diagram of Ardara aureole	247
(b)	AFM phase diagram of Ardara aureole	247
28 (a)	AKF phase diagram of Barnesmore aureole	247
(b)	AFM diagram of Barnesmore aureole	247

Figure		Follows page
29 (a)	AKF phase diagram of Thorr aureole	247
(b)	AFM diagram of Thorr aureole	247
30 (a)	AKF phase diagram of the Main Donegal granite aureole	247
(b)	AFM phase diagram of the Main Donegal granite aureole	247
31	AKFM phase diagram of Fanad aureole	247
32	A'KFM phase diagram of Fanad aureole	247
33	AKFM phase diagram of Ardara aureole	247
34	A'KFM phase diagram of Ardara aureole	247
35	AKFM phase diagram of Barnesmore aureole	247
36	A'KFM phase diagram of Barnesmore aureole	247
37	AKFM phase diagram of Thorr aureole	247
38	A'KFM phase diagram of Thorr aureole	247
39	AKFM phase diagram of the Main Donegal Granite aureole	247
40	A'KFM phase diagram of the Main Donegal Granite aureole	247
41	AKF diagram of all aureoles	247
42	A'KF phase diagram of all aureoles	247
43	AFM phase diagram of all aureoles	247
44	A'FM phase diagram of all aureoles	247
45	AKFM phase diagram of all aureoles	247

Figure		Follows page
46	Thompson phase projection of all aureoles	247
47	Plot of rocks on AKFM tetrahedron	258
48	Aluminium silicate phase diagram showing the movement of kyanite-rocks to the stability field of andalusite	258

PART ONE

FLUORESCENT X-RAY SPECTROSCOPY - A MEANS OF SILICATE ANALYSIS

CHAPTER ONE

FLUORESCENT X-RAY SPECTROGRAPHIC ANALYSIS OF SILICATE ROCKS

I. INTRODUCTION

Whatever is the method used for analysing silicate rocks, the reliability i. e. the source and amount of errors involved in this method, must be estimated before using the resulting data to draw conclusions. This reliability is determined by both the precision and accuracy of the method in use and its assessment involves the statistical analysis of the data obtained. To follow is a comparative summary of the reliability of some of the commonly used methods in silicate analysis. The statistical terms used in the discussion are:-

n — number of observations, analyses, readings, etc.

X — amount of element, number of counts (in X-ray analysis).

$\bar{X}$ — arithmetic mean of Xs.

d — deviation of an observation from the mean.

S — standard deviation or the uncertainty of a single observation $= \sqrt{\frac{\Sigma d^2}{n-1}}$.

Sc — standard counting error (for X-ray work only where X is the number of counts) $= \sqrt{X \text{ or } \bar{X}}$

$= \sqrt{\frac{1}{X} + \frac{1}{X}}$ in case of standard unknown

using standard for comparison - simple ratio.

$S_{\bar{x}}$ standard error or the error of the arithmetic mean = $\frac{S}{\sqrt{n}}$

C relative deviation of a single observation or the coefficient of variation = $\frac{S}{\bar{X}} \times 100$

E relative error of the mean = $\frac{C}{\sqrt{n}}$

The reliability of the conventional wet chemical methods has been discussed at length bt Fairbairn et al., (1951), Fairbairn and Shairer (1952) and Fairbairn (1953) in a cooperative investigation of a Granite G_1 and a Diabase W_1 as well as a synthetic glass of granitic composition. The results of this investigation shocked the geologists who were accustomed to use the analytical results without questioning their reliability.

Three interesting facts arise in connection with the conventional wet chemical methods, namely:-

1. Interlaboratory precision is much lower than had been supposed.
2. From the accuracy and precision point of view, for Si and Al the method is precise but not accurate due to bias in determination whereas for Mg, Ca, Na, and K, it is relatively less precise but more accurate.
3. By virtue of the dependence of some determinations on others as well as the bias in the Si and Al determination, the summation of the results of rock analysis near to 100% is not an assurance of their correctness.

For these reasons, coupled with the facts that conventional methods require long time, high costs and special skill, systems of the so-called rapid analysis of silicates have been proposed (Shapiro

and Brannock 1952, 1956, Corey and Jackson 1953, Bannerjee and Colliss 1955, Riley 1958). A criticism of the rapid method was presented by Mercy (1956) who showed that single determinations by rapid methods of:

a. SiO_2, total iron, FeO, MgO, CaO, Na_2O, K_2O and P_2O_5 are all precise and accurate.
b. TiO_2 is accurate but moderately precise.
c. Al_2O_3, Fe_2O_3 show moderate accuracy and precision.
d. MnO shows poor accuracy but moderate precision.
e. H_2O^+ shows poor accuracy and precision.

The following table is a compilation of Mercy's data of accuracy and precision based on six analyses of each of a granite from the Rosses and an older gradodiorite from the dioritic phase of Thorr District, both from Co. Donegal, Eire.

TABLE 1

ACCURACY AND PRECISION OF RAPID METHOD COMPILED FROM MERCY, 1956

Element	Accuracy		Precision	
	C	Range of error C	C	E*
SiO_2	0.6%	(+1) - (-1) %	0.42%	0.16%
TiO_2	3-6%	always +ve error	6.9%	3.2%
Al_2O_3	1-2%	(+2.8)-(4.3)%	3.0%	1.0%
Total Fe	1.7%	always -ve error	2.1%	0.58%
MnO	20.0%	always -ve error	7.4%	1.4%
MgO	2.0%		2.2%	1.2%
CaO	3.0%		0.88%	0.33%
Na_2O	3.5%		1.8%	0.69%
K_2O	4.4%		3.0%	1.4%
P_2O_5	10.0%		2.6%	0.66%

* six analyses each in duplicate

In the period of the last 15 years, X-rays as a tool for chemical analysis has been universally and successfully tried particularly after the development of high intensity sealed X-ray tubes with stable power sources, highly sensitive counters, crystals of large spacing and high diffracting power, and reliable electronic counting systems. This provides another method for silicate analysis which is more rapid and would be better, and might outdate, the wet chemistry if proved to be reliable.

To follow is a discussion of the analytical method used in the present work and itsrelaibility.

II. SAMPLE PREPARATION - PELLETIZATION

Sample preparation is basically a method by which a homogeneous reproducible specimen surface can be presented in an adequate way to the X-ray spectrograph. Once these parameters are satisfied, the choice of a particular method rather than another will depend on the time factor and the ease with which the specimen is prepared from the sample.

The commonly used ways of preparing samples for X-ray fluorescence are fusion and direct pelletization of the powder. Besides being lengthy, fusion technique also has the disadvantages of difficulty in attaining reproducibility (Chodos and Engel, 1961), possibility of contaminations from the different equipments used (Baird et al., 1961), and loss in intensity particularly of Mg, Al, and Na (Hornung). Therefore, direct briquetting was investigated and proved to be reproducible and more practical as will be shown later.

Briquettes were prepared in the following way:-

1. The powdered specimen (about 2 grams for each pellet) was mixed with bakelite resin to the ratio of 6:1 and the mixture was carefully homogenised for 20 minutes in a ball-mill.

2. The homogenised mixture was poured into $1\frac{1}{2}$" steel mold and backed with a known amount of pure cellulose powder which was kept standard for all the pellets.

3. The powder was compressed gradually against highly polished steel discs or glass discs up to 30 tons on ram, kept there for 20 seconds and then the pressure was released slowly.

4. The briquettes produced were baked for $\frac{1}{2}$ hour at 110°C, face up in an oven.

The bakelite is used here as a thermo-roasting binder that gives a robust and durable briquette. Briquettes of pure powders, although would result in higher intensities, proved to be practically difficult to prepare and to handle.

The use of the glass discs as pads against which the powder is pressed is better than the polished steel discs. The fact that one glass disc is used for preparing one pellet, results in briquettes whose surfaces are not only mirror-like (Volborth, 1963), but also reproducible. Moreover, it saves the time consumed in the frequent polishing of the steel discs. Worth mentioning is the fact that only in very rare cases, the glass discs cracked during releasing the pressure. Yet, checks made on such pellets showed that the latter are free from any glass (SiO_2) contaminations. The glass discs were put directly on a steel ram having a smooth surface. It was noticed that if a soft tissue is put between the glass disc and the

steel ram, the glass disc shattered completely into small pieces.

The cellulose backing is useful in that it gives an adequate space for labelling.

III. STANDARD USED - EXTERNAL STANDARD

As the rocks concerned in the present work are all metamorphic pelites, a wide range of composition is unlikely to be displayed. Therefore, a carefully analysed rock of this group (GL-10) can be satisfactorily used as an external standard to which the "unknowh" rock can be compared. This method has the following advantages:-

1. The ultimate reliability is achieved when both the standard and the unknown of nearly similar composition, are identically prepared.

2. The comparison with such a standard can compensate for the absorption and enhancement effects encountered in thick samples of composite nature and, indeed, it is the easiest way to do so.

3. Comparing the unknown with the standard as quickly as is convenient can eliminate errors due to the instability and drift in the electronic system.

4. Errors due to goniometer setting particularly that evolving from resetting the goniometer to the 2θ value corresponding to maximum intensity, can be eliminated if the standard and the unknown are interchanged without disturbing the goniometer.

IV. EQUIPMENT

A Siemens-make Krystallofex-4 in conjunction with a G. S. type recording and counting console were used.

For quantitative analysis, a constant X-ray radiation intensity is required. This intensity is proportional to the current in the X-ray tube and to the square root of the tube voltage. As specified by the makers, both the current and the voltage in the X-ray tube of Krystallofex-4 are stabilized to an accuracy of 0.1%, fluctuations of the mains voltage of 220 V. between +10 and -10% are taken into account.

X-ray tubes with chromium and tungsten anodes were used. Both tubes have beryllium windows with a very low absorption factor.

For manganese, a tungsten-anode tube was used for two reasons:-

1. Manganese X-ray fluorescent intensity is much higher when using tungsten radiation compared to a chromium one.

2. When a chromium tube is used, there is an overlap of MnKa and CrK_B. Although this overlap can be resolved by using suitable secondary collimation and a scintillation counter, yet, a great loss in fluorescent intensity will be marked.

For the other elements, i.e. Na, Mg, Al, Si, P, Ca, Fe, K, and Ti, chromium-anode tube gives much higher intensity for all the elements except for Fe, being according to Jenkins (oral communication), nearly $^2/_3$ of that of tungsten-anode tube.

The radiation counting console is provided with single-impulse counting and impulse-preselecting facilities, an electronic clock with time preselection, and an impulse-height analyser. This type of measuring apparatus is suitable for use with Geiger-Muller, proportional and scintillation counter tubes.

A gas flow proportional counter was used in preferential to a Geiger-Muller counter because, according to Parrish and Kohler (1956), Liebhafsky et al., (1960), it has the following advantages:-

1. The voltage signals produced by the counter are proportional to the energy of the X-ray quanta that produced the pulses.
2. It eliminates the non-linearity problems.
3. It makes possible to apply simple electronic pulse height discrimination techniques giving a lower background and a higher peak/background ratio. This is particularly important when powder specimens that have a complex spectral distribution are used.

In preference to a scintillation counter, gas-flow proportional counter provides better energy of resolution (2. 5 times).

Recording was automatically done by an electronic print-out recorder attached to the counting console. This recorder prints out the number of counts over a pre-specified fixed interval of time.

In the present work, fixed time rather than fixed counts was used in measuring the intensity. This is because:-

1. Using a fixed counts procedure, the collection of the same number of counts on the background as on the peak takes a very long time particularly if the background intensity is

very low relative to that of the peak - a situation which is met in most of the elements analysed for.

2. Statistically, it has been shown by Heinrich (1959), Birks and Brown (1962) that there is no advantage in using a fixed counts procedure instead of a fixed time one. Gaylor (1962) goes even further in stating that fixed time is never worse and nearly always better than fixed counts.

V. GONIOMETER SETTINGS

For the determination of 2θ of the peak and the background of the different elements, a 2θ scan over the peak was first performed and automatically recorded on the chart recorder. Then counts were taken by the stepwise scanning of the approximate region in which the peak occurs at intervals of 0.02° and plotted graphically to locate the exact position of the point of maximum intensity. The goniometer was always rotated in one direction to avoid errors arising from backlash in the adjustment of the goniometer drum.

When rock sample was used, a slight shift in the 2θ of the peak is noticed compared with samples of the pure element or its simple salt. This may be due to the difference in the chemical state in which the element is present in the two samples.

VI. INSTRUMENTAL CONDITIONS - PULSE HEIGHT ANALYSIS (P. H. A.)

As means of separating X-ray photons into definite measurable spectral lines, a gypsum crystal in conjunction with a pulse height

selector were used.

The use of the crystal alone is not convenient because of:

1. Loss of intensity by a factor of the order of 10^6 (Liebhafsky et al., 1960).
2. Diffraction of lines in odd orders that may give rise to line interference and/or relatively high background, both of which cannot be eliminated by using the crystal alone (Heinrich, 1960).

For these reasons, a pulse height selector was used in conjunction with the crystal. By definition, the pulse height selector is "a circuit designed to select and pass voltage pulses in a certain range of amplitude" (The International Dictionary of Physics and Electronics). Pulse height selection is, therefore, a process of separating the characteristic X-rays from the specimen according to their energies rather than wavelength. The range of pulse height that passes the selector is called a "window". This window has a "base" or a lower threshold and a height or "channel", both of which are measurable in volts. The base and the channel can be adjusted to select and pass pulses lying between the energy limits of the selector settings for counting and reject the undesired ones.

A systematic approach for setting the pulse height selector is necessary. In the present work, this was done as described hereafter.

A. Choice of Counter Voltage, Base Line and Channel Width

Samples used for the present investigations are the pure elements or their pure simple salts, referred to here as Elementary

Standards.

Without using the channel, the base line is set at different voltages and a stepwise scan across counter voltages at each base line setting is then performed. In the present work, the counter voltage was changed by steps of 15 volts. Counts are taken at suitable rate and the average of three readings is plotted against the corresponding counter voltage. The INTEGRAL curves produced in this way are of the type shown in Fig. 1a.

The figure shows that counts increase rapidly until they reach a maximum level and then remain constant over a certain range of counter voltages forming a plateau characteristic of proportional counters. According to Parrish and Kohler (1956), this plateau represents the voltage range which will produce pulse amplitudes greater than the discrimination level i. e. once the applied voltage exceeds the minimum required to make all pulses greater than the threshold or the base line, no further increase in intensity is obtained when the counter voltage is increased. As is to be expected, the higher the base line voltage, the higher is the counter voltage required to reach this plateau of maximum counts.

Inspection of these integral curves for the different elements shows two interesting features:

1. There is a wide range of voltages that can be applied on the counter without changing the intensity.

2. The higher the atomic number of the element, the shorter is the wavelength of its spectral line and the lower is the counter voltage required to get maximum counts at a given base line.

Further increase in counter voltage will cause a sudden rise

in counts corresponding to the Geiger counter region where proportionality does not hold anymore.

The same procedure mentioned above in producing integral curves is repeated using the channel this time. DIFFERENTIAL curves of the type examplified in Fig. 1 b and c are produced, each at a particular base line setting. These curves show that counts increase to a value similar or very close to that obtained in integral curves, remain unchanged at this level over a certain range of counter voltages and then drop rapidly. This drop indicates that at this level, the pulses are amplified to such a degree that they exceed the upper threshold of the pulse height discriminator.

From these graphs, a complete picture of the appropriate combinations of counter voltage, base line and channel width that give a stable maximum counts for a particular element, are known. Eventually, different sets of conditions that would not be affected by slight fluctuations in the voltage of these three variables, can be specified.

As to the choice of a base line, it is to be noted that the higher the base line, the narrower becomes the plateau of stable maximum counts at a given channel width (cf. Figs. 1 b and c). Hence it is advisable to use as low base line as convenient. Heinrich (1960) pointed out that raising the base line not only offers no advantages, but also results, in certain cases, in a loss of efficiency in the separation of energy levels.

Regarding the choice of the counter voltage, it is preferable to maintain it at a level slightly above that necessary to reach the maximum counts. As Heinrich (1960) points out, this "minimizes the passing of noise pulses smaller than the desired signal."

Fig. 1

Pulse height analysis.

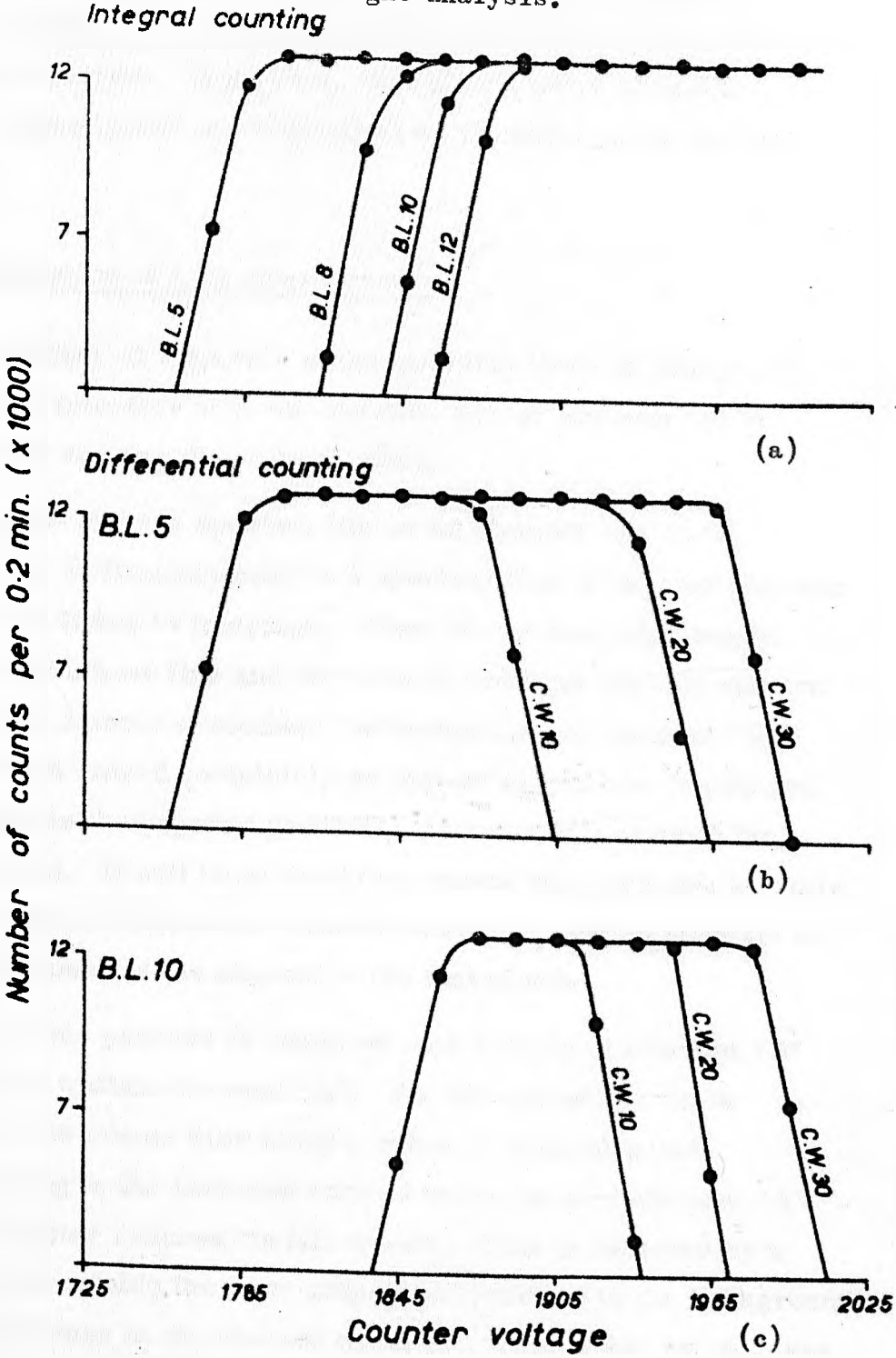

The setting of the channel width at a particular voltage depends on whether or not there are elements that might interfere with that of interest. If present, this interference should be carefully investigated and eliminated as is explained in the next section..

B. Elimination of Line Interference

The effect of elements whose spectral lines of odd orders are liable to interfere with the spectral line of interest can be elininated by varying the channel width.

Suppose that the spectral line of an element "A" to be measured is sufficiently near to a spectral line of another element "B" which is liable to interfere. First we set the pulse height selector on the base line and the counter voltages already chosen. Then using a sample of element "A" containing no element "B", the channel is closed completely so that no counts are registered. The channel is then opened gradually (at steps of 2 volts in the present work). It will be noticed that counts will increase steadily until they reach a maximum whereby they will remain constant no matter how much is the channel width increased.

The same process is repeated on a sample of element "B" that does not contain element "A". As the channel width is increased, the counts rise along a range of channel width corresponding to the increase noticed in the case of element "A" before the latter reaches its full counts. This is followed by a plateau representing the first order contributions to the background Further increase in the channel width will bring about an increase

in counts that corresponds to higher order contributions to the background and/or the interfering spectral line of element "B" depending on whether an immediate second plateau and/or sharp increase in counts is produced. It is evident that the range of channel width to be used is that producing the first plateau. The choice of a point in the middle of this plateau is a suitable one, being not affected by slight fluctuation in the channel voltage. The classic example of measuring Al in the presence of Ti is illustrated in Fig. 2a.

C. Background and Peak/Background Ratio

A background will be always present when the intensity of an X-ray line is measured for any specimen in general, and when using powder specimens of composite nature in particular. Components that contribute to the background are primarily reflections at higher orders of characteristic and non-characteristic radiations all of which are Bragg angle-dependent and secondarily scattered X-rays, detector noise, radioactivity and cosmic rays. The background, therefore, may vary considerably from one specimen to another.

The background becomes an important problem and, indeed a critical one, in the determination of light elements of low intensities. As pointed out by Parrish and Kohler (1956) and later by Liebhafsky et al., (1960), the problem becomes worse when a scintillation counter is used instead of a proportional counter because of the former's less energy of resolution.

More important still is the peak/background ratio which must

be attained as high as possible or at least higher than the lower limits of X-ray detectability. Parrish and Kohler (1956) showed that the peak/background ratio is a function of the analyzer transmission.

Eventually, pulse height selection would be expected to eliminate the higher order contributions to the background, thus improving P/B ratio. This was found to be true by varying the channel width. Changes in the base line proved to have a very little effect, if not at all, on the P/B ratio. Worth mentioning is that according to Liebhafsky et al., (1960), the pulse height selection also filters out scattered X-rays as well as the phototube noise when differences in energy are large enough.

Practically, the problem is approached by doing a stepwise channel width scan with the goniometer set at the peak and another scan with the goniometer set at the background, using the specimen to be analysed in both cases (Fig. 2 b). From the curves produced, the channel width that gives a good P/B ratio without a considerable loss of counts on the peak, can be known.

D. Conditions Used In Analysis

Table 2 shows the instrumental conditions chosen for the different elements analysed for.

Fig. 2

Pulse height analysis.

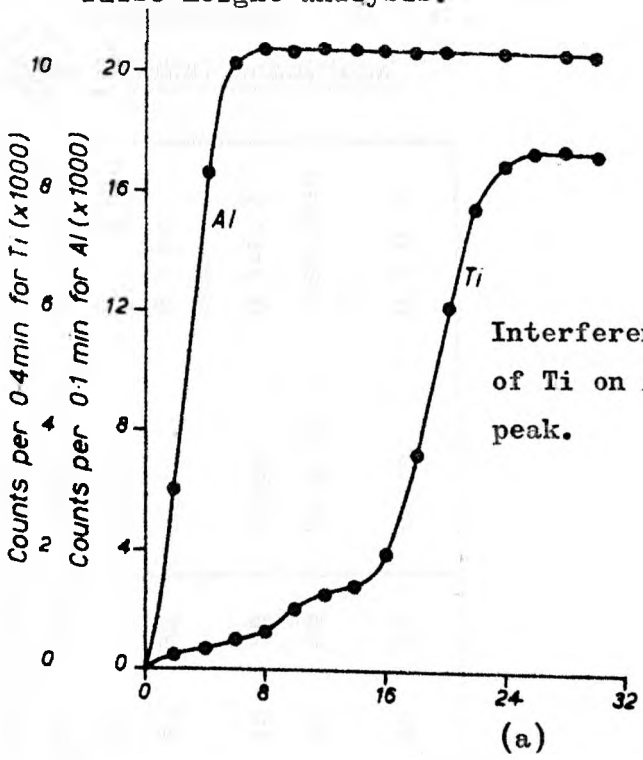

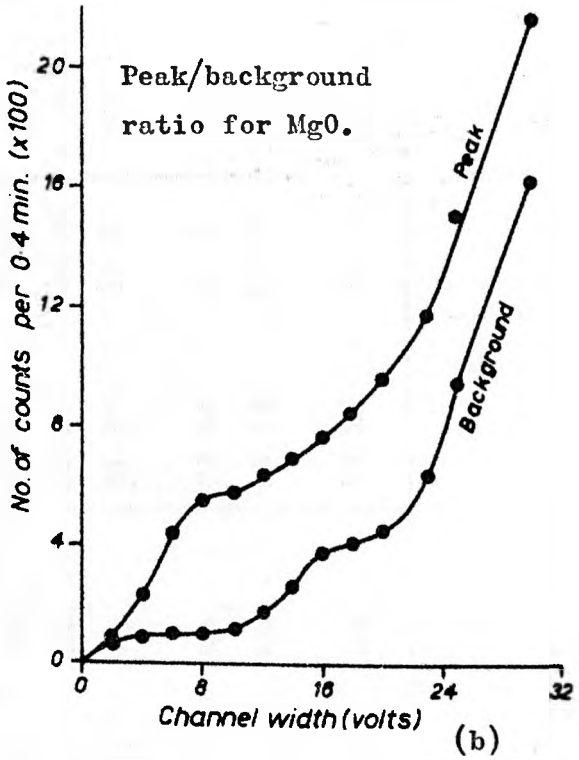

TABLE 2

Experimental Conditions

Element	Characteristic radiation	Goniometer settings Peak 2θ	Goniometer settings Bkgd 2θ	Target excitation Radiation	Kv	mA	Analysing crystal	Vacuum Torr
Si	Ka_1	55.98	57.22	Cr	40	30	Gyps.	0.1
Ti	Ka_1	20.98	20.26	Cr	40	30	Gyps.	0.1-0.2
Al	Ka_1	66.70	68.23	Cr	40	30	Gyps.	0.1
Fe	Ka_1	29.66	30.56	Cr	40	30	Gyps.	0.1-0.2
Ca	Ka_1	25.67	24.85	Cr	40	30	Gyps.	0.1-0.2
Mg	Ka_1	81.27	82.27	Cr	40	30	Gyps.	0.1 or less
K	Ka_1	28.64	27.75	Cr	40	30	Gyps.	0.1-0.2
Na	Ka_1	53.52	54.25	Cr	40	40	K.A.P.	less than 0.1
Mn	Ka_1	32.21	33.15	W	40	36	Gyps.	0.1-0.2

TABLE 2 (CONTINUED)

Counter	Pulse Height Analysis				Counting Rate in Min.
	Amplification	Counter volt	Base line volt	Channel width	
Gas flow proportional counter. Mixture of 90% Argon + 10% Methane	10x4	1980	8	15	0. 4
	10x4	1860	8	15	0. 4
	10x4	1920	5	10	1. 0
	10x4	1815	5	14	0. 4
	10x4	1900	12	12	0. 4
	10x4	1980	8	8	1. 0
	10x4	1910	10	12	0. 2
	10x4	1995	5	12	1. 0
	10x4	1852	10	10	0. 4
	10x4	1912	5	9	1. 0

VII. RELIABILITY OF THE METHOD USED

X-ray emission spectrography is not an absolute method of determining the amounts of elements present. According to Liebhafsky et al., (1960) if the comparison is "properly" carried out, the reliability of a comparative X-ray emission method is measured by its precision. The term "properly" includes the use of a standard so reliable that it may be considered to contain the elements of interest at (or very close) the true weight fraction known.

A. Sources of Errors

Errors may be (a) mechanical and electrical particularly due to the instability of counter electronics, i.e. machine reproducibility, or (b) due to the nature of the specimens (pelletizing, grain size, sample surface etc.).

Yet, an error which is not only important but also unavoidable is the Standard Counting Error "Sc". It results from fluctuations that cannot be elininated as long as quanta are counted because X-ray quanta are emitted randomly and not regularly in time (Macdonald, 1964). This Sc equals to $\sqrt{\bar{X}}$ or $\sqrt{\frac{1}{X_{standard}} + \frac{1}{X_{unknown}}}$ in case of using a comparison standard for the establishment of simple ratio (proof of these equations is explained at length in Liebhafsky et al., 1960). This error is significant in that it can be used as "a criterion for judging the operating conditions for X-ray emission spectrography" (Liebhafsky et al., 1960).

Hence, a comparison between Sc and S gives a clue for the reliability of the analytical results. The identity of these two standard errors is an indication that the different conditions of analysis were satisfactory over the period required to take the data.

For the different tests of reproducibility, the rock which will be used as a standard during the actual course of analysis (GLIO) was crushed to different grain sizes and 30 pellets were prepared. The following table outlines the procedure of crushing and the conditions of each pellet. (Table 3).

Each of the following aliquots was homogenised for 30 minutes and about 10 grams of each were mixed with bakelite resin to the ratio of 6 : 1, then homogenised for 20 minutes. Five portions (about 2 grams each) of every grain size were pelletized as explained earlier. Pellets No. 1 - 25 were pressed against glass discs (using a fresh disc for each pellet) and those numbered 27 - 31 were pressed against highly polished steel discs.

Two points should be noted in the above mentioned way of crushing and preparing the samples:-

1. Although the powder is crushed to pass the 100, 200 or 300 mesh screens, yet this does not necessarily mean that the overall grain size is 150, 76 or 53μ respectively. In fact the greatest bulk of the powder is far below these grain sizes because using the tema crusher results in transforming the major part of the powder into very fine dust.

2. It can be argued that sieving the powder after crushing would result in some sort of mineral separation, particularly if the

TABLE 3

Aliquot Number	Pellets Number	Grain Size
1	1 - 5 and 27	Small pieces of the rock crushed in Tema for 40 secs. and finished with the ball mill and manual agate mortar to pass 100 m esh.
2	6 - 10 and 28	-100 mesh powder (from aliquot No. 1) further crushed in Tema for 30 secs. and finished with the ball mill and manual agate mortar to pass 200 mesh.
3	11 - 15 and 29	-100 mesh powder (from aliquot No. 1) further crushed in the Tema for 50 secs. and finished with the ball mill and manual agate mortar to pass 300 mesh.
4	16-20 and 30	-200 mesh powder (from aliquot No. 2) further crushed in Tema for 20 secs. finished with ball mill and manual agate mortar to pass 300 mesh. The whole lot was split in two halves.
5	21-25 and 31	The first half was further crushed in the ball mill for $\frac{1}{2}$ hour (aliquot No. 4. pellets 16 - 20 and 30). The second half was further crushed in the ball mill for 1 hour (aliquot No. 5. pellets 21 - 25 and 31).

rock contains platy minerals. Yet, sieving was necessary to ensure that the whole powder is below a certain grain size. This problem of separation was overcome by homogenising the powder into a ball mill homogeniser for 30 minutes after it has been sieved.

B. Machine Reproducibility - Long and Short Term Variations

During this test, each pellet remained undisturbed during the whole sets of readings. For each pellet, count readings were taken for a number of equal consecutive counting intervals. These readings were then subdivided sequentially into sets of 10 each (the time necessary for measuring both the standard and the specimen in the usual analysis).

The results and the statistical analysis of this test is shown in Table 4.

Inspection of Table 4 shows that for short term deviation within sets, the standard counting error and the standard deviation can be considered identical. The slight increase of the standard deviation over the standard counting error in the very few cases in Table 4 is insignificant and, indeed, for comparisons of this sort, it can never be eliminated.

The same applies to the two standard errors calculated for the long term deviation. In the case of aluminium, for example, over a working period of 2 hours, the standard deviation is greater than the standard counting error only by 0.01% of the amount of Al present; a difference which is insignificant at all.

Element	Pellet No.	Av. counts on peak	P/B ratio	Short Term Deviation within sets: Set No.	Sc	C%	s	C%	Long Term Deviation: Degrees of freedom	Sc	C%	s	C_c%
Si	13	22100	67	1	148	0.67	165	0.75	49	149	0.67	176	0.79
				2	149	0.67	187	0.84					
				3	149	0.67	156	0.70					
				4	149	0.67	139	0.62					
				5	149	0.67	166	0.75					
	1	25568			160	0.63	183	0.72					
	6	24600			157	0.64	222	0.90					
	11	24554			157	0.64	164	0.67					
	16	24654			157	0.64	124	0.50					
	21	24503			157	0.64	134	0.55					
Ti	1	18400	22	1	136	0.74	156	0.85	31	136	0.74	155	0.84
				2	136	0.74	128	0.70					
				3	136	0.74	185	1.00					
	13	15997		1	126	0.79	193	120	27	126	0.79	121	0.77
				2	126	0.79	64	0.40					
				3	126	0.79	103	0.64					
	24	17431		1	132	0.67	165	0.95	52	132	0.76	148	0.85
				2	132	0.76	167	0.96					
				3	132	0.76	99	0.57					
				4	132	0.76	115	0.66					
				5	132	0.76	178	1.02					
Fe	1	19802	23		141	0.71	195	0.98					
	6	20246			142	0.70	108	0.53					
	11	20454			143	0.70	205	1.00					
	16	20334			142	0.70	123	0.60					
	21	20409			143	0.70	128	0.63					

TABLE 4 (CONTINUED)

Element	Pellet No.	Av. counts on peak	P/B ratio	Short Term Deviation within sets: Set No.	Sc	C%	s	C%	Long Term Deviation: Degrees of freedom	Sc	C%	s	C_c%
Al	21	7527	18	1	86	1.15	127	1.70	113	87	1.16	88	1.17
				2	87	1.16	83	1.10					
				3	87	1.16	54	0.72					
				4	87	1.16	56	0.75					
				5	87	1.16	66	0.88					
				6	87	1.16	56	0.75					
				7	87	1.15	94	1.24					
				8	87	1.15	88	1.17					
				9	87	1.15	86	1.14					
				10	87	1.15	75	0.99					
				11	88	1.16	86	1.13					
Ca	1	18401	21	1	135	0.74	110	0.60	32	136	0.74	134	0.73
				2	136	0.74	112	0.61					
				3	136	0.74	121	0.66					
	10	17257		1	132	0.76	110	0.45					
				2	132	0.76	77	0.45					
				3	131	0.76	99	0.58					
	13	16541		1	129	0.78	121	0.73	29	129	0.78	114	0.69
				2	128	0.78	88	0.53					
				3	129	0.78	122	0.74					
Mg	11	353	2.5	1	18	5.45	21	6.36	37	19	5.38	22	6.23
				2	19	5.43	20	5.71					
				3	19	5.21	17	4.66					
				4	19	5.18	15	4.25					
	29	337		1	18	5.26	23	6.73	23	18	5.34	17	5.00
				2	18	5.44	16	4.83					

TABLE 4 (CONTINUED)

Element	Pellet No.	Av. counts on peak	P/B ratio	Short Term Deviation within sets: Set No.	Sc	C%	s	C%	Long Term Deviation: Degrees of freedom	Sc	C%	s	C_c%
K	1	21725	42	1	148	0.68	161	0.74	88	147	0.68	168	0.77
				2	148	0.68	155	0.71					
				3	148	0.68	122	0.56					
				4	147	0.68	166	0.77					
				5	147	0.68	106	0.49					
				6	147	0.68	170	0.79					
				7	147	0.68	55	0.30					
				8	147	0.68	153	0.71					
				9	147	0.68	170	0.79					

Sc: standard counting error

s: standard deviation or the uncertainty of a single observation

C%: relative deviation of a single observation or the coefficient of variation expressed in per cent of the amount present.

C_c%: relative deviation of the counting error

Since it is intended in the actual course of rock analysis to use intensity ratio i. e. immediate comparison of the unknown rock with a carefully analysed rock used as a standard, instead of the direct use of number of counts, there was no point to determine the long term deviations over working periods of a day or more.

It can, therefore, be concluded that the spectrograph system is satisfactorily stable over the periods necessary to collect the data of analysis.

C. Effect of Grain Size and Pelletization on Reproducibility

In this test, the 5 pellets of each grain size were analysed for the different elements using a pellet of another rock as a comparison standard to calculate the X-ray intensity ratio (= No. of counts of sample/No.of counts of the standard). The results of this test and the statistical analysis of the data is shown in Table 5.

Inspection of Table 5 shows that the standard deviation is less than the standard counting error, suggesting that there is no added error due to pelletization and the method adopted for sample preparation is satisfactory. The table also shows that it is not necessarily the fine-grained powders which would give higher precision.

The -300 mesh-size powder will be used because:-

1. Further crushing would not improve the precision.
2. The mica in a coarse powder might tend to chip off the rock.
3. For consideration of accuracy which will be mentioned later,

TABLE 5

Effect of Grain Size and Pelletization on Reproducibility

Element	Pellet Nos. *	Average of 5 ratios	S	C%	$S\bar{x}$	E	Sc	Cc%
Si	1 - 5	1.0518	0.282	0.44	0.126	0.20	0.589	0.92
63.69	6 - 10	1.0825	0.300	0.47	0.134	0.21	0.583	0.92
	11 - 15	1.1016	0.488	0.76	0.218	0.34	0.577	0.91
	16 - 20	1.1153	0.271	0.43	0.121	0.19	0.565	0.89
	21 - 25	1.1139	0.342	0.54	0.153	0.24	0.571	0.90
Ti	1 - 5	0.8431	0.005	0.55	0.002	0.25	0.012	1.33
0.90	6 - 10	0.8317	0.006	0.66	0.003	0.30	0.012	1.33
	11 - 15	0.8311	0.005	0.55	0.002	0.25	0.012	1.33
	16.- 20	0.8083	0.007	0.78	0.003	0.35	0.012	1.33
	21 - 25	0.8080	0.007	0.78	0.003	0.35	0.013	1.44
Al	1 - 5	0.7998	0.198	1.16	0.088	0.52	0.304	1.78
17.05	6 - 10	0.7991	0.134	0.79	0.060	0.35	0.306	1.79
	11 - 15	0.7984	0.102	0.60	0.046	0.27	0.304	1.78
	16 - 20	0.7816	0.148	0.87	0.066	0.39	0.306	1.79
	21 - 25	0.7882	0.104	0.61	0.046	0.27	0.306	1.79
Total	1 - 5	1.4956	0.022	0.22	0.010	0.10	0.121	1.21
iron	6 - 10	1.5260	0.026	0.26	0.011	0.11	0.121	1.21
as	11 - 15	1.5306	0.051	0.51	0.023	0.23	0.121	1.21
Fe_2O_3	16 - 20	1.5385	0.064	0.64	0.029	0.29	0.121	1.21
9.99	21 - 25	1.5402	0.051	0.51	0.023	0.23	0.121	1.21

TABLE 5 (CONTINUED)

Element	Pellet Nos.	Average of 5 ratios	S	C%	$S\bar{x}$	E	Sc	Cc%
Mn	1 - 5	1.0188	0.0027	3.86	0.0012	1.73	0.0016	2.28
0.07	6 - 10	1.0045	0.0018	2.57	0.0008	1.15	0.0016	2.28
	11 - 15	1.0049	0.0013	1.86	0.0006	0.83	0.0016	2.28
	16 - 20	1.0162	0.0012	1.71	0.0005	0.76	0.0016	2.28
	21 - 25	1.0262	0.0013	1.86	0.0006	0.83	0.0016	2.28
Mg	1 - 5	0.8100	0.074	3.89	0.033	1.74	0.214	11.26
1.90	6 - 10	0.6209	0.021	1.11	0.009	0.49	0.214	11.26
	11 - 15	0.5984	0.076	4.00	0.034	1.79	0.220	11.58
	16 - 20	0.5506	0.074	3.89	0.033	1.73	0.222	11.68
	21 - 25	0.5424	0.077	4.05	0.034	1.79	0.224	11.79
Ca	1 - 5	1.0995	0.0024	0.31	0.0011	0.14	0.0080	1.04
0.77	6 - 10	1.0427	0.0041	0.53	0.0018	0.23	0.0082	1.06
	11 - 15	1.0224	0.0039	0.51	0.0017	0.22	0.0082	1.06
	16 - 20	1.0377	0.0033	0.43	0.0015	0.19	0.0081	1.05
	21 - 25	1.0473	0.0027	0.35	0.0012	0.16	0.0081	1.05
Na	1 - 5	1.0585	0.036	1.88	0.016	0.84	0.178	9.32
1.91	6 - 10	0.9809	0.058	3.04	0.026	1.36	0.178	9.32
	11 - 15	1.0274	0.047	2.46	0.021	1.10	0.182	9.53
	16 - 20	0.9866	0.050	2.62	0.022	1.17	0.178	9.32
	21 - 25	0.9857	0.041	2.15	0.018	0.96	0.179	9.37

TABLE 5 (CONTINUED)

Element	Pellet Nos.	Average of 5 ratios	S	C%	$S\bar{x}$	E	Sc	Cc%
K	1 - 5	1.1839	0.020	0.61	0.009	0.28	0.028	0.86
3.25	6 - 10	1.1631	0.027	0.83	0.012	0.37	0.028	0.86
	11 - 15	1.1484	0.020	0.61	0.009	0.28	0.028	0.86
	16 - 20	1.0940	0.013	0.40	0.006	0.18	0.028	0.86
	21 - 25	1.0673	0.029	0.89	0.013	0.40	0.028	0.86
P	1 - 5	0.9922	0.0028	3.50	0.0013	1.57	0.0056	7.00
0.08	6 - 10	0.9255	0.0008	1.00	0.0004	0.45	0.0058	7.25
	11 - 15	0.9384	0.0023	2.87	0.0010	1.28	0.0058	7.25
	16 - 20	0.8998	0.0009	1.13	0.0004	0.51	0.0060	7.50
	21 - 25	0.8988	0.0010	1.25	0.0004	0.56	0.0060	7.50

* Refer to Table 3 for the grain size of these pellets

S, Sx and Sc are expressed as oxide per cent

C and E are expressed as per cent of the amount present

Sc is the standard counting error of simple ratio

Cc is the relative deviation of the counting error

-300 mesh powder proved to give more accurate results than -200 powder.

Since it is intended to use three pellets for each rock instead of five during the actual course of analysis, three pellets of the -300 mesh powder were measured and the results are statistically analysed as shown in Table 6.

Table 6.

Effect of Pelletization on the Reproducibility of 3 Pellets

Element	% oxide	S	C%	$S\bar{x}$	E%
Si	63.69	0.341	0.54	0.197	0.31
Ti	0.90	0.005	0.56	0.003	0.32
Al	17.05	0.150	0.88	0.087	0.51
Fe	9.99	0.032	0.32	0.018	0.18
Mn	0.07	0.0005	0.71	0.0003	0.41
Mg	1.90	0.015	0.79	0.009	0.46
Ca	0.77	0.002	0.26	0.001	0.15
Na	1.91	0.036	1.88	0.021	1.08
K	3.25	0.021	0.64	0.012	0.37
P	0.08	0.0006	0.75	0.0003	0.43

In both Tables 5 and 6, since S is smaller than Sc, it can be concluded that the standard deviation noticed between the pellets is due to the unavoidable standard counting error. It follows that if the counting is increased (lower Sc), the precision between the pellets should improve. To test this assumption, the 5 pellets of the -300 mesh powder were analysed and the counting was increased to nearly 300,000 for Si, Fe, K; 80,000 for Al and 5,000 for Mg.

TABLE 7

Effect of Pelletization on the Reproducibility of 5 Pellets at High Counting Rate

Element	S	C%	$S\bar{x}$	E	Sc	Cc%
Si (63.69)	0.085	0.11	0.038	0.06	0.153	0.24
Al (17.05)	0.02	0.12	0.009	0.05	0.08	0.47
Fe (9.99)	0.01	0.10	0.004	0.04	0.03	0.30
Mg (1.90)	0.01	0.53	0.004	0.24	0.03	1.58
k (3.25)	0.006	0.18	0.003	0.08	0.008	0.25

The results of this test (Table 7) show a great improvement in S which is, in turn, lower than Sc. Again this indicates that there is no added error due to pelletization and the precision required from the analysis is dependent on the choice of a particular standard counting error to suit the work for which the analysis is done.

D. The Effect of Grain Size of Intensity

It has been for a long time recognized that although X-ray fluorescence intensity is unaffected by the physical state of the elements, yet the extent to which the powder is ground has a considerable effect. Claisse (1956 in Claisse and Samson 1961) showed by experiment that, in general, the fluorescence intensity increases as the grain size decreases.

Later, Claisse and Samson (1961) theoretically predicted and experimentally verified in quantitative terms the effect of grain size on X-ray fluorescene intensity. They theoretically showed that for a given wavelength, when the grain size is very large or very

small, the intensities are independent of grain size although they differ from each other by a factor of 12. Yet, these two extremes are separated by a "transition zone" occurring between 5μ - 1 mm, a range which "encloses all the grain sizes that can be produced or that are utilized in X-ray fluorescence analysis"(p. 344). Their experiments proved the existence of such a zone. Moreover, the authors (ibid) pointed out that the belief of the necessity of pulverizing the sample as much as possible to by-pass the transition zone, has no basis and in fact in the case of light elements, the transition zone is displaced toward very fine grain sizes..

In view of these findings, this grain size effect is investigated in the present work. Column 3 of Table 5 and Figure 3 show the results of this investigation. From these results, it is clear that not all the intensities of all the elements increase with decreasing grain size.

This discrepancy has been mentioned and/or investigated by Hornung ( ), Chodos and Engel (1961) and Volborth (1963 and 1964). Chodos and Engel (1961) pointed out that the presence of mica which is difficult to grind and often form large specks or powder surfaces, apparently has a great effect on X-ray analysis. Hornung ( ) and Volborth (1963, 1964) further investigated this effect and their observations, together with those of the present work are outlined in Table 8.

Volborth (1964) explained this discrepancy in the following way. A micaceous mineral like biotite will increase its total relative surface than non-micaceous minerals upon further grinding; an effect which is further enhanced by pelletizing at high pressure.

TABLE 8

Element	Effect of grinding on Intensity			
	Hornung( )	Volborth (1963)	Volborth*(1964)	Present work
Si	increase	decrease	decrease** -1%mG-1	increase
Ti	slight decrease	increase considerably	increase -20%	decrease
Al	increase	increase considerably	increase -4%	decrease
Fe	decrease	increase considerably	regularly increase 34% in G-1 0.5% in W-1	increase
Ca	increase	decrease	decrease -7%	decrease followed by increase
Mg	increase	increase considerably	increase -8-17%	decrease
K	increase	increase-sporadic and slight if not at all	decrease 4%	decrease
Mn	-	increase considerably	increase -59%	decrease followed by increase
P	-	-		decrease
Na	-	-	increase 2.3%	decrease

TABLE 8 (CONTINUED)

* The figures represent the per cent increase or decrease of the amount present. The calculations are based on expressing the intensities in per cent so that one number, either the highest or the lowest corresponds to the recommended values of Stevens et al., for G-1 and W-1 (U. S. Geol. Surv. Bull. 1113, 1960).

** The decrease is greate in G-1 than in W-1

Fig. 3

Effect of grain size on X-ray intensity.

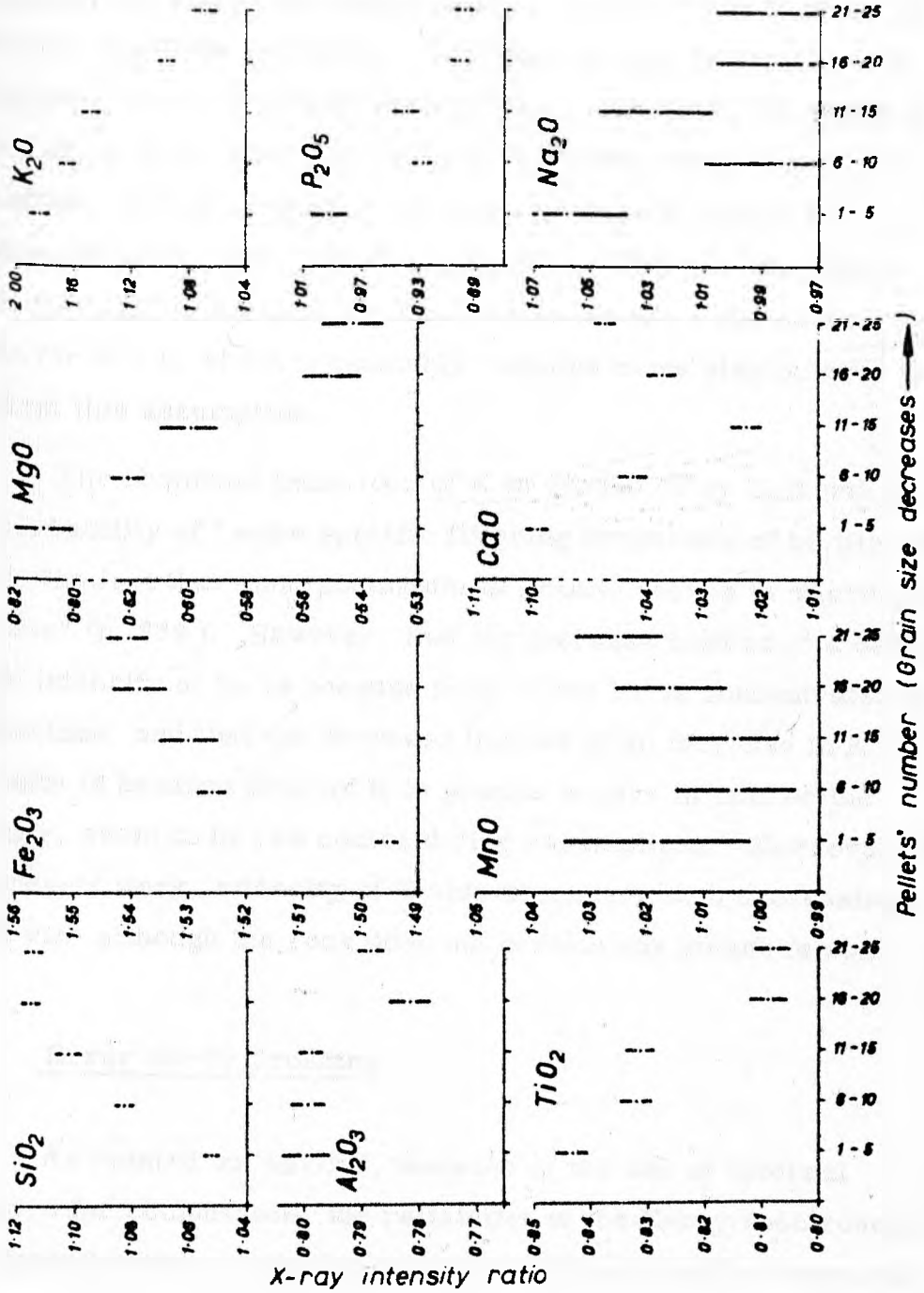

This results in high intensity readings for the elements which compose the biotite. This assumption can account for his observed decrease or increase in the intensity of the different elements except for Na where one would expect a decrease and K where an increase should be predicted. This discrepancy is explained by Volborth by the assumption that for Na " apparently the effect of diminishing grain size is greater here because of the very soft radiation. Besides, most of the sodium is concentrated in plagioclase and not in biotite". (p. 638). However, the figure 2-3% increase in Na given by Volborth is for G - 1 and no data is given for W - 1, which presumably contains more plagioclase, to confirm this assumption.

The abnormal behaviour of K is attributed by Volborth to the probability of "some specific filtering properties of biotite mica and to the fact that most potassium in granite occurs in microcline perthite" (p. 639). However, that the increase instead of a decrease in the intensity of Na is because most of the Na is concentrated in plagioclase, and that the decrease instead of an increase in K intensity is because most of K in granite occurs in microcline perthite, seem to be two contradicting assumptions. Moreover, in the present work, intensity of K also decreases with decreasing grain size although the rock does not contain any potash felspar.

E. Error due to Crushing

As pointed out earlier, because of the use of external standard for comparison, the reliability of the X-ray spectroscopy will depend mainly on the fact that the unknown must be prepared

exactly as the standard. Crushing is by far the most important step in preparation which is likely to introduce a big error. As shown in the previous section, the X-ray intensity of the different elements will either increase or decrease with varying grain size.

To test the precision of the grinding technique adopted in the present work, three aliquots of the -100 mesh powder of GL-10 were ground separately to -300 mesh. Three pellets of each aliquot were prepared and the X-ray intensity ratio was determined for all the elements. Table 9 shows the result of this test.

It can be seen from this table that the difference between the averages of the three aliquots is small and insignificant. In fact it is sometimes smaller than the difference between pellets of the same aliquot. Moreover, S is always lower than Sc, i. e. there is no added error due to crushing.

Therefore, it can be concluded that the error due to crushing the -100 mesh powder to -300 mesh is within the precision of pelletizing the powder of one aliquot, which in turn lies within the standard counting error.

VIII. ANALYTICAL DATA

Thirty three chemically analysed rock powders were used in the analyses by X-ray fluorescence to calibrate and check the reliability of the method. Appendix 1 shows a list of these rocks for any future reference. Two series of tests were done:

1. Test No. 1. was performed on a -200 mesh powder. The standard used for comparison (Gl-10, specimen text No. 12)

TABLE 9

PRECISION OF CRUSHING ROCK GL - 10

Element	Pellet No.	X-ray Intensity Ratio Aliquot No. 1.	Aliquot No. 2.	Aliquot No. 3.	Statistical Data Total Average	S Ratio	S Oxide	C%
SiO_2	1	1.0156	1.0131	1.0118				
63.69	2	1.0145	1.0134	1.0111	1.0129	0.0012	0.07 (Sc=0.153)	0.11
	3	1.0119	1.0126	1.0120				
	Av.	1.0140	1.0130	1.0116				
TiO_2	1	1.0105	0.9942	0.9989				
0.80	2	1.0044	0.9928	0.9984	1.0001	0.0073	0.006 (Sc=0.012)	0.62
	3	1.0095	0.9945	0.9976				
	Av.	1.0081	0.9938	0.9983				
Al_2O_3	1	1.0219	1.0298	1.0029				
17.05	2	1.0060	1.0010	1.0236	1.0169	0.0024	0.041 (Sc=0.304)	0.24
	3	1.0029	1.0271	1.0167				
	Av.	1.0169	1.0193	1.0144				
Fe^{3+}	1	0.9936	0.9978	0.9909				
(tot.)	2	0.9923	1.0059	0.9975	.9960	0.0098	0.098 (Sc=0.21)	0.98
9.99	3	0.9916	1.0058	0.9904				
	Av.	0.9925	1.0032	0.9922				
MnO	1	1.0052	1.0043	0.9994				
0.07	2	0.9900	1.0002	1.0002	0.9988	0.0026	0.0002 (Sc=0.0016)	0.60
	3	0.9967	1.0014	0.9922				
	Av.	0.9973	1.0019	0.9973				
MgO	1	0.9724	0.9261	0.9905				
1.90	2	0.9954	0.9198	0.9909	0.9732	0.0227	0.043 (Sc=0.22)	2.26
	3	1.0000	0.9953	0.9680				
	Av.	0.9893	0.9471	0.9831				

TABLE 9 (CONTINUED)

Element	Pellet No.	X-ray Intensity Ratio Aliquot No. 1.	Aliquot No. 2.	Aliquot No. 3.	Total Average	Statistical Data S Ratio	S Oxide	C%
CaO	1	0.9899	0.9914	0.9890				
0.77	2	0.9858	0.9942	0.9922				
	3	0.9922	0.9974	0.9915	0.9905	0.0026	0.002 (Sc=0.008)	0.26
	Av.	0.9893	0.9943	0.9909				
K_2O	1	1.0023	0.9881	1.0035				
3.25	2	0.9864	0.9856	0.9949				
	3	1.0101	0.9917	0.9993	0.9958	0.0063	0.020 (Sc=0.028)	0.61
	Av.	0.9996	0.9885	0.9992				

and for calculation of the X-ray intensity ratio, was also a -200 mesh powder (aliquot No. 2 of Table 3, p. 20).

2. Test No. 2 and No. 2 repeated were done on a -300 mesh powder. The standard (specimen 12) used for this test was also crushed to pass 300 mesh

Unless otherwise indicated, three pellets per each rock powder were prepared as described earlier.

A. Chemical Composition of Rock GL 10 used as a Standard

Table 10 shows the results of chemical analysis of rock GL 10 (specimen 12) done by rapid method. In fact, not only the standard GL 10 but also all the other rocks, the analyses of which is mentioned in the present work, are analysed by the same method.

The method of analysis is described by Riley (1958). A brief outline of this method is to follow.

All the elements except FeO and H_2O are analysed for in two solutions viz. solution A and B.

Solution A: is used for the determination of silica. The solution is prepared by fusing the rock with sodium hydroxide and the fusion product is dissolved in water. Silica is determined in the acidified solution by the molybdenum blue method.

Solution B: is prepared by attacking the rock with hydrofluoric and perchloric acids. Elements to be determined in solution B are total iron as Fe_2O_3, alumina, titania, manganese oxide, calcium oxide, magnesium oxide, sodium oxide, potassium oxide and phosphorous pentoxide.

TiO_2 is determined photometrically by means of the yellow compound formed by the addition of hydrogen peroxide to the acid solution after suppressing the interference of iron with phosphoric acid.

Al_2O_3 is determined photometrically. It is extracted with a solution of 8-hydroxyquinoline in chloroform at pH 5 after complexing iron as the ferrous dipyridyl complex. Any remaining fluoride is complexed by beryllium sulphate. Correction for titanium interference is considered.

Total Iron is determined photometrically after it is reduced with hydroxyl amine at pH 4.8 - 5.0 and complexed as the red ferrous dipyridyl complex.

Manganese is determined photometrically by oxidation to permanganate using potassium periodate in acid solution.

Sodium and potassium oxides are determined by flame photometry using ammonium sulphate as a spectroscopic buffer and after removing iron, aluminium and titanium by means of ion exchange resin.

P_2O_5 is determined photometrically by a single solution molybdenum blue method using ascorbic acid as the reducing agent.

CaO and MgO are determined with titration versus ethylenediamine-tetraacetic acid after the removal of interfering elements.

TABLE 10

Chemical Analysis of GL 10 (Specimen 12) *

Oxide	(a)	(b)	(c)	Average
SiO_2	63.89	63.50	-	63.69
TiO_2	0.79	0.80	0.80	0.80
AL_2O_3	17.03	17.11	17.00	17.05
Fe_2O_3 (total)	10.02	9.97	9.98	9.99
MnO	0.07	0.07	0.07	0.07
MgO	1.96	1.85	1.89	1.90
CaO	0.66	0.92	0.72	0.77
Na_2O	1.90	1.91	1.92	1.91
K_2O	3.25	3.23	3.26	3.25
H_2O	1.77	1.75	-	1.76
P_2O_5	0.08	0.08	0.08	0.08
FeO	8.17	8.23	-	8.20
Fe_2O_3				0.88
Total				100.36

* Analyst: M. Brotherton - Geology Dept.
Liverpool University.

B. Results

The precision of analysis is high as predicted earlier; so high that the same results were obtained using powders of different grain size or different pellets of the same powder. The only condition to get such precision is that the rock used as a standard is ground to the same grain size as that of the unknown.

The precision of the determination of each element will be discussed later at length in due turn. But at this stage, it can be pointed out that there is no problem whatsoever with the precision when pellets of the same size powder are used.

Regarding the accuracy of the results, the one-point calibration proved to be unsatisfactory in most cases, particularly for the results of silica. The most possible explanation for this discrepancy is that the pre-assumption that the straight calibration line relating the per cent oxide and the intensity ratio should go to the origin (i.e. at $x = 0$, $y = 0$), is false. Consequently, there should be an intercept and in the equation of the straight line $y = bx + a$ (where b is the slope of the line and a is the intercept on the y-axis) $a \neq 0$.

Another disadvantage of this one point-calibration method is that for elements present in very low concentrations (e.g. Mn, P, etc.) or for elements like Ca and Mg, the error which is very likely present in the chemical analysis of the standard will have a great effect on the results obtained by X-ray. An excellent illustration of this will be demonstrated in the case of Mn.

To solve this calibration problem and to test for the validity

of the assumptions just mentioned, silica was chosen for investigation on account of the facts that it is present as a major constituent and the X-ray results show great deviation from those of the chemical analysis.

(i) Silica

The precision of the X-ray spectrographic determination of SiO_2 is shown in Table 11. Compared with Table 5 it is evident that the precision is below the standard counting error.

Pellets used in Test No. 2. were redetermined by X-ray (Test 2 repeated) together with other five rocks (Specimen Nos. 15, 16, 22, 31, 32). Then the intensity ratio of all the pellets used in Test No. 1, Test No. 2 and No. 2 repreated were plotted against the results of the chemical analysis. The line relating the intensity ratio and the chemical analysis was drawn; both the slope and the intercept were calculated by the least square method.

The use of the least square method is justifiable on the basis that the chemical analyses of the rocks were done by different analysts at different times, hence the errors in the analyses will be random. Fig. 4a shows this silica calibration line.

The equation of the silica calibration curve is:

$$y = 42.399\,x + 21.1951$$

$$SiO_2\% = (42.3999 \times \text{Intensity Ratio}) + 21.1951$$

Table 12 shows the results of chemical analysis, X-ray analysis calculated from the simple ratio (one-point calibration) and X-ray analysis calculated using the equation of the silica graph

TABLE 11

Precision of X-ray Spectrographic Determination of SiO_2

Specimen	No. of Pellets	SiO_2% $\bar{X}$	S	C%	$S_{\bar{x}}$	E%
Test No. 1. (-200 Mesh)						
1	3	57.62	0.264	0.46	0.152	0.27
2	3	76.01	0.321	0.42	0.185	0.24
3	3	70.07	0.532	0.76	0.307	0.44
4	3	60.53	0.248	0.41	0.143	0.24
5	3	59.69	0.470	0.79	0.271	0.46
6	3	63.26	0.273	0.43	0.158	0.25
10	5	77.67	0.275	0.35	0.123	0.16
13	5	62.86	0.391	0.62	0.166	0.28
Test No. 2. (-300 Mesh)						
1	3	57.31	0.314	0.55	0.181	0.32
2	3	76.37	0.511	0.67	0.295	0.37
3	3	70.24	0.505	0.72	0.292	0.41
4	3	60.62	0.025	0.04	0.014	0.02
5	3	59.18	0.149	0.25	0.086	0.14
5a	3	59.18	0.309	0.52	0.178	0.30
6	3	63.00	0.274	0.43	0.158	0.25
7	3	58.64	0.271	0.46	0.156	0.27
8	3	62.79	0.539	0.86	0.311	0.50
9	3	58.96	0.618	1.05	0.360	0.61
10	3	77.30	0.552	0.71	0.319	0.41

TABLE 11 (CONTINUED)

$\bar{X}$: Arithmetic mean

S : Standard deviation of a single observation (amount of oxide)

$S\bar{x}$: Standard error of the arithmetic mean (amount of oxide)

C% : Relative deviation of a single observation (in per cent of the amount of oxide present)

E% : Relative error of the mean (in per cent of the amount of oxide present)

(least square). Notice the immense improvement in the accuracy of the results calculated by the least square equation.

Further test on the method was done on other seven rocks taken as unknowns. The results are shown in Table 13 together with the data of chemical analysis.

The deviation and standard deviation in per cent silica from the chemical analysis are shown in Table 14, none of the results was discarded from the calculation because of high or low values. This gives a measure of the accuracy of the X-ray method assuming that the chemical data are accurate and represent the arithmetic means.

Worth noticing is that the accuracy decreases with coarser grain size. This is to be expected because with coarse powders, the

TABLE 12

Comparison of X-ray Spectrographic Data with Chemical Data for SiO_2

Specimen	Chemical Analysis	X-ray Spectrographic Data					
		Test No. 1		Test No. 2.		Test 2 repeated	
		One-point calibration	Least square	One-point calibration	Least square	One-point calibration	Least square
1	56.31	54.73	57.62	54.07	57.19	54.25	57.31
2	77.06	82.34	76.01	82.75	76.29	82.88	76.37
3	68.58	73.41	70.07	73.74	70.28	73.68	70.24
4	61.16	59.09	60.53	59.53	60.82	59.23	60.62
5	59.35	57.82	59.69	57.06	59.18	57.06	59.18
6	63.45	63.19	63.26	62.75	62.97	62.79	63.00
7	59.34	-	-	56.10	58.53	56.24	58.64
8	63.21	-	-	62.59	62.86	62.48	62.79
9	58.89	-	-	56.66	58.92	56.73	58.96
10	76.76	84.82	77.67	84.57	77.50	84.28	77.30
11	62.44	-	-	61.75	62.30	61.45	62.10
12	63.69		63.60		63.60		63.60
13	62.65	61.42	62.86	-	-	-	-
15	64.25	-	-	-	-	64.46	64.11
16	72.36	-	-	-	-	74.84	71.36
22	66.89	-	-	-	-	69.38	67.38
31	54.87	-	-	-	-	50.94	55.11
32	68.87	-	-	-	-	68.55	67.83

TABLE 13

Comparison of X-ray Spectrographic Data with Chemical Data for SiO_2 using Seven Unknown Rocks and the Least Square Equation

Specimen	Chemical Analysis	X-ray Analysis
18	63.11	62.95
19	61.90	61.39
20	62.52	61.77
21	60.55	60.42
24	55.77	55.66
26	76.27	76.03
27	50.72	50.78

TABLE 14

Deviation of SiO_2% from the Chemical Analysis

(d = SiO_2% X-ray analysis - SiO_2% Ch. An.)

Specimen	d Test 1	d Test 2	d Test 2 rept.
1	+1.31	+0.88	+1.00
2	-1.05	-0.77	-0.69
3	+1.49	+1.70	+1.66
4	-0.63	-0.27	-0.54
5	+0.34	-0.17	-0.17
6	-0.19	-0.48	-0.45
7	-	-0.81	-0.70
8	-	-0.65	-0.42
9	-	+0.03	+0.07
10	+0.91	+0.64	+0.54
11	-	-0.11	-0.30
12	-0.09	-0.09	-0.09
13	+0.21	-	-
15	-	-	-0.14
16	-	-	-1.00
18	-	-	-0.16
19	-	-	-0.51
20	-	-	-0.75
21	-	-	-0.13
22	-	-	+0.49
24	-	-	-0.11
26	-	-	-0.24
27	-	-	+0.06
31	-	-	+0.34
32	-	-	-1.04
	n = 9 s = 0.90	n = 12 s = 0.74	n = 24 s = 0.63

biotite flakes with the tendency to lie parallel to the pellet surface would greatly affect the results. Therefore only the -300 mesh results (Test 2 repeated) will be considered in the calculations and discussions to follow.

It is difficult, however, to estimate how much of this error is attributed to the chemical analysis and how much to the X-ray analysis. Yet, even standing as they are, the present results are better than those of Hooper (1964) where s = 1.10% $si0_2$ out of 60% $Si0_2$ as the mean oxide present. They are comparable with Volborth (1963) who quotes s = 0.61 and $Sx^- = 0.16$ for 19 analyses the result of one of which (No. 9 in his Table A5) was discarded apparently because of the 1.36% $Si0_2$ deviation it gives whereas four analyses were not included in his calculations because of lack of gravimetric data. Accordingly, and assuming x^- = 52%, 65% and 77% $Si0_2$, he gives the following data as the relative deviations and errors representing the $Si0_2$ encountered:

$C_{52\%} = 1.17$ $E_{52\%} = 0.31$

$C_{65\%} = 0.94$ $E_{65\%} = 0.25$

$C_{77\%} = 0.79$ $E_{77\%} = 0.21$

On the basis of 53 analyses (discarding three of the original 56 analyses as being unacceptable) Volborth (1963) concludes that for n = 53, s = 0.89 and $Sx^- = 0.12$ in per cent $Si0_2$. Accordingly,

$C_{52\%} = 1.71$ $E_{52\%} = 0.24$

$C_{65\%} = 1.37$ $E_{65\%} = 0.19$

$C_{77\%} = 1.15$ $E_{77\%} = 0.16$

Similar calculations from the data of the present work where n = 24, s = 0.67 and Sx^{-} = 0.15, would give

$C_{52\%}$ = 1.21 $E_{52\%}$ = 0.25

$C_{65\%}$ = 0.97 $E_{65\%}$ = 0.20

$C_{77\%}$ = 0.81 $E_{77\%}$ = 0.17

Again, the results of the present work are comparable to those of Volborth (1963) if not better than them.

(ii) Titanium oxide

The instrumental conditions for TiO_2 determination are listed in Table 2. The precision of the method is shown in Table 15.

The precision is by all means superior to that of the chemical analysis. In the present work C is 2-1% of the amount of oxide present for 7 specimens and less than 1% for 15 specimens.

Compared with the chemical methods, the following are the figures for TiO_2 precision given by different authors:-

C = 6.9 (Mercy, 1956 by rapid methods)

C = 9.23, 4.31 (Stevens and others, 1960, for G-1 and W-1 respectively by direct reading spectrometer)

C = 23.20, 22.56 (Fairbairn and others, 1951, for G-1 and W-1 respectively, all analyses)

C = 16.59, 18.34 (Stevens and others, 1960, for G-1 and W-1, all analyses)

C = 5.76, 6.54 (Stevens and others, 1960 - preferred value)

Compared with other X-ray data, Volborth (1963) quotes C = 5.0 and 0.5 for G-1 and W-1 respectively and a range of 0.7 - 1.5 for other five rocks.

As to the accuracy of TiO_2 determination, again the one-point calibration proved to be inadequate, as shown in Table 16. The fact that all the X-ray results are lower than the chemical analysis suggests that the colourimetrically determined 0.80% TiO_2 of GL-10 (Table 10) is lower than the true value, thus representing a further contribution to the error of the one-point calibration applied to TiO_2 determination.

Similar to the case of SiO_2, an equation was derived by the least square method using the X-ray intensity ratio on the x-axis and the data of the chemical analysis on the y-axis. The equation is:

$$y = 0.9142\,x + 0.0206 \quad \text{or}$$

$$TiO_2\% = (0.9142 \times \text{Intensity ratio}) + 0.0206$$

Calculated on this basis, the X-ray results are shown in column marked least square in Table 16 and the calibration graph is shown in Fig. 4b. The results in this column are the ones to be considered in further calculations or comparisons.

Assuming that the chemical data are accurate and represent the arithmetic mean, the minus or plus deviations from the chemical analysis are shown in the column marked "d" in Table 16. The standard deviation calculated is S = 0.06% TiO_2 for -200 mesh and 0.057% TiO_2 for -300 mesh. The deviations range from -0.10 to +0.09 for the 200 mesh and from +0.09 to +0.08% TiO_2 for the 300 mesh powder. Such symmetrical plus and minus deviation indicates

TABLE 15

PRECISION OF X-RAY SPECTROGRAPHIC DETERMINATION OF TiO_2

Specimen	No. of Pellets	TiO_2% $\bar{X}$	s	C%	$S_{\bar{x}}$	E%*
Test No. 1. (-200 Mesh)						
1	3	1.33	0.007	0.53	0.004	0.31
2	3	0.53	0.007	1.32	0.004	0.76
3	3	0.63	0.010	1.59	0.006	0.92
4	3	1.00	0.012	1.20	0.007	0.69
5	3	1.15	0.007	0.61	0.004	0.35
6	3	0.92	0.016	1.74	0.009	1.00
10	5	0.51	0.000	0.00	0.000	0.00
11	3	0.80	0.007	0.88	0.004	0.51
13	5	0.55	0.005	0.91	0.002	0.41
Test No. 2. (-300 Mesh)						
1	3	1.33	0.007	0.53	0.004	0.31
2	3	0.54	0.007	1.30	0.004	0.75
3	3	0.62	0.007	1.13	0.004	0.65
4	3	0.98	0.000	0.00	0.000	0.00
5	3	1.15	0.007	0.61	0.004	0.35
5a	3	1.15	0.007	0.61	0.004	0.35
6	3	0.93	0.000	0.00	0.000	0.00
7	3	1.04	0.007	0.67	0.004	0.39
8	3	0.84	0.010	1.19	0.006	0.69
9	3	1.09	0.007	0.64	0.004	0.37
10	3	0.51	0.000	0.00	0.000	0.00
14	3	0.82	0.007	0.85	0.004	0.49
17	3	0.88	0.007	0.79	0.004	0.46

* For the meaning of these statistical terms, refer to Table 11, (p. 44).

TABLE 16

COMPARISON OF X-RAY SPECTROGRAPHIC DATA WITH CHEMICAL DATA FOR TiO_2

Specimen	Chemical Analysis	X-Ray Spectrographic Data					
		Test No. 1.			Test No. 2.		
		One-pt. calibr.	Least square	Deviation	One-pt. calibr.	Least square	Deviation
1	1.32	1.14	1.33	+0.01	1.14	1.33	+0.01
2	0.56	0.45	0.53	-0.03	0.46	0.54	-0.02
3	0.54	0.54	0.63	+0.09	0.53	0.62	+0.08
4	0.91	0.86	1.00	+0.09	0.84	0.98	+0.07
5	1.24	0.98	1.14	-0.10	0.99	1.15	-0.09
5a	1.24	-	-	-	0.98	1.15	-0.09
6	0.86	0.80	0.92	+0.06	0.80	0.93	+0.07
7	1.02	-	-	-	0.89	1.04	+0.02
8	0.91	-	-	-	0.71	0.84	-0.07
9	1.04	-	-	-	0.94	1.09	+0.05
10	0.54	0.43	0.51	-0.03	0.43	0.51	-0.03
11	0.82	0.68	0.80	-0.02	0.69	0.81	-0.01
11a	0.82	-	-	-	0.64	0.75	-0.07
12	0.80	0.80	0.93	(Definite colourimetric error)			
13	0.59	0.46	0.55	-0.04	-	-	-
14	0.82	-	-	-	0.70	0.82	0.00
17	0.87	-	-	-	0.75	0.88	+0.01
19	0.89	-	-	-	0.83	0.91	+0.02
			n = 9			n = 16	
			s = 0.06			s = 0.057	

Figure 4.

The error bar limits on this and subsequent similar figures are the standard deviation of the X-ray precision results and the results for accuracy of rapid analysis in Mercy (1956).

Fig. 4

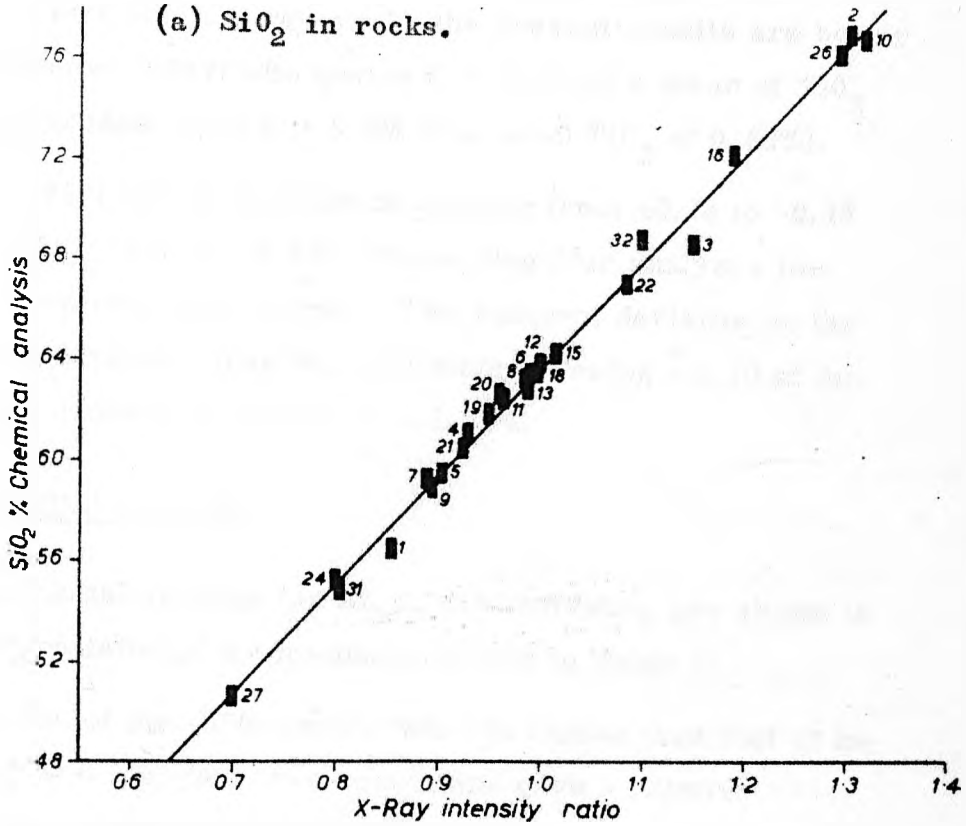
(a) SiO_2 in rocks.
SiO_2 % Chemical analysis
X-Ray intensity ratio
76
72
68
64
60
56
52
48
0·6
0·7
0·8
0·9
1·0
1·1
1·2
1·3
1·4

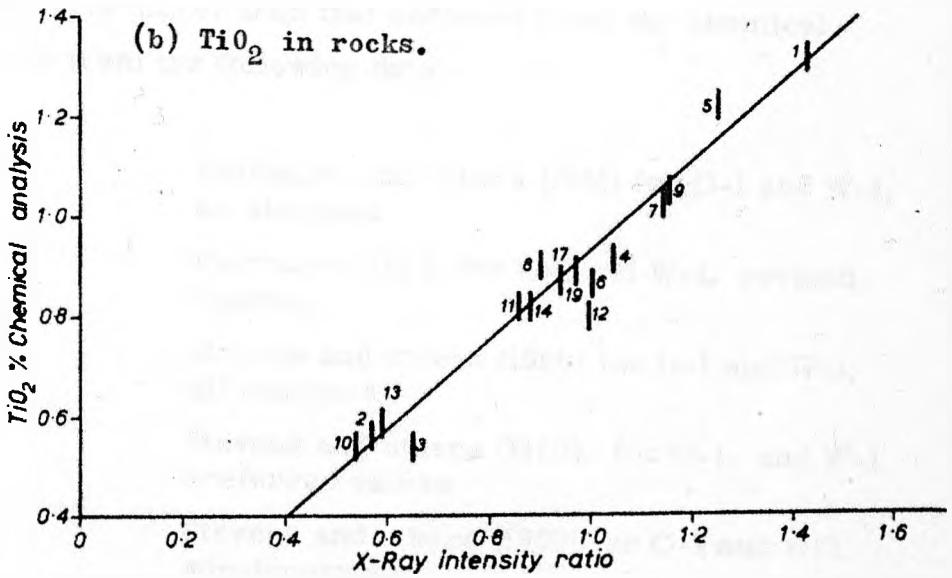
(b) TiO_2 in rocks.
TiO_2 % Chemical analysis
X-Ray intensity ratio
1·4
1·2
1·0
0·8
0·6
0·4
0
0·2
0·4
0·6
0·8
1·0
1·2
1·4
1·6

that there is no bias in X-ray spectrographic analysis.

Compared with other X-ray work, the present results are better than those of Hooper (1964) who quotes C = 11.4% of a mean of TiO_2 of 0.6% (in the present work C = 6.9% of a mean TiO_2 of 0.87%).

Volborth (1963) quotes a deviation ranging from +0.18 to -0.13 for a range of TiO_2 of 0.19 - 1.63% (discarding four analyses for having doubtful colorimetric error). The range of deviation in the present work is narrower than that of Volborth, being $\pm$ 0.10 at the most for a TiO_2 concentration of 0.54 - 1.32%.

(iii) Aluminium oxide

The instrumental settings for Al_2O_3 determination are shown in Table 2. The precision of the method is shown in Table 17.

The precision of the -300 mesh powder is higher than that of the 200 mesh. Out of 8 analyses, two specimens gave a relative deviation of about 1.5% whereas the other 6 specimens were less than 1% of the amount of Al_2O_3 present.

This precision is higher than that achieved from the chemical methods as shown from the following data:-

C = 3.21, 5.61	Fairbairn and others (1951) for G-1 and W-1, all analyses
C = 2.21, 3.3	Fairbairn (1952) for G-1 and W-1, revised figures.
C = 2.60, 4.16	Stevens and others (1960) for G-1 and W-1, all analyses
C = 1.19, 1.19	Stevens and others (1960), for G-1, and W-1, preferred values
C = 3.6, 2.5	Stevens and others (1960) for G-1 and W-1, spectrographic

C = 3.0 Mercy (1956), rapid chemical methods

Compared with other X-ray data, Volborth (1963) quotes C = 0.63, 0.82, and 0.23 for G-1, W-1, and a syenite rock respectively. The present data of precision are comparable to those of Volborth.

As to the accuracy of the method, Figure 5a shows the plots of X-ray intensity ratio versus the results of chemical analysis. Table 18 shows the deviations of the 16 rocks analysed to be within the range of $\pm$ 0.50% alumina. The sign and magnitude of these deviations bear no relation whatsoever to the amount of silica in the rocks, hence an enhancement effect is unlikely to be responsible for these deviations. Yet, the fact that both the (-200) and (-300) mesh powders gave identical results, and that the deviations show a symmetrical distribution regarding their positive and negative signs, exclude the possibility of any bias to be present in the X-ray analysis. Most of these deviations can be, therefore, due to errors in the chemical data.

(iv) Total iron as Fe_2O_3

The instrumental conditions for iron determination is shown in Table 2. The precision of the method is shown in Table 19.

As shown in this table, the reproducibility of the fine powder is greater than that of the coarse powder in spite of the still high-reproducibility of the latter. For -200 mesh powders, out of 8 analyses, the relative deviation of only one is 1.6%, three are between 1 - 0.5% and four have relative deviation less than 0.5% of the amount present. For -300 mesh, out of 11 analyses only one has a

TABLE 17

PRECISION OF X-RAY SPECTROGRAPHIC DETERMINATION OF Al_2O_3

Specimen	No. of Pellets	Al_2O_3% $\bar{X}$	s	C%	$S_{\bar{x}}$	E%*
Test No. 1. (-200 Mesh)						
3	3	15.34	0.076	0.50	0.044	0.29
4	3	19.37	0.101	0.52	0.058	0.30
5	3	19.47	0.255	1.31	0.147	0.76
6	3	18.31	0.101	0.55	0.058	0.32
11	3	19.24	0.201	1.04	0.116	0.60
13	5	16.72	0.166	0.99	0.074	0.44
Test No. 2. (-300 Mesh)						
3	3	15.17	0.090	0.59	0.052	0.34
4	3	19.29	0.158	0.82	0.091	0.47
5	3	19.41	0.140	0.72	0.081	0.42
5a	3	19.41	0.140	0.72	0.081	0.42
6	3	18.11	0.160	0.88	0.092	0.51
7	3	19.93	0.291	1.46	0.170	0.84
8	3	20.33	0.183	0.90	0.106	0.52
14	3	17.82	0.290	1.63	0.167	0.94

* For the meaning of these statistical terms, refer to Table 11, p. 44 .

TABLE 18

COMPARISON OF X-RAY SPECTROGRAPHIC DATA WITH THE CHEMICAL DATA FOR Al_2O_3

Specimen	Chemical Analysis	X-Ray Spectrographic Data			
		Test No. 1.		Test No. 2.	
		$\%Al_2O_3$	Deviation	$\%Al_2O_3$	Deviation
1	21.73	22.44	+0.71	22.21	+0.48
3	15.11	15.34	+0.23	15.17	+0.06
4	19.79	19.37	-0.42	19.29	-0.50
5	18.92	19.47	+0.55	19.41	+0.49
6	18.06	18.31	+0.25	18.11	+0.05
7	20.05	-	-	19.93	-0.12
8	19.85	-	-	20.33	+0.48
9	19.49	-	-	20.01	+0.52
11	19.49	19.24	-0.25	19.15	-0.34
12	17.05	17.05	0.00	17.05	0.00
13	16.52	16.72	+0.20	-	-
14	18.32	-	-	17.82	-0.50
19	18.99	-	-	19.12	+0.13
21	20.36	-	-	20.16	-0.20
23	18.93	-	-	18.97	+0.04
25	16.52	-	-	16.91	+0.39
		$n = 8$		$n = 15$	
		$s = 0.41$		$s = 0.36$	

relative deviation of about 1%, two are between 1 - 0.5% and eight have a relative deviation less than 0.5% of the amount present. The range of Fe_2O_3 concentration is 4 - 10%.

This precision is very high and superior to that of chemical methods as shown from the following figures:-

C = 13.76, 2.88	Fairbairn and others for G-1 and W-1, all analyses (1951)
C = 13.90, 2.49	Stevens and others (1960) for G-1 and W-1, all analyses
C = 2.5, 5.91	Stevens and others (1960) for G-1 and W-1, spectrographic
Average C = 2.1	Mercy (1956) - Colorimetric

Compared with other X-ray data, Volborth (1963) gives a 'C' range of 0.12 to 1.60.

The calibration graph for Fe_2O_3 determination is shown in Fig. 5b. Table 20 shows the results of the X-ray spectrographic analysis compared with those of the chemical analysis. Assuming that the chemical data are accurate and represent the arithmetic mean, the plus and minus deviations of X-ray from chemical results are shown in the same table.

Volborth (1963) quotes a deviation range of -1.55 to +0.88% Fe_2O_3 (excluding the data for iron-ground specimens). The range of deviation in the present work is much narrower than that of Volborth, being +0.25 to -0.54. It can, therefore, be concluded that both the accuracy and precision of the present work are better than those of Volborth (1963).

TABLE 19

PRECISION OF X-RAY SPECTROGRAPHIC DETERMINATION OF TOTAL IRON AS Fe_2O_3

Specimen	No. of Pellets	Fe_2O_3% $\bar{X}$	s	C%	$S_{\bar{x}}$	E%*
Test No. 1. (-200 Mesh)						
1	3	9.44	0.026	0.28	0.015	0.16
3	3	9.27	0.067	0.72	0.039	0.42
4	3	7.72	0.032	0.41	0.018	0.24
5	3	8.52	0.070	0.82	0.040	0.47
6	3	7.89	0.035	0.44	0.020	0.25
10	5	4.17	0.031	0.74	0.014	0.33
11	3	5.02	0.081	1.61	0.047	0.93
13	5	5.50	0.027	0.49	0.012	0.22
Test No. 2. (-300 Mesh)						
1	3	9.34	0.095	1.02	0.055	0.59
2	3	3.69	0.013	0.35	0.008	0.20
3	3	9.21	0.010	0.11	0.006	0.06
4	3	7.59	0.025	0.33	0.014	0.19
5	3	8.55	0.007	0.08	0.004	0.05
6	3	7.75	0.010	0.13	0.006	0.08
7	3	7.79	0.042	0.54	0.024	0.31
8	3	6.31	0.025	0.40	0.014	0.23
9	3	9.21	0.061	0.66	0.035	0.38
10	3	4.06	0.013	0.32	0.008	0.18
14	3	7.24	0.013	0.18	0.008	0.10

* For the meaning of these statistical terms, refer to Table 11, p. 44 .

TABLE 20

COMPARISON OF X-RAY SPECTROGRAPHIC DATA WITH THE CHEMICAL DATA OF Fe_2O_3

Specimen	Chemical Analysis	X-Ray Spectrographic Data			
		Test No. 1.		Test No. 2.	
		$\%Fe_2O_3$	Deviation	$\%Fe_2O_3$	Deviation
1	0.52	9.44	-0.08	9.34	-0.18
2	3.69	3.96	+0.27	3.94	+0.25
3	9.23	9.27	+0.04	9.21	-0.02
4	7.50	7.72	+0.22	7.59	+0.09
5	9.09	8.52	-0.57	8.55	-0.54
6	7.99	7.89	-0.10	7.75	-0.24
7	7.88	-	-	7.79	-0.09
8	6.37	-	-	6.31	-0.06
9	9.20	-	-	9.21	-0.01
10	3.81	4.17	+0.34	4.06	+0.25
11	4.93	5.02	+0.09	4.98	+0.05
12	9.99	9.99	0.00	9.99	0.00
13	6.01 (5.51-6.53)	5.50	-0.51	-	-
14	7.00	-	-	7.24	+0.24
15	8.12	-	-	8.25	+0.13
18	7.12	-	-	7.24	+0.12
19	8.00	-	-	7.93	-0.07
20	6.99	-	-	7.22	+0.23
21	9.44	-	-	9.19	-0.25
22	8.39	-	-	8.37	-0.02
		$n = 10$		$n = 19$	
		$s = 0.31$		$s = 0.20$	

Fig. 5

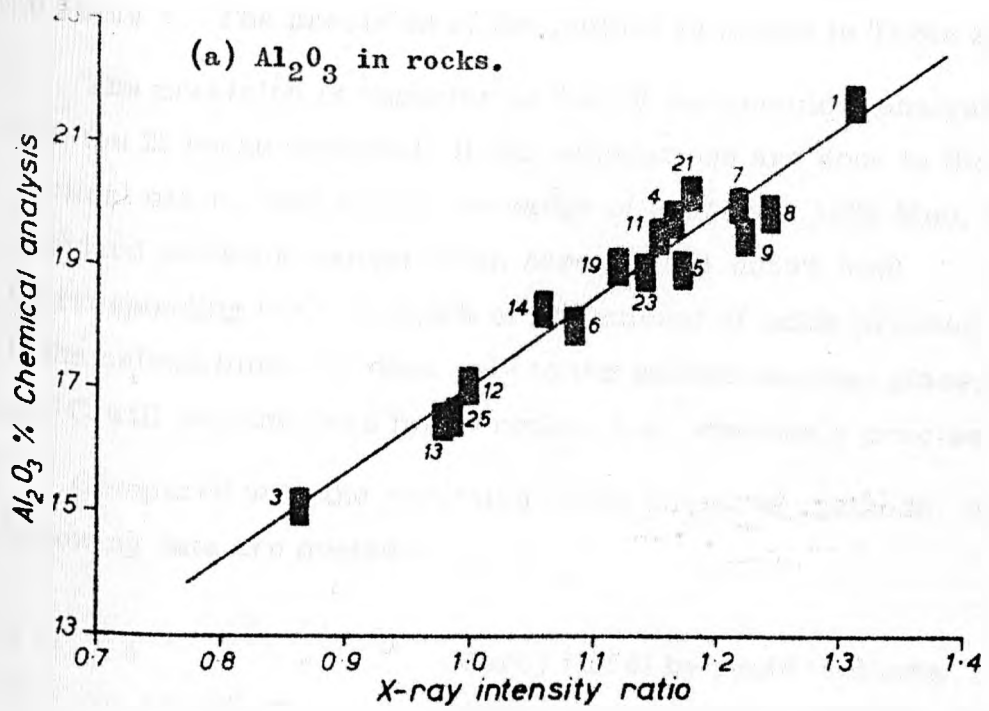
(a) Al_2O_3 in rocks.
Al_2O_3 % Chemical analysis
X-ray intensity ratio
13
15
17
19
21
0·7
0·8
0·9
1·0
1·1
1·2
1·3
1·4
1
21
7
4
8
11
9
19
5
23
14
6
12
25
13
3

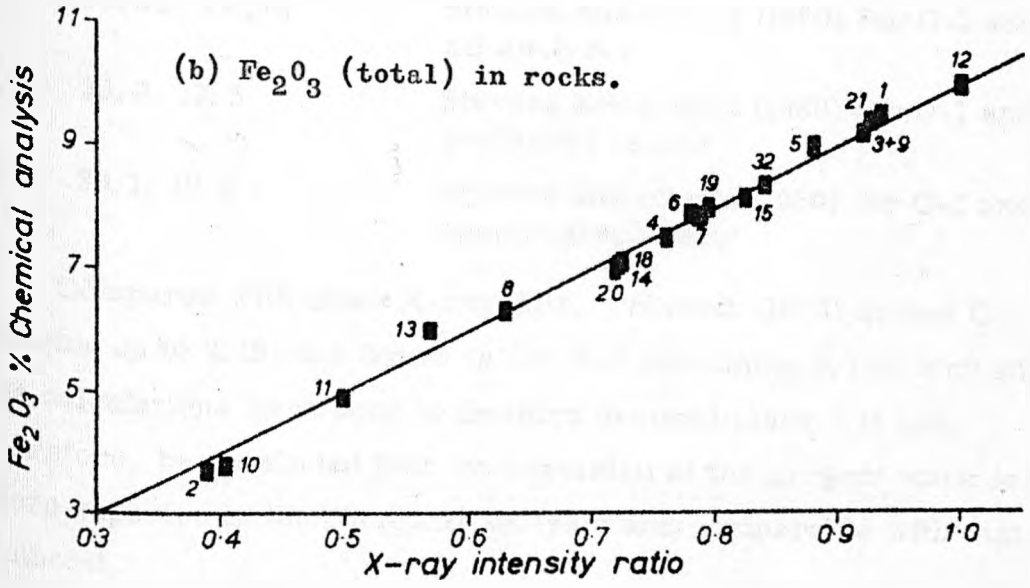
(b) Fe_2O_3 (total) in rocks.
Fe_2O_3 % Chemical analysis
X-ray intensity ratio
3
5
7
9
11
0·3
0·4
0·5
0·6
0·7
0·8
0·9
1·0
12
21
1
3+9
5
32
19
6
15
4
7
18
14
20
8
13
11
2
10

(v) Manganese as MnO

The instrumental conditions for MnO determination are listed in Table 2. The precision of the method is shown in Table 21.

The precision is superior to that of the chemical analysis. For the 21 rocks analysed, if the calculations are done to the third decimal place, then within the range of 0.046 - 0.191% MnO, the standard deviation ranges from zero up to 0.0050% MnO (corresponding to C = 2.61% of the amount of oxide present). Yet, if the calculations are done only to the second decimal place, S and C will become zero for 19 rocks, i.e. absolutely precise.

Compared with the precision of the chemical methods, the following data are quoted:-

C = 7.4	Mercy (1956) by rapid methods
C = 36.33, 40.77	Fairbairn and others (1951) for G-1 and W-1
C = 33.62, 32.33	Stevens and others (1960) for G-1 and W-1, all analyses
C = 20.0, 12.5	Stevens and others (1960) for G-1 and W-1, preferred values
C = 33.1, 10.9	Stevens and others (1960) for G-1 and W-1, spectrographically

Compared with other X-ray data, Volborth (1963) quotes C ranging up to 2.15, the figure is for W-1 containing 0.18% MnO and the calculations were done to the third decimal place. It can, therefore, be concluded that the precision of the present work is far more superior to the chemical analysis and comparable with that of Volborth.

TABLE 21

Precision of X-Ray Spectrographic Determination of Mn0

Specimen	No. of Pellets	Mn0% $\bar{X}$	s	C%	$S_{\bar{x}}$	E%*
Test No. 1. (-200 Mesh)						
1	3	0.147	0.0023	1.56	0.0013	0.90
4	3	0.088	0.0015	1.70	0.0008	0.98
5	3	0.122	0.0031	2.54	0.0018	1.46
6	3	0.093	0.0015	1.61	0.0008	0.93
10	3	0.077	0.0010	1.30	0.0006	0.75
11	3	0.115	0.0015	1.31	0.0008	0.75
13	3	0.114	0.0010	0.88	0.0006	0.51
Test No. 2. (-300 Mesh)						
1	3	0.148	0.0036	2.43	0.0021	1.40
3	3	0.191	0.0050	2.61	0.0029	1.50
4	3	0.094	0.0010	1.06	0.0006	0.61
5	3	0.120	0.0010	0.83	0.0006	0.48
5a	3	0.118	0.0017	1.44	0.0010	0.83
6	3	0.103	0.0034	3.30	0.0019	1.90
7	3	0.094	0.0000	0.00	0.0000	0.00
8	3	0.046	0.0010	2.17	0.0006	1.25
9	3	0.087	0.0031	3.56	0.0018	2.05
10	3	0.077	0.0015	1.95	0.0008	1.12
17	3	0.091	0.0015	1.64	0.0008	0.94
21	3	0.057	0.0000	0.00	0.0000	0.00
23	3	0.108	0.0010	0.92	0.0006	0.53
25	3	0.091	0.0000	0.00	0.0000	0.00

* For the meaning of these statistical terms, refer to Table 11. p. 44.

TABLE 22

Comparison of X-Ray Spectrographic Analysis with the Chemical Data of MnO

Specimen	Chemical Analysis	X-Ray Spectrographic Data Test No. 1. % MnO	Deviation	Test No. 2. % MnO	Deviation
1	0.14	0.15	+0.01	0.15	+0.01
2	0.05	0.07	+0.02	0.07	+0.02
3	0.19	0.19	0.00	0.19	0.00
4	0.09	0.09	0.00	0.09	0.00
5	0.13	0.12	-0.01	0.12	-0.01
5a	0.13	-	-	0.12	-0.01
6	0.10	0.09	-0.01	0.10	0.00
7	0.10	-	-	0.09	-0.01
8	0.05	-	-	0.05	0.00
9	0.08	-	-	0.09	+0.01
10	0.08	0.08	0.00	0.08	0.00
11	0.12	0.12	0.00	0.12	0.00
12	0.07	0.08	+0.01	0.08	+0.01
13	0.11	0.11	0.00	-	-
17	0.09	-	-	0.09	0.00
21	0.05	-	-	0.05	0.00
23	0.11	-	-	0.11	0.00
25	0.08	-	-	0.09	+0.01
		n = 10		n = 17	
		s = 0.009		s = 0.008	

Regarding the accuracy of the method, with the known poor precision of MnO chemical determination as well as its poor accuracy (C = 20% always negative error - Mercy, 1956), the least square method proved to be of great value for such situation. Using the X-ray intensity ratio and the data of chemical analysis, the equation of Mn calibration graph is:-

$$MnO\% = (0.0628 \times \text{Intensity Ratio}) + 0.0192$$

The calibration graph is shown in Figure 6a.

Calculated on this basis, the X-ray data are shown alongside the chemical analysis in Table 22.

From the 23 rocks analysed, 12 rocks including the tonalite standard T-1, showed no deviation from the chemical analysis, whereas the other 11 rocks showed deviations range +0.02 to -0.01% MnO. This symmetrical distribution of positive and negative deviations suggests that there is no bias in the X-ray spectrographic analysis and that the deviations are probably due to errors in the chemical data.

The accuracy of the present work is superior to that shown by Volborth (1963) who quotes a deviation range of +0.042 to -0.026% MnO for a concentration range of 0.04 - 0.18% MnO.

(vi) Calcium oxide

The instrumental setting for the determination of CaO is shown in Table 2. The precision of the method is shown in Table 23.

The precision of the X-ray determination of CaO is very high and for the range of concentration investigated it seems to be independent

of the amount of CaO present. For a concentration as low as 0.16% CaO the standard deviation is 0.0027 corresponding to a relative deviation of 1.69% of the amount of calcium present. For concentrations higher than this, the relative deviation hardly exceeds 1% of the CaO present. These figures of precision are superior to those of the chemical methods as shown from the following data:-

C = 0.88	Mercy (1956) by rapid methods
C = 9.66, 10.96	Fairbairn and others 1951 for G-1 and W-1 containing 1.40 and 10.96% CaO respectively, all analyses
C = 8.95, 1.46	Stevens and others 1960 for G-1 and W-1, all the 60 analyses
C = 5.05, 0.74	Stevens and others 1960 for G-1 and W-1, preferred values
C = 13.0, 6.3	Stevens and others 1960, spectrographic

Compared with other X-ray data, Volborth (1963) quotes a relative deviation range of 0.34 - 0.15 for a range of concentration of 1.46 - 10.94; four rocks being analysed.

Regarding the accuracy of the method, the equation of the calcium calibration curve (Fig. 6b) calculated by the least square method is:

CaO% = (1.0635 x Intensity Ratio) - 0.2022

Table 24 shows the X-ray spectrographic data alongside with the chemical data. The minus and plus deviations of the X-ray from those of the chemical analyses are shown in the same table.

Chemically, calcium and magnesium oxides were determined according to the method described by Riley (1958). They are

"determined on solution B by titration with ethylenediaminetetra-acetic acid after removal of interfering elements, except manganese, by extraction of their oxidates at pH 4.9 - 5.1 with chloroform in a continuous extractor." Both calcium and magnesium oxides are determined on this extracted solution by using E. B. T. as indicator whereas CaO alone is determined using calcon as indicator. By simple calculation, Mg oxide can be then determined. Titration is done using photoelectric titrator.

The titration for Ca proved to be always laborious and difficult to determine the end point precisely. The sort of precision obtained is demonstrated from the carefully analysed GL10 (Table 10). The separate triplicate determinations gave CaO% = 0.66, 0.92, and 0.72 (S = 0.12% CaO and C = 15.6% of the amount present).

With such a low precision, the deviation of the X-ray data from the chemical analysis is decidedly mostly due to a chemical error rather than inaccurate X-ray determination.

As to the deviation noticed in the standard Tonalite T-1, it is interesting to note that from the results of analysis of this rock, the greater than 5% CaO is only given by conventional method. But when done with the rapid chemical method, the results by different analysts were as follows: 4.86 (average of 6), 4.9, 4.90 (average of 6). Only one analyst gave a result of more than 5% by rapid method. It seems that CaO% determined by conventional method is higher than that determined by rapid chemical method. Since the calculation of X-ray determination in the present work is based on specimens chemically analysed by rapid method, the deviation of 0.46% CaO in standard T-1 will decrease considerably if the present X-ray

TABLE 23

Precision of X-Ray Spectrographic Determination of CaO

Specimen	No. of Pellets	CaO% $\bar{X}$	s	C%	$S_{\bar{x}}$	E%*
Test No. 1. (-200 Mesh)						
1	3	0.44	0.0046	1.04	0.0027	0.60
2	3	0.39	0.0042	1.08	0.0025	0.62
3	3	0.68	0.0042	0.62	0.0024	0.36
4	3	0.60	0.0055	0.92	0.0032	0.53
5	3	0.16	0.0027	1.69	0.0016	0.98
6	3	1.17	0.0070	0.60	0.0040	0.35
10	5	0.78	0.0027	0.35	0.0012	0.16
11	3	3.31	0.0251	0.76	0.0145	0.44
13	5	4.85	0.0151	0.31	0.0068	0.14
Test No. 2. (-300 Mesh)						
1	3	0.46	0.0047	1.02	0.0027	0.59
2	3	0.40	0.0023	0.57	0.0013	0.33
3	3	0.71	0.0036	0.51	0.0021	0.29
4	3	0.63	0.0036	0.57	0.0021	0.33
5	3	0.17	0.0036	2.12	0.0021	1.22
5a	3	0.17	0.0034	2.00	0.0020	1.15
6	3	1.18	0.0059	0.50	0.0034	0.29
7	3	2.03	0.0046	0.23	0.0027	0.13
8	3	0.34	0.0015	0.44	0.0009	0.25
9	3	0.86	0.0080	0.93	0.0046	0.54
10	3	0.80	0.0053	0.66	0.0031	0.38
14	3	0.44	0.0021	0.48	0.0012	0.28
17	3	1.22	0.0029	0.24	0.0017	0.14

* For the meaning of these statistical terms, refer to Table II, p. 44.

TABLE 24

Comparison of X-Ray Spectrographic Data with Chemical Data for CaO

Specimen	Chemical Analysis	X-Ray Spectrographic Data					
		Test No. 1.			Test No. 2.		
		One-pt. calibr.	Least square	Deviation	One-pt. calibr.	Least square	Deviation
1	0.28	0.46	0.44	+0.16	0.48	0.46	+0.18
2	0.64	0.42	0.39	-0.25	0.44	0.40	-0.24
3	0.75	0.64	0.68	-0.07	0.66	0.71	-0.04
4	0.39	0.58	0.60	+0.21	0.60	0.63	+0.24
5	0.21	0.14	0.16	-0.05	0.15	0.17	-0.04
5a	0.21	-	-	-	0.15	0.17	-0.04
6	0.91	0.99	1.17	+0.26	1.01	1.18	+0.27
7	1.91	-	-	-	1.62	2.03	+0.12
8	0.36	-	-	-	0.39	0.34	-0.02
9	1.02	-	-	-	0.77	0.86	-0.16
10	0.70	0.71	0.78	+0.08	0.73	0.80	+0.10
11	3.17	2.54	3.31	+0.14	2.58	3.36	+0.19
11a	3.17	-	-	-	2.44	3.17	0.00
12	0.77		0.86	+0.09		0.86	+0.09
13	5.19	3.57	4.85	-0.34	-	-	-
14	0.63	-	-	-	0.46	0.44	-0.19
17	1.10	-	-	-	1.03	1.22	+0.12
19	1.47	-	-	-	1.13	1.37	-0.10
21	0.58	-	-	-	0.57	0.58	0.00
			n = 10 s = 0.20			n = 18 s = 0.15	

Fig. 6

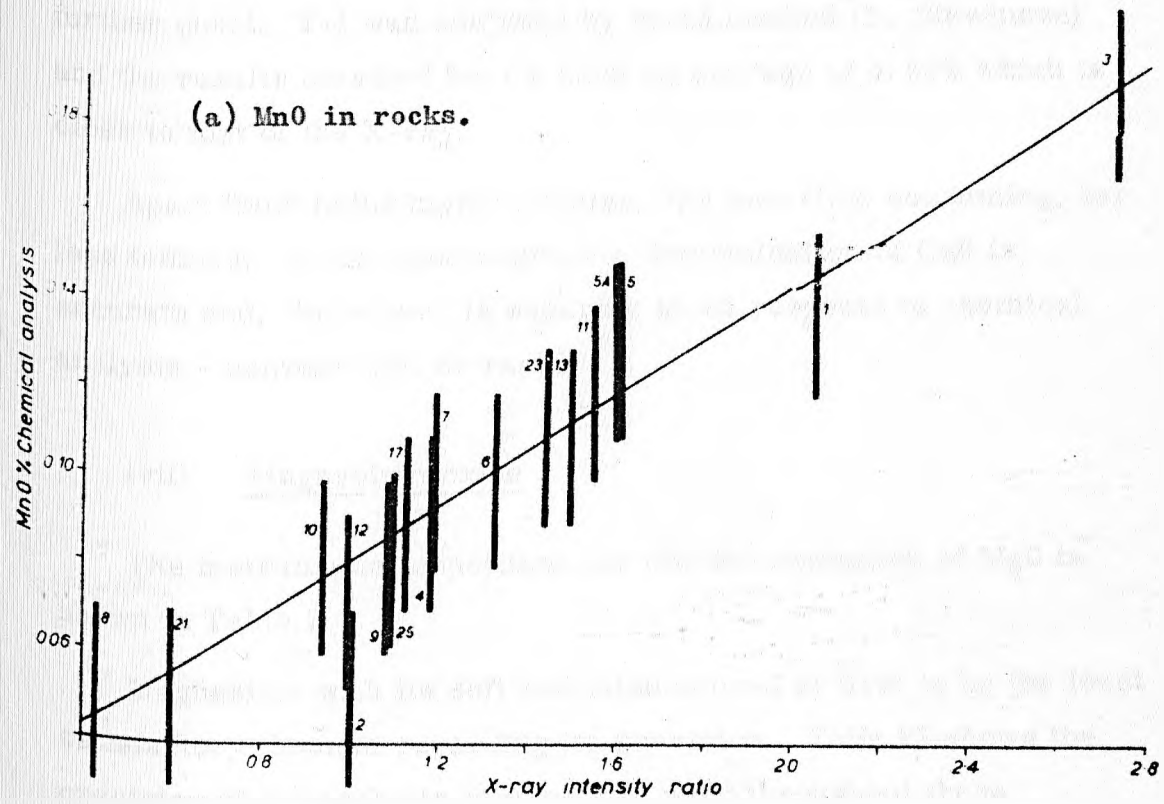
(a) MnO in rocks.
MnO % Chemical analysis
X-ray intensity ratio
0·08
1·2
1·6
2·0
2·4
2·8
0·06
0·10
3
5A
5
1
11
23
13
7
17
6
10
12
4
9
25
8
21
2

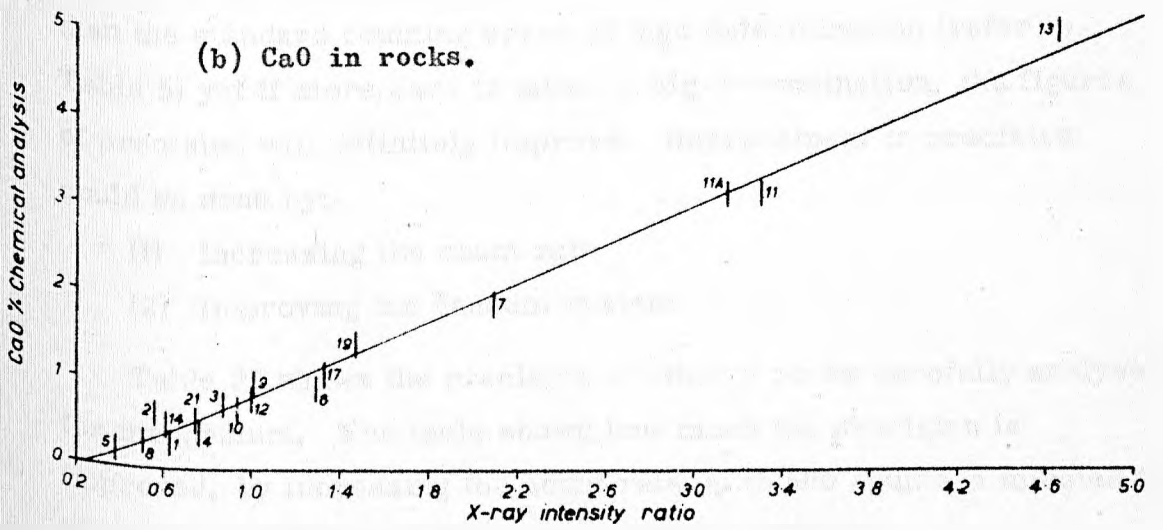
(b) CaO in rocks.
CaO % Chemical analysis
X-ray intensity ratio
0·2
0·6
1·0
1·4
1·8
2·2
2·6
3·0
3·4
3·8
4·2
4·6
5·0
0
1
2
3
4
5
13
11A
11
7
19
17
16
9
12
10
21
3
14
2
5
8
1
4

result is compared to those of rapid chemical method alone. As a further check, T-1 was analysed by rapid method (B. Stevenson) and the results obtained for Ca have an average of 4.86% which is close to that of the X-ray.

Apart from being highly precise, far less time consuming, far less tedious; X-ray spectrographic determination of CaO is accurate and, therefore, is superior in all respects to chemical analysis - conventional or rapid.

(vii) Magnesium oxide

The instrumental conditions for the determination of MgO is shown in Table 2.

Magnesium with its soft radiation proved at first to be the least satisfactory element regarding its precision. Table 25 shows the precision of the analysis of the rocks used throughout these preparatory stages of X-ray fluorescence analysis. Although the figures of deviations shown in Table 25 are comparable to or less than the standard counting error of MgO determination (refer to Table 5) yet if more care is taken in Mg determination, the figures of precision will definitely improve. Improvement in precision could be done by:-

(1) Increasing the count rate

(2) Improving the vacuum system

Table 26 shows the precision of other 9 rocks carefully analysed for magnesium. The table shows how much the precision is improved, by increasing the count rate up to 500 counts/5 minutes for 1% MgO, providing that the vacuum used is efficient.

TABLE 25

Precision of X-Ray Spectrographic Determination of MgO

Specimen	No. of Pellets	MgO% $\bar{X}$	s	C%	$S_{\bar{x}}$	E%*
Test No. 1. (-200 Mesh)						
1	3	2.41	0.18	7.47	0.10	4.31
2	3	1.46	0.08	5.48	0.04	3.16
3	3	2.34	0.14	5.98	0.08	3.45
4	3	2.79	0.30	10.75	0.17	6.21
5	3	3.51	0.41	11.68	0.24	6.83
6	3	1.38	0.07	5.07	0.04	2.93
10	5	1.39	0.17	12.23	0.08	5.47
13	5	2.10	0.26	12.09	0.11	5.50
Test No. 2. (-300 Mesh)						
1	3	2.61	0.22	8.43	0.13	4.87
3	3	1.97	0.10	5.08	0.06	2.93
5	3	3.25	0.27	8.31	0.15	4.80
5a	3	2.85	0.18	6.31	0.10	3.64
6	3	1.26	0.17	13.49	0.10	7.79
7	3	1.56	0.19	12.18	0.11	7.03
9	3	1.66	0.15	9.04	0.09	5.22
14	3	3.39	0.20	5.90	0.11	3.41
17	3	1.96	0.08	4.08	0.05	2.35

* For the meaning of these statistical terms, refer to Table 11, p. 44 .

TABLE 26

Precision of X-Ray Spectrographic Determination of MgO

Specimen	No. of Pellets	MgO% $\bar{X}$	s	C%	$S_{\bar{x}}$	E%*
19	3	1.83	0.06	3.28	0.03	1.89
21	3	1.77	0.02	1.13	0.01	0.65
23	3	2.93	0.06	2.04	0.03	1.17
24	3	2.86	0.12	4.19	0.07	2.42
26	3	2.66	0.08	3.01	0.04	1.74
27	3	1.37	0.09	6.57	0.05	3.79
28	3	1.78	0.02	1.46	0.01	0.84
29	3	5.25	0.10	1.90	0.06	1.09
30	3	2.31	0.07	3.03	0.04	1.75

* For the meaning of these statistical terms, refer to Table 11 , p. 44 .

This precision is almost better than that of the conventional chemical methods as shown from the following data.

C = 35.32, 72.6	Fairbairn and others (1951) for G-1 and W-1 containing 0.39 and 6.53% MgO respectively. All analyses.
C = 32.15, 5.29	Stevens and others (1960) for G-1 and W-1, all 60 analyses.
C = 14.6 1.51	Stevens and others (1960) for G-1 and W-1, preferred values.
C = 6.6, 3.0	Stevens and others (1960) for G-1 and W-1, spectrographic determination.

Compared to other X-ray analysis, the present data are not better than those of Volborth (1963) who used the specially designed Al-target X-ray tube developed by Professor Burton L. Henke and also increased the count rate to collect 64,000 counts.

Regarding the accuracy of the method, Fig. 7a shows the calibration graph and Table 27 shows the results of the X-ray analysis compared with those of chemical analysis. The -300 mesh powder proved to be more accurate than the -200 mesh. Hence the results of the -300 mesh powder are the ones to be considered in the following discussions.

The fact that the deviations show a symmetrical distribution regarding their positive and negative signs, suggests the absence of any bias in the X-ray determination of Mg. For the 25 rocks analysed (Test No. 2. Table 27), the frequency of deviation is as follows:-

For a deviation of $\pm$ 0.45 - 0.40% MgO : four rocks
$\pm$ 0.39 - 0.30% MgO : three rocks
$\pm$ 0.29 - 0.20% MgO : six rocks
$\pm$ 0.19 - 0.10% MgO : four rocks
less than $\pm$ 0.10% : eight rocks

However, most of this error is believed to be in the chemical determination because the very likely present error in the chemical determination of calcium will affect the accuracy of the chemical analysis of magnesium due to their interdependence. In fact, it is more than just a coincidence that the large positive or negative deviations in Mg corresponds to a deviation in Ca with the opposite sign.

As to the tonalite standard T-1, the X-ray result of the -200 mesh was higher than the preferred chemical value by 0.21% MgO. However, two interesting points arise:-

1. The more accurate -300 mesh powder always showed lower results than the -200 mesh (Table 27). Consequently, this +0.21% MgO deviation will be significantly reduced, have a -300 mesh powder for tonalite been used.
2. The analysis of tonalite by the rapid method in our laboratories (Stevens) gave a result of 2.11% MgO which is very close to the X-ray result of 2.10%.

Therefore, it can be concluded that the X-ray fluorescence analysis of Mg is as precise and accurate, if not better, as the chemical analysis. In terms of speed and labour involved, the chemical methods (conventional or rapid) do not stand a chance in comparison with fluorescence method. Moreover, a pre-knowledge of the amount of Ca is not a necessary requisite for the determination of Mg by X-ray spectroscopy, the reverse holds for the chemical methods.

Finally, although the present data of precision are not as good as those of Volborth (1963), yet the present accuracy is better than his. Volborth (1963) quotes a deviation range of +1.07 (for MgO concentration of 3.01%) to -0.21 (for 4.42% MgO). For his dedrifted results (less accurate as stated by Volborth) the deviation range is +2.01 to -0.86%

TABLE 27

Comparison of X-Ray Spectrographic Analysis with the Chemical Data for MgO

Specimen	Chemical Analysis	X-Ray Spectrographic Analysis			
		Test No. 1.		Test No. 2.	
		% MgO	Deviation	% MgO	Deviation
1	3.02	2.41	-0.61	2.61	-0.41
2	1.20	1.46	+0.26	1.52	+0.32
3	2.26	2.34	+0.08	1.97	-0.29
4	2.90	2.79	-0.11	2.82	-0.08
5	3.07	3.51	+0.44	3.25	+0.18
5a	3.07	-	-	2.85	-0.12
6	1.61	1.38	-0.23	1.26	-0.35
7	1.83	-	-	1.56	-0.27
8	1.39	-	-	1.50	+0.11
9	1.74	-	-	1.66	-0.08
10	1.35	1.39	+0.04	1.56	+0.21
11	1.44	1.77	+0.33	1.41	-0.03
12	1.90	1.90	0.00	1.90	0.00
13	1.89	2.10	+0.21	-	-
14	2.94	-	-	3.39	+0.45
17	1.81	-	-	1.96	+0.15
19	1.89	-	-	1.83	-0.06
21	1.69	-	-	1.77	+0.08
23	3.15	-	-	2.93	-0.22
24	2.89	-	-	2.86	+0.03
25	3.05	-	-	2.82	-0.23
26	2.75	-	-	2.66	-0.09
27	1.80	-	-	1.37	-0.43
28	2.19	-	-	1.78	-0.41
29	4.91	-	-	5.25	+0.34
30	2.10	-	-	2.31	+0.21
		n = 10		n = 25	
		s = 0.31		s = 0.25	

MgO. In the present work, the highest deviation is +0.45% MgO; the same rock has a Ca deviation of -0.17%, which suggest that most of the error is due to an error in the chemical results.

(viii) Potassium oxide

The instrumental setting for K_2O determination are listed in Table 2. The precision of the method is shown in Table 28.

Apart from the fantastic speed of K_2O determination by X-ray (five minutes for 3 pellets of one specimen) the precision is very high and for the range of K_2O% investigated (1.23 - 5.35), standard deviation does not vary with concentration. The highest deviation is 0.071% K_2O (corresponding to 1.27% of the amount of oxide present -5.60%) whereas the highest relative deviation was 1.77% of the amount present - 1.64% K_2O (corresponding to S = 0.029% K_2O).

This precision is superior to that of the chemical and spectrographic methods as shown from the following quoted figures:

C = 3.0	Mercy (1956), rapid method
C = 8.41, 24.61	Fairbairn and others (1951) for G-1 and W-1, all analyses
C = 7.26 19.00	Stevens and others (1960) for G-1 and W-1, all analyses
C = 2.74 and 4.68	Stevens and others (1960) for G-1 and W-1, preferred values
C = 11.7	Stevens and others (1960), for G-1 spectrographic

Compared with other X-ray data, the present results are comparable to those of Volborth (1963), who gives C range of 0.6 - 1.6.

As to the accuracy of the method, the equation for calculating K_2O% by the least square method was derived from the X-ray intensity

ratio and the results of the chemical analysis. The calibration graph is shown in Fig. 7b and the equation of the graph is

$$K_2O\% = (3.0612 \times \text{Intensity Ratio}) - 0.0342$$

from which the intercept on the y-axis is -0.0342% K_2O. As to the negative sign of the intercept, although its amount (0.03%) can be neglected on account of being small, yet Volborth (1963) has a similar negative intercept amounting to 0.25% K_2O on his potassium calibration curve.

Calculated by this equation, the results of X-ray analysis in comparison with chemical analysis are shown in Table 29. Assuming that the chemical data are accurate and represent the arithmetic mean, the plus or minus deviations from the chemical data are shown in the same table.

The range of deviation is 0.42 to +0.35 with a standard deviation of 0.20 over a range of 1.23 - 5.35% K_2O concentration. Only three analyses out of the 24 done, showed such high deviation. The fact that such relatively high deviation is consistent in both the 200 and 300 mesh powders suggests an error in the chemical analysis rather than inaccurate X-ray data due to the effect of grain size on K_2O intensity.

The present results compare very well with Volborth (1963) who quotes a similar range of deviation from +0.43 to -0.35 over a range of 1.47 - 5.43% K_2O. It is agreed with Volborth that such symmetrical distribution of points on either side of the calibration curve may indicate an error in the chemical analysis rather than inaccurate X-ray data. It is also agreed that with such a range of deviation, the X-ray data can be considered at least as accurate as the chemical methods.

TABLE 28

Precision of X-Ray Spectrographic Determination of K_2O

Specimen	No. of Pellets	$K_2O\%$ $\bar{X}$	s	C%	$S\bar{x}$	E%*
Test No. 1. (-200 Mesh)						
1	3	3.23	0.038	1.70	0.022	0.98
2	3	2.73	0.060	2.20	0.035	1.27
3	3	1.64	0.029	1.77	0.017	1.02
4	3	3.80	0.025	0.66	0.014	0.38
5	3	5.44	0.051	0.94	0.029	0.54
6	3	3.32	0.007	0.21	0.004	0.12
10	5	2.60	0.013	0.50	0.006	0.22
11	3	1.48	0.021	1.42	0.012	0.82
13	5	1.18	0.010	0.85	0.004	0.38
Test No. 2. (-300 Mesh)						
1	3	3.22	0.020	0.62	0.012	0.36
2	3	2.62	0.029	1.11	0.017	0.64
3	3	1.57	0.023	1.46	0.013	0.84
4	3	3.75	0.021	0.56	0.012	0.32
5	3	5.38	0.016	0.30	0.009	0.17
5a	3	5.24	0.071	1.35	0.041	0.78
6	3	3.27	0.040	1.22	0.024	0.70
7	3	3.78	0.020	0.53	0.012	0.30
8	3	4.52	0.032	0.71	0.018	0.41
9	3	4.04	0.010	0.25	0.006	0.14
10	3	2.54	0.030	1.18	0.017	0.68
12	3	3.52	0.050	1.42	0.029	0.82
14	3	3.05	0.026	0.85	0.015	0.49

* For the meaning of these statistical terms, refer to Table 11, p. 44.

TABLE 29

Comparison of X-Ray Spectrographic Data with Chemical Data for K_2O

Specimen	Chemical Analysis	X-Ray Spectrographic Data					
		Test No. 1.			Test No. 2.		
		One-pt. calibr.	Least square	Deviation	One-pt. calibr.	Least square	Deviation
1	2.87	3.47	3.23	+0.36	3.46	3.22	+0.35
2	2.35	2.97	2.73	+0.38	2.82	2.62	+0.27
3	1.68	1.80	1.64	-0.04	1.70	1.57	-0.11
4	3.88	4.09	3.80	-0.08	4.02	3.75	-0.13
5	5.35	5.82	5.44	+0.09	5.75	5.38	+0.03
5a	5.35	-	-	-	5.60	5.24	-0.11
6	3.32	3.56	3.32	0.00	3.51	3.27	-0.05
7	4.00	-	-	-	4.05	3.78	-0.22
8	4.52	-	-	-	4.84	4.52	0.00
9	4.46	-	-	-	4.33	4.04	-0.42
10	2.42	2.80	2.60	+0.18	2.74	2.54	+0.12
11	1.64	1.61	1.48	-0.16	1.61	1.48	-0.16
12	3.25	-	-	-	3.25	3.03	-0.22
13	1.23	1.29	1.18	-0.05	-	-	-
14	3.04	-	-	-	3.28	3.05	+0.01
17	3.70	-	-	-	3.78	3.52	-0.18
			n = 9			n = 15	
			s = 0.21			s = 0.20	

Fig. 7

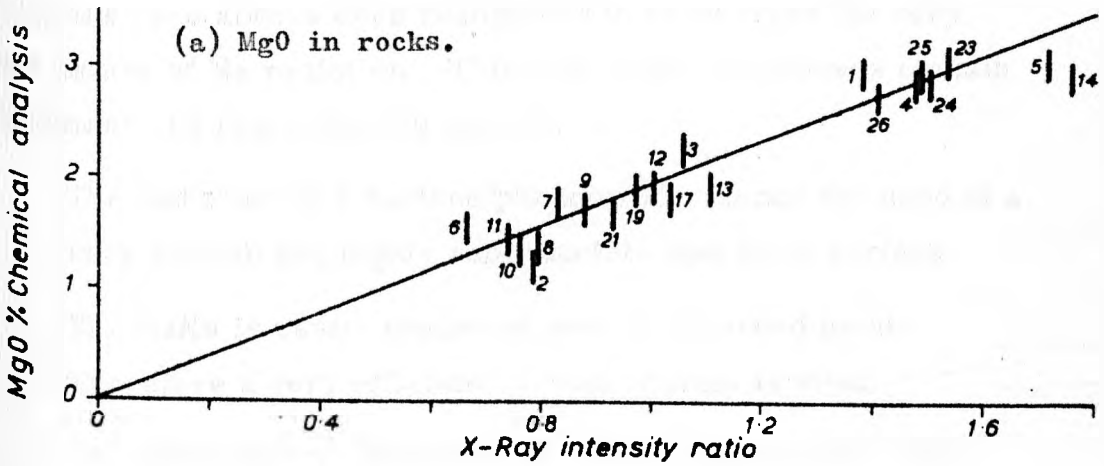
(a) MgO in rocks.
MgO % Chemical analysis
X-Ray intensity ratio
0
0·4
0·8
1·2
1·6
1
2
3
25
23
5
14
26
4
24
12
3
9
7
13
17
19
6
11
21
10
8
2

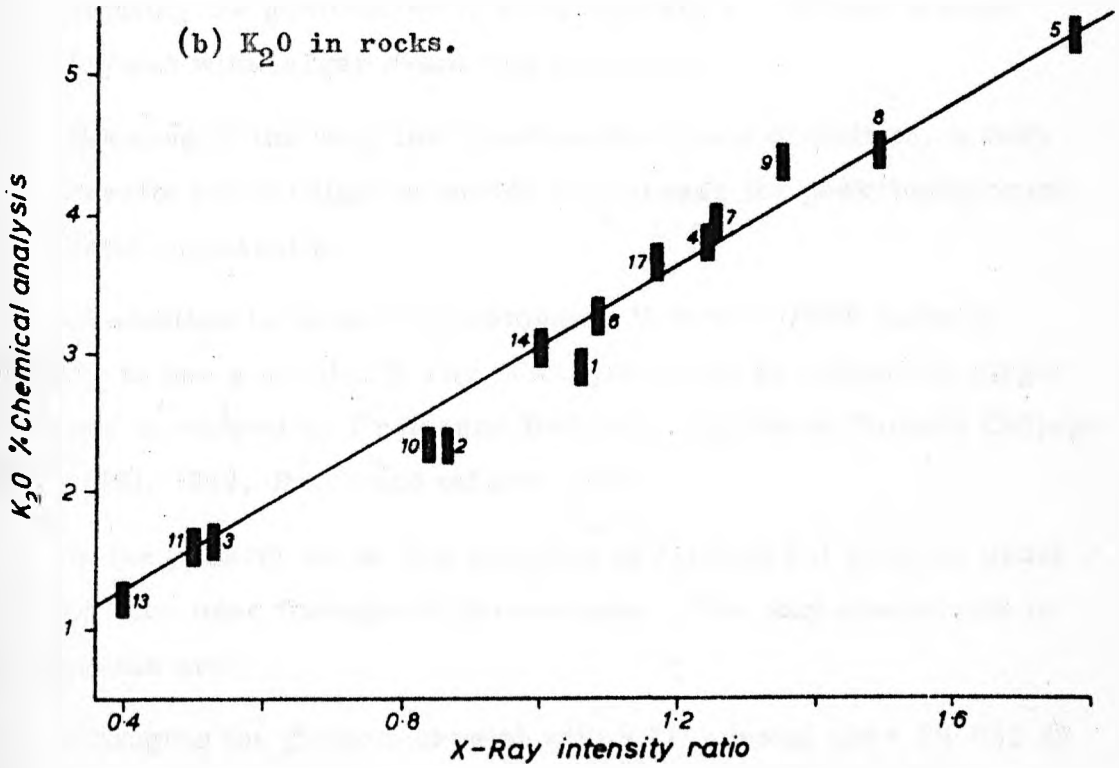
(b) K_2O in rocks.
K_2O % Chemical analysis
X-Ray intensity ratio
0·4
0·8
1·2
1·6
1
2
3
4
5
5
8
9
7
4
17
6
14
1
10
2
11
3
13

(ix) Sodium oxide

In the X-ray spectrographic analysis of sodium, certain difficulties have always been recognised to arise from the very "soft" nature of Na radiation. This last property imposes certain restrictions and requirements namely:-

1. The radiation is a surface phenomenon, hence the need of a very smooth and highly reproducible specimen surface.

2. The NaKa is easily scattered and/or absorbed by air. Therefore a very efficient vacuum system is vital.

3. The wavelength of NaKa is 11.9090 A. This means that if gypsum crystal (2d = 15.198 A) is used then the goniometer should be turned to 103.09° to satisfy the Bragg equation. The geometry of the Siemens apparatus used does not allow rotating the goniometer to such high angle. Hence, another crystal with larger d-spacing is needed.

4. Because of the very low fluorescence yield of sodium, a very careful pulse height selection to increase the peak/background ratio is essential.

In addition to these requirements, Volborth (1963) found it necessary to use a special X-ray tube namely the prototype Al-target X-ray tube developed by Professor Burton L. Henke at Pomana College (Henke, 1961, 1962, Baird and others, 1962).

In the present work, the analysis is carried out with the usual Cr-target tube used throughout the analysis. The only alterations in the apparatus are:-

1. Changing the gypsum crystal with KAP crystal (2d = 26.632 A)

to compensate for the restricted rotational angle of the goniometer (the highest angle is about 84^{o} in Siemens).

2. Changing the beryllium window of the gas flow proportional counter with the still thinner polycarbonate film (2 microns thick). This minimises the absorption of the characteristic Na radiation.

The instrumental conditions are listed in Table 2. The precision of the method is shown in Table 30. Counts were collected over a period of 5 minutes for either the peak and the background. Notice the relative low sodium concentration in the rocks under consideration.

From Table 30, the relative deviation range is 0.73 - 5.77% for a range of 0.93 - 3.61% Na_2O.

Compared with chemical analysis, the following are the figures of precision for Na_2O determination:

C = 1.8	Mercy (1956) by rapid analysis
C = 7.99, 10.20	Fairbairn and others (1951) for G-1 and W-1 respectively, all analysis
C = 7.06, 9.76	Stevens and others (1960) for G-1 and W-1, all analysis
C = 3.3, 5.3	Stevens and others (1960) for G-1 and W-1, preferred values
C = 8.6, 4.3	Stevens and others (1960) for G-1 and W-1, spectrographic determination

Compared with other X-ray work, Volborth (1963) quotes C = 0.13, 0.55, 0.10 for Na_2O concentrations of 10.73, 10.75, and 4.11 respectively.

The present data of precision is better than those of the chemical analysis but lower than those of Volborth. Precision of rocks containing

Na_2O as high as 10% was not tried. Yet, taking in consideration the facts that (a) no sophisticated alterations are made to the equipment, (b) the low concentration of sodium in the rocks under consideration, and (c) the relatively short time interval used in collecting the counts, then, these figures of precision are adequately good.

As to the standardisation of the method, the calibration graph is shown in Fig. 8a. Calculated by the least square method, the equation of the graph is:- $Na_2O\%$ = 1.68 X-ray intensity ratio + 0.19.

On this basis, the X-ray results, the chemical analysis and the deviations between the two are shown in Table 31.

For the 13 rocks analysed, the deviation range is +0.22 to -0.23% Na_2O; only 4 rocks show high deviations of 0.23 to 0.17%, the rest have deviations less than 0.10%. This range of deviation is much narrower than that of Volborth who quotes a deviation of +0.37 to -0.42.

Therefore, the X-ray spectrographic determination of sodium can be considered adequate even when using the usual sealed Cr-target X-ray tube.

(x) Phosphorus oxide

The instrumental setting for P_2O_5 determination is shown in Table 2. The precision of this determination is shown in Table 32.

For such a light element present in very low concentration, the precision proved to be excellent although the time taken for accumulating the X-ray counts was relatively short (5 minutes per pellet). For 22 analyses done, the highest deviation was 0.007 for

TABLE 30

Precision of X-Ray Spectrographic Determination of Na_2O

Specimen	No. of Pellets	$Na_2O\%$ $\bar{X}$	s	C%	$S\bar{x}$	E%*
19	3	1.31	0.05	3.81	0.03	2.20
20	3	2.74	0.02	0.73	0.01	0.42
22	3	2.15	0.08	3.72	0.05	2.15
23	3	3.13	0.06	1.91	0.03	1.10
24	3	1.78	0.05	2.81	0.03	1.62
25	3	3.61	0.03	0.83	0.02	0.48
27	3	1.56	0.09	5.77	0.05	3.33
28	3	1.41	0.08	5.67	0.05	3.27
29	3	0.93	0.04	4.30	0.02	2.48
30	3	1.92	0.05	2.60	0.03	1.50
32	3	1.14	0.06	5.26	0.03	3.04

* For the meaning of these statistical terms, refer to Table II, p. 44 .

TABLE 31

Comparison of X-Ray Spectrographic Analysis with the Chemical Data of Na_2O

Specimen	Chemical Analysis	X-Ray Analysis	Deviation
11	5.33	5.55	+0.22
12	1.91	1.87	-0.04
19	1.52	1.31	-0.21
20	2.74	2.74	0.00
22	1.98	2.15	+0.17
23	3.20	3.13	-0.07
24	2.01	1.78	-0.23
25	3.61	3.61	0.00
27	1.55	1.56	+0.01
28	1.36	1.41	+0.05
29	1.00	0.93	-0.07
30	2.01	1.92	-0.09
32	0.97	1.14	+0.17

n = 13
s = 0.14

P_2O_5 concentration of 0.10% (corresponding to C = 7.00% of the amount of oxide present). Longer counting time would improve these figures, but this was found to be unnecessary for an element like phosphorus.

It would be doing injustice if these figures of precision are to be compared with those of conventional chemical methods as shown from the following data:-

C =	65.12, 29.48	(Fairbairn and others, 1951, for G-1 and W-1 containing 0.11 and 0.14% P_2O_5 respectively)
C =	24.39, 47.71	(Stevens and others (1960) for G-1 and W-1)
C =	55.10, 40.51	(Stevens and others, 1960, for G-1 and W-1, all analyses)

No data for phosphorus X-ray spectrographic determination is given by Volborth (1963) to be compared with the present work.

As to the accuracy of the method, the application of the least square method to the X-ray intensity ratio versus the data of chemical analysis gave the following equation:

$$P_2O_5\% = (0.0427 \times \text{Intensity Ratio}) + 0.0373$$

The application of the least square is of great use to reduce the random error in the chemical analysis. The calibration graph is shown in Fig. 8b.

The results of the X-ray spectrographic analysis compared with the chemical data are shown in Table 33. Assuming that the chemical data are accurate and represent the arithmetic mean, the deviation of the X-ray data calculated by the least square equation, from the chemical analysis are shown in Table 33.

It is to be noted that the deviation for the Tonalite standard T-1 is

TABLE 32

Precision of X-Ray Spectrographic Determination of P_2O_5

Specimen	No. of Pellets	P_2O_5% $\bar{X}$	s	C%	$S\bar{x}$	E%*
Test No. 1. (-200 Mesh)						
1	3	0.09	0.0063	7.00	0.0036	4.04
2	3	0.06	0.0035	5.83	0.0020	3.37
3	3	0.07	0.0015	2.14	0.0009	1.24
4	3	0.08	0.0028	3.50	0.0016	2.02
5	3	0.05	0.0006	1.20	0.0003	0.69
6	3	0.09	0.0064	7.11	0.0037	4.10
10	5	0.08	0.0020	2.50	0.0009	1.12
11	3	0.10	0.0023	2.30	0.0013	1.33
13	5	0.16	0.0038	2.37	0.0017	1.06
Test No. 2. (-300 Mesh)						
1	3	0.10	0.0034	3.40	0.0020	1.96
2	3	0.07	0.0037	5.28	0.0021	3.05
3	3	0.08	0.0055	6.87	0.0032	3.97
4	3	0.08	0.0046	5.75	0.0026	3.32
5	3	0.07	0.0033	4.71	0.0019	2.72
5a	3	0.06	0.0032	5.33	0.0018	3.08
6	3	0.09	0.0050	5.56	0.0029	3.21
7	3	0.09	0.0046	5.11	0.0026	2.95
8	3	0.09	0.0060	6.67	0.0034	3.85
9	3	0.10	0.0070	7.00	0.0040	4.04
10	3	0.09	0.0025	2.78	0.0014	1.60
12	3	0.09	0.0057	6.33	0.0033	3.65
14	3	0.09	0.0067	7.44	0.0039	4.30

* For the meaning of these statistical terms, refer to Table 11, p. 44.

TABLE 33

Comparison of X-Ray Spectrographic Data with Chemical Data for P_2O_5

Specimen	Chemical Analysis	X-Ray Spectrographic Data					
		Test No. 1.			Test No. 2.		
		One-pt. calibr.	Least square	Deviation	One-pt. calibr.	Least square	Deviation
1	0.19	0.10	0.09	-0.09	0.13	0.10	-0.09
2	0.06	0.05	0.06	0.00	0.06	0.07	+0.01
3	0.04	0.07	0.07	+0.03	0.09	0.08	+0.04
4	0.10	0.08	0.08	-0.02	0.09	0.08	-0.02
5	0.05	0.04	0.05	0.00	0.06	0.06	+0.01
5a	0.05	-	-	-	0.06	0.06	+0.01
6	0.09	0.10	0.09	0.00	0.10	0.09	0.00
7	0.03	-	-	-	0.09	0.08	+0.05
8	0.11	-	-	-	0.14	0.11	0.00
9	0.13	-	-	-	0.12	0.10	-0.03
10	0.10	0.08	0.08	-0.02	0.10	0.09	-0.01
11	0.05	0.13	0.10	+0.05	0.12	0.10	+0.05
12	0.08	0.08	0.08	0.00	0.08	0.08	0.00
13	0.14	0.23	0.16	+0.02	-	-	-
14	0.16	-	-	-	0.10	0.09	-0.07
17	0.10	-	-	-	0.09	0.09	-0.01
			n = 10 s = 0.04			n = 15 s = 0.04	

Fig. 8

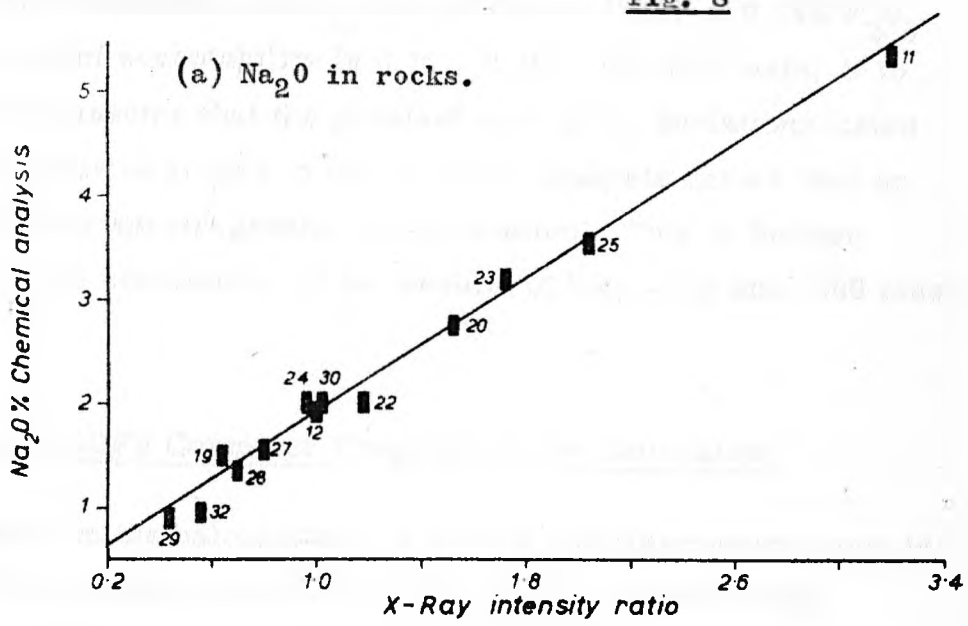
(a) Na_2O in rocks.
Na_2O % Chemical analysis
X-Ray intensity ratio
0·2
1·0
1·8
2·6
3·4
1
2
3
4
5
11
25
23
20
24
30
22
12
19
27
28
32
29

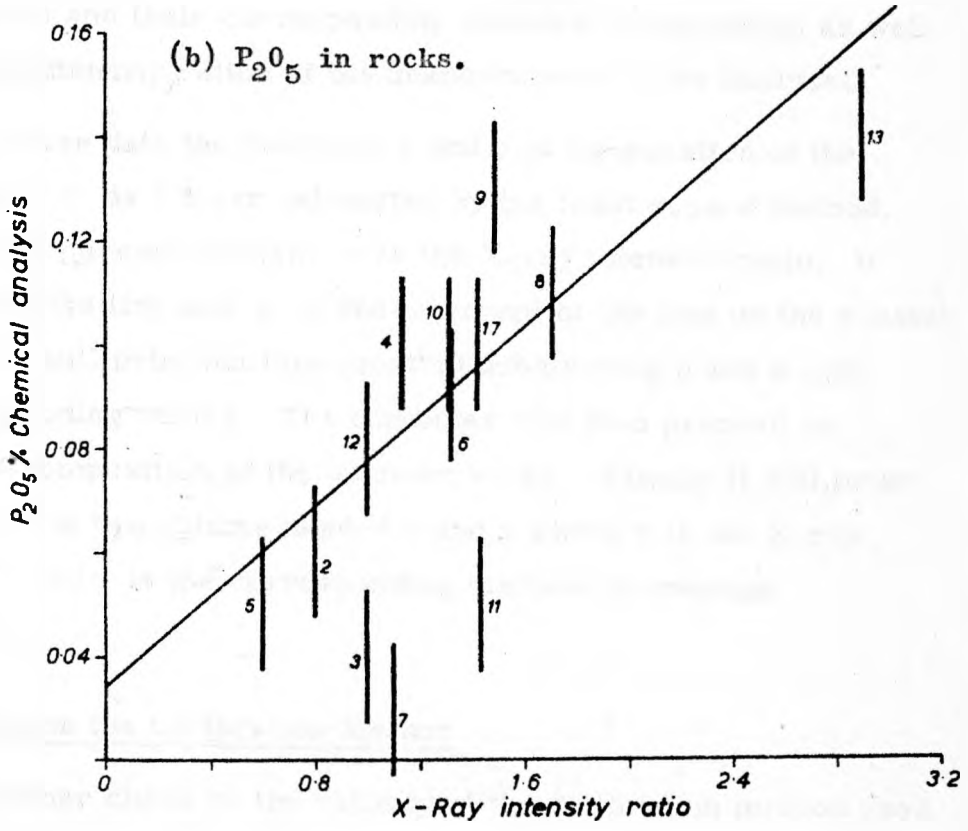
(b) P_2O_5 in rocks.
P_2O_5 % Chemical analysis
X-Ray intensity ratio
0·16
0·12
0·08
0·04
0
0·8
1·6
2·4
3·2
13
9
8
10
17
4
6
12
2
5
11
3
7

0.02 from the arithmetic mean of the preferred value of 0.14% P_2O_5 (adopted limits of acceptability is 0.10 - 0.16). On this basis, it is satisfactory to assume that the greatest part of the deviations listed in the table is due to errors in the chemical analysis rather than an inaccurate X-ray spectrographic determination. This is further confirmed by the consistency of the results of both -200 and -300 mesh powders.

C. An Algol KDF9 Computer Programme for Calculation

To speed up the calculations, a simple computer programme is devised. The computer is given the data used to construct the calibration g raph, namely the X-ray intensity ratio of the chemically analysed rocks and their corresponding chemical composition as well as the X-ray intensity ratios of the unknown rocks to be analysed.

From these data the functions a and b in the equation of the straight line $y = bx + a$ are calculated by the least square method, (where y is the percent element, x is the X-ray intensity ratio, b is the slope of the line and a is the intercept of the line on the y-axis). The computer will print out this equation substituting b and a with their corresponding values. The computer will then proceed to calculate the composition of the unknown rocks. Finally it will print out the results in two colums headed x and y where x is the X-ray intensity ratio and y is the corresponding element percentage (Appendix III).

D. A Check on the Calibration Method

As a further check on the validity of the calibration method used throughout this work, a rock (GL 31) of nearly the same amount of

silica as that of the standard GL 10 was chosen. Using the existing silica as an "internal standard" to which the counts of all other elements are related, the ratios counts of element/counts of silica for all the elements in both the standard GL-10 and the " unknown" GL-31 were calculated. The percent elements of the unknown was then calculated using these ratios and the chemical analysis of the standard GL-10.

Results obtained by this method alongside with the results obtained by the external standard method used throughout this work are shown in Table 34.

The agreement between the results obtained by the two methods proves the validity of the calibration already used and possibly furnishes another way of calibration in X-ray spectrography, viz. using the counts of an element already present in the sample provided that the percent of this element is known to be present in the same amount in both the standard and the unknown.

E. Mica Effect

The effect of the presence of micaceous minerals on the accuracy of the results of X-ray spectrographic analysis has been mentioned and discussed by Volborth (1963, 1964), Chodos (1961) and Baird et al., (1961). This effect was mentioned earlier in this work when the effect of grain size on the intensity of X-ray was investigated (p. 31).

According to Volborth (1964), further grinding of a micaceous rock would result in a decrease in intensity for each of Si, Ca, Na and an increase in intensity of each of Al, Fe, Mn, Mg, K, Ti. These changes in intensity would take place on the basis of comparing the chemical composition of biotite to that of granite.

TABLE 34

Element	Standard Rock GL-10			"Unknown" Rock GL-31 (Pellet No. 194)				
	% Chemical	Counts Peak-Bckgd.	Ratio Element/ Silica	Counts Peak-Bckgd.	Ratio Element/ Silica	Ratio "unknown" / Ratio standard GL 10	% Element	% Calculated by external standard
SiO_2	(63.60)	61200		61567				
TiO_2	(0.93)	39995	0.6335	37790	0.6138	0.9393	0.87	0.88
Al_2O_3	17.05	7088	0.1158	7887	0.1281	1.1061	18.86	18.97
Fe_2O_3	9.99	47705	0.7795	39280	0.6380	0.8185	8.18	8.23
MnO	0.07	3776	0.0617	3699	0.0601	0.9738	0.07	0.07
MgO	1.90	223	0.00364	189	0.00307	0.8425	1.60	1.61
CaO	(0.86)	40802	0.6667	21088	0.3425	0.5138	0.44	0.35
K_2O	3.25	103530	1.6917	116175	1.8870	1.1154	3.63	3.64
Na_2O	1.91	70	0.00114	90	0.00146	1.2782	2.44	2.35
P_2O_5	0.08	182	0.00297	193	0.00313	1.0538	0.08	0.08

In practice, however, Volborth found that this assumption is valid except for Na and K which behaved opposite to expectation.

Table 8 (p. 33) shows the effect of grinding on the X-ray intensity of the different elements as noticed by Hornung ( ), Volborth (1963, 1964) and as noticed in the present work. In view of the contradictions shown in this table, four rocks of different modal amounts of biotite and/or muscovite were tested to investigate this mica effect. The results of the analysis are shown in Table 35. From this table, it can be concluded that for the pelitic schists and gniesses under investigation, ground similarly to an equivalent grain size of -300 mesh, the mica effect is negligible and is practically non-existing.

(ix) Summary and Discussion of the reliability of X-ray spectrographic analysis

At this stage, the question arises as to which is the more reliable, X-ray spectrochemical analysis or the wet chemical methods.

Before dealing with this question, a summary of the different factors that affect the reliability of the X-ray method and which factors were discussed and tested for on the previous pages, is given below.

A. Factors affecting the precision:-

(a) Electronics stability which was tested by using a single pellet and taking counts for the different elements over a prolonged time (Table 4).

(b) Errors due to the pelletization of the same powder into a number of pellets. This was checked for all the elements using powders of different grain sizes. The X-ray intensity ratios of five pellets of each grain size were measured and the results are shown in Tables 5, 6 and 7.

TABLE 35

Comparison of X-ray spectrographic and chemical analyses of rocks containing different amounts of mica

Specimen	Modal Anal.		SiO_2%		TiO_2	
	Biotite	Muscovite	Chemical	X-ray	Ch.	X-ray
7	30	1	59.34	58.64	1.02	1.04
8	5	45	63.21	62.79	0.91	0.84
19	35	00	61.90	61.39	0.89	0.91
21	30.6	25.8	60.55	60.42	0.86	0.99

TABLE 35 (CONTINUED)

Specimen	Total Fe as Fe_2O_3		MnO		K_2O	
	Ch.	X-ray	Ch.	X-ray	Ch.	X-ray
7	7.88	7.80	0.10	0.09	4.00	3.78
8	6.37	6.31	0.05	0.05	4.52	4.52
19	8.00	7.93	0.05	0.06	4.45	4.54
21	9.44	9.20	0.05	0.05	4.30	4.46

TABLE 35 (CONTINUED)

Specimen	MgO		CaO	
	Ch.	X-ray	Ch.	X-ray
7	1.83	1.56	1.91	2.03
8	1.39	1.50	0.36	0.34
19	1.89	1.83	1.47	1.37
21	1.69	1.77	0.58	0.58

(c) Errors due to crushing the -100 mesh powder to the -300 mesh used in pelletization. This was tested by crushing three separate alliquots of the -100 mesh powder. The result is shown in Table 9.

B. Factors Affecting the Accuracy:-

(a) Errors due to the calibration technique i. e. the use of least square method for some elements and the direct straight ratio (one point calibration) for others. This was tested for and found valid as shown by the results obtained for standard tonalite T-1 and also by using the existing silica as internal standard (Table 32).

(b) Errors due to the possibility that the unknown is not crushed exactly as the standard. This was implicitly tested among the precision tests (errors due to crushing).

(c) Errors due to the so-called mica effect. This error was shown to be absent under the present working conditions (Table 35).

(d) Errors due to interelements effect in both the unknownand the standard and in particular the Si-Al problem. The discussion of this error will also entail the answer to the question set at the beginning as to which is the more accurate X-ray or wet chemistry. To this important subject, a more detailed investigation was done and is discussed in the next section.

C. Interelement or Matrix Effect

The interelement effect includes:-

(a) The matrix absorption or the absorption of the fluorescent radiation of an element by other elements in the matrix. Thus, if the element under investigation is in a matrix of high absorption, the intensity of its characteristic radiation will be relatively reduced while it is emerging from the specimen.

(b) Matrix enhancement : occurs when the characteristic radiation of an element has sufficient energy to excite the characteristic radiation of another element. The result will be a relative increase in the intensity of the enhanced element. An example of this effect is the enhancement of alumina by silica.

However, it is to be stated from the beginning that all the rocks under investigation are pelitic schists and gneisses with relatively small elemental differences and hence the discussion to follow is not concerned with gross problems arising from very widely different matrices.

For a long time, the matrix effect was considered as an obstacle in X-ray spectrographic analysis of rocks. Yet, there is no justifiable reasons to assume that for the normal silicate rocks where variations in the chemical compositions are not great, the matrix will affect the accuracy of X-ray spectrographic analysis. Even in the classical example of Si-Al mutual absorption and enhancement, experiments in the present work showed that with a range of 50 - 76% silica, no such alumina enhancement was detected.

It is interesting to mention that Volborth (1963) introduced a correction factor of an enhancement in Al amounting to 0.88% to be brought about by a known difference in Si of 20%. However, should this hold true, one would expect an absorption correction for Si by Al, a correction not mentioned by Volborth since his Si results were accurate enough.

On the other hand, Orrell and Gidley (1964) noticed a reduction in Si radiation which they attributed to the "strong absorption of Si-Ka by Al atoms in the matrix " (p. 23). A graphical correction was then developed as follows (p. 23): " A series of spectrographically pure SiO_2 standards from 0 to 100% at 10% intervals were made up and examined to obtain the theoretical linear calibration. A further series of standards containing a fixed amount of SiO_2 and varying amount of Al_2O_3, was then examined and the reduction in the count-rate due to Al absorption was used to construct an empirical count ratio correction chart. " By this method, the authors (ibid) were able to obtain a linear calibration curve for silica. However, if this holds true, one would expect an enhancement correction for Al by Si. Such a correction was not mentioned by the authors since their Al results gave directly a linear calibration curve.

In summary, here are two works in each of which the Si-Al problem was recognised, yet in one work (Volborth, 1963) only the enhancement of Al by Si was corrected for, whereas in the other work (Orrell and Gidley, 1964) only the absorption of Si by Al was corrected for.

To approach and test the problem of interelement effect, two separate aliquots of -100 mesh powders of three chemically analysed rocks (Specimens 28, 29 and 30) and GN.4457 were crushed to -300 mesh and three pellets per each aliquot were prepared. Pellets of the

first aliquot were analysed for some of the major elements by X-ray fluorescence in the usual way, i. e. using GL-10 as a standard for comparison. The results compared with those of the chemical analysis as well as the deviations are shown in Table 36.

Now knowing that all factors affecting the reliability of X-ray fluorescence other than the interelements effect have been already tested for and proved absent, then these deviations are either due to the presence of interelements effect or an error in the chemical analysis.

Therefore, the pellets of the second aliquot were analysed using another rock of different chemical composition than that of GL-10, as a standard. The X-ray intensity ratio of these pellets is shown in the last column of Table 36. Presumably, if an interelements effect is present, the X-ray analysis of the three rocks using another standard of different chemical composition and hence of different interelements effect, this analysis will give different results than those produced by using GL-10.

Graphs for the different elements were then drawn plotting this latter X-ray intensity versus the results of chemical analysis, as well as versus the results of X-ray analysis when GL-10 was used as a standard.

Figure 9a shows the plots of silica. Both the X-ray and chemical analyses of rock 28 agree whereas the other two rocks gave lower values than the chemical results. Assuming that the data of Specimen 28 represents the true SiO_2 content, then a straight calibration line cannot be drawn through the plots of intensity ratio versus results of chemical analysis without bringing about large deviations in the other two rocks. Yet, such a linear calibration curve can be drawn using the

TABLE 36

Element	Specimen	Chemical Analysis	X-Ray Anal. using GL 10 as standard	Deviation X-ray Chem.	X-ray intensity ratio Standard used	X-ray intensity ratio Ratio spec/stand
SiO_2	28	57.39	57.42	+0.03	A_{29}b	0.9920
	29	60.87	59.20	-1.67		1.0285
	30	59.04	57.81	-1.23		0.9942
TiO_2	28	1.08	1.20	+0.12	A_{29}b	1.0243
	29	0.84	0.88	+0.04		0.7574
	30	1.19	1.17	-0.02		0.9810
Al_2O_3	28	22.46	21.75	-0.71	A_{29}	0.8955
	29	19.92	20.40	+0.48		0.8515
	30	23.74	23.43	-0.31		1.0090
Total Iron as Fe_2O_3	28	9.66	9.47	-0.19	A_{29}b	1.3843
	29	6.11	7.03	+0.92		1.0390
	30	6.38	6.86	+0.48		0.9886
MgO	28	2.19	1.78	-0.41	A_{14}	0.3617
	29	4.91	5.25	+0.34		0.9787
	30	2.10	2.31	+0.21		0.3981
CaO	28	0.39	0.53	+0.14	A_{29}	0.7752
	29	0.30	0.19	-0.11		0.3793
	30	0.57	0.87	+0.30		0.9941
K_2O	28	4.56	4.47	-0.09	A_{29}b	1.6257
	29	2.99	3.07	+0.08		1.1068
	30	2.74	2.77	+0.03		0.9908

plots of intensity ratio versus results of X-ray analysis with a deviation of $\pm$ 0.2% SiO_2 (solid line in the graph). Better still is the dashed "best" straight line giving a deviation of $\pm$ 0.1% silica for the three rocks.

The agreement of X-ray results using two different standards suggests the absence of the interelements effect. The better fit of the calibration curve plotted using the X-ray results suggests that the deviations of the X-ray analysis from the chemical analysis is due to an error in the latter.

Figure 9b shows the results of titania treated in the same way as silica. Again the X-ray results gave a better calibration curve suggestive of being more accurate than the chemical data.

For alumina, the results are shown in Figure 10a. Again, the X-ray analysis proved to be more accurate than the chemical data and the curve shown in the figure can be considered the correct calibration curve. Yet, because of the special interest of the Si-Al enhancement, another three rocks of widely varying silica contents (26, 27 and 33) were chemically analysed. These three rocks were also analysed by X-ray fluorescence and treated in a similar way to that of three rocks under investigation. The results of these analyses are shown in Table 37.

As is noticed from this table, all the three rocks show a positive deviation of 1% alumina. Yet they show no sign of enhancement whether the SiO_2 content is similar to that of the standard GL-10 (63.69% SiO_2) as in the case of (33), or much higher as in the case of (26), or much lower as in the case of (27).

Now, if the X-ray intensity ratio shown in the last column of

Fig. 9

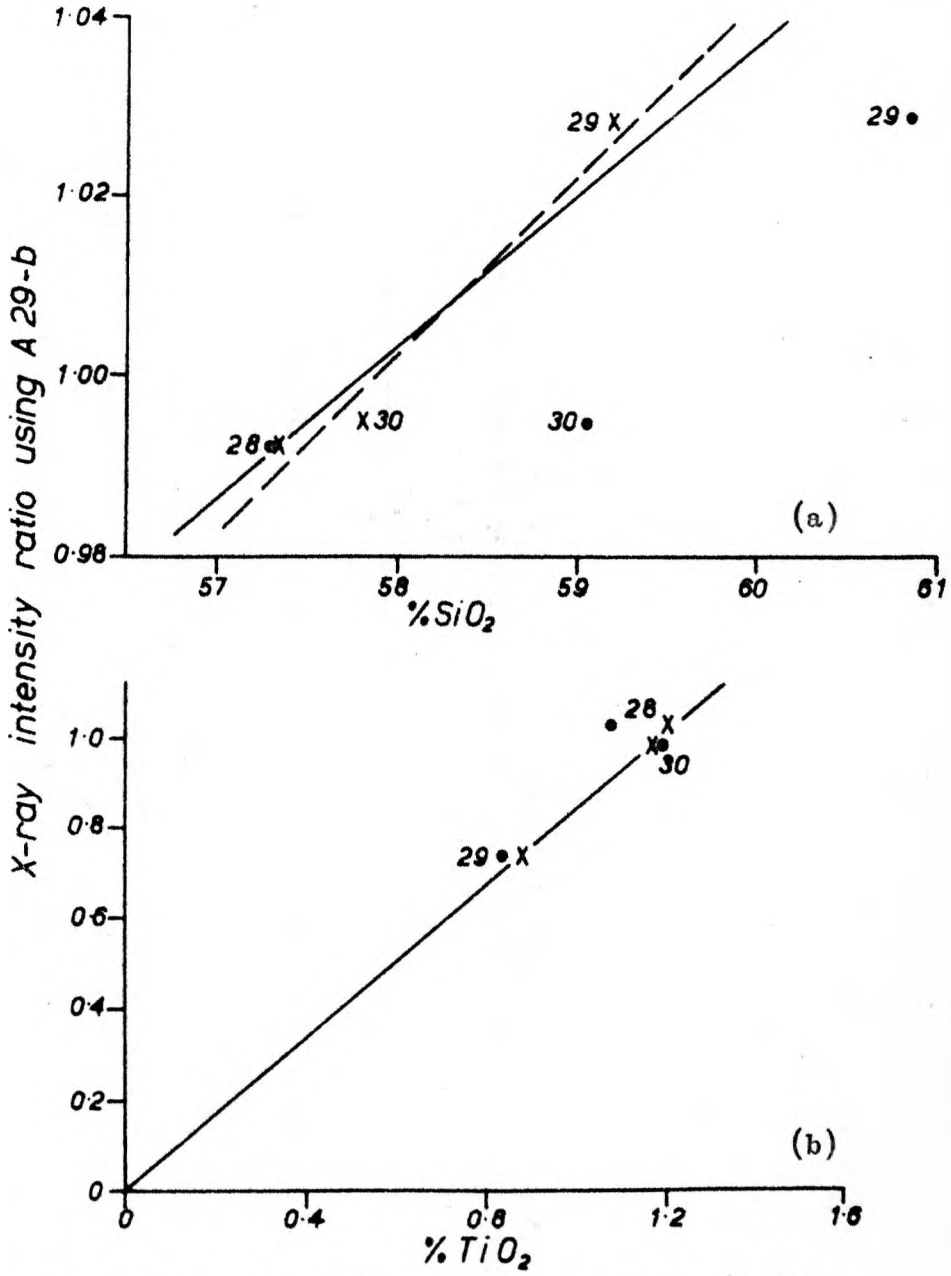

• Intensity ratio vs. results of chemical analysis

x Intensity ratio vs. X-ray analysis using GL10 standard

TABLE 37

Specimen No.	SiO_2% Chemical	SiO_2% X-ray	Al_2O_3% Chemical	Al_2O_3% using GL-10 as standard	Deviation X-Ch.	X-Ray Intensity Ratio using Rock A-29 as a standard
26	76.27	76.03	10.03	11.13	+1.10	0.4627
27	50.72	50.78	29.79	31.21	+1.49*	1.3211
33	64.59	63.50	17.92	18.82	+0.90	0.7825

* This rock had an undissolved residue which would reduce the Al deviation to approximately 1.09%

Table 37 is plotted versus the results of chemical and X-ray analyses shown in the 3rd and 4th columns respectively, and if the calibration curve shown in Fig. 10a was traced, the result will be Figure 10b, Notice that the calibration curve exactly fits the plots of intensity ratio versus the X-ray results, thus suggesting that the positive bias of about 1% alumina is due to an error in the chemical analysis.

For the determination of total iron as Fe_2O_3, Figure 11a shows that the calibration curve with as low a deviation as $\pm$ 0.05% Fe can only be drawn through plots using the X-ray analysis. This shows that the deviations in iron determination for the three rocks (28, 29 and 30) are due to chemical error. Other chemically analysed three rocks (Specimens 7, 8 and 9) were treated in the same way. Table 38 shows the results of this analysis.

Figure 11b shows the plot of these results. It is to be noticed that exactly the same calibration curve as that in Fig. 11a was produced. This reproducibility of calibration curve is suggestive of its correctness and hence the more accuracy of the X-ray analysis.

However, a third set of chemically analysed three rocks (26, 27 and 33) showed a positive bias in X-ray analysis. The X-ray intensity ratios of these three rocks were determined using the A-29 rock standard used in the above six rocks, as well as another rock GL-45 as another standard. The result of this analysis is shown in Table 39.

The plot of X-ray intensity ratio using A-29 as a standard versus the data of chemical analysis and X-ray analysis using GL-10 as a standard, is shown in Fig. 11c. Here, two different calibration lines with low deviations can be drawn (solid and dashed lines in the graph).

Fig. 10

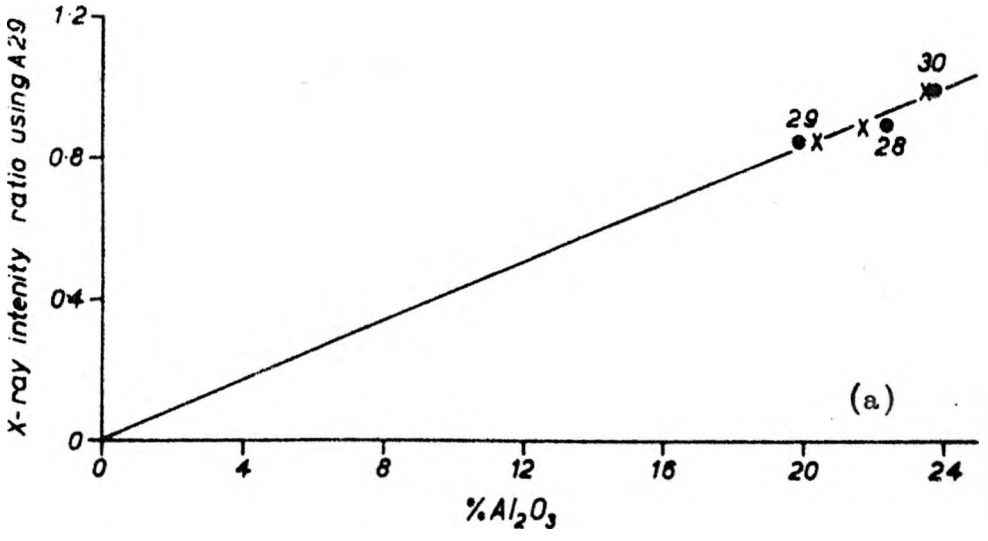

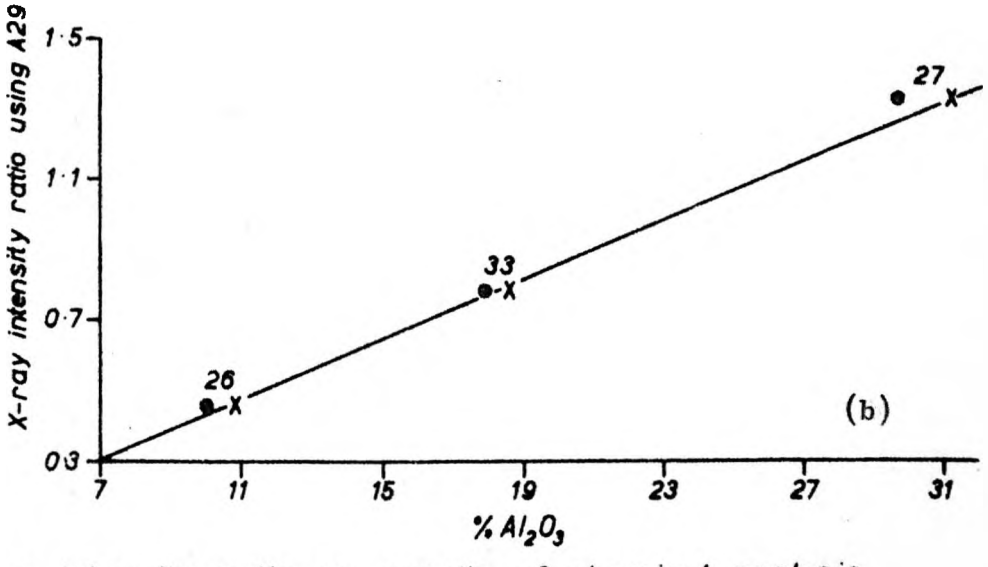

• Intensity ratio vs. results of chemical analysis

x Intensity ratio vs. X-ray analysis using G.L 10 standard

Specimen	Fe_2O_3% Chemical	Fe_2O_3% X-ray using GL-10 Standard	Deviation X-ray-Ch.	X-ray Int. Rat. using A29 as St.
7	7.88	7.79	-0.09	1.1634
8	6.37	6.31	-0.06	0.9580
9	9.20	9.21	+0.01	1.3886

TABLE 38

TABLE 39

Specimen	Fe_2O_3% Chemical	Fe_2O_3% X-ray using GL-10 as standard	Deviation X-ray Chemical	X-ray Intensity Ratio using A-29 as a standard	X-ray Intensity Ratio using GL-45 as a standard
26	6.31	6.93	+0.62	1.0180	0.7247
27	5.12	5.37	+0.25	0.7918	0.5595
33	7.90	8.25	+0.35	1.2150	0.8652

Yet only the solid line fits with the other two calibration curves shown in Figs. 11a and b. Moreover, if the carefully analysed GL-10 is calculated back from the two calibration curves of Fig. 11c, the correct value of 99.9% Fe_2O_3 can only be produced from the solid line, the dashed line giving a value of 9.25%. Since the solid line is produced from points relating the X-ray intensity ratio to the results of X-ray fluorescence analysis, one can conclude that the X-ray analytical data are the accurate ones.

Further still, the last column of Table 39 shows the X-ray intensity ratio of the three rocks using a third different standard of different composition and hence of different interelements effect. The plots and the calibration curve using these intensity ratios are shown in Figure 11d. If the standard GL-10 is calculated from this graph, the solid line will give the correct value of 9.99% Fe_2O_3 whereas the dashed line will give a value of 9.25% - exactly similar to the situation met in the curves of Fig. 11c. This again confirms the validity of the above conclusions regarding the absence of interelement effect and the more accuracy of X-ray data.

The accuracy of both magnesium and calcium determinations were examined and the results are shown in Figs. 12a and b. For both elements, the accuracy can be argued either way. Yet, the fact that for two rocks out of the three analysed, a negative deviation in one element corresponds to a positive deviation in the other, shows that part of the deviation is due to chemical error. This is because, in chemistry, the determination of Ca and Mg is inter-dependent whereas in X-ray each element is determined independently from the other.

For K_2O, there is an agreement in the results of both chemical

Fig. 11

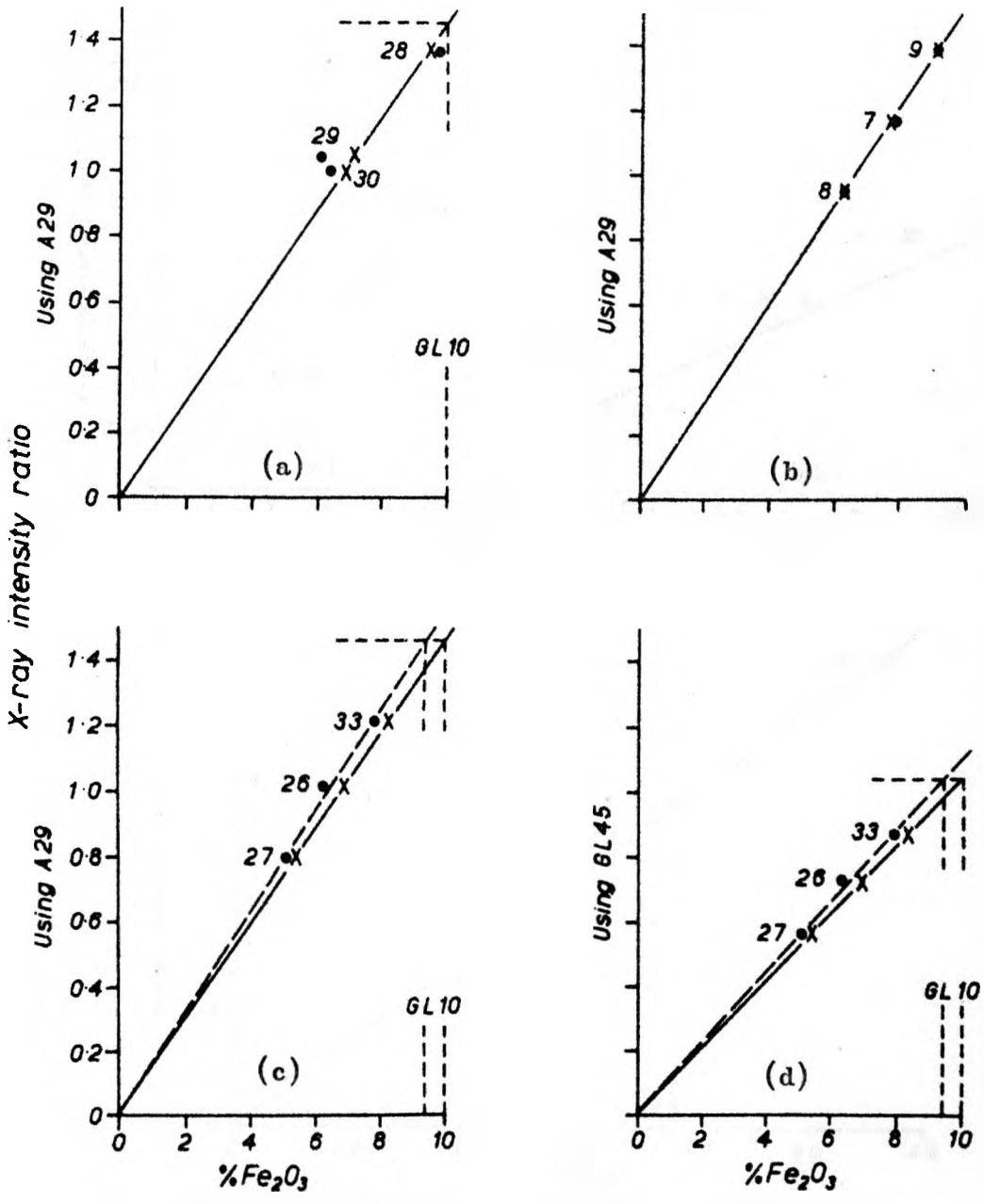

• Intensity ratio vs. results of chemical analysis
x Intensity ratio vs. X-ray analysis GL10 standard

Fig. 12

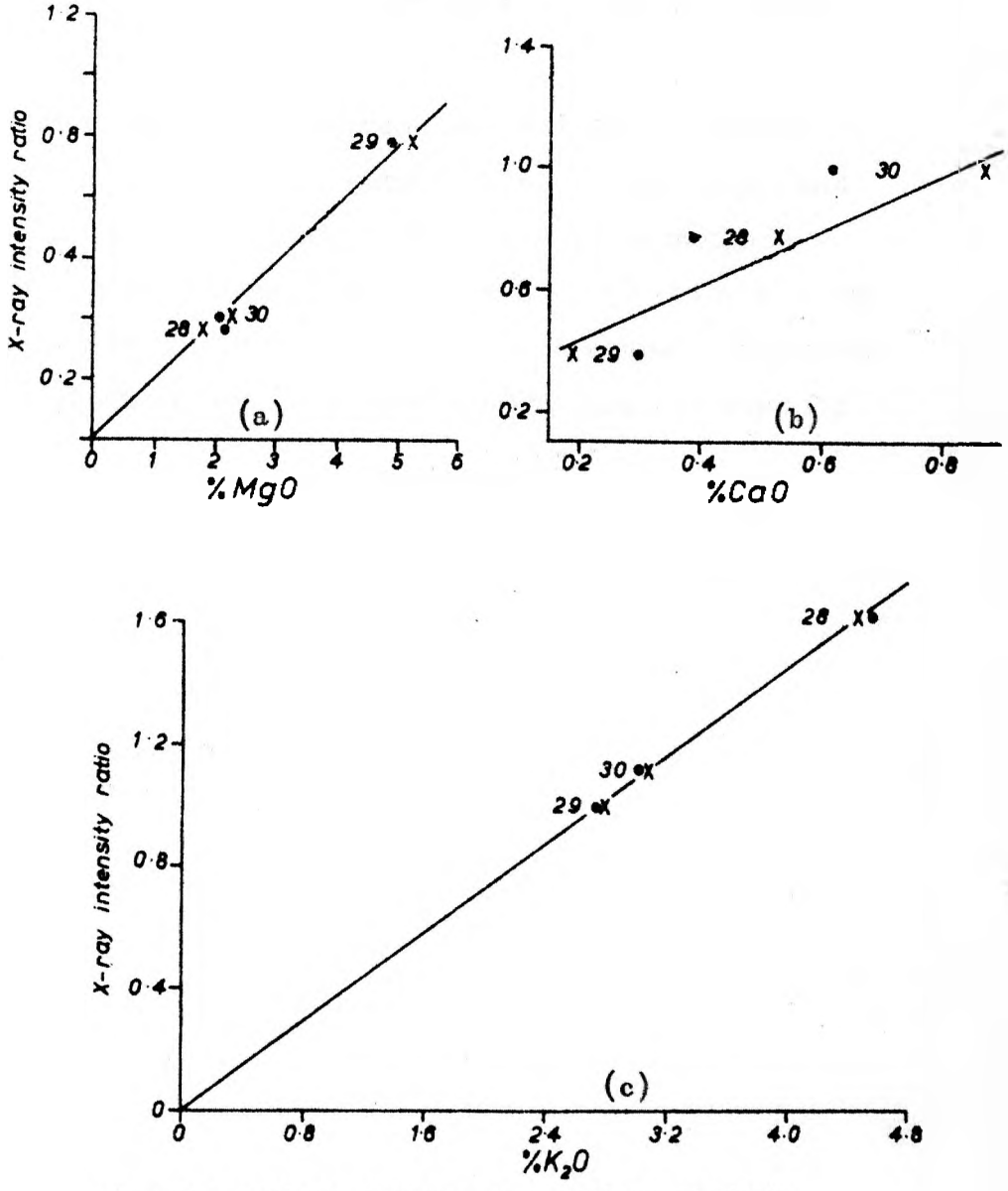

• Intensity ratio vs. results of chemical analysis
X Intensity ratio vs. X-ray analysis using GL10 standard

and X-ray analysis with a deviation of $\pm$ 0.10% K_2O. Figure 12c shows the plots of the analytical data of Table 34. Worth mentioning is that potassium is the fastest element to analyse by X-ray. The three pellets of one rock take only 5 minutes to determine the K content.

In conclusion, the X-ray fluorescence analysis of silicate rocks proved to be a successful means to achieve more rapid and as or more accurate results compared with chemical methods - conventional or rapid. The main factors of this success are, first, the rocks analysed are all pelites with no wide elemental variations and, second, a group of chemically analysed pelites was used for calibration.

CHAPTER TWO

FLUORESCENT X-RAY SPECTROGRAPHIC MICRO-ANALYSIS OF SILICATE MINERALS

I. INTRODUCTION

As has been shown earlier in this work, X-ray spectroscopy is reliable rapid method for silicate analysis. For all the major elements, one pellet per rock proved to be adequate for analysis and the amount of powdered sample used to prepare one pellet is 2 grams. However, with small amounts of geological samples i. e. samples of limited size such as minerals, extraterrestial materials as tektites, chondrules, etc. a 2 gm. sample is difficult or impossible to obtain in many cases. Hence, there is a need to develop a method by which few milligrams of silicate sample can be easily and efficiently analysed.

It should be noted that not only the limited sample size is the single criterion by which the developed method would be successful, but also the following criteria should be taken into consideration:

1. The developed method must not involve the complete destruction of the sample, i. e. the sample should be recovered after the analysis.
2. The amount of labour and the different steps involved in the sample preparation should be kept to a minimum.
3. The need of sophisticated equipments should be kept to a minimum.

II. GENERAL CONSIDERATIONS

One of the important features in X-ray spectroscopy is that the characteristic fluorescent intensity decreases with decreasing atomic number of the elements. This decrease is due to the lower fluorescent yield of the low atomic number elements and the absorption of the characteristic fluorescent radiation by air, diffracting crystal, detector window and the specimen itself. The softer the radiation, the more pronounced is the absorption. With light elements as sodium and magnesium, the volume of the sample reacting with the primary X-ray is those atoms at or near the spectrum surface. Hence the surface of the specimen should be very smooth and highly reproducible from one specimen to another.

On the other hand, with "hard" radiations as those of Fe, the volume of the sample reacting with primary X-ray is greater. Therefore, the sample must be "infinitely" thick i. e. no increase in the characteristic X-ray intensity of the element is brought about by increase in the sample thickness. Rose and others (1964) pointed out that the infinite depth is reached for Ca at less than 100 microns and for Mg at less than 50 microns.

III. PREVIOUS WORK

To the best of the writer's knowledge, the important micro or semi-micro analysis done on silicate samples is that of Rose and others in 1962, 1964 and 1965.

In 1962, Rose and others described three methods of preparing specimens using 250 milligram sample, namely:

1. Mechanically mixing the sample with 4 parts of boric acid.
2. Fusing the sample with 1.250 gms. of $Li_2B_4O_7$.
3. Fusing the sample with equivalent amount of La_2O_3 and 1.000 gm. $Li_2B_4O_7$.

In the second and third preparation techniques, fusion was made in graphite crucibles at 1000°C for 8-10 min. Then boric acid was added to the cooled bead to bring the weight of the bead up to a certain value. The whole lot was then ground in a mixer grinder to pass a 325-mesh screen. Finally the sample was pelleted using boric acid as backing.

The authors (ibid) determined CaO, Fe_2O_3 and SiO_2 and concluded that with the use of the heavy absorber La_2O_3, there was an improvement in the calibration lines. They also concluded that the third method of preparation " has been used to analyse successfully a variety of materials with results agreeing within one percent of the chemical determination" (1962, p. 82).

In 1964, Rose and others applied the above mentioned third way of sample preparation except that they used only 50 mg. of sample, 50 mg. La_2O_3, 340mg. $Li_2B_4O_7$. They analysed six samples of tektites for 7 major elements having the following range of chemical composition:

SiO_2	72.3 - 74.4
Al_2O_3	11.1 - 11.4
Total Fe	5.28 - 6.17
CaO	2.36 - 2.91
K_2O	2.17 - 2.29
MnO	0.10 - 0.11
TiO_2	0.67 - 0.70

Notice how narrow is the range of chemical composition.

In 1965, Rose et al., in a further attempt to reduce the amount of sample used, pointed out that they applied the $La_2O_3/Li_2B_4O_7$ fusion technique successfully to a sample as small as 25 mg. a quantity which "represents a practical lower limit for the $Li_2B_4O_7$. La_2O_3 fusion technique" (p.155). Consequently, they developed a new method to analyse fewer milligrams of sample.

In this technique (Rose et al., 1965), an accurately weighed 4-10 mg. sample is decomposed for several hours in 1 ml. 5:2:3 $HF:HNO_3:H_2O$, the solution is then evaporated to dryness, then 1 ml. 1:1 HNO_3 is added to the residue after each evaporation. The silica-free nitrates thus produced, are dissolved in 1 ml. of 1:4 HNO_3. The solution is then very carefully absorbed onto 500 mg. of powdered chromatographic paper, mixed carefully and thoroughly with tephlon, dried overnight, then ground in a boron carbide mortar and, finally, carefully pressed into a pellet using powdered chromatographic paper as backing. By this technique, the authors (ibid) determined Al_2O_3, total iron, K_2O, CaO, TiO_2, and MnO on G-1, W-1, six tektites and five synthetic glasses. The X-ray data agreed well with the reported chemical values of these oxides.

Critically speaking, although Rose et al., (1962, 1964, 1965) techniques are good and gave X-ray data agreeing with the reported chemical analysis, yet several points arise in connection with their sample preparation techniques:

1. The sample is completely destroyed.
2. Unless the quantity of the specimen is 25 mg. or more, silica cannot be determined.

3. The technique by which the sample is prepared is very lengthy, involving many steps and a list of precautions. Bearing in mind that we are dealing with less than 10 mg. (Rose et al., 1965), the fusion of such small quantity, its dissolution, mixing, grinding as well as its frequent transferring into different vessels, increase the possibility of loss of material as well as the introduction of contaminations.

IV. PRELIMINARY WORK

The present work was initiated by Dr. M. P. Atherton as a project for the Honours Degree Students in the Geology Department, Liverpool University; namely, S. P. Harris, P. J. Hill and H. F. Shaw. Together with the present author, the whole team tried to develop a method using few milligrams of chemically analysed biotites available in the Department. One of these biotites which will be referred to as "Biotite Standard" is pure biotite which has been chemically analysed by three analysts for five times. Table 40 shows the result of these analyses.

The problem became divisible in two parts:

1. The preparation of the sample in a simple way, adequate for its presentation to the spectrograph.
2. Standardisation of the method i. e. the transformation of the X-ray data into percentage element oxide.

As to the preparation of the sample, the easiest way was to mount few flakes of biotite by sticking them directly on cellotape, the latter is, in turn, mounted on the sample holder.

TABLE 40

Chemical Analysis of Biotite Standard

Oxide	1	2	3	4	5	6
SiO_2	36.70	36.75	35.88	35.88	36.52	
TiO_2	3.04	2.97	3.03	4.16	2.42	
Al_2O_3	16.28	16.13	16.25	15.97	16.03	
Fe_2O_3	2.31	2.31	2.93	2.86	2.52	
FeO	20.76	20.76	20.43	20.43	20.29	
MnO	0.54	0.51	0.50	0.50	0.37	0.48
MgO	7.62	7.85	8.15	7.94	8.09	7.82
CaO	-	-	0.10	0.10	-	
Na_2O	0.17	0.16	0.16	0.18	0.15	
K_2O	9.72	9.74	9.62	9.34	9.58	
H_2O	3.07	3.07	3.07	3.07	(3.07)	
-	-	-	-	-	-	
Total	100.24	100.27	100.12	100.43	99.04	
Total Iron As Fe_2O_3	25.37	25.37	25.63	25.56	25.06	24.82

Analysts: M. Edmunds, M. Brotherton, J. Mather.

As to the standardisation of the method, the direct comparison between the X-ray intensities of the unknown and an analysed external standard was not possible because:

1. The surface area and/or the volume of the biotite cannot be kept constant from one sample to another.
2. There is no guarantee that the specimen is "infinitely" thick.

It was, therefore, thought to use an element which is already present in the biotite as an internal standard to which the X-ray intensities of the other elements are related. Then, the X-ray intensity ratios thus calculated for the unknown, can be compared to the X-ray intensity ratio calculated in the same way for the chemically analysed standard.

A requisite for this calibration method is the pre-knowledge that the element to be used as an internal standard should be present in the same amount in all the specimens. The validity of this calibration technique was investigated earlier on two rocks having the same amount of silica and the results were shown in Table 34. (p. 89).

Silica in biotites would provide a fairly reasonable internal standard for a semiquantitative analysis. For 28 analysed biotites (Deer, Howie and Zussmann, 1962) 14 of which are of igneous origin and the other 14 are metamorphic, the variance σ^2 was found to be 1.10% and 2.51% SiO_2 for igneous and metamorphic biotites respectively.

Unfortunately, the results of this analysis proved to be imprecise and inaccurate.

Pelletization technique was then tried. The biotite sample was mechanically mixed with twice its weight bakelite resin and the mixture

was pelletized. The same calibration technique was used. The results showed slight improvement in precision but there was no improvement in accuracy. The main reason was that the specimens were still not "infinitely" thick and the surface area to the sample volume was not constant.

V. THE ANALYSIS OF 5-8 MILLIGRAMS OF SILICATE MINERALS

From the foregoing discussion, it became evident that to attain precision and accuracy, the sample should be infinitely thick, the surface should be smooth and the ratio surface area to effective thickness should be constant.

After a number of trials, the present author arrived to the following technique of analysis using 5 mg. of biotite and 8 mg. of garnets.

A. Sample Preparation

The main equipments needed were two small sieves, $\frac{1}{2}$" and $\frac{1}{4}$" diameter each. The mesh screens of these sieves can be easily replaced. For this purpose the sieves were made in the Department's workshop as follows:

Two rectangular plates of perspex were cut 2" x 1.5" each. A $\frac{1}{2}$" or $\frac{1}{4}$" hole was drilled in the middle of the 2 perspex pieces. The mesh screen is to be put between the two plates to cover this central hole. The two plates are held together by 4 screws and nuts drilled at the 4 corners of the plates. When these nuts are tightened, the mesh screen is held securely. It is advisable to bevel the edge around

the central hole of the upper perspex plate.

As mesh screens, Bolting Cloth was used. Two sizes were chosen namely 25N (about 61 microns ≡ 240 B. S. S. mesh) and 10N (about 124 microns ≡ 120 B. S. S. mesh). The 25N and 10N Bolting Cloth were used for the $\frac{1}{2}$" and $\frac{1}{4}$" sieves respectively. For each specimen, a new piece of Bolting Cloth was used. This ensured the absence of any contaminations from one specimen to another due to sieving.

Approximately 5 mg. of biotites is crushed manually in a small agate mortar for few minutes. The powder is then sieved with the help of a small brush to pass the 25N mesh screen of the $\frac{1}{2}$" sieve. This 61 microns or less biotite powder is received into a small watch glass. The $\frac{1}{4}$" sieve is placed directly on a glass disc and the powder is then transferred to the mesh hole (the glass disc is one of those used in preparing the rock pellets described before p. 6). The powder is then brushed to pass the 10N mesh screen of the $\frac{1}{4}$" sieve. This will be found easy due to the large size of the mesh holes compared to the powder grain size. With practice, this final sieving can be done to produce a heap of biotite on the glass plate, with a more or less uniform thickness.

This last sieving is done with the glass plate placed on the platten of the hydraulic press. The die or the supporting ring of the press is put on top of the platten. Cellulose powder is then sieved gently with the help of a brush and a wide screen ordinary sieve until the hole of the die is filled. The idea of sieving the cellulose is to let it "showers" around the biotite heap and finally covering it completely while the biotite is still held in place without any disturbance.

Pressure is then gradually increased up to 30 tons/ram, then kept there for 30 seconds. The pressure is then released gently and steadily. The result will be a cellulose pellet in the middle of which the biotite powder is pressed. The whole surface has a mirror finish.

The above mentioned sample preparation technique has the following advantages:

1. The preparation of one pellet takes about 15 minutes.
2. Particular or high skill is not required.
3. Contamination of the sample is very unlikely.
4. Accurate weighing is not needed.
5. Loss of small amounts of the sample due to grinding and/or sieving is insignificant since the 5 mg. are more than what is needed to produce and "infinitely" thick specimen.
6. No need for a variety of equipments and materials.
7. Most important is that the biotite can be recovered from the pellet by scratching it with a needle.

B. Sample Presentation to the X-ray Spectrograph

No matter what is the degree of care taken in sieving and pelletising, the very outer edges of the biotite circle will be seen to thin out and diffuse into the surrounding cellulose. The degree of thinning out differs from one specimen to another. Therefore, masking the outer edges of the specimen was necessary.

A lead mask was separately done as follows:

On the platten of the hydraulic press, cellulose powder, then lead powder, then cellulose powder were sprinkled in the given order.

The whole lot was then pressed to 30 tons/ram. This produced a lead disc sandwiched between two cellulose sheets. The amount of cellulose and lead used were just enough to produce the thinnest possible disc which would prevent the characteristic Fe Ka radiation to pass through to the detector. This was checked by using pure iron oxide pellet.

A hole, smaller in diameter than that of the biotite circle was drilled in this mask. The mask was then glued on one of the sample holders. One sample holder carrying one particular mask was used throughout the analysis of each element. This eliminates the errors due to:

1. The thickness of the mask.
2. The size of the hole in the mask.
3. The position of the exposed area of the specimen relative to the primary X-ray beam and the crystal.

By this method, a specimen which has reproducible smooth surface and constant surface area is presented to the spectrograph. As to the effective thickness of the specimen, 5 mg. sample proved to be as effectively deep as 30 mg. prepared in the same way. This was tested for Fe and Ti and both pellets gave the same number of counts.

C. Instrumental Conditions

The same instrumental conditions as those used for rock analysis and shown in Table 2, p. 17 were used here with very slight changes. For Mg determination, the counter window was changed from beryllium to the very thin polycarbonate film of 2 micron thickness.

Also the count rate for most of the elements was changed to suit the present lower count conditions.

D. Calibration

The immediate and direct comparison with an external standard of nearly the same composition as that of the unknown, is by far the best method of calibration as discussed earlier (p. 7). Therefore, a carefully analysed mineral will be used as a standard to which other unknown samples of the same mineral are compared.

E. The Background and its Effect on Calibration

The area of the sample irradiated is much smaller than the area of the beam from the X-ray tube. Hence, the background measured will be due to the sample and the sample mask. Therefore, the background counts should be subtracted from the total counts before constructing the calibration g raph.

This was found to be true for most of the elements. The direct comparison between the total counts of the unknown and the standard after subtracting the background counts, gave a good calibration graph in the form of a straight line passing in most cases through the origin. The slope of the line was constant for different measurements of different pellets.

However, for iron and silica, it was found that good calibration graphs are produced only if the total counts were used i. e. the background counts are not subtracted. Moreover, if the sample mask was changed, the slope and intercept of the calibration graph are changed. The reason for this is not yet clearly understood. Yet this meant that a new calibration graph is to be constructed each time the iron

and/or silica are measured in one batch of specimens.

This problem was solved by choosing three chemically analysed specimens that have the best fit on the calibration graph after a repeated series of measurements. The X-ray intensities of these three specimens are measured with each batch of specimens. The results of the three known specimens are then analysed by the least square method and the equation of the straight line ($y = bx + a$) of the calibration g raph under this particular condition of analysis, can be calculated. Knowing the slope and the intercept of the calibration line, the per cent element can be calculated for the X-ray intensity ratios of the unknowns.

The computer programme shown earlier (p. 87) will be of great value in this situation. In practice, what will be needed, then, is only extra three measurements when a batch of unknowns is analysed. The computer programme will carry out all the necessary calculations.

F. Precision of the Method

The precision of the method was tested on three pellets of the biotite standard (using 5 mg. of biotite for each pellet) as well as on three pellets of garnet (using 8 mg. for each pellet). The results and the statistical analysis of this test are shown in Tables 41 and 42.

From these tables, it is evident that sample preparation and presentation is highly precise. The standard deviation of a single pellet is in most of the cases much lower than the standard counting error. In few cases, the two deviations were comparable.

It can, therefore, be concluded that with such high precision,

TABLE 41

Precision of X-ray Spectrographic Microanalysis of Biotite
(3 pellets, 5 mg. each)

Element	Pellet No.	Chemical Analysis	N_T Counts on Peak	N_B Counts on Bckgd.	$N_T - N_B$	Time of Count Mins.	Av. $\bar{N}$	S Counts
SiO_2	1	36.34	12583	2825	9758	10	9794	34
	2		12650	2825	9825	10		
	3		12624	2825	9799	10		
TiO_2	1	3.00	28166	8874	19202	4	19163	164
	2		28017	8874	19133			
	3		27939	8874	19065			
Al_2O_3	1	16.13	11032	3840	7192	8	7139	48
	2		10938	3840	7098			
	3		10968	3840	7128			
Total Iron as Fe_2O_3	1	25.27	19334	7790	11544	4	11583	109
	2		19288	7790	11498			
	3		19496	7790	11706			
MnO	1	0.48	4116	3146	970	2	1017	57
	2		4147	3146	1001			
	3		4227	3146	1081			
MgO	1	7.93	1467	875	592	7	588	4
	2		1520	935	585			
	3		1591	1005	586			
K_2O	1	9.60	60547	7278	53269	4	53094	238
	2		60468	7278	53190			
	3		60100	7278	52822			

Elem.	S % element	C % of the amount present	Sx^- counts	Sx^- % Element	E % of the amount present	Standard Counting Error		
						Sc Counts	Sc % element	Cc % of the amount present
SiO_2	0.13	0.36	19	0.08	0.21	124	0.46	1.27
TiO_2	0.026	0.83	95	0.015	0.48	192	0.031	9.99
Al_2O_3	0.11	0.68	27	0.06	0.39	121	0.27	1.67
Fe_2O	0.24	0.95	63	0.14	0.55	165	0.34	1.34
MnO	0.02	4.16	33	0.01	2.40	65	0.03	6.25
MgO	0.05	0.63	2	0.03	0.36	50	0.67	8.45
K_2O	0.04	0.41	137	0.02	0.24	260	0.05	0.52

TABLE 41 (CONTINUED)

TABLE 42

Precision of X-Ray Spectrographic Microanalysis of Garnet*
(3 pellets, 8 mg. each)

Element	Pellet No.	Chem. Analysis	N_T Counts on Peak	N_B Counts on Bckgd.	$N_T - N_B$	Time of Count Mins.	Av. N^-	S Counts
SiO_2	1		13563	1465	12098			
	2	39.35	13730	1465	12265	10	12162	90
	3		13588	1465	12123			
TiO_2	1		9625	8762	863			
	2	0.04	9617	8762	855	4	843	27
	3		9547	8762	812			
Al_2O_3	1		5750	2830	4920			
	2	21.34	5781	2830	4951	5	4940	18
	3		5780	2830	4950			
Total Iron as Fe_2O_3	1		24716	7366	17395			
	2	28.30	24804	7366	17438	4	17328	154
	3		24518	7366	17152			
MnO	1		19939	3307	16632			
	2	9.14	20161	3307	16854	2	16727	161
	3		20002	3307	16695			
CaO	1		45059	7143	37916			
	2	2.60	44932	7143	37789	4	37692	283
	3		44515	7143	37372			
MgO	1		1328	1112	216			
	2	1.59	1311	1080	231	7	224	7.5
	3		1294	1060	224			

TABLE 42.(CONTINUED)

Elem.	S % element	C % of the amount present	Sx^- Counts	Sx^- % element	E of the amount present	Standard Counting Error Sc Counts	Sc % element	Cc % of the amount present
SiO_2	0.29	0.73	52	0.16	0.42	117	0.38	0.96
TiO_2	0.001	3.25	15	0.0007	1.88	31	0.0015	3.75
Al_2O	0.08	0.37	10	0.04	0.21	88	0.38	1.78
Fe_2O	0.25	0.88	89	0.14	0.51	157	0.25	0.88
MnO	0.08	0.87	93	0.05	0.50	142	0.08	0.87
CaO	0.02	0.76	163	0.01	0.44	212	0.014	0.54
MgO	0.053	3.33	4	0.03	1.92	36	0.255	16.04

* The Garnet used is "EDM. LM-18"

only one pellet of 5 mg. of biotite or 8 mg. of garnet, can safely be used for analysis.

G. Analytical Data and the Accuracy of the Method

Twelve to fourteen biotites and five garnets which had been chemically analysed were used to test the accuracy of the method.

Appendix II shows details of these minerals for future reference.

(i) Silica

The results of the analysis of silica is shown graphically in Fig. 13a. The comparison between the chemical and X-ray data is shown in Table 43. The deviations of the X-ray analysis are shown in the same table.

Worth mentioning is that the X-ray intensity ratio used in drawing the silica calibration graph was calculated without subtracting the background from the total counts. The equation of the straight calibration line is:

$$SiO_2\% = 31.88 \text{ X-ray Intensity Ratio} + 4.68$$

For a range of 34.09 - 37.02% SiO_2, the deviations range was +0.22 to -0.32%. Assuming that the chemical data are accurate and represent the arithmetic mean, the standard deviation of the X-ray results from the chemical values was calculated as:

$$S = 0.17\% \ SiO_2$$
$$\bar{Sx} = 0.05\% \ SiO_2$$

TABLE 43

Comparison of X-ray Spectrographic Data and Chemical Analysis of SiO_2 in Biotites

Specimen No.	Chemical Analysis	X-Ray Spectrographic Analysis	
		SiO_2%	Deviations X-ray-Chemical
1	37.02	37.08	+0.06
2	36.08	35.90	-0.18
3	34.09	34.11	+0.02
4	34.68	34.69	+0.01
5	34.47	34.57	+0.10
6	35.64	35.36	-0.28
7	35.63	35.77	+0.14
8	36.41	36.55	+0.14
9	35.87	35.55	-0.32
10	35.23	35.34	+0.11
11	34.29	34.37	+0.06
12	36.34	36.56	+0.22

Assuming that $\bar{x}$ = 34% and $\bar{x}$ = 37% (The lowest and highest values of silica in the minerals analysed), the relative deviation in terms of per cent of the amount present is:

$C_{34\%} = 0.50$ $E_{34\%} = 0.14$

$C_{37\%} = 0.46$ $E_{37\%} = 0.13$

(ii) Aluminium oxide

The results of the analysis of aluminium oxide are shown graphically in Fig. 13b. The comparison between the chemical and the X-ray data is shown in Table 44.

The standard deviation of the X-ray analysis from the chemical data is:

$S = 0.29\%\ Al_2O_3$ $S\bar{x} = 0.08\%\ Al_2O_3$

Assuming that $\bar{x}$ = 18.29 and 20.68% representing the lowest and highest alumina content in the samples analysed, then the coefficient of variation and the relative error in terms of per cent of the amount present are:

$C_{18.29} = 1.58$ $E_{18.29} = 0.04$

$C_{20.68} = 1.40$ $E_{20.68} = 0.04$

In view of the facts that:

1. the statistical figures of accuracy are comparable to those of the precision of the analysis, and
2. the symmetrical distribution of the deviations with regards to their positive and negative signs, indicates that there is no bias

TABLE 44

Comparison of X-ray Spectrographic Data with Chemical Data for Al_2O_3 in Biotites

Specimen No.	Chemical Analysis	X-Ray Analysis	Deviation X-ray - Chemical
1	20.62	21.15	+0.53
2	18.29	18.22	-0.07
3	19.60	19.66	+0.06
4	20.68	20.20	-0.48
5	19.74	19.65	-0.09
6	19.75	19.73	-0.02
7	18.85	19.05	+0.20
8	19.46	19.35	-0.11
9	20.07	20.37	+0.30
10	20.39	20.39	0.00
11	20.45	19.99	-0.46
12	16.13	16.30	+0.17

Figure 13.

The error bar limits on this and subsequent similar figures are the standard deviation of the X-ray precision results and the results for accuracy of rapid analysis in Mercy (1956).

Fig. 13

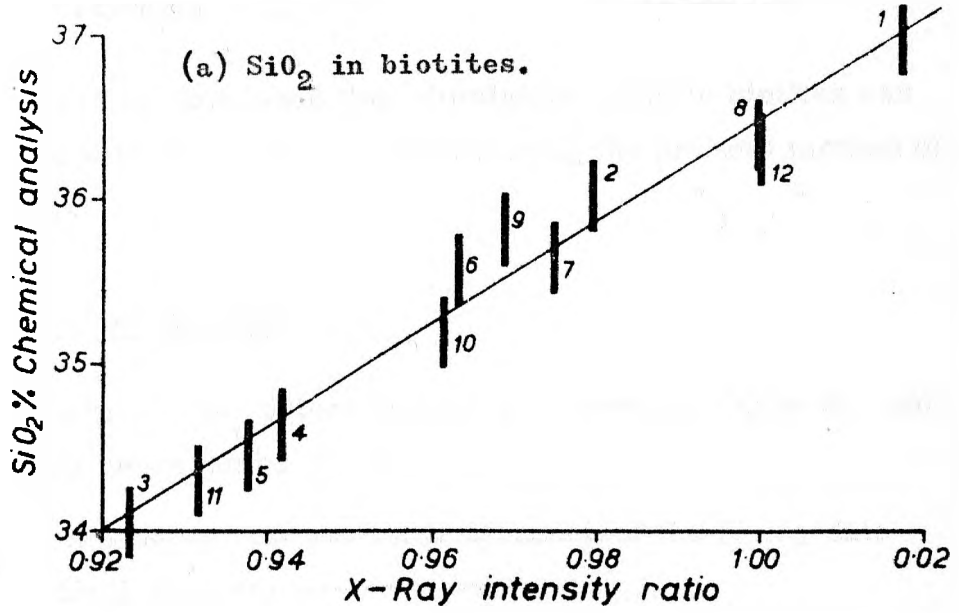
(a) SiO_2 in biotites.
SiO_2 % Chemical analysis
37
36
35
34
0·92
0·94
0·96
0·98
1·00
0·02
X-Ray intensity ratio
1
2
3
4
5
6
7
8
9
10
11
12

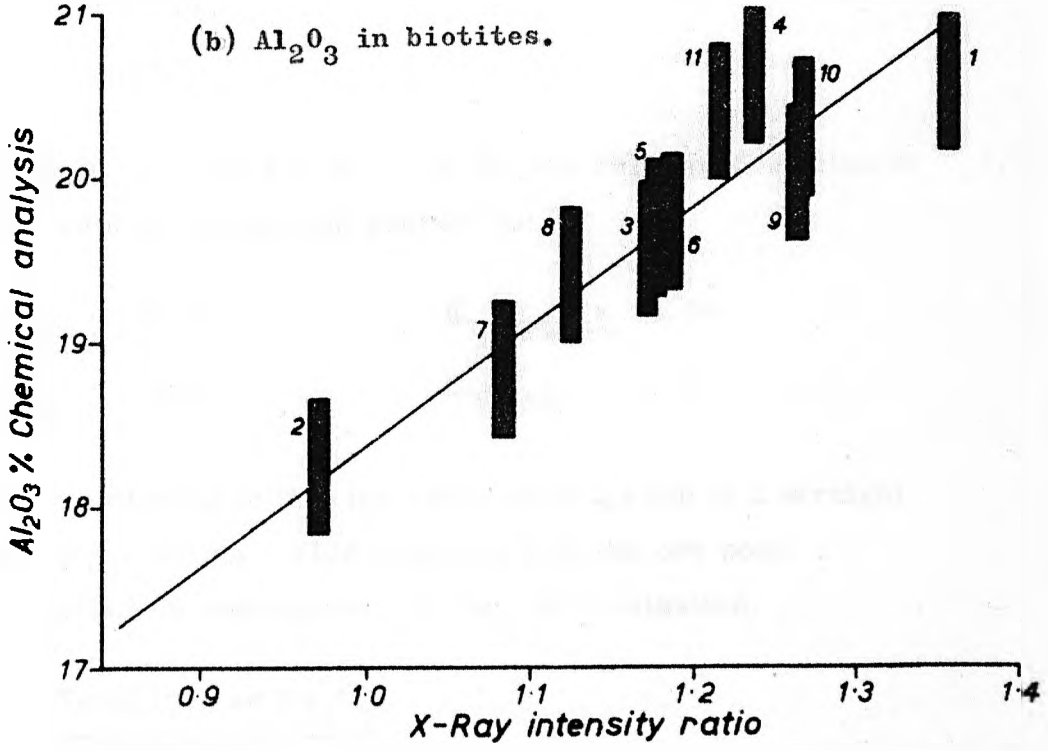
(b) Al_2O_3 in biotites.
Al_2O_3 % Chemical analysis
21
20
19
18
17
0·9
1·0
1·1
1·2
1·3
1·4
X-Ray intensity ratio
1
2
3
4
5
6
7
8
9
10
11

in the X-ray analysis towards either higher or lower results than the chemical analysis,

therefore, it can be concluded that aluminium oxide in biotites can be determined with reasonable accuracy using the present method of X-ray analysis.

(iii) Titanium oxide

The results of TiO_2 determination are shown in Table 45. and are graphically represented in Fig. 14a.

For these results, the standard deviation of the X-ray data from the chemical analysis is:

$S = 0.16\%\ TiO_2$

$Sx^- = 0.04\%\ TiO_2$

Assuming that $x^- = 1.40$ and $x^- = 3.39$, the relative deviation in terms of per cent of the amount present is:

$C_{1.40\%} = 11.14$ $\qquad$ $E_{1.40\%} = 3.04$

$C_{3.39\%} = 4.72$ $\qquad$ $E_{3.39\%} = 1.26$

Worth mentioning is that the calibration graph is a straight line passing to the origin. This suggests that the one point calibration method is satisfactory in TiO_2 determination.

(iv) Total Iron as Fe_2O_3

Iron was determined twice using the same set of pellets but

TABLE 45

Comparison of X-ray Spectrographic Data and Chemical Analysis of TiO_2 in Biotites

Specimen No.	Chemical Analysis	% Oxide	Deviation X-ray-Chem. An.
1	1.60	1.52	-0.08
2	1.74	1.68	-0.06
3	2.83	2.90	+0.07
4	2.95	2.90	-0.05
5	3.02	2.90	-0.12
6	2.25	2.18	-0.07
7	1.57	1.48	-0.09
8	1.53	1.57	+0.04
9	1.58	1.58	0.00
10	2.01	1.91	-0.10
11	3.39	3.00	-0.39
12	3.00	3.00	0.00
13	1.57	1.75	+0.18
14	1.40	1.71	+0.31

Fig. 14

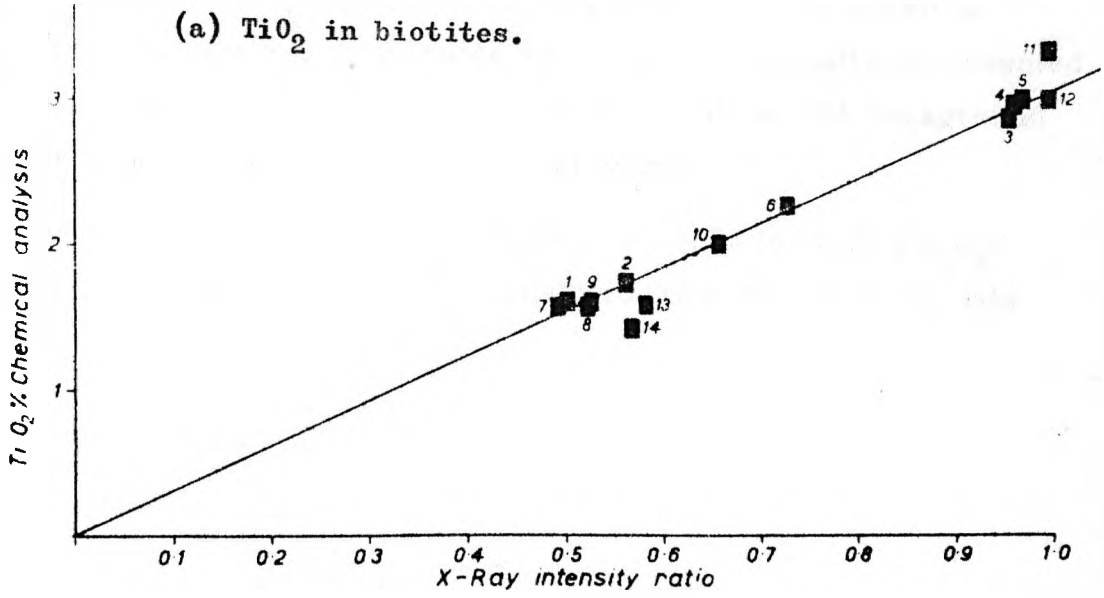
(a) TiO_2 in biotites.
TiO_2 % Chemical analysis
X-Ray intensity ratio
1
2
3
0·1
0·2
0·3
0·4
0·5
0·6
0·7
0·8
0·9
1·0

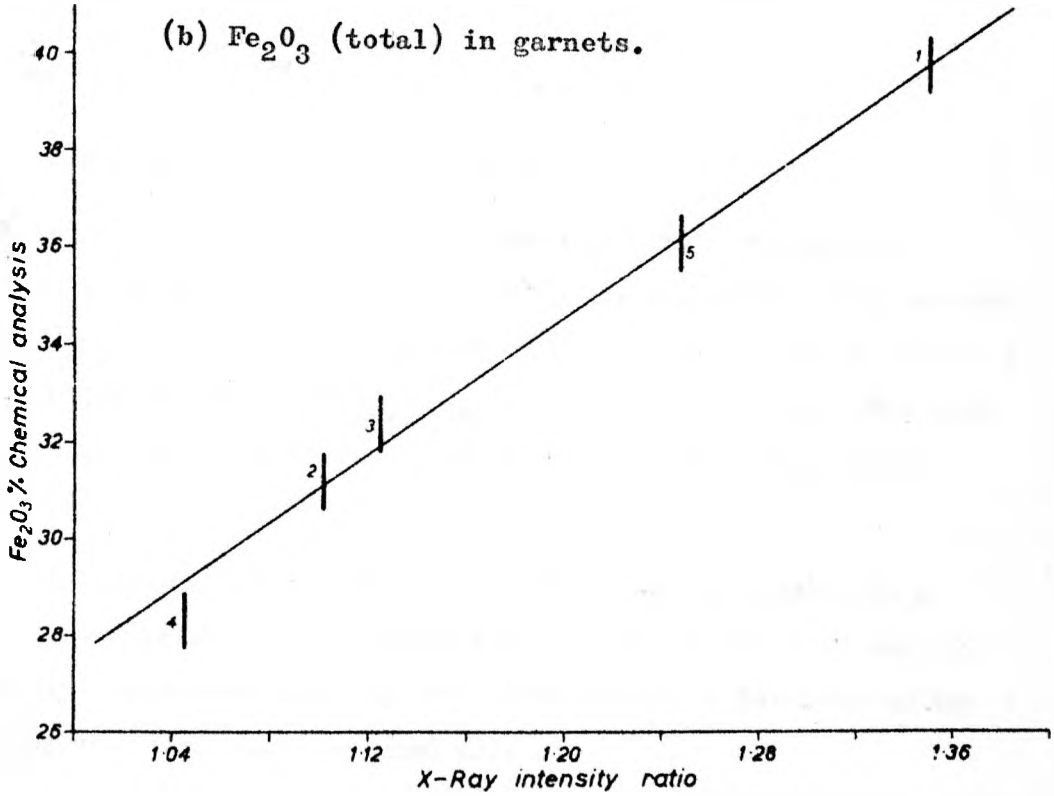
(b) Fe_2O_3 (total) in garnets.
Fe_2O_3 % Chemical analysis
X-Ray intensity ratio
26
28
30
32
34
36
38
40
1·04
1·12
1·20
1·28
1·36

using different hole size mask for each test. Test No. 1. was done using a mask with a big hole. The results of this test is shown in column marked Test No. 1. in Table 46 and are graphically represented in Fig. 15a. In calculating the X-ray intensity ratios, the background counts were not subtracted from the total counts.

For this test, the range of deviation is +1.23 to -1.08 Fe_2O_3. The standard deviation of the X-ray analysis from the chemical data is:

$$S = 0.62\% \ Fe_2O_3$$
$$S\bar{x} = 0.17\% \ Fe_2O_3$$

Assuming that $\bar{x} = 16.42$ and $\bar{x} = 27.71$, then

$$C_{16.42\%} = 3.77 \qquad E_{16.42\%} = 1.05$$
$$C_{27.71\%} = 2.24 \qquad E_{27.71\%} = 0.62$$

(figures are in per cent of the amount present).

However, these figures of accuracy are not satisfactory regarding the high fluorescent yield of Fe Ka radiation. The sample preparation itself was shown earlier to be precise (Table 41, p. 119) with S = 0.24% Fe_2O_3 and $C_{25.27\%} = 0.95$. Therefore, this high deviation was thought to be due to sample mispresentation and a second test was done.

In the second test (Test No. 2 in Table 46), a mask with a smaller hole was used. The results are shown in Table 46 and are graphically represented in Fig. 15b. The standard deviation of the X-ray analysis from the chemical data is:

TABLE 46

Comparison of X-Ray Spectrographic Data and Chemical Analysis of Total Iron as Fe_2O_3 in Biotites and Garnets

Specimen No.	Chemical Analysis	X-Ray Spectrographic Analysis Test No. 1. (Fig. 15a) % oxide	Deviation X-ray-Chem. An.	Test No. 2. (Fig. 15b) % oxide	Deviation X-ray-Chem. An.
1	16.42	16.67	+0.25	16.98	+0.56
2	21.61	22.84	+1.23	21.70	+0.09
3	27.71	27.88	+0.17	27.78	+0.07
4	25.54	25.02	-0.52	25.84	+0.30
5	23.74	22.66	-1.08	23.37	-0.37
6	22.64	22.61	-0.03	22.52	-0.12
7	23.66	23.42	-0.24	23.32	-0.34
8	21.06	21.46	+0.40	21.49	+0.43
9	21.72	21.67	-0.05	21.18	-0.54
10	22.69	23.31	+0.62	23.11	+0.42
11	22.23	21.72	-0.52	21.84	-0.39
12	25.27	26.27	+1.00	26.15	+0.88
13	18.62	18.43	-0.19	18.52	-0.10
14	24.92	25.27	+0.35	25.05	+0.13
Garnets (Fig. 14b)					
1	39.83	40.02	+0.19		
2	31.20	30.97	-0.23		
3	32.39	31.83	-0.56		
4	28.30	28,90	+0.60		
5	36.02	36.12	+0.10		

Fig. 15

Fe_2O_3 (total) in biotites.

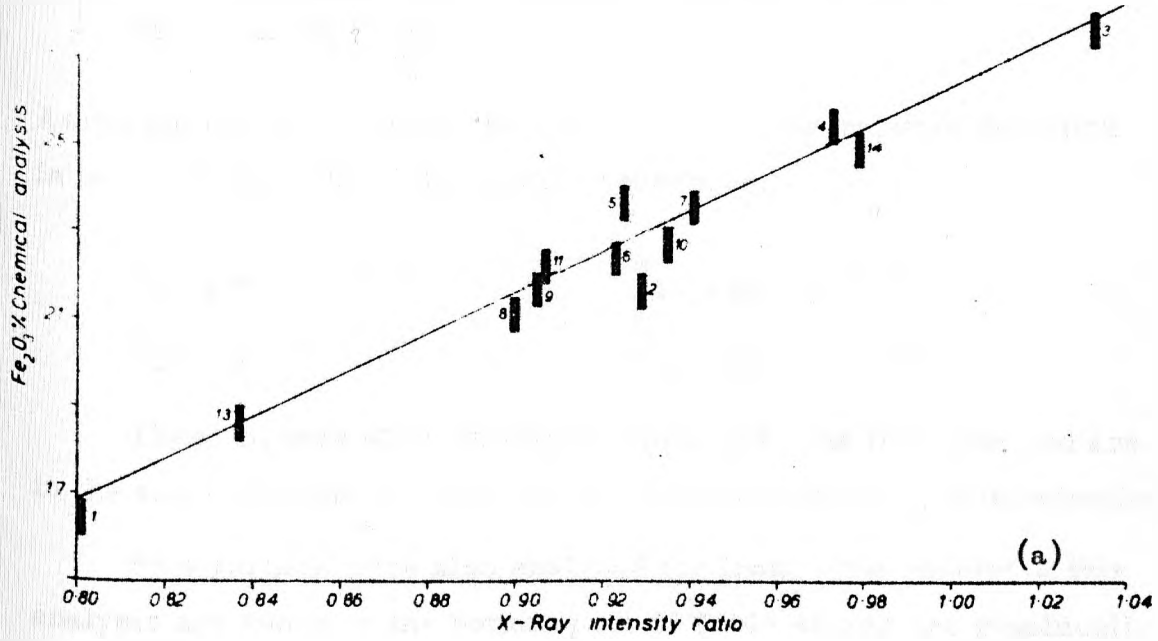

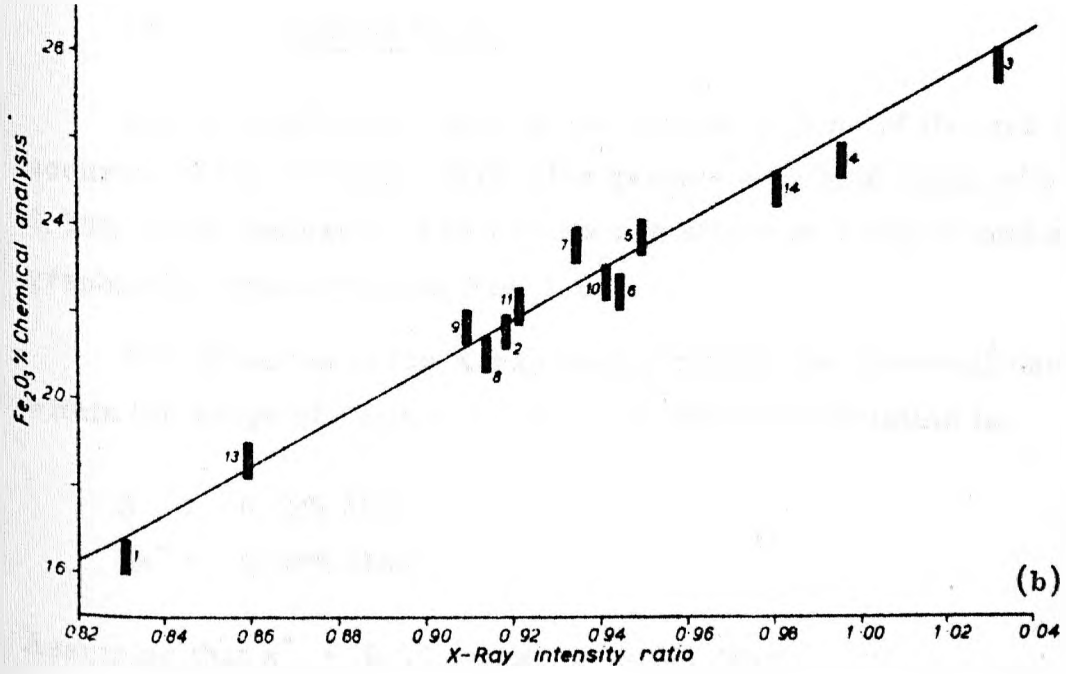

$S = 0.42\%\ Fe_2O_3$

$S_{\bar{x}} = 0.11\%\ Fe_2O_3$

Assuming that $\bar{x} = 16.42$ and $\bar{x} = 27.71$, the relative deviation in terms of per cent of the amount present is:

$C_{16.42\%} = 2.55$ $\qquad$ $E_{16.42\%} = 0.71$

$C_{27.71\%} = 1.51$ $\qquad$ $E_{27.71\%} = 0.42$

These figures show an improvement over the first test and are in the same time satisfactory for the accuracy of Fe_2O_3 determination.

Five garnets were also analysed for iron. The results of this analysis are shown in the bottom part of Table 46 and are graphically represented in Fig. 14b. The range of deviation is the same as that of the biotites.

(v) Manganese Oxide

MnO was not determined in the biotite because of its lack of accurate chemical data. Yet, five garnets with MnO range of 0.75-9.30% were analysed. The results are shown in Table 47 and are graphically represented in Fig. 16a.

The deviation of the X-ray analysis from the chemical data is within the range of +0.16 to -0.11. The standard deviation is:

$S = 0.12\%$ MnO

$S_{\bar{x}} = 0.05\%$ MnO

Assuming that $\bar{x} = 0.75$ and $\bar{x} = 9.30$, then,

TABLE 47

Comparison of X-ray Spectrographic Data and Chemical Analysis of MnO in Garnets

Specimen No.	Chemical Analysis	X-ray Spectrographic Analysis	
		MnO%	Deviation X-ray-Chem. Anal.
1	0.75	0.75	0.00
2	9.30	9.30	0.00
3	0.91	0.80	-0.11
4	9.14	9.05	-0.09
5	6.17	6.33	+0.16

$C_{0.75\%} = 16.00$ $E_{0.75\%} = 7.15$

$C_{9.30\%} = 1.29$ $E_{9.30\%} = 0.57$

It can be concluded that the method is accurate enough for MnO determination.

(vi) Calcium Oxide

As in the case of manganese, CaO was analysed for only in the garnets. The results are shown in Table 48 and are graphically represented in Fig. 16b.

For a range of 0.17-8.63% CaO, the deviation of the X-ray data from the chemical analysis was +0.10 to -0.45. Only one specimen (Garnet No. 1) showed this high 0.45% deviation. The standard deviation is

$S = 0.23\%$ CaO

$S_{\bar{x}} = 0.10\%$ CaO

Assuming the $\bar{x} = 2.65$ (the average CaO composition of the five garnets analysed), then,

$C_{2.65\%} = 8.68$ $E_{2.65\%} = 3.77$

(vii) Magnesium Oxide

Magnesia in biotites and garnets were analysed. The results are shown in Table 49 and are graphically represented in Figs. 17a and b. Worth mentioning is that the calibration graph is in the form of a straight line passing to the origin. This means that direct comparison

TABLE 48

Comparison of X-ray Spectrographic Data and Chemical Analysis of CaO in Garnets

Specimen No.	Chemical Analysis	X-ray Spectrographic Analysis	
		CaO%	Deviation X-ray - Chem. Anal.
1	1.20	0.75	-0.45
2	0.67	0.68	+0.01
3	8.63	8.69	+0.06
4	2.60	2.70	+0.10
5	0.17	0.23	+0.06

Fig. 16

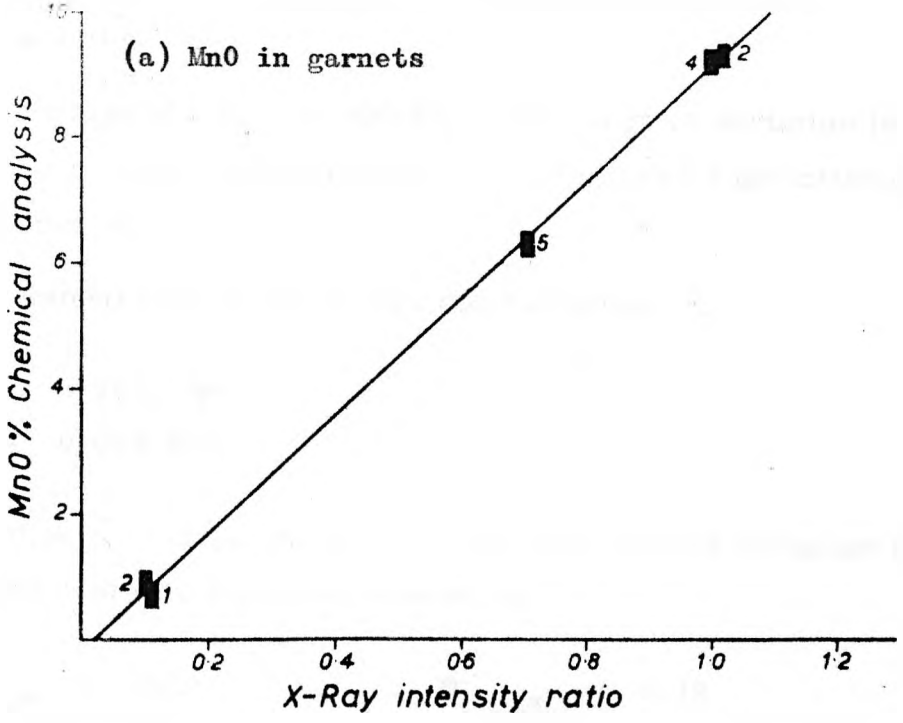
(a) MnO in garnets
MnO % Chemical analysis
X-Ray intensity ratio
0·2
0·4
0·6
0·8
1·0
1·2
2
4
6
8
4
2
5
2
1

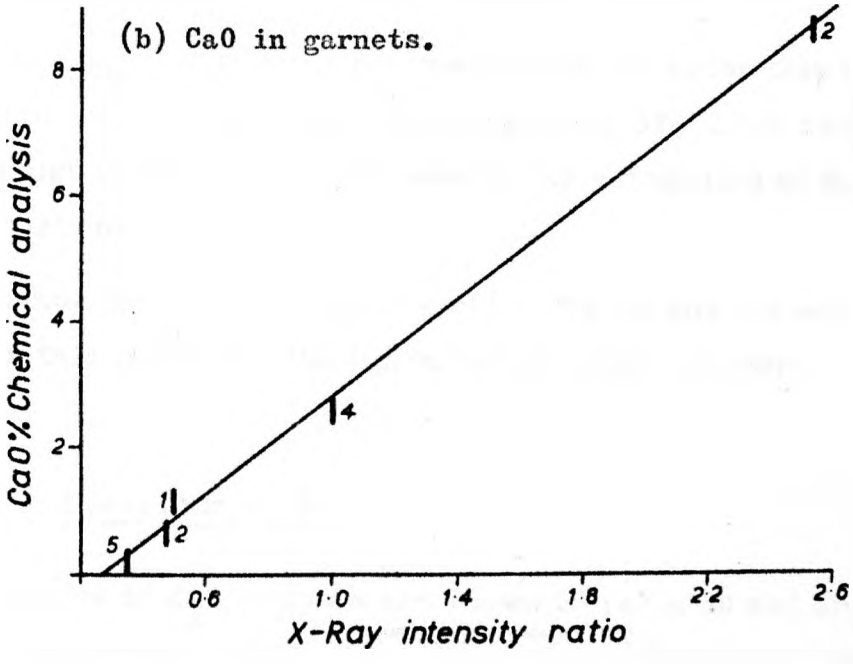
(b) CaO in garnets.
CaO % Chemical analysis
X-Ray intensity ratio
0·6
1·0
1·4
1·8
2·2
2·6
2
4
6
8
2
4
1
2
5

between two X-ray intensity ratios i. e. one point calibration technique is valid.

For a range of 1. 02 - 12. 81% MgO, the range of deviation is +0. 44 to -0. 52. Only one specimen out of 18 showed a deviation of -0. 93% (Garnet No. 1).

The standard deviation in MgO determination is:

$S = 0.25\%$ MgO

$S_{\bar{x}} = 0.06\%$ MgO

Assuming that $\bar{x} = 1.02$ and $\bar{x} = 12.81$, the relative deviation in terms of per cent of the amount present is:

$C_{1.02\%} = 24.50$ $\quad$ $E_{1.02\%} = 6.12$

$C_{12.81\%} = 1.95$ $\quad$ $E_{12.81\%} = 0.49$

The figure $C_{1.02\%} = 24.50$ is not realistic in the sense that all the garnet speciments with low MgO concentration (1. 02 - 1. 59) never showed the high deviation of 0. 25% used in the calculation of the above relative deviations.

Regarding the low fluorescent yield of Mg Ka and the soft character of this radiation, the figures of accuracy are very satisfactory.

(viii) Potassium oxide

The results of K_2O analysis are shown in Table 50 and are graphically represented in Fig. 18. The standard deviation of the X-ray analysis from the chemical data is:

TABLE 49

Comparison of X-ray Spectrographic Data and Chemical Analysis of Magnesium Oxide in Biotites and Garnets

Specimen No.	Chemical Analysis	X-Ray Spectrographic Analysis	
		MgO%	Deviation X-ray - Chemical
Biotites			
1	12.81	12.91	+0.10
2	9.68	10.12	+0.44
3	5.44	5.79	+0.35
4	5.55	5.36	-0.19
5	8.40	8.65	+0.25
6	8.91	9.10	+0.19
7	8.93	8.60	-0.33
8	10.60	10.40	-0.20
9	10.02	9.72	-0.30
10	8.84	8.32	-0.52
11	8.33	8.14	-0.19
12	8.09	8.10	+0.01
14	9.78	9.88	+0.10
Garnets			
1	3.26	2.33	-0.93
2	1.21	1.31	+0.10
3	1.02	1.01	-0.01
4	1.59	1.75	+0.16
5	1.34	1.20	-0.14

Fig. 17

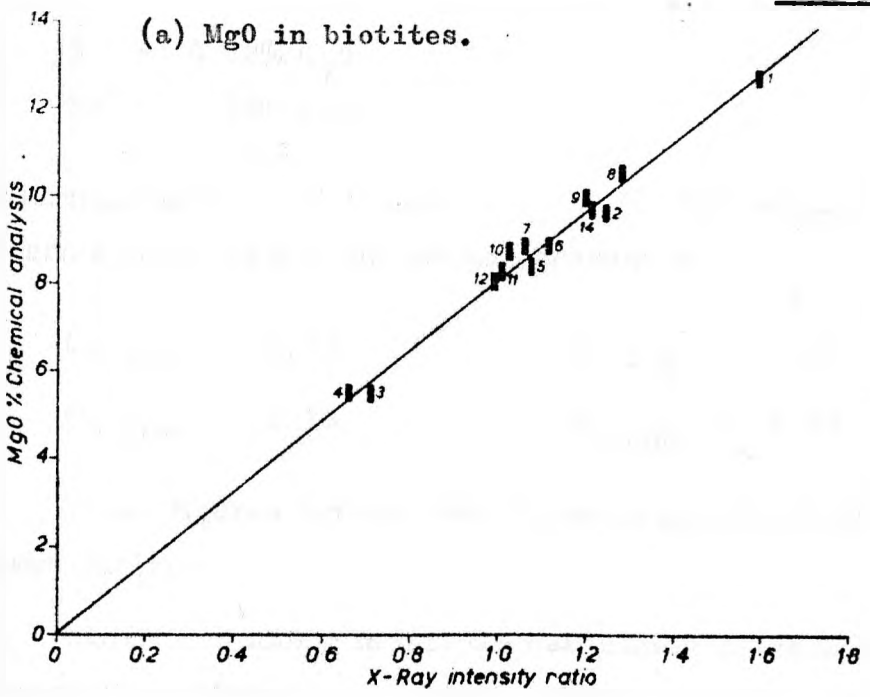
(a) MgO in biotites.
MgO % Chemical analysis
X-Ray intensity ratio
0
2
4
6
8
10
12
14
0·2
0·4
0·6
0·8
1·0
1·2
1·4
1·6
1·8

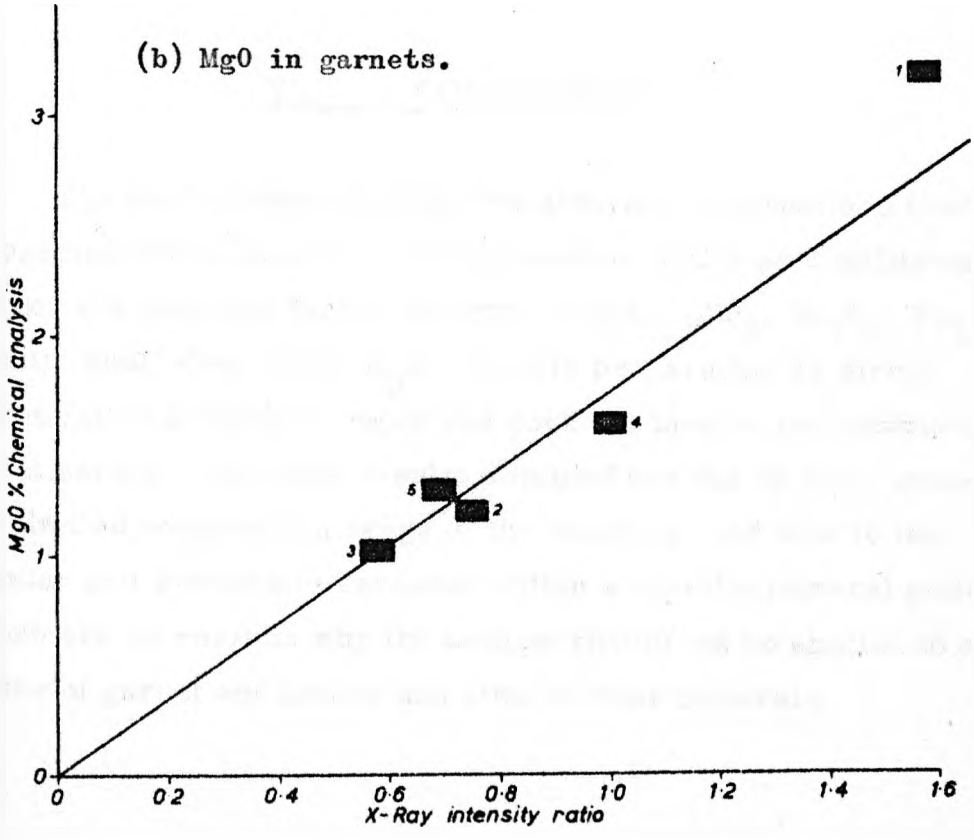
(b) MgO in garnets.
MgO % Chemical analysis
X-Ray intensity ratio
0
1
2
3
0·2
0·4
0·6
0·8
1·0
1·2
1·4
1·6

$S = 0.22\% K_2O$

$Sx^- = 0.06\% K_2O$

Assuming that $x^- = 7.51$ and $x^- = 9.60$, the relative deviation in terms of per cent of the amount present is:

$C_{7.51\%} = 2.92$ $\quad$ $E_{7.51\%} = 0.80$

$C_{9.60\%} = 2.29$ $\quad$ $E_{9.60\%} = 0.63$

These figures indicate that the accuracy of K_2O determination is satisfactory.

Worth mentioning is that the calibration graph of K_2O is a straight line passing to the origin. Hence, the use of one point calibration technique is valid and can be applied for K_2O determination.

VI. CONCLUSIONS

The method described for the analysis of garnet and biotite is precise and accurate. 5 milligrams of biotite or 8 milligrams of garnet are required for the analysis of SiO_2, TiO_2, Al_2O_3, Fe_2O_3 (total), MnO, CaO, MgO, K_2O. Sample preparation by direct pelletization is simple, rapid and does not involve the destruction of the minerals. The good results obtained are due in some measure to the limited composition range of the samples, and also to the regular and systematic variation within a specific mineral suite. There are no reasons why the method should not be applied to other suites of garnet and biotite and also to other minerals.

TABLE 50

Comparison of X-ray Spectrographic Data and Chemical Analysis of K_2O in Biotites

Specimen No.	Chemical Analysis	X-ray Spectrographic Analysis	
		% Oxide	Deviation X-ray - Chem. An.
1	8.74	8.74	0.00
2	7.51	7.61	+0.10
3	8.79	9.23	+0.44
4	8.74	8.69	-0.05
5	9.37	9.27	-0.10
6	9.10	8.88	-0.22
7	8.20	8.37	+0.17
8	8.38	8.68	+0.30
9	8.84	8.89	+0.05
10	8.63	8.79	+0.16
11	9.44	9.21	-0.23
12	9.60	9.60	0.00
13	8.32	8.33	+0.01
14	8.73	8.33	-0.40

Fig. 18

K_2O in biotites.

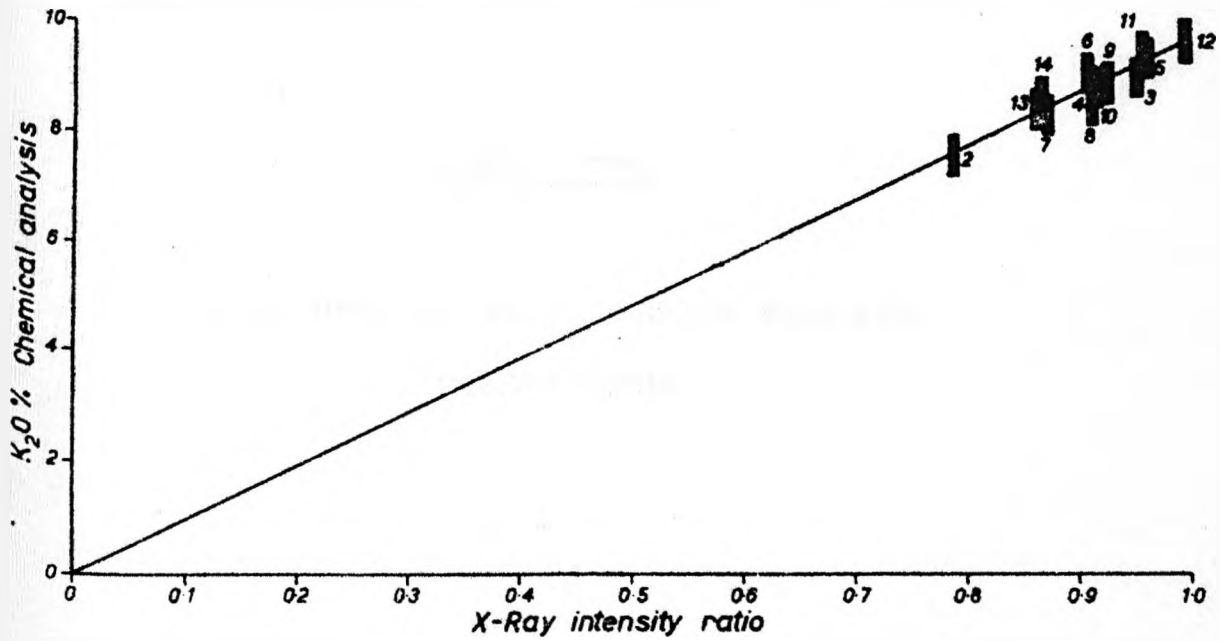

PART TWO

A REVIEW OF THE ALUMINIUM SILICATE POLYMORPHS

Andalusite, sillimanite and kyanite are trimorphic minerals of the compound Al_2SiO_5. It is believed that their stability fields consist of 3 divariant areas bound by univariant equilibrium lines and their phase diagram can assume either of 2 patterns viz. one consisting of two univariant equilibrium lines with no point in common or else consisting of three univariant equilibrium lines having one common invariant point, i. e. a triple point.

The wide occurrence of these minerals either individually or in pairs or sometimes all the three polymorphs together in metamorphic rocks (Hietanen, 1956), makes the study of the system Al_2O_3 - SiO_2 very attractive to metamorphic petrologists and experimentalists as it appears to afford a clue to the relationships between temperature and pressure of metamorphism.

The determination of the equilibrium relations between the trimorphs is usually approached by three different ways: hypothetical, experimental or on the basis of geological occurrences and petrological data. A comprehensive discussion of the aluminium silicate polymorphs is given by Pitcher, 1965. A brief outline of the previous work done on these polymorphs with a particular emphasis on work done after Pitcher's 1965 review is given below.

Because of the unreliability of the existing thermochemical data as well as the small differences in the thermochemical constants of the aluminium silicates, the construction of a phase diagram based on these data does not provide a model which is consistent with petrological data. Thus, the phase diagrams of Fyfe et al., (1958) and Kumagai and Ito (1959) consist of two univariant equilibrium lines with no common triple point. Both diagrams indicate that kyanite is the high pressure polymorph, andalusite is the low-pressure

high-temperature polymorph and sillimanite is the low pressure and low-temperature polymorph. However, after the accumulation of more thermodynamic and experimental results (e. g. Skinner et al., 1961; Pankratz and Kelly, 1964; Evans, 1965; Newton, 1966a and B; Weill, 1966; Holm and Kleppa, 1966;) Fyfe (1967) analysed the available data and constructed a phase diagram which assumed an inverted Y-shape, i. e. with a common invariant triple point. On the other hand, Karpov (1967) considers that all the work that has been done on the Al_2O_3 - SiO_2 system gives a rather indeterminate and inconsistent picture. He considered that calculations of the stability of aluminium silicate modifications lack the necessary values for the standard enthalpies of formation of the three polymorphs and "only very recently, thanks to the successful measurement of the enthalpies of formation of kyanite, andalusite, sillimanite and mullite from oxides at 695°C made by Holm and Kleppa (1966) using the method of dissolution in fused oxides, have such calculations been possible" (p. 143). Consequently, on the basis of thermodynamic data and independently of experimental research, Karpov (1967) presents his phase diagram which assumes the inverted-Y shape. However, the P-T values, slope of the phase boundaries and the position of the triple point are completely different from those in Fyfe's (1967) phase diagram.

On geological grounds, Miyashiro (1949) suggested his inverted-Y phase diagram which shows kyanite to be stable at high pressures - low temperature, sillimanite at moderate pressure-high temperature and andalusite at low pressure and temperature. This general form of phase diagram is now accepted and confirmed to some extent by experimentalists through their attempts to define the slope and position of the field boundaries.

The experimental work on the Al_2O_3 - SiO_2 system is based on studying the P and T conditions of either the independent synthesis of each polymorph or the inversion of one polymorph to another, but real progress was not made until after the identification of mullite by Bowen et al., (1924) and the development of simple hydrothermal techniques in the late 1940's. The experimental results were, not unexpectedly, subject to doubts, changes and criticisms. Thus Roy and Osborn (1954) could not distinguish sillimanite from mullite in attempts to synthesise the former. They were also unable to reproduce the earlier synthesis experiments of Michel-Levy (1950) and Balconi (1941). Roy (1954) and Roy and Roy (1955) synthesised andalusite with the use of seed crystals or impurities (e.g. Ca^{2+}, Mg^{2+}) but later Aramaki and Roy (1959 and 1963) discovered that it was a new polymorph and suggested a whole family of ordered disordered phases of the aluminium silicates which would affect the P-T curves of the system. Earlier, Aramaki and Roy (1958) were unable to synthesise kyanite below 600°C at up to 5 K bars either in the Al_2O_3 - SiO_2 - H_2O system or with the addition of various mineralizers. On the other hand, Coes (1955) synthesised the three polymorphs from kaolin at 10 - 20 K bar and a temperature of 700-900°C in the presence of Na salt producing andalusite, and fluorides producing sillimanite; kyanite formed easily as a by-product appearing simultaneously with sillimanite and andalusite. Carr and Fyfe (1960) showed that in experiments using different starting materials, the pressure/temperature field in which a phase or assemblage of phases may be synthesized need not be identical with that in which it is stable (Pitcher, 1965). Roy and Roy (1955) stress the importance of the presence of impurities when attempting to correlate experimental

equilibrium data with natural occurrences "since in nature a host of impurities are available" (p. 174).

Clark et al., (1957) and Clark (1961) in determining the kyanite-sillimanite boundary found that reversible transformation was obtained only above 1300°C. In 1957, extrapolation to lower temperature and pressures ranges was done by computation and in 1961, Clark used additional synthesis experiments to carry the boundary to 1000°C. This work was criticized by:-

(1) Fyfe (1967) who considers that extrapolation at lower T is a difficult matter. Moreover, "in a synthesis experiment involving two polymorphs it is normal for one to nucleate and grow more readily than the other. If such synthesis is carried out in a region where reaction between polymorphs is sluggish, the polymorph formed more readily may persist. This is impossible at temperatures where reversal is rapid. Hence, a synthesis experiment need correctly reflect equilibrium only under conditions where reaction rates are known to be fast." (p. 70).

(2) Kitarov et al., (1963) argue that extrapolation of the phase line of Clark (1961) was done without taking into account other reactions which complicate the picture of the stable phase diagram. Consequently, the part of the diagram illustrating the kyanite-sillimanite phase boundary in the section above 900°C is relatively fully characterised whereas the position of other boundaries around fields of stability of separate phases remain uncertain, as do the position of the triple point.

Khitarov et al., (1963) determined the line kyanite-sillimanite in the lower temperature range (400-875°C and 9-15.7 K bar). They also succeeded in determining the line andalusite-sillimanite and gave a triple point value of 390°C/9 K bar. Independently, Bell (1963) using the same type of apparatus as that of Khitarov et al., (1963) arrived to a triple point at 300 ± 50°C/ 8 ± 0.5 K bar, a value which is near to that of Khitarov et al.

The results of both works have been criticized by Winkler (1965, 1967) who considers that the P-T estimates are low and contradict petrographic observations. He bases his criticism on the following grounds:-

(1) The coexistence of andalusite, kyanite and sillimanite in the staurolite zone - the lower part of amphibolite facies, "it is known with certainty that a temperature around 550°C must have been realized for these rocks to form" (Winkler, 1965, p. 165).

(2) If the data were correct, "the upper stability limit of pyrophyllite ought to transgress the field of stability of sillimanite in a relatively large range of pressure between 4-11 K bars" (ibid. p. 165).

The work of Khitarov et al., (1963) has been also criticized by Holm and Kleppa (1966) on the basis that Khitarov's kyanite-sillimanite curve has a too low a slope to be consistent with Clark's (1961) data and with the Clausius-Clapeyron relation and his sillimanite-andalusite-mullite-quartz non-variant point is completely out of line in view of Holm and Kleppa's (1966) data.

It is worth noticing that in the experimental determination of

the aluminium silicate phase diagram, the andalusite-kyanite boundary is in most cases a tentative attempt. Thus, Bell (1963) did not give any P-T data on the andalusite-kyanite equilibrium and Khitarov et al., (1963) were unable to determine the boundary between the two polymorphs. However, Weill (1963) showed that a carefully weighed andalusite crystal sealed with 30 mg. kyanite and 50 mg. distilled water and subjected to 3 K bar at 700°C gained 3.2% weight. On this evidence, Weill (ibid. p. 946) "believes this is to be the first unambiguous demonstration of the laboratory synthesis of andalusite."

For the position of the invariant triple point between kyanite, andalusite and sillimanite, the following values are quoted (see also Fig. 19):-

Based on petrological (+ experimental) data:-

Hietanen (1956)	about	400°C	
Schuiling (1957)		540°C	3.4 K bar
Sobolev (1960)		550°C	13 K bar (tentative)
Schuiling (1962)		550°C	7.5 K bar
Winkler (1965)		570°C	7.5 K bar
Winkler (1967)		595 ± 10°C	6.5 ± 0.5 K bar

Based on experimental work:-

Clark et al. (1957)	275°C	8.2 K bar (tentative)
Bell (1963)	300 + 50°C	8 ± 0.5 K bar
Khitarov et al. (1963)	390°C	9 K bar

Based on thermodynamics and thermochemical data:-

Waldbaum (1965)	340°C	8.7 K bar
Weill (1966)	410°C	2.4 K bar
Holm and Kleppa (1966)	477°C	5.9 K bar
Fyfe (1967)	430-470°C	2.1-2.8 K bar
Karpov (1967)	528°C	7.25 K bar

Apart from these criticisms and discrepancies in the determination of the phase relation between aluminium silicate polymorphs, the application of the experimental phase diagram to natural occurrences is open to other criticisms:-

(1) Natural system has not yet been closely simulated in the laboratory (Pitcher, 1965). According to Green (1963), the main aspects of this dissimilarity are that the experimental system is saturated with water and is not saturated with other minerals of natural assemblages. Indeed, the host of impurities found in natural rocks relative to the aluminium silicates are bound to affect their stability.

(2) According to Chinner (1966), the application of the aluminium silicate phase diagram to geothermometry depends for its validity on the two assumptions that the natural occurrences reflect equilibrium under P-T conditions of crystallisation and that pressure and temperature were the sole external controls.

(3) Rates of nucleation and growth are as important factors as temperature and pressure (c.f. Rast, 1965; Rutland, 1965).

(4) There is the possibility that the aluminium silicate polymorphs

Fig. 19

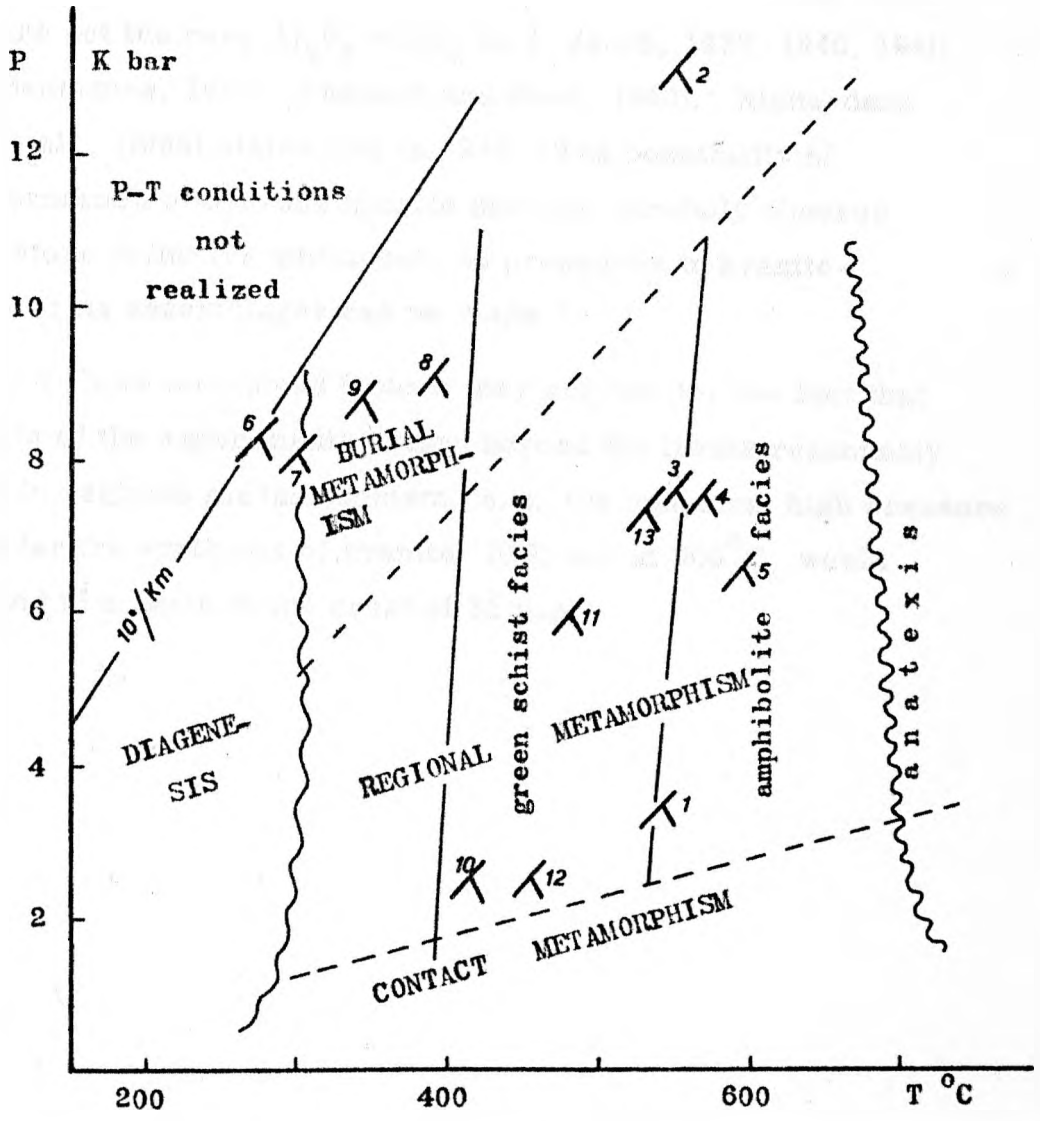

Kyanite–andalusite–sillimanite triple point.

Petrological: (1) Schuiling 1957; (2) Sobolev 1960; (3) Schuiling 1962; (4) Winkler 1965; (5) Winkler 1967; Experimental: (6) Clark et al 1957; (7) Bell 1963; (8) Khitarov et al 1963; Thermodynamic data: (9) Waldbaum 1965; (10) Weill 1966; (11) Holm and Kleppa 1966; (12) Fyfe 1967; (13) Karpov 1967. Position of facies boundaries after Winkler 1967.

> are not the pure $Al_2O_3 + SiO_2$ (c.f. Jacob, 1937, 1940, 1941; Henriques, 1957; Pearson and Shaw, 1960). Richardson et al., (1965) states that (p. 248) "The possibility of formation of hydrous kyanite must be carefully checked before definitive statements on pressures in kyanite-bearing assemblages can be made."

The above mentioned factors may account for the fact that the results of the experiments extend beyond the limits reasonably accepted in regional metamorphism, e.g. the unnatural high pressure required for the synthesis of kyanite, 10 K bar at 500°C, would correspond to a depth in the crust of 35 Km.

PART THREE

THE ALUMINIUM SILICATES-BEARING ROCKS IN THE CONTACT AUREOLES OF COUNTY DONEGAL GRANITES

INTRODUCTION

The wide variation in the mode of emplacement of the Granites in Co. Donegal, Eire, and the contact metamorphism associated with them provide an excellent situation to study the factors involved in the development of the different forms of aluminium silicates in the Granites' aureoles namely, andalusite, kyanite, sillimanite and fibrolite (Figs. 20, 21). The Granites are all of the high-level type and their intrusion can be ascribed to a late episode in the Caledonian drama (Read, 1961). They are intruded in an epizonal assemblage of folded sedimentary rocks and basic sills of Dalradian age (Pitcher and Read, 1963).

Part Three of the present thesis deals with the aluminium silicates bearing rocks occurring in the aureoles of 5 Donegal Granites, namely, the western Fanad granodiorite aureole, the aureole and enclaves of Thorr granodiorite, the Barnesmore granite aureole, the northern aureole of the Ardara pluton and the aureole of the Main Donegal granite. This part is divided in two chapters. The first chapter deals with the petrology of these rocks, their spatial arrangement in relation to the granites as well as the textural characteristics of the aluminium silicate minerals. In the second chapter, the results of the chemical and modal analyses are presented, followed by the discussion and interpretations of these results.

Fig. 20

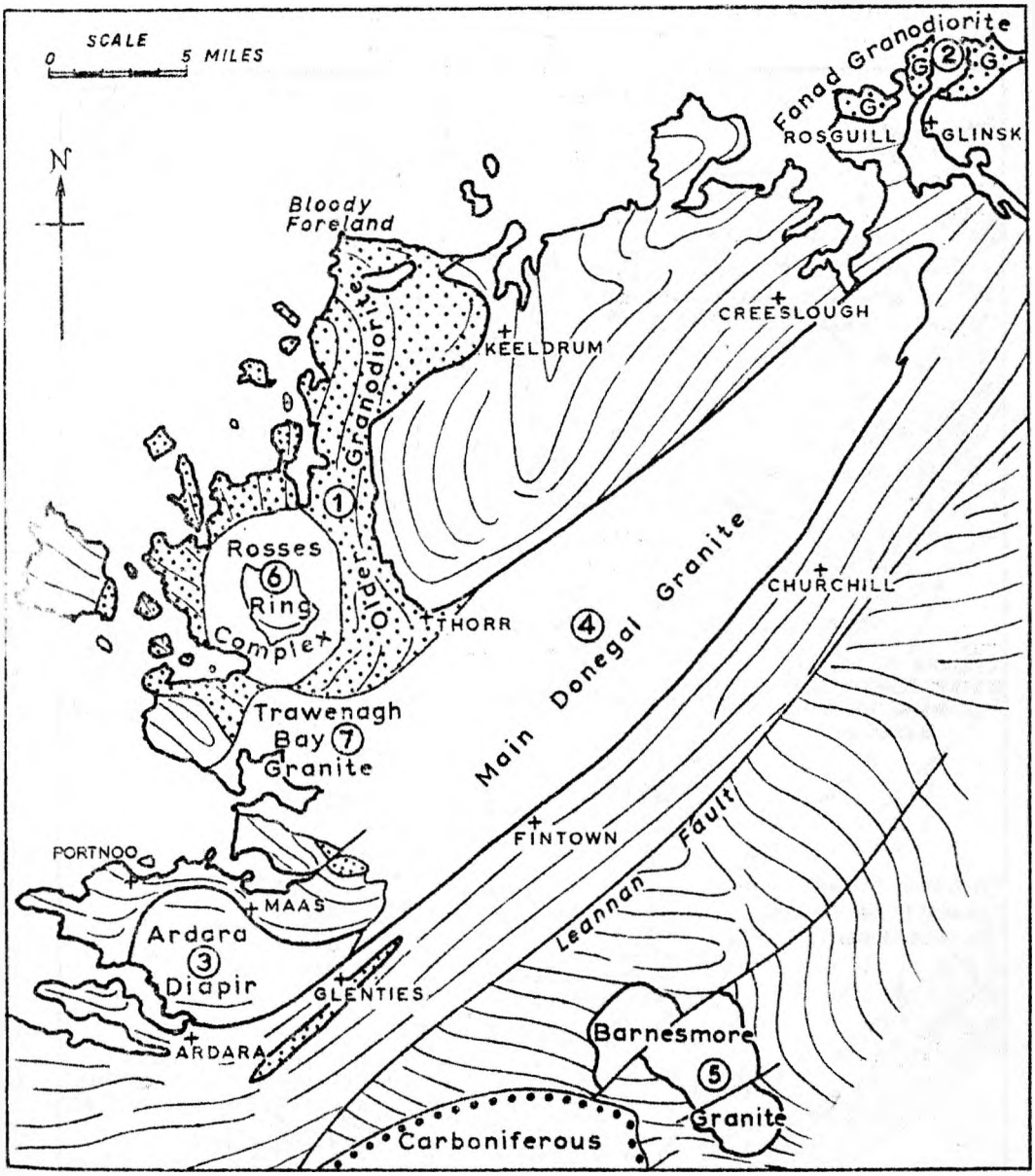

Geological sketch map of Donegal showing the distribution of 7 granite bodies (After Pitcher and Read 1963).

(1) Thorr Granodiorite
(2) Fanad granodiorite
(3) Ardara Granodiorite
(4) Main Donegal Granite
(5) Barnesmore Granite
(6) Rosses Granite
(7) Trawenagh Bay Granite.

Fig. 21

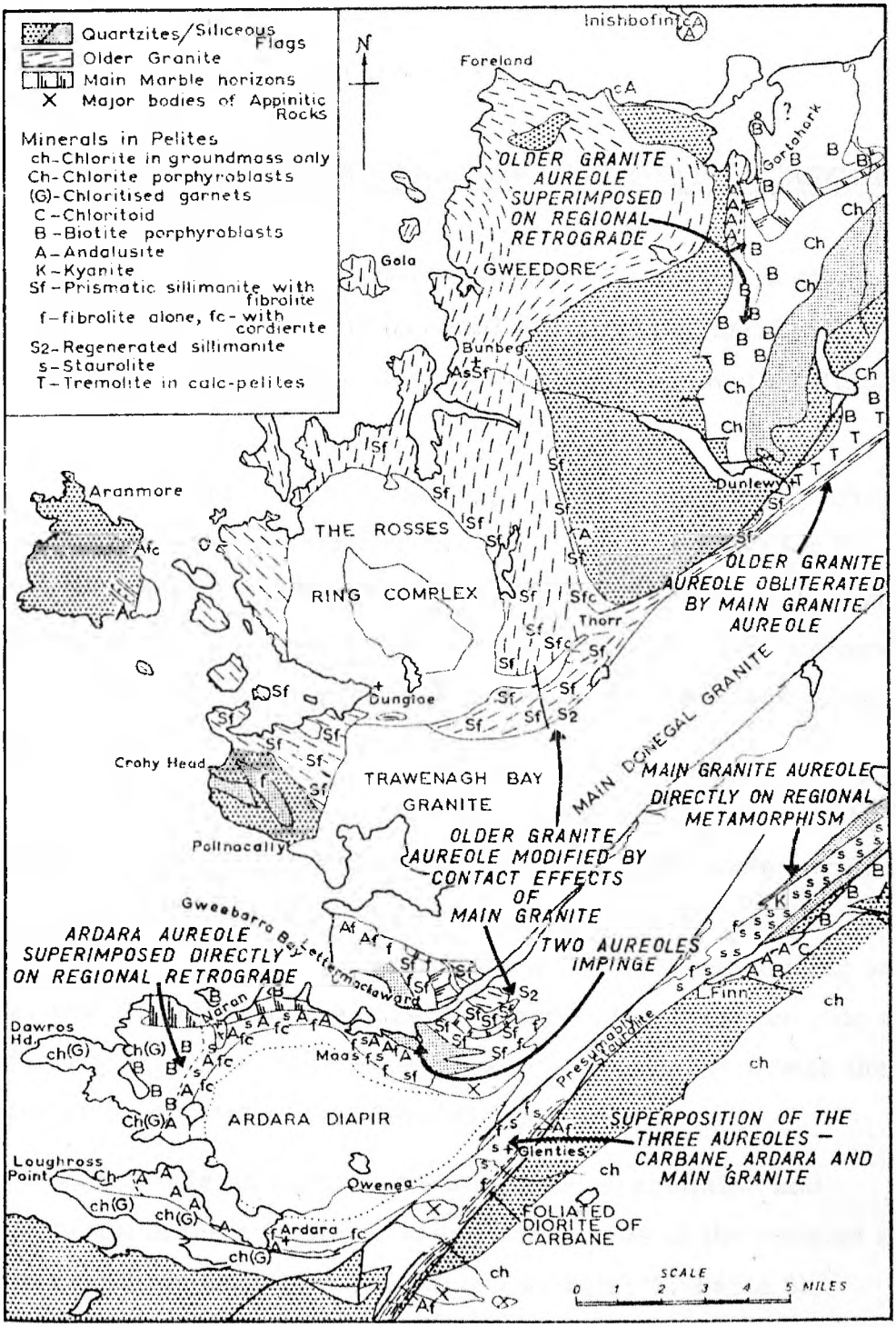

Geological sketch map of the western part of Donegal showing the distribution of metamorphic minerals (After Pitcher and Read 1963).

CHAPTER ONE

PETROLOGY

I. THE WESTERN FANAD GRANODIORITE AUREOLE

The geology of the Fanad Granodiorite complex is given by Hull et al., (1891), that of the Rosguill area by Knill and Knill, (1961) and a detailed study of the contact in the western Fanad by Pitcher and Read (1963).

The effect of contact metamorphism is studied in a pelitic horizon striking northwards into the Granite contact. In the regional parts, the rock is a fine grained quartz-chlorite-muscovite-garnet schist. With increasing metamorphism, it develops into a coarse biotite-rich hornfels with porphyroblasts of andalusite and mica-cordierite knots.

The regional rocks are evenly dipping and the schistosity is puckered in the strike direction. With advancing metamorphism, this uniform structure is obliterated in the hornfelses by the development of a winding heterogeneous structure. According to Pitcher and Read (1963), the aureole represents a metamorphic and metasomatic static recrystallisation which is associated with the reactive emplacement of the Fanad Granodiorite.

To follow is an outline of the mineral description and reconstitution in the aureole as seen in the rocks of the present study. For the modal amounts of these minerals, refer to Table 51.

Quartz is fine grained in the regional rocks. With increased metamorphism, it coarsens and segregates along the old schistosity

and along the new strain slip cleavage.

Feldspar: Plagioclase gradually enters the granulose rocks. It is mainly of andesine composition.

Iron ore: In the regional rocks, it forms elongated grains lying within the schistosity. In highly metamorphosed rocks, such alignment is still preserved in the spongy andalusite.

Chlorite-Biotite: In the regional and least metamorphosed schists, chlorite occurs as green knots that sometimes contain garnets, as rims around garnets, as well as pale green flakes formed after biotite in the groundmass. At about 1500 yards from the contact with the Granite, the first signs of biotite replacing chlorite appear. With increased metamorphism, the chlorite knots and rims and that in the groundmass are replaced by biotite. The biotite flakes usually lie within the schistosity but sometimes cut across it. In the coarse hornfels, the knots consist of deep brown biotite and muscovite flakes. Spongy crystals of andalusite may accompany the knots and in highly altered rocks, they contain cordierite. The overall change in biotite with increasing metamorphism is the deepening of its brown colour as well as an increase in size rather than in amount. In the 22 specimens analysed, the modal amount of biotite fluctuates between 14.8 - 40.9 with no general trend as the granite contact is approached.

Chlorite reappears as a retrograde mineral in the hornfelses, especially when fibrolite and shimmered andalusite are present.

Muscovite is dominant in the regional rocks but shows a general diminution with increased metamorphism. The modal amount of muscovite shows a gradual decrease from 36.1 - 2.8% as the

contact is approached (from specimen 4 to 22 in Fig. 22).

Garnet occurs in the regional rocks as kernels in the chlorite knots as well as big porphyroblasts (sometimes up to 5mm. across) which are chlorite rimmed. These garnets contain trails of inclusions set at varying angles to the schistosity. Sometimes, they are sieved with quartz inclusions. With advancing metamorphism, these garnets start to disappear and small perfectly idiomorphic fresh looking pink garnets reappear in the now biotite knots (Pl. 1a). These are considered as regenerated new garnets and are sometimes associated with remnants of the regional garnets (c. f. Atherton and Edmunds, 1966). Frequently, garnet occurs as inclusions in andalusite.

Andalusite appears first as thin slender crystals which gradually increase in size. Small subidiomorphic crystals occur in the groundmass at about 1100 yards from the Granite contact. Most of these andalusites have square outlines. Oblong crystals set at different angles or across the foliation also occur. The andalusite clearly overprints the groundmass preserving its schistose structure as indicated by the parallel alignment of mica and elongated grains of iron ore.

At about 1050 yards from the Granite contact, the andalusite develops as large spongy crystals lying within the schistosity along the biotite-muscovite bands. The andalusite here clearly replaces parts of the mica bands (Pl. 1b). The edges of the andalusite are in many cases ill-defined and the groundmass mica are seen to pass imperceptibly into andalusite. Idiomorphic basal sections of andalusite are present but infrequent. So far, no andalusite is noticed in the biotite knots.

At about 1000 yards from the Granite contact, andalusite appears in the biotite knots, sometimes containing garnet as inclusions (Pl. 1c). With increased metamorphism and the development of the hornfelsic texture, andalusite is present throughout the rock. Pink pleochroic idiomorphic to subidiomorphic crystals are seen together with the spongy type.

Andalusite is sometimes altered to shimmer aggregates. Nearer to the contact, it is partly replaced with coarse sillimanite.

Fibrolite is well developed at about 450 yards from the granite contact although it starts a few yards further away as occasional very minute wisps associated with biotite. Fibrolite occurs commonly as meandering bundles replacing the brown biotite. In cases where replacement is incomplete, the biotite becomes yellow and paler in colour. Sometimes, fibrolite aggregates form oblong masses with inclusions of iron oxide elongated in one direction parallel to the fibrolite elongation (Pl. 1d). The fibrolite in these masses is mingled with or coarsened to slender sillimanite prisms.

Fibrolite sometimes follows the grain boundaries of the pre-existing minerals including andalusite. In the latter case, there is no direct relation between the fibrolite and the andalusite except a purely mechanical one. However, in very few cases, small patches as well as needles of fibrolite are seen as inclusions in andalusite (Pl. 1e, f, 2a)

Sillimanite: Within the first 250 yards of fibrolite occurrence, coarse sillimanite crys tals are not seen. The first development of sillimanite is seen at about 230 yards from the granite contact where it occurs as slender prisms mingled with fibrolite (Pl. 2b).

Few yards nearer to the contact, stout prisms of sillimanite partly replace andalusite (Pl. 2c). Also, it sometimes develops in the groundmass independently from andalusite. In agreement with Pitcher and Read (1963), the coarse sillimanite is the later and the more stable form.

Potash feldspar first appears in rocks at about 600 yards from the granite contact. Its distribution is sporadic and occurs as well developed crystals or else mixed with plagioclase in a perthitic texture.

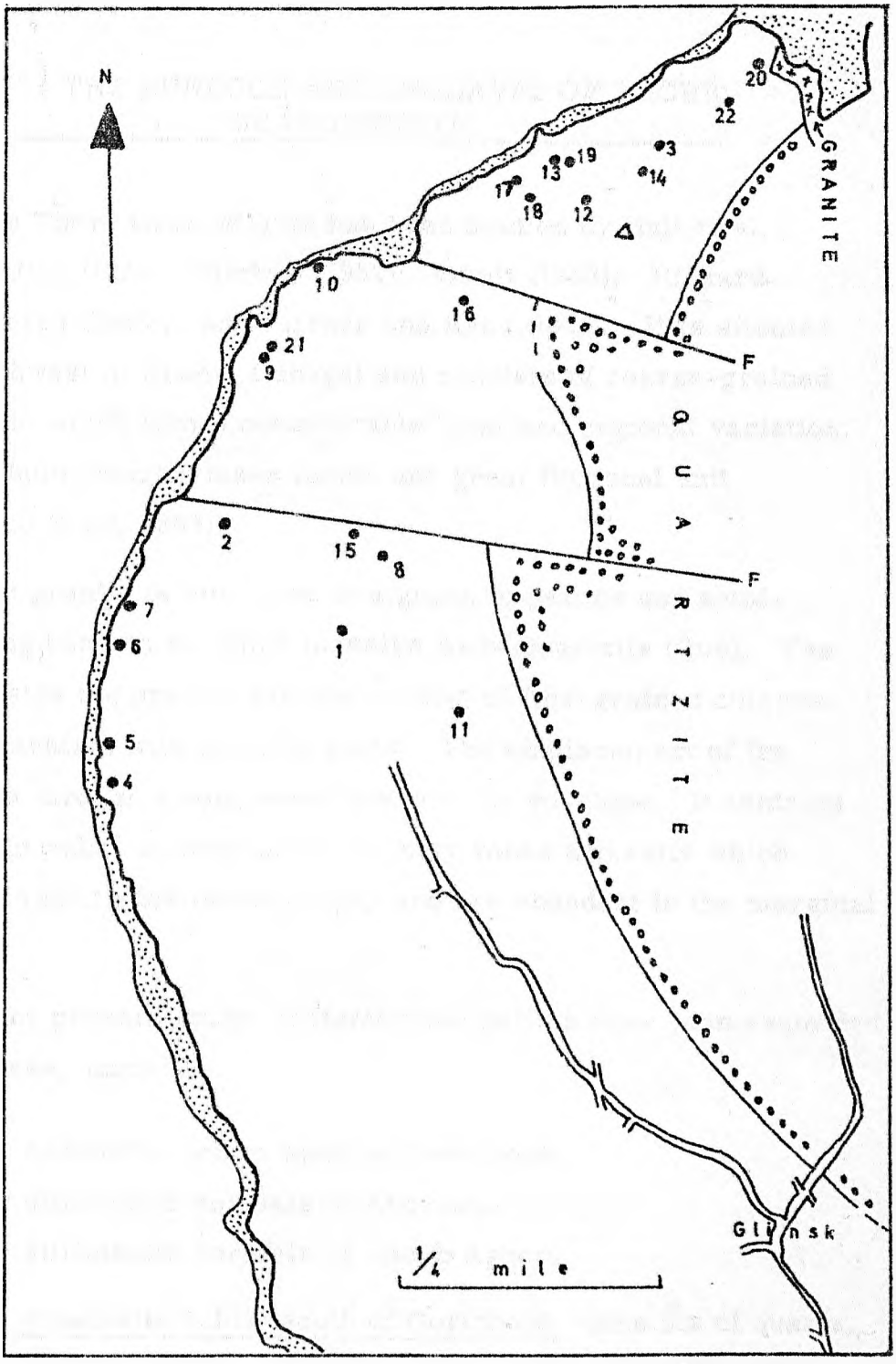

Geological sketch map of Fanad Aureole showing the localities of the specimens used in analysis. (Geology after Pitcher and Read 1963)

II. THE AUREOLE AND ENCLAVES OF THORR GRANODIORITE

The Thorr Granodiorite has been studied by Hull et al., (1891); Whitten (1955); Pitcher (1953); Gindy (1953); Rickard (1957); Mercy (1960); and Pitcher and Read (1963). It is situated in the northwest of County Donegal and consists of coarse-grained granodiorite which shows considerable local and regional variation. Yet, the whole granitic mass forms one great fluxional unit (Pitcher and Read, 1963).

The granite is emplaced in a group of pelites and semi-pelites lying beneath the thick massive Ards Quartzite (ibid). The pelites outside the granite aureole consist of fine-grained chlorite-muscovite schists with chlorite knots. The emplacement of the granite was through strong reactions with its envelope. It contains innumerable relict masses of the country rocks and rafts which preserve a relict ghost stratigraphy and are abundant in the marginal zone.

In the present study, metamorphic pelites have been examined in three areas, namely:-

1. The andalusite schist south of Gortahork.
2. The sillimanite hornfels of Ardveen.
3. The sillimanite hornfels of Lough Agher.

The andalusite schist south of Gortahork consists of quartz, plagioclase, brown biotite, muscovite, iron oxide, chlorite and andalusite. Knots of biotite are frequent and the host schistosity sweeps around these knots. The andalusite occurs as large

porphyroblasts overprinting the groundmass and incorporating much of its materials as inclusions. It mainly replaces parts of the mica bands (Pl. 2d). Trails of elongated grains of iron oxide are seen to pass undisturbed from the groundmass into the andalusite. The andalusite is clearly of static growth and is similar to that of the Fanad Granite aureole described earlier.

In the pelitic enclaves of Ardveen and Lough Agher, sillimanite and fibrolite are abundant. The rock has a hornfelsic texture and consists of quartz, plagioclase, deep brown biotite, muscovite, fibrolite, sillimanite, iron oxide and with or without garnet as well as potash feldspar. Late chlorite is seen in some thin sections.

Fibrolite replaces the biotite and forms the usual vein-like winding through the rock. It also occurs as small isolated patches as well as individual wisps. These patches are sometimes included in sillimanite (Pl. 2e). Fibrolite also fringes the pre-existing minerals including sillimanite.

Sillimanite occurs as slender prisms coarsened from fibrolite as well as elongated densely-packed robust prisms (Pl. 2f). Isolated individual prisms are sometimes seen replacing the biotite.

In conclusion, the schists and hornfelses of the Thorr Granodiorite district are characterised by andalusite, sillimanite and fibrolite. Crystallisation of andalusite was static and took place later than the structures induced by the emplacement of the granitic rocks. Sillimanite and fibrolite are abundant in the hornfelses of the pelitic enclaves. Fibrolite seems to have started to grow earlier than sillimanite and continued to grow after the

development of sillimanite. The early fibrolite is represented by inclusions in sillimanite as well as the mats from which slender sillimanite prisms develop. The late fibrolite is represented by the fringes following the boundaries of sillimanite robust crystals.

III. THE BARNESMORE GRANITE AUREOLE

The Barnesmore granite and its aureole have been studied by Walker and Leedal (1954), Smart (1962), Pitcher and Read (1963). The granite is an oval shaped isolated pluton, about 20 square miles in extent. It is emplaced into steeply dipping metagreywackes consisting of quartzo-feldspathic granulite with intercalations of coarse oligoclase-muscovite-biotite pelitic schists. The contacts are sharp and have an outward dipping.

The emplacement of the pluton has no structural effect on its envelope, hence Walker and Leedal (1954) envisaged a mechanism of simple cauldron subsidence to be involved in the granite emplacement. The metamorphic aureole is relatively narrow and the thermal effects are limited (100-200 yards). The contact metamorphism is well shown by the intercalated mica-schists which produce true pelitic hornfelses in a narrow marginal zone, few yards in width, at the granite contact. The granulite bands associated with the pelitic hornfelses are coarsened and their feldspar becomes conspicuous.

In the present study, only the bands of mica schists and the pelitic hornfelses are considered.

The regional mica-schists consist of quartz, feldspar, biotite, muscovite, chlorite, apatite and iron ore. Feldspar is mainly oligoclase. It is sometimes intergrown with biotite. Biotite is of a greenish colour and is usually aligned along the foliation. It is not as abundant as muscovite and is sometimes partly altered to chlorite. Apatite is a common accessory mineral.

Pelitic schists in the outer part of the aureole do not show great mineralogical changes from those of the regional rocks. The only evidence of thermal effect is the development of irregular small andalusite crystals. Oligoclase is still preserved and is only

recrystallised. Biotite retains its original greenish colour.

True pelitic hornfelsesare restricted to the narrow innermost zone of the aureole. Here, the rocks are characterised by conspicuous large andalusite which occurs as spongy porphyroblasts as well as small idioblastic crystals. Pleochroism is sometimes in patches from colourless to pink. Various degrees of alteration of andalusite to shimmer aggregates are seen. Sometimes the alteration products coarsen to muscovite. According to Smart (1962, p. 59), the two forms of andalusite possibly "record two phases of contact metamorphism such as may have resulted from the two phases of intrusion : the xenoblastic form may have grown under the influence of a second wave of heat from the sheet complex."

Biotite is greenish to greenish-brown in colour. Alteration to chlorite is very common. Together with muscovite, it forms a hornfelsic texture. Oligoclase occurs as recrystallised granular aggregates, cordierite as irregular hexagonal and elongated grains completely altered to mica. Fibrolite is sporadic and not common. It replaces the mica both in the groundmass as well as in the andalusite crystals. Sometimes, fibrolite fringes the andalusite. Microcline and orthoclase sometimes form the main feldspar of the rock.

In conclusion, the Barnesmore aureole is static. Its narrow extent is a result of the quickly cooled low-temperature Barnesmore granite.

IV. THE NORTHERN AUREOLE OF ARDARA PLUTON

A. Introduction and Synopsis of Previous Work

The Ardara pluton, its aureole and the surrounding country rocks have been studied in detail by the Geological Survey of Ireland (1891), Mithal (1952), Akaad (1954, 1956a, 1956b), Pitcher and Sinha (1958), Pitcher and Read (1963) and Jones and Galwey (1964).

The granite pluton of Ardara (about 5 miles in diameter) is a composite circular body consisting of a granodiorite core surrounded by a relatively narrow, highly foliated biotite hornblende tonalite. The foliation is parallel to the margin of the pluton.

The pluton was emplaced by two upwellings of magma and grew diapirically by exertion of pressure outward on the country rocks. The intruded northern country rocks are the Rosbeg semi-pelites and the Clooney pelites. According to Akaad (1956b), the contact effects extend to a distance of over one mile and the northern part of the aureole can be divided in the following zones:-

1. The outermost part of the aureole where biotite appears in the regional muscovite-chlorite phyllonites to replace the chlorite pseudomorphs after garnet. Quartz also coarsens.

2. The inner aureole which is further divided into:-
   (a) Outer andalusite zone, 220-250 yards wide, with staurolite.
   (b) Inner sillimanite zone, 120-140 yards wide, with garnet, A cordierite sub-zone of the sillimanite zone at the immediate contact with the granite is recognized.

According to Akaad (ibid), andalusite resulted from two phases of crystallisation related to the two phases of intrusion of the diapir. This is shown by the fact that some andalusites have pleochroic cores surrounded by mantles of poikilitic chiastolite with trains of inclusions parallel to the schistosity of the groundmass. He further thought that the core has rotated prior to the deposition of the mantle.

In the andalusite hornfelses, Akaad gives the sequence of mineral development as staurolite and garnet, followed by two separate phases of andalusite development which in turn is followed by fibrolite and finally muscovite. "The sillimanite hornfels is entirely devoid of andalusite but along the outer boundary of the sillimanite zone, they generally contain pseudomorphs of fibrolite after chiastolite and andalusite" (ibid, p. 387).

On the other hand, Pitcher and Read (1963), distinguished two modes of occurrence of andalusite. The first is in the outer part of the andalusite zone. It occurs as augen-knots within the axial plane schistosity which in detail can be seen to be a strain-slip. There are many cases where this pattern inside the andalusite unit is discordant to that outside the unit. The second type of andalusite is in the inner part of the andalusite zone. Andalusite is idiomorphic, lacking the strain slip arrangement and lying in a finer groundmass. It is pleochroic with trail-free cores. The authors (ibid) agree with Akaad on the two stages of andalusite growth but do not confirm Akaad's conclusion that the core has rotated before the deposition of the mantle around it.

Pitcher and Read (1963) made the following comments:-

I. Andalusite can be assumed to be of slightly later growth than staurolite, but "both are aureole minerals growing together under very similar conditions. They do not record two separate

metamorphic episodes or great difference in physical controls." (p. 282).

2. The bulk of sillimanite and fibrolite does not form directly from andalusite, and the two minerals are of independent growth.

In their conclusion, the authors (ibid) point out that in the innermost part of the aureole, crystallisation outlasted the deformation caused by the granite. They are sceptical about Akaad's two distinct stages in the thermal process and state that "the essential unity of the structural pattern in the aureole shows that only one event is involved, the higher temperatures of the innermost aureole permitting the dominance of crystallisation over those of deformation" (p. 283).

The petrochemistry of the Cleengort pelitic schist horizon both within and outside the contact aureole of Ardara has been symmetrically studied in detail by Pitcher and Sinha (1958). In their method of sampling, the two authors (ibid) chose eight lines of traverse normal to the strike and spanning the outcrop of the Cleengort schist. Five rectangular sampling areas were marked out across each traverse.

In the regional rocks outside the influence of the aureole, the only significant variation is exhibited by magnesium "in which a slight decrease is followed by a rapid and progressive increase in the direction of the limestone" (ibid. p. 401).

Inside the aureole, Cleengort pelites showed little or no change across the outcrop for the elements silicon, aluminium, total iron, phosphorus and manganese. On the other hand, "magnesium continued to vary systematically and almost in the same manner in the several traverses" (ibid. p. 402). The rate of change is so nearly identical to that outside the aureole that there cannot have been significant migration of magnesium in the aureole rocks. The same applies to titanium for which progressive changes were noticed in both regional and aureole schists. Calcium showed no significant differences.

Potassium values are somewhat higher than those in the regional schists but there is a general lack of contrast between potassium values of the two environments. Sodium shows a considerable uniformity although relatively high values do sometimes occur. These represent small additions of sodium at the immediate contacts of the Ardara pluton. Values of $H_2O + 110^{o}$ are, not unexpectedly, lower in the hornfelse.

Pitcher and Sinha (1958) showed that the high magnesia rocks run in a zone adjacent to the Portnoo limestone. In both the regional and the aureole rocks, the points showing an abrupt increase in magnesium are not always in the same position relative to the limestone boundary. Yet, this difference in relative positions of some points disappears if the top of the lower semi-pelitic horizon lying immediately above the Portnoo Limestone is used as the reference line instead of the limestone boundary.

From the foregoing observations, Pitcher and Sinha concluded that the contact metamorphism involved a dehydration but was otherwise largely isochemical in nature. Also, metamorphic zonation of the aureole, as has been described by Akaad (1956b) is not a result of original compositional differences.

B. Description of the Aureole

The object of the following description is to record the textural features and then deduce the mutual relations of the coexisting minerals in the aluminium silicate-bearing rocks. For this purpose, 63 specimens were collected from the northern inner aureole of Ardara for microscopic study. According to the present study, this part of the aureole can be distinguished into the following zones as the granite is approached:-

1. The kyanite-bearing andalusite schist.

2. The kyanite-free andalusite schist.

3. The coarse sillimanite hornfels.

1. The kyanite-bearing andalusite schist:-

A dark-grey schist forming the outer part of the inner aureole. In the field, andalusite forms stumpy thick prisms, distinctively grey in colour and appears to be augened.

In thin sections, the rock consists of quartz, feldspar, biotite, muscovite, chlorite, staurolite, garnet, kyanite, andalusite and occasionally fibrolite. The rock is highly schistose with porphyroblasts of andalusite, feldspar and occasionally staurolite.

The elongated quartz grains and the brown mica flakes mark the schistosity, which is distinctly crenulated. It is worth mentioning that the garnet, -chlorite schists outside the aureole show similar foliation and puckering. The only difference is that in the aureole rocks, the biotite takes the place of the chlorite in the regional schists. The biotite flakes are brown and contain pleochroic haloes. These flakes are not always segregated into bands. Occasionally, quartz and crenulated biotite form spectacular augen-like units lying between the schistose biotite. The schistosity of the groundmass sweeps around these units.

Partial or complete retrogression of biotite to chlorite is evident. The replacing chlorite occurs as green flakes either growing across the biotite or else replacing it in situ. Intermediate stages of biotite chloritization are common. This retrogression is accompanied by partial or complete shimmerisation of the coexisting andalusite.

Andalusite porphyroblasts form augen-knots which overprint and lie in the well developed schistosity and include parallel trails of the groundmass materials, e. g. quartz, staurolite, garnet, kyanite, fibrolite and iron ore. Commonly, andalusite overgrows the augen-

like units of quartz-biotite mentioned above. The original structure of these units is preserved in the andalusite knots and betrayed by the signoidally arranged quartz inclusions as well as the microfolds exhibited by them. The cleavage of the andalusite is not interrupted nor deviated by these microfolds (pl. 3a, b, c) nor does it show undulose extinction. Andalusite is also seen to grow and merge imperceptibly into the folded biotite.

Plagioclase (albite-oligoclase) show similar textural characteristics to those of andalusite. Many instances have been seen where the twin laminae are straight and overprints the sigmoidal quartz inclusions (pl. 3d, e).

From the andalusite and plagioclase textures, it is apparent that these two minerals overprint the groundmass structures. The texture exhibited by knots of these two minerals could easily be mistaken as textures evolving from rotated porphyroblasts. Therefore, it must be emphasized that the growth of these two minerals was mainly static and no rotation or movement whatsoever took place during their growth.

Staurolite occurs commonly as irregular grains although subidiomorphic crystals growing in the biotite are not uncommon. Sometimes, staurolite cuts across the biotite. It also grows over the puckers of the groundmass and contains curved trails of inclusions which are sometimes continuous with the groundmass structure, i. e. similar to andalusite, staurolite overprints the groundmass structure. In some slides, staurolite occurs as clusters of small grains as well as individual small crys tals dissiminated all over the rock (pl. 4a, b). It is also seen as inclusions in the andalusite and feldspar crystals (pl. 3f).

Garnet is not common. It occurs as fractured crystals which

are often replaced with chlorite. It also occurs as inclusions in andalusite.

Kyanite (not recorded by Akaad, 1956b and noted only in one slice by Pitcher and Read, 1963), occurs as small prisms which lie in the biotite but in the majority of cases they are at small angle or set across the biotite folia (pl. 4c, d). When kyanite cuts across the biotite, the latter is not disturbed nor attenuated along the kyanite boundaries. In some cases, kyanite is seen to pass imperceptibly into biotite (pl. 4e). As with the staurolite, kyanite is also seen to occur as numerous small grains (pl. 4b), as well as inclusions in the feldspar and the andalusite porphyroblasts (pl. 4f, 5a). An interesting case was noticed where a long kyanite prism lies across, and undisturbed by, the curved inclusions in a plagioclase porphyroblast (pl. 5b). When occurring as inclusions in andalusite, kyanite prisms lie at different angles to the andalusite cleavage with no crystallographic relation between the two minerals.

As to the relation between the kyanite and staurolite, both minerals generally have the same textural characteristics and the two are sometimes seen in parallel growth (pl. 5c).

Fibrolite occurs as sporadic twirls decolourising and replacing the biotite. In some instances, it appears that staurolite, kyanite and andalusite enclose the fibrolite or parts of the fibrolitised biotite (pl. 5d, e, f). Therefore, these minerals are thought to be later than this enclosed fibrolite.

From the foregoing description, one can draw the following picture as to the possible sequence of metamorphic crystallisation in the kyanite-bearing andalusite zone of the aureole: An early fibrolite formation followed by kyanite-staurolite. Finally andalusite and

plagioclase overprinted the groundmass and enclosed kyanite, staurolite and fibrolite. The crystallisation of these minerals was static. However, the sequence of minerals given above does not mark distinct and different episodes of metamorphism. A mineral included in the other does not show any resorption or destruction. In fact, the staurolite included in andalusite shows in most cases better developed faces than that found in the groundmass.

2. The kyanite-free andalusite schist:-

This part of the aureole is characterised by the absence of kyanite and the frequent development of perfectly idioblastic andalusite set in a finer grained groundmass.

In thin sections the idioblastic andalusites are rimmed with graphite and contain trails of the groundmass material. The trails are in most cases concordant with the groundmass. The groundmass schistosity is seen sometimes to sweep around the andalusite crystals.

Andalusite consists of almost inclusion - free pleochroic cores which are optically different from the andalusite mantle around it. The cores are always surrounded by a thin zone of fine inclusions (Akaad, 1956b, fig. 2., Pitcher and Read, 1963, fig. 15). These cores are good evidence of two stages of growth and there is certainly a difference in type between the core and the margin.

Alteration of andalusite to shimmer aggregates as well as to stout flakes of biotite and muscovite generally increases as the contact is approached. This is also accompanied by an increase in the amount of fibrolite. The replacing biotite and muscovite grow inwards and the resulting flakes are arranged with their length perpendicular to the original andalusite edges.

Fibrolite develops from the biotite of the groundmass and the mica resulting from the alteration of andalusite. Fibrolite also occurs as veins fringing, sweeping around and transecting the andalusite.

Garnets occur in some rocks of this part of the aureole. These garnets are small, euhedral and are seen as inclusions in andalusite and feldspar porphyroblasts as well as concentrations along certain bands in the groundmass.

Staurolite is seen in some thin sections as euhedral to subhedral grains normally included in the andalusite. In one thin section it has been seen as inclusion in the andalusite core.

The sequence of events in this part of the aureole as seen from thin sections can be outlined as follows: The crystallisation of garnet-staurolite, the development of andalusite in two stages followed by recrystallisation and growth of large micas in the andalusite and finally the development of fibrolite.

3. The coarse-sillimanite hornfels:-

A brownish grey hornfels which is free of kyanite, distinctly less schistose and contains less andalusite than the andalusite zone.

In thin sections, the rock is fine grained consisting of sillimanite, fibrolite, biotite, muscovite, quartz, and esitic plagioclase, garnet and occasional andalusite. Nearer to the contact, cordierite is also found.

Sillimanite forms stout prisms and increases in size towards the granite contact. There are few instances in the innermost part of the sillimanite zone where composite crys tals of sillimanite exhibit shapes reminiscent of andalusite. The writer agrees with

Pitcher and Read (1963) that andalusite in this case may have been produced at an early stage and finally replaced by sillimanite, but the growth of the great bulk of the fibrolite and even much of what is there of the stouter sillimanite is quite independent of this early andalusite, i. e. there is no textural indication of polymorphic transformation.

Fibrolite replaces the mica. It is also found as inclusions in garnet as well as patches in some sillimanite crystals. Quite often, fibrolite occurs as vein-like bundles winding through the rock and bordering the existing mineral grains, including sillimanite. Coarsening of fibrolite into sillimanite is also frequent.

Andesitic plagioclase is a main constituent of the groundmass. It also occurs as pokilitic porphyroblasts. Muscovite forms flakes either replacing the aluminium silicates or intersecting the biotite. It also occurs as porphyroblasts set across, but not affected by, later shear planes. Both plagioclase and muscovite are of later formation.

Garnet is common. It forms irregular or corroded large grains. Cordierite occurs as subidioblastic grains which are sometimes altered.

C. Comments and Conclusions

The main comments and conclusions arising from the present study and concerning the aluminium silicate minerals in the Ardara Aureole can be summarised as follows:-

1. The inner aureole can be divided into 3 zones based on the type of aluminium silicates present. These zones are: (Fig. 23).

(i) An outer kyanite-bearing andalusite schist.

(ii) A middle kyanite-free andalusite schist.

(iii) An inner kyanite-free coarse-sillimanite hornfels.

2. Andalusite, kyanite, fibrolite, sillimanite, staurolite, feldspar and garnet are all aureole minerals of static crys tallisation. Each mineral overprints the groundmass structure and encloses the already existing minerals.

3. Kyanite forms a zone about 80-120 yards wide on the northern part of the aureole. This mineral is always associated with andalusite, staurolite and sometimes with fibrolite. Significantly, it cuts across the biotite folia and is sometimes enclosed in the andalusite; indicating that the kyanite is later than the biotite and earlier than the andalusite.

4. In the kyanite-bearing andalusite zone, the sequence of crystallisation as seen from the textural evidences is as follows:-

(i) Fibrolite replacing biotite.

(ii) Kyanite-staurolite and sometimes garnet.

(iii) Andalusite-plagioclase.

The occurrence of fibrolite at an early stage of metamorphism may indicate a sharp rise in temperature at the early stages of the granite emplacment. It seems that fibrolite can easily replace biotite once the temperature rises. Whether or not an aqueous phase is involved in this reaction is difficult to decide. This sudden rise in temperature is also suggested by the spectacular development of numerous small crystals as well as clusters of staurolite and kyanite peppering the rock. It is very likely that rapid heating caused supersaturation which led to a fast rate of nucleation of these two minerals.

The big augen-like porphyroblasts of staurolite, andalusite and feldspar overprint the structure of the groundmass. These minerals are static and there is no movement involved during their crystallisation. It is thought that the sygmoidally arranged inclusions they contain and the augen shape they assume is inherited from the already augened quartz-biotite knots which they overprint. However, the possibility that the porphyroblasts have been augened later is not completely excluded.

5. The middle part of the aureole is a kyanite-free andalusite schist. Here, thermal effects are superimposed on the regional structure and consequently, the latter is obliterated.

6. Staurolite in this part of the aureole is less common compared with its frequent development in the outer kyanite-bearing andalusite schist. From the modal analysis, all the 7 kyanite-bearing andalusite schists contained staurolite whereas it was recorded in 5 rocks out of the 9 kyanite-free andalusite schists.

7. The andalusite in the kyanite-free andalusite schist is mainly the chiastolitic variety. It differs from that of the outer part of the aureole mainly in two aspects, viz. the marked idiomorphic habit as well as the two stages of its formation. The latter is indicated by the presence of a pleochroic pink core surrounded by a mantle. The core is almost inclusion-free, which indicates a slow rate of crystallisation whereas the mantle is full of inclusions and indicates a faster rate of growth. However, both stages of andalusite growth are static. In this respect, the author does not agree with Akaad (1956b) that the core has rotated prior to the deposition of the mantle.

8. Fibrolite develops from biotite. It decolourises and replaces the biotite. There seems to be two phases of fibrolite

development. The first is the very early fibrolite mentioned before and the remnants of which are still seen in the kyanite-bearing andalusite schist. The second phase is clearly seen in the middle as well as the inner parts of the aureole. Here, fibrolite fringes the existing minerals including sillimanite. It also replaces the biotite formed after chiastolite. Fibrolite sometimes coarsens to give sillimanite.

The author does not agree with Akaad's statement (1956b, p. 387), "The development of fibrolite pseudomorphs after chiastolite at the boundary of the andalusite zone appears to be the result of late changes in the physical conditions of thermal metamorphism causing the sillimanite zone to advance into the andalusite zone." It is evident from the present study that fibrolite develops mainly from mica. Direct and straightforward pseudomorphism of fibrolite after chiastolite has not been seen. What appears as a fibrolite pseudomorph is either a development of fibrolite aggregates or else fibrolite formed from the mica which had replaced andalusite, i. e. the development of fibrolite from andalusite is not a direct reaction but it is accomplished through an intermediate phase of andalusite alteration to mica.

9. The materials for fibrolite and sillimanite growth are independent of the early andalusite.

10. There is no textural evidence of polymorphic transformation of one aluminium silicate into the other.

11. The microscopic examination of the aureole rocks shows that the proposed limits of the kyanite-bearing andalusite zone (Fig. 23) coincides in general with a line connecting the points of the abrupt

magnesium change shown by Pitcher and Sinha (1958). The significance of this relationship will be discussed at length when the chemical analysis of the rocks is considered in a later chapter.

Fig. 23

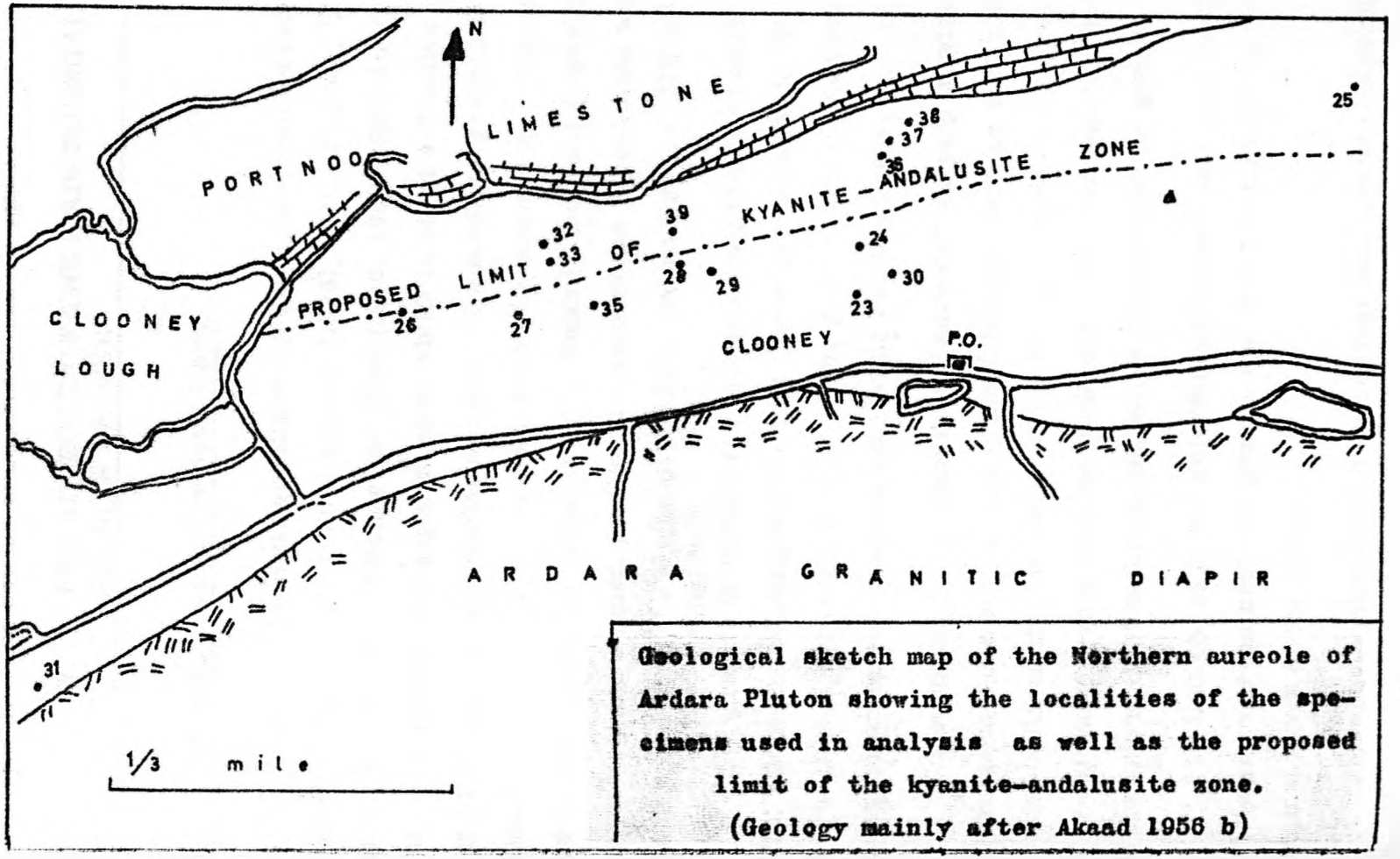

Geological sketch map of the Northern aureole of Ardara Pluton showing the localities of the specimens used in analysis as well as the proposed limit of the kyanite-andalusite zone.
(Geology mainly after Akaad 1956 b)

V. THE AUREOLE OF THE MAIN DONEGAL GRANITE PROPER

A. Introduction and Previous Work

The Main Donegal granite proper and its aureole have been studied by Hull et al., (1891), Andrew (1928), McCall (1954), Tozer (1955), Read (1958), Pitcher and Read (1959, 1960, 1963) and Berger (1967). It forms an elongated mass which is about 4-5 miles in width and 36 miles long and consists mainly of a medium-grained biotite granodiorite varying to a coarse-grained granodiorite. The granite was intruded into Dalradian country rocks (mainly the Creeslough Succession and a small portion of Kilmacrenan Succession) with its length parallel to the strike of the intruded rocks, i. e. NE-SW.

The granite is banded and contains long trains of country rock rafts. Both the banding and the raft trains are parallel to the country rock walls. The marginal parts of the granite are sheeted and show strong foliation with marked mullioning and boudinage.

Surrounding the granite is an "aureole" varying in width between 1-1½ miles and containing high grade minerals such as staurolite, kyanite, sillimanite and andalusite. Rocks outside this "aureole" are completely devoid of these minerals. The "aureole" is deformed and the intensity of deformation increases towards the granite contact.

The last phase of the deformation history involved flattening restricted to areas near the granite and is superimposed on the marginal parts of the pluton.

The above-mentioned field settings are already established and agreed to by previous workers on the Main Donegal granite. Yet,the

interpretation and the significance of these facts are controversial. The latest two comprehensive works on the granite and its aureole are those of Pitcher and Read (1959, 1960) and Berger (1967). A brief outline of these two works is therefore given.

Pitcher and Read (1959) visualize the Main Donegal granite as a magmatic intrusion under conditions of high temperature and powerful directed pressure, and flowing in a southwardly direction. They explain the banding of the granite and raft trains to be due to this primary magmatic flow and the marginal cataclasis is due to the drag of the consolidating granite against its walls.

The authors (1960) pointed out that the main structural effects of the granit emplacement can be seen in the aureole schists as the tightening of the open folds found in the country rocks as well as the development of planar, linear and mullioning structures. These structures are identical to those in the marginal parts of the granite.

The granite has a pronounced wide aureole of contact schists. The aureole rocks are primarily of low metamorphic grade but towards the granite contact intense new structures and high-grade mineral assemblages have replaced the regional character. The high grade minerals grew during the movement producing the structures in the aureole.

Berger (1967) in his study of the Main Donegal granite concludes that while it is impossible to disprove the notion that the granite was forcefully emplaced, yet, most of its structural features are the result of a powerful deformation which was superimposed on the pluton prior to its complete consolidation at its present crustal level.

In the area around the granite, Berger recognises 5 phases of deformation (F1-F5). The relation between these 5 phases and the

granite can be outlined as follows:- Three episodes (F1-F3) predate the emplacement of the granite (F3 increases in intensity towards the area now occupied by the granite), F4 was superimposed while the granite was still hot and able to respond to stresses by recrystallization, F5 caused further deformation in the envelope though by this time the granite must have been cool enough to react by "cold" cataclasis.

Therefore, the Main Donegal granite proper was emplaced into a pre-existing large-scale shear zone. The structures in the granite envelope, though apparently indicating uniformity of deformation between the granite and its carapace, are considered to be composite in origin. The early regional structures were invaded by the granite and tightened coaxially by subsequent movements.

Regarding the relation between the phases of deformation and the mineral development in the pelites around the granite, the following summary is compiled from Berger's conclusions (p. 593-594):- During a static interval between F2 and F3 garnets and plagioclase porphyroblasts formed while kyanite, staurolite and possibly sillimanite formed in areas of most intense deformation. After F3 and the emplacement of the Granite, andalusite, fibrolite and regenerated garnets form the true aureole minerals related to the Granite.

According to Berger (ibid), the granite was emplaced into a pre-existing "root-zone" of intensely deformed and high metamorphosed rocks and much of the apparent aureole actually pre-dates the emplacement of the Granite.

B. Description of the Aluminium Silicate Bearing Rocks in the Aureole

Presented with the controversy whether the granite has a staurolite kyanite, andalusite-bearing aureole or not, it is natural to examine the status of these minerals and their relationship to the granite. Therefore, in the present study, specimens from six localities where aluminium silicates occur, were collected for petrographic and chemical studies. The localities are shown in Fig. 24. and include:-

Southern side of the granite

(1) Fintown area (F)

(2) Glenaboghil (Bo)

(3) Lough Reelan area (LR)

Northern side of the granite

(4) Glenkeo (G) (northeastern end of the granite)

(5) Lackagh Bridge (LB)

(6) Owennagreeve River area (R)

Regarding the stratigraphy of the Dalreadian rocks adjacent to the Main Donegal granite, the aureole on the southeast of the granite consists of rocks of the Fintown succession which is divisible into the following members:

Youngest
- Lough Finn Dark Pelites and Limestones
- Fintown Siliceous Flags
- Glendowan Pelites and Limestones
- Staghall Semi-pelitic Group
- Glaggan Lough Limestones
- Losset Pelites and Semi-pelites

Fig. 24

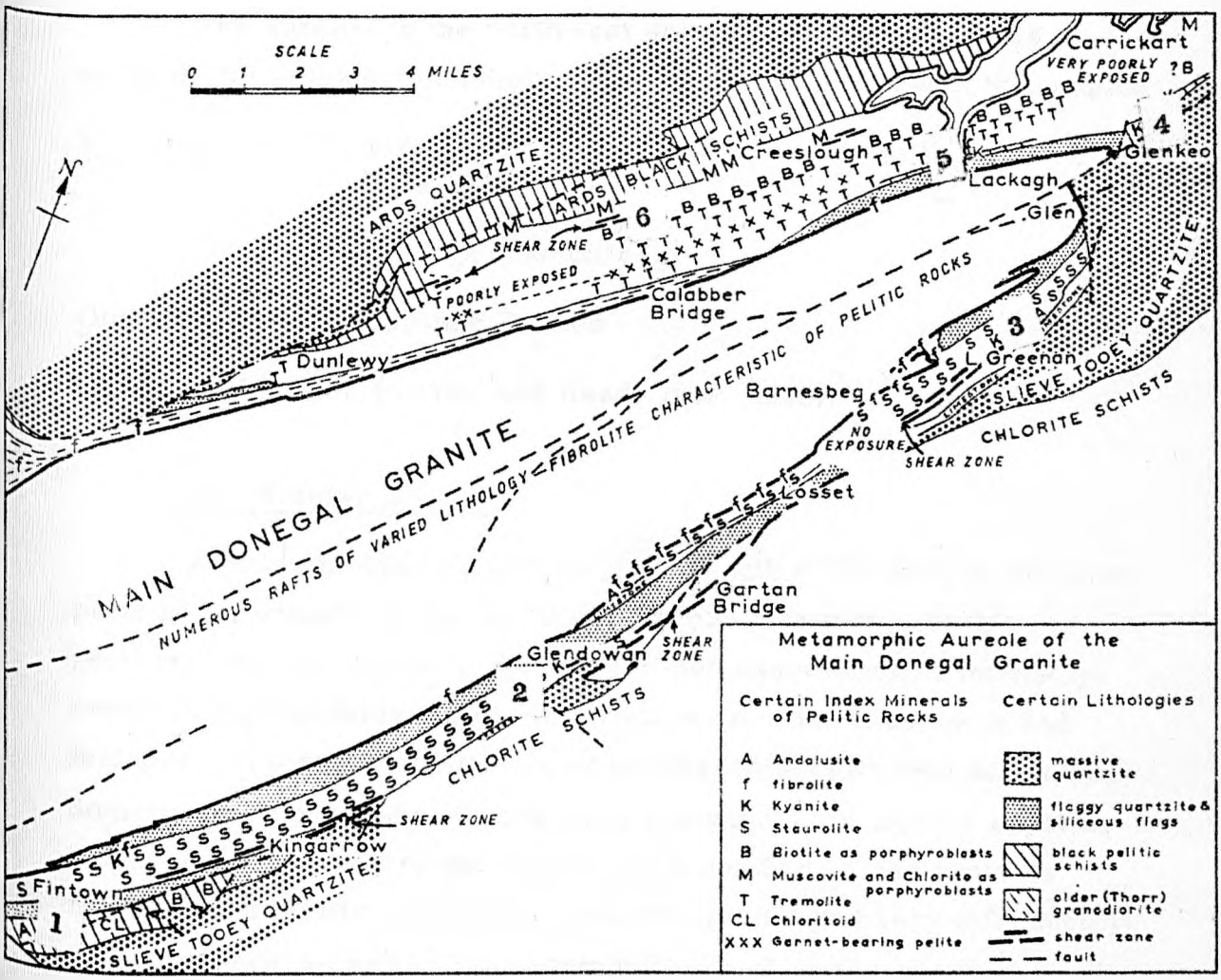

Diagramatic map of the Main Donegal Granite (After Pitcher and Read 1963) showing the localities described in the present study.

(1) Fintown area
(2) Glenaboghil
(3) Lough Reelan
(4) Glenkeo
(5) Lackagh Bridge
(6) Owennagreeve River.

Oldest — Glenieraragh quartzite

The aureole to the northwest and north of the granite is made of the following members of the North-West Donegal Succession:-

Youngest
- Ards Quartzite
- Ards Pelites
- Cresslough Group
- Lackagh Quartzite

Oldest — Lackagh Pelites

(Stratigraphy after Pitcher and Read, 1959, 1960).

(1) Fintown area:-

Andalusite-bearing schists occur south of Fintown in the outer parts of the staurolite-garnet main aureole rock type. In thin sections, the andalusite is set in a foliated association of intensely crenulated groundmass minerals: quartz, biotite, muscovite and feldspar. It forms well-developed porphyroblasts as well as stripes. Sometimes, the porphyroblasts show rectangular or square crystals having well defined straight edges. It is pleochroic and contains inclusions of biotite, graphite, iron ore, garnet and very infrequently perfect staurolite crystals. Commonly, graphite forms a rim bordering the andalusite. In few cases, graphite inclusions tend to form the cross characteristic of chiastolite (pl. 6a). Although the inclusions in andalusite show such variable mineralogy, yet their amount is small. In fact, many crystals are inclusions-free except for minute grains of dark graphite and/or iron ore.

The andalusite grows mainly in the mica-rich bands and show the following relationships:

(1) Curved andalusite stripes intimately follow the intense puckers and crenulations of the groundmass, yet, the andalusite does

now show undulose extinction (pl. 6b).

(2) The groundmass materials pass undeflected into the andalusite crystals (pl. 6c, 6d). Remnants of these materials with their characteristic puckers are enclosed and preserved in some andalusite crystals (pl. 6e).

(3) Usually, the schistosity of the groundmass is not deflected against the andalusite porphyroblasts. Only one case was seen where the schistosity seemed to sweep around andalusite (pl. 6f). In this case, the andalusite apparently overprinted an already augened site and, in fact, the deformation is ealier than the andalusite growth.

From these textural relationships, it is clear that the andalusite development is static and overprints the groundmass minerals. It is definitely later than the foliation and the intense puckering of the groundmass.

This mode of andalusite development is similar in every respect to the andalusite in the kyanite-bearing schists of the Ardara aureole described earlier.

Another feature displayed by the Fintown andalusite is that some rectangular cross sections consist of a core which is optically different from the rest of the crystal. In many cases, the occasional trails of inclusions in the mantle stop suddenly against the core. At the edge of the core, the growing andalusite often evades a quartz grain or a mica flake and the consequently deposited andalusite mantle includes such grains (pl. 7a).

In thin sections where andalusite is completely altered to shimmer aggregates, it was noticed that under polarised light, certain parts of this shimmer are clearer and contain less dark

materials than the rest of the shimmer (pl. 7b). Yet, under crossed nicols, both parts have the same characteristics. It is very likely that the clear parts of the shimmer aggregates represent the original andalusite cores. This Fintown cored andalusite recalls that of the inner part of the andalusite zone of Ardara described earlier (p. 167).

Staurolite is uncommon in the andalusite-bearing schists. It is recorded as small euhedral six-sided crystals included in andalusite (pl. 7c).

The sites of regional garnets are represented by large biotite knots which sometimes contain new regenerated garnets. Invariably, the host schistosity sweeps around these knots (pl. 7d). Yet, there also occur numerous small crystals of garnet growing over the schistosity of the groundmass. The crystals are euhedral to subhedral and are of buff colour (pl. 7e). These crystals represent new thermal garnets formed later than the structures seen in the groundmass.

Muscovite is abundant, forming up to 36% of the rock. It is full of dark inclusions. Biotite is less common than muscovite (up to 20%). It forms red brown flakes which contain pleochroic haloes and dark inclusions.

Effects of retrogressive metamorphism in sheer zones are seen in most of the thin sections. Here, chlorite knots replace the garnets, the andalusite is altered to shimmer aggregates and the biotite of the groundmass is chloritised.

It can therefore, be concluded that garnet and staurolite developed earlier than andalusite. The andalusite growth is static as

it overprints the minerals and structures of the groundmass. Two stages of andalusite growth are recognised and are shown by an andalusite core surrounded with a mantle. Judging by the amount of inclusions, the core has a slower rate of growth than the mantle. However, there is no indication of a time gap between the two stages of andalusite growth.

(2) Glenaboghil schists:-

Kyanite occurs in the contact schists of Glenaboghil, 1. 5 miles northeast of Fintown, at about half a mile from the Granite contact. Samples from two parallel traverses, 1. 8 miles apart and normal to the granite contact, were collected. Examination of thin sections of these samples showed that in the western traverse, kyanite is abundant and is associated with fibrolite, whereas in the eastern traverse, only fibrolite is present.

The Glenaboghil schists present a clue to the relation between the aluminium silicate minerals and the granite metamorphism. A brief petrographic account is given accompanied by as many microphotographs as possible to show the textures displayed by the constituent minerals.

The Glenaboghil schists consist of quartz, plagioclase, brown biotite, muscovite, garnet, staurolite, fibrolite, tourmaline,iron ore, chlorite and with or without kyanite.

Biotite and muscovite are the main schistosity markers. They are occasionally segregated into bands. The biotite is partly replaced with fibrolite. Modal analysis showed that the amount of fibrolite increases towards the granite.

Overprinting this mica are numerous small euhedral to sub-

hedral grains of garnet of buff dusky colour (pl. 7f, 8a). Clusters of these garnets are sometimes seen (pl. 8b). The garnets also overprint the partly fibrolitised mica (pl. 8c, 8d) as well as well-developed fibrolite aggregates (pl. 8e). In both cases, fibrolite is partly enclosed in the garnets. From this observation, together with the nature of the individual and clusters of garnet crystals, the garnet is believed to be of thermal origin.

Kyanite occurs as prisms as well as stout irregular grains. It mainly overprints biotite. The mica is not disturbed nor attenuated by the small kyanite crystals (pl. 8f, 9a, 9b) but with large kyanites, the host schistosity sweeps around the kyanite porphyroblasts. It is interesting to notice that frequently, the kyanite encloses crystals of the garnet described before (pl. 9c).

Staurolite shows the same textural characteristics displayed by the kyanite. Again it encloses the garnet (pl. 9d). Plagioclase occurs as porphyroblasts as well as g rains in the groundmass. The porphyroblasts often include the garnet as well as small prisms of kyanite (pl. 9e, f, 10a).

From these relationships, one can conclude that the sequence of aureole metamorphic minerals development is as follows:
An early development of fibrolite followed by garnet, then staurolite-kyanite and finally plagioclase feldspar.

The significance of these conclusions are:-

(i) Kyanite, staurolite and plagioclase porphyroblasts, all containing inclusions of garnet are aureole minerals.

(ii) The development of early fibrolite supports the conclusions mentioned earlier in the Ardara aureole. Fibrolite seems to form easily at the early stages of metamorphism, probably due to a surge of heat, and continues to grow throughout the aureole

metamorphic history as long as thermal conditions are suitable.

(3) Lough Reelan area:-

Andalusite-kyanite schists occur in a well exposed narrow belt of the Losset Pelites, about 50 yards across, with schists rich in staurolite on the northwest, and platy schists to the southeast. The schists are coarse and contain well developed andalusite crys tals as well as quartz-andalusite sweats out.

In thin sections, the schists are well foliated and consist of quartz, plagioclase, brown biotite, muscovite, garnet, staurolite, kyanite and with or without andalusite and fibrolite. Tourmaline and iron ore are common accessories.

Kyanite forms elongated prisms lying within or cutting across the biotite (pl. 10c, d, e, 11c). It is also seen in parallel growth with staurolite (pl. 10f). Kyanite occurs in most of the specimens collected and is more abundant than what was originally indicated by Pitcher and Read (1960).

Staurolite occurs as euhedral to subhedral grains. It contains inclusions of quartz, garnet and iron ore. Spongy crystals with idioblastic outlines are frequent. Normally, the host schistosity sweeps around big staurolite porphyroblasts. Andalusite occurs as big spongy crystals as well as irregular elongated grains which tend to lie along the foliation. It contains inclusions of quartz, biotite, garnet as well as euhedral crystals of staurolite (pl. 11a, b) and elongated small prisms of kyanite (pl. 11b). The size of the staurolite and kyanite inclusions is much smaller than that of the minerals developed outside the andalusite.

It is evident, therefore, that staurolite and kyanite are earlier

than andalusite. From the difference in the size of staurolite and kyanite within and outside the andalusite, it is probable that these two minerals continued their growth after the andalusite started to develop.

(4) Glenkeo kyanite schists:-

Kyanite is well developed in the dark schists belonging to the black Ards Pelites in the vicinity of Glenkeo, 1.5 miles due south of Carrickart.

In thin sections, the schists consist of quartz, feldspar, biotite, muscovite, garnet, graphite, iron ore, traces of fibrolite, kyanite with or without staurolite. In the staurolite-free schists, the modal kyanite ranges up to 16% whereas in the staurolite-bearing schists, kyanite is only in the range of 1-2%, whereas staurolite ranges up to 11%.

Quartz, muscovite and biotite form a foliated base for the big crystals of kyanite, staurolite and the smaller garnet. In the kyanite schists, augens of decussate texture occur within the foliated schistose rock and the host schistosity is seen to sweep around these augens. The augens consist of quartz, biotite and numerous kyanite prisms showing clear hornfelsic texture (pl. 11d). The kyanite is undeformed (pl. 12e) and the original schistosity is marked by parallel graphite trails contained only within the augens.

Outside these augens, the rock is perfectly foliated and is affected by a strain slip cleavage producing a puckering well shown by the arrangement of the folia. Elongated kyanite prisms, generally aligned along the foliation, are abundant. They are remarkably affected by this strain slip cleavage. The effect is seen on the kyanite as zig-zagging (pl. 11e, f) (F4 according to Berger, 1967)

combined sometimes with folding (pl. 12a, b) as well as strong folding accompanied by the snapping of the kyanite prisms (pl. 12c).

Besides this deformed kyanite, there also occur undeformed crystals set at different angles to the foliation. Schistosity adjacent to these kyanites is not disturbed and in few cases, trails of dark materials folded in the same way as the groundmass, pass through these kaynites (pl. 12d).

Garnet occurs as small euhedral to irregular grains. Staurolite occurs as idioblastic crystals full of quartz inclusions which are discordant with the groundmass. The groundmass schistosity sweeps around the staurolite porphyroblasts. Staurolite sometimes includes garnet (pl. 12f, 13a).

(5) Lackagh Bridge schists:-

At about 1/3 mile north of Lackagh Bridge, kyanite-bearing schists occur at the bottom of the Cresslough group and are exposed on the shore 500 yards from the main granite contact. The schists bear aligned kyanite and are interbedded with Lackagh Bridge type-quartzite.

Thin sections from this area do not add any new information other than that mentioned before. The rock consists of quartz, plagioclase, light-brown biotite, muscovite, iron ore, graphite, tourmaline, kyanite and occasional fibrolite. Staurolite is absent.

Kyanite occurs as large crystals either aligned in or set across the foliation. It contains dark graphitic inclusions which are set at high angles (sometimes normal) to the rock schistosity (pl. 13b). Normally, the host schistosity sweeps around the kyanite crystals (pl. 13c). The kyanite is sometimes partly to completely altered to shimmer aggregates.

(6) Owennagreeve River area:-

Kyanite-bearing schists occur in the Owennagreeve stream to the northeast of Calabber Bridge and at about 1,000 yards from the granite contact. The schists consist of quartz, plagioclase, light-brown biotite, muscovite, iron ore, graphite, tourmaline, kyanite with or without staurolite. The rock is highly foliated and the schistosity is puckered by a strain-slip cleavage. The foliated mica and quartz form the base in which small kyanite and staurolite are set with the host schistosity sweeping around them. Again, these schists do not add any new information other than that mentioned before.

C. Conclusions

The main conclusions regarding the aluminium silicates in the rocks surrounding the Main Donegal granite can be outlined as follows:-

In agreement with Pitcher and Read (1963) and disagreement with Berger (1967), the carapace around the Main Donegal granite is a true aureole of the granite and the minerals it contains, namely, fibrolite, kyanite, staurolite and andalusite are aureole minerals, in the sense that they result from the granite effect. This conclusion is supported by:-

(1) The textural characteristics of the aluminium silicates described earlier, particularly the appearance of early fibrolite as well as the inclusion of garnet in kyanite, staurolite and andalusite.

(2) The neat arrangement of these high grade minerals in a zone of nearly uniform thickness all the way around the granite.

(3) The complete absence of these high grade minerals in rocks

outside the aureole.

The order of crystallisation can be synthesised as follows:-

(1) An early fibrolite decolourising and replacing the biotite.

(2) Small garnets overprinting biotite and fibrolite.

(3) Staurolite and kyanite including garnets.

(4) Feldspar and andalusite including garnet, kyanite and staurolite.

It seems likely that the crystallisation of the kyanite outlasted the deformation of the aureole. This assumption arises from the fact that in some thin sections, kyanite occurs in two different ways in relation to the schistosity of the rock. Both occurrences are often seen in the same thin section and can be described briefly as follows:-

(1) Kyanite crystals with the host schistosity sweeping around them.

(2) Kyanite overprinting the groundmass and lying at different angles to the schistosity without disturbing it. It also includes folded trails of dark materials passing from the groundmass.

The aureole of the Main Donegal granite recalls that of Ardara pluton described earlier. The common features between the two aureoles are:-

(1) The sequence of crys tallisation of the aluminium silicates is the same.

(2) Crystallisation of the aluminium silicates is static.

(3) Fibrolite seems to replace biotite at an early stage of the metamorphism and continues to develop as long as the thermal

conditions are appropriate.

(4) Andalusite crystallises in what appears to be two phases resulting in the development of a core which is optically and texturally different from the andalusite mantle. It must be emphasized that the distinction between the two phases is not one of time but mainly of different rates of growth of the core and the mantle.

(5) Staurolite and kyanite ~~and~~ included in andalusite and feldspar do not show any resorption, i. e. no time gap apparent.

(6) There is no sign of polymorphic transformation of one aluminium silicate to another.

Plate 1.

(a) Small idiomorphic aureole garnet growing in the new biotite knot. (Fanad, x75)

(b) Andalusite overprinting and replacing parts of a mica band. (Fanad, x37)

(c) Andalusite growing in the new biotite knot and including garnet. (Fanad, x40)

(d) Fibrolite aggregates forming an oblong mass and containing elongated grains of iron oxide parallel to the fibrolite elongation. (Fanad, x37)

(e) Fibrolite needles enclosed in andalusite. (Fanad, x37)

(f) Same as (e) between crossed nicols.

Abbreviations :

A : andalusite
B : biotite
F : fibrolite
G : garnet

Plate 1.

(a)

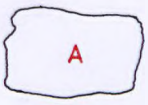

(b)

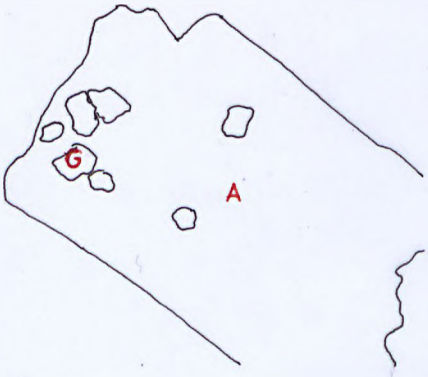

(c)

(d)

(e)

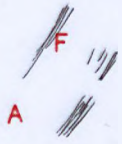

(f)

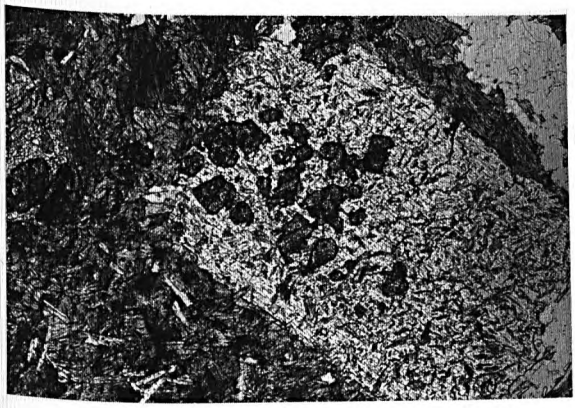

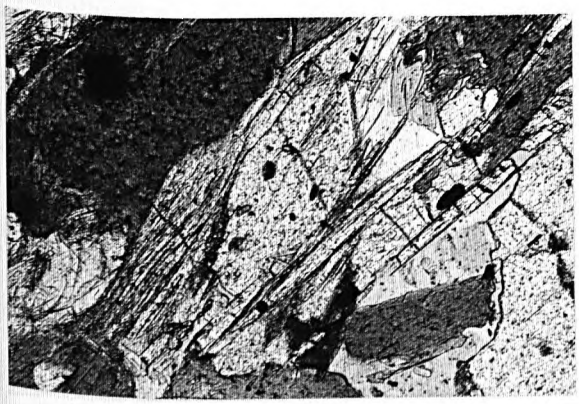

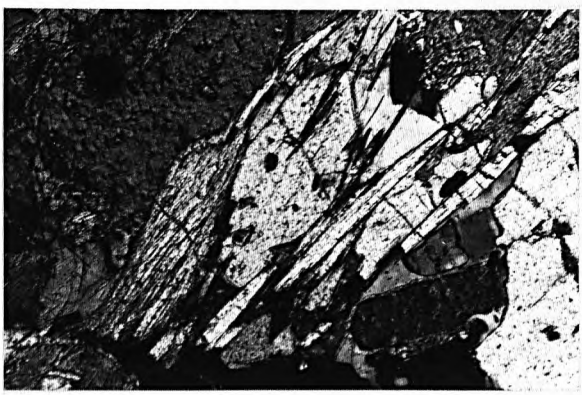

Plate 1.

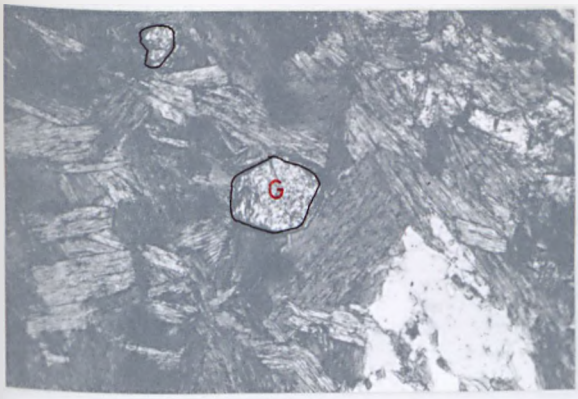

(a)

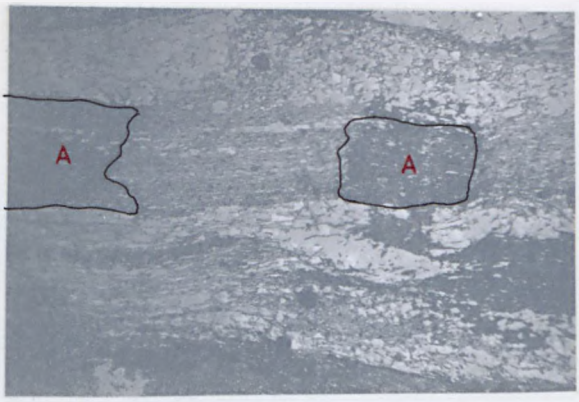

(b)

(c)

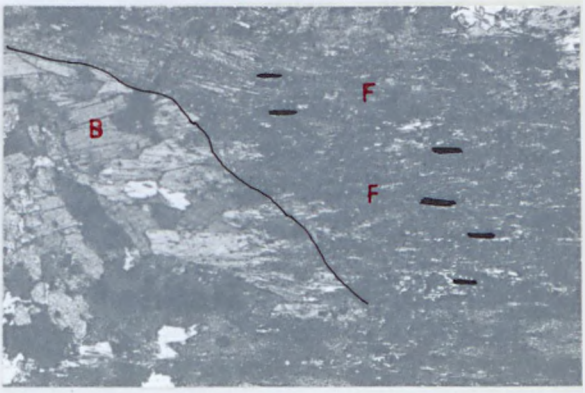

(d)

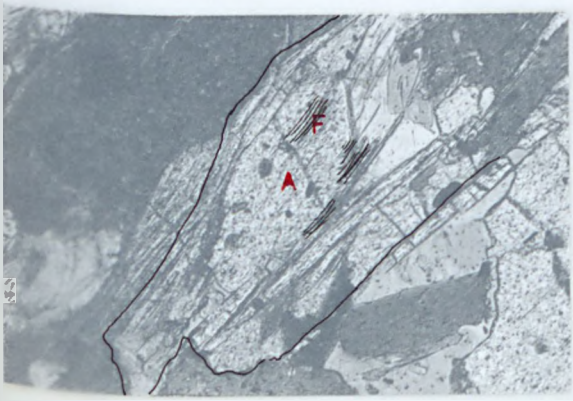

(e)

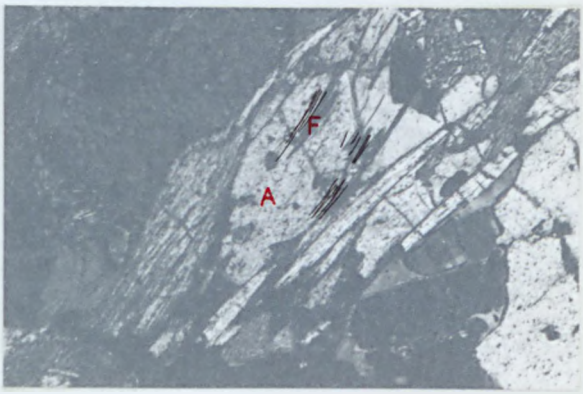

(f)

Plate 2.

(a) Fibrolite patches included in andalusite. (Fanad, x75)

(b) Slender sillimanite prisms mingled with fibrolite. (Fanad, x75)

(c) Sillimanite prisms partly replacing andalusite and growing parallel to the andalusite cleavage. Both minerals share the same c-axial direction. Crossed nicols. (Fanad, x40)

(d) Andalusite replacing parts of a mica band. Notice the elongated ore inclusions lying parallel to the rock schistosity. (South Gortahork, x35)

(e) Fibrolite patches included in a large sillimanite crystal. (Lough Agher, x37)

(f) Densely packed sillimanite prisms. (Ardveen, x35)

Abbreviations :

A : andalusite
B : biotite
F : fibrolite
S : sillimanite

Plate 2.

(a)

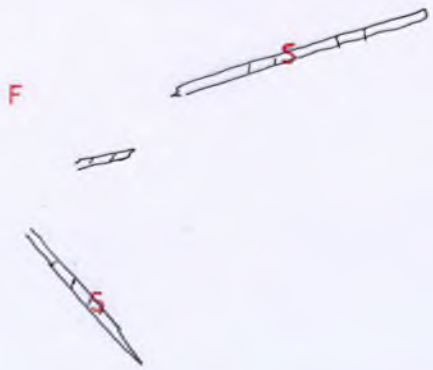

(b)

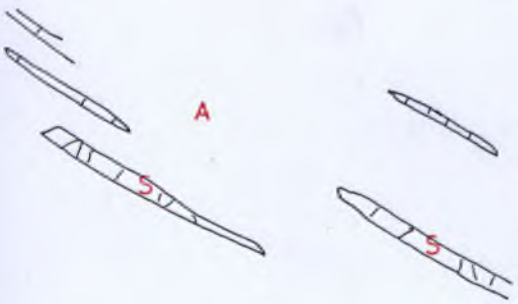

(c)

(d)

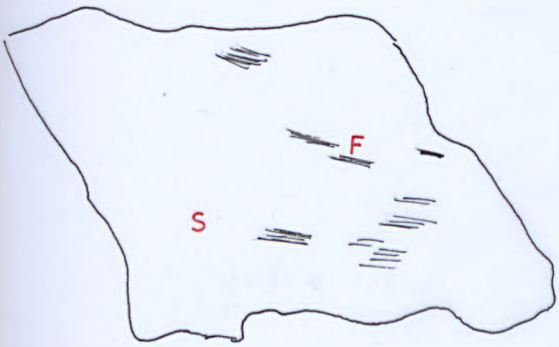

(e)

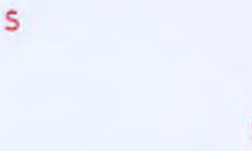

(f)

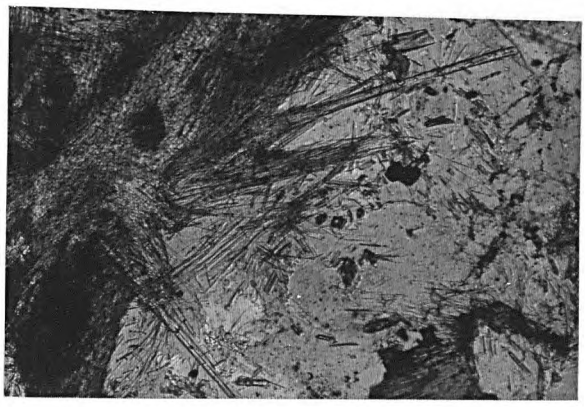

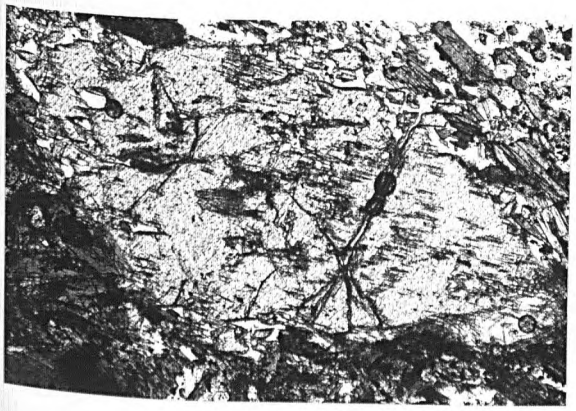

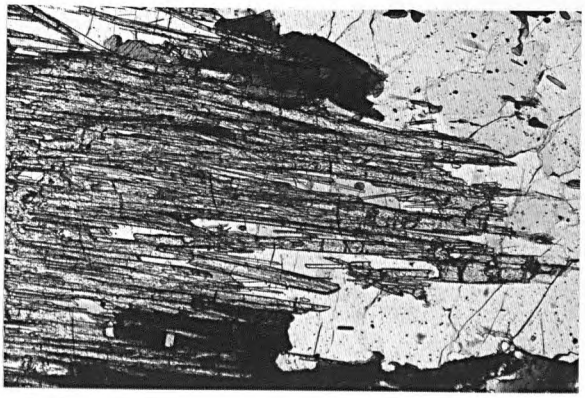

Plate 2.

(a)

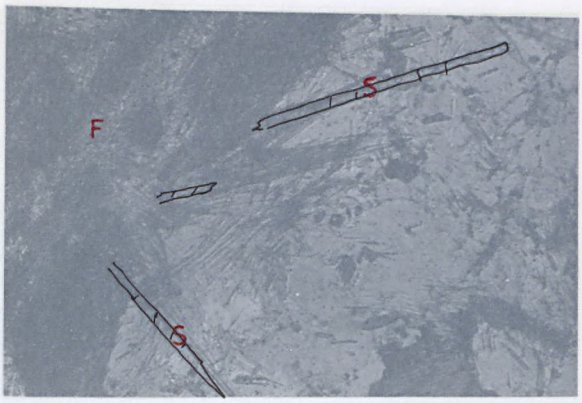

(b)

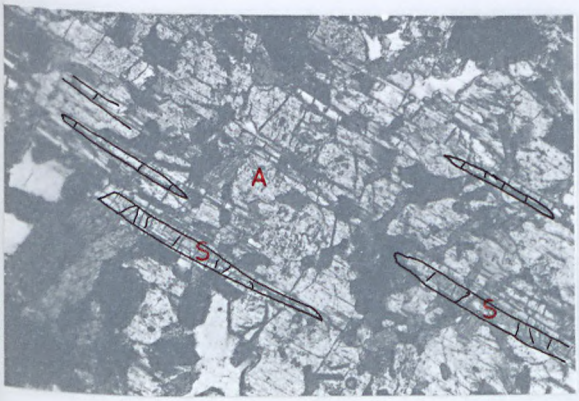

(c)

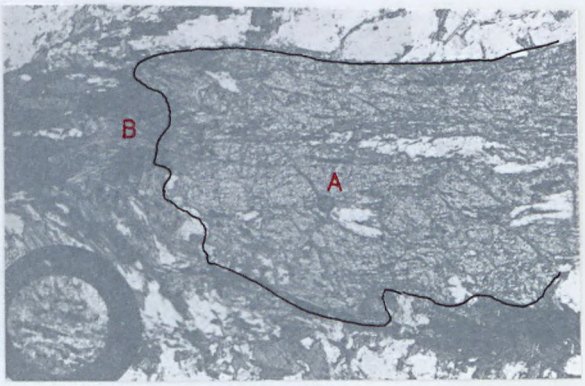

(d)

(e)

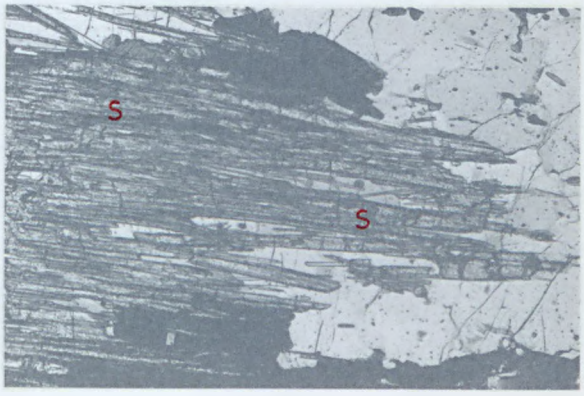

(f)

Plate 3.

(a) Andalusite overprinting the groundmass puckers and incorporating its materials as inclusions. (Ardara, x37)

(b) Andalusite overprinting the groundmass puckers. Crossed nicols. (Ardara, x14)

(c) Andalusite augen overprinting groundmass puckers and containing sygmoidally arranged quartz grains. (Ardara, x15)

(d) Plagioclase porphyroblast with straight twin laminae and curved quartz inclusions. Crossed nicols. (Ardara, x75)

(e) Plagioclase porphyroblast showing straight twin laminae not affected by the curved quartz inclusions. Crossed nicols. (Ardara, x37)

(f) Staurolite crystal with well defined faces occurring as an inclusion in andalusite. (Ardara, x37)

Abbreviations :

A : andalusite
P : plagioclase
St : staurolite

Plate 3.

(a)

(b)

(c)

(d)

(e)

(f)

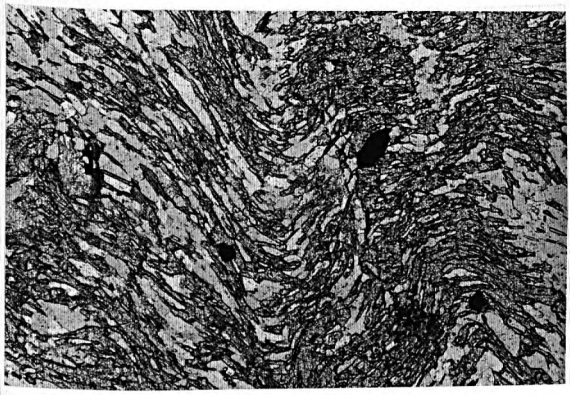

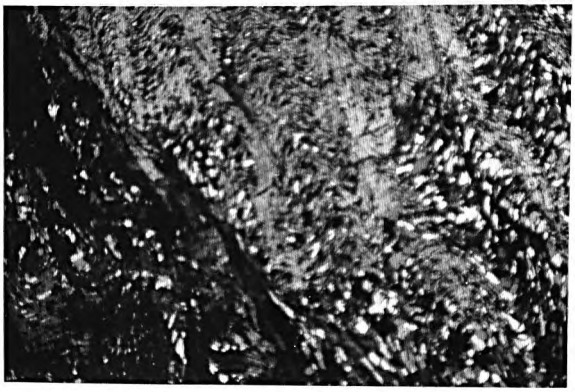

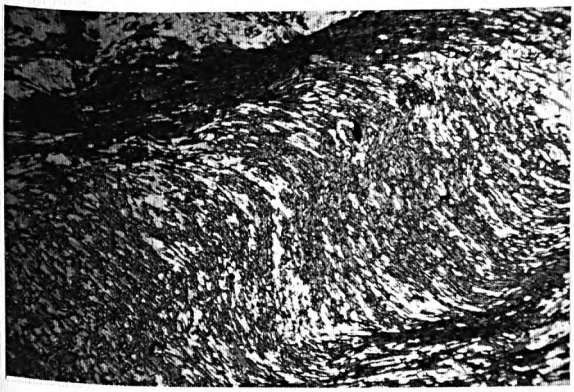

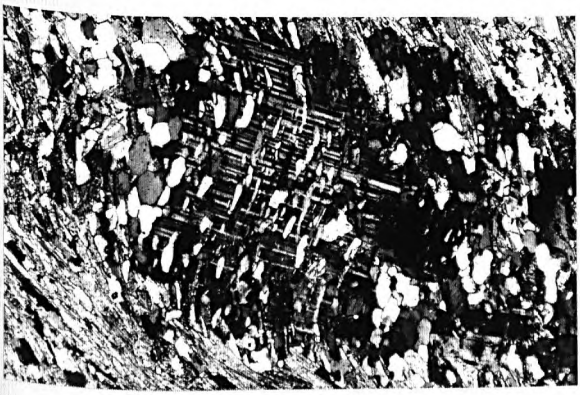

Plate 3.

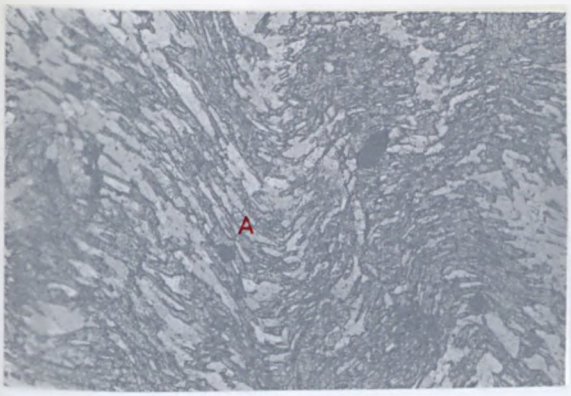

(a)

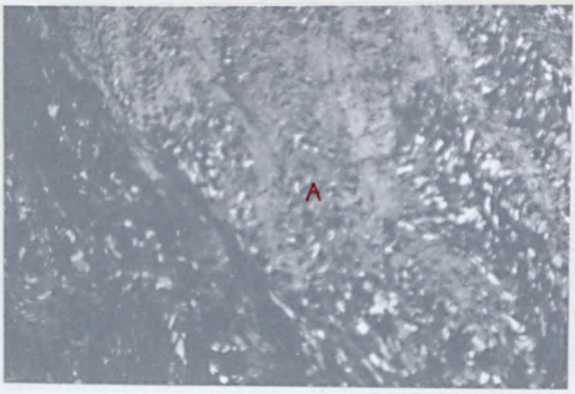

(b)

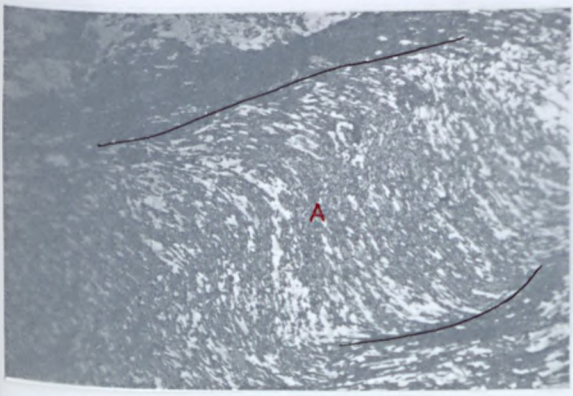

(c)

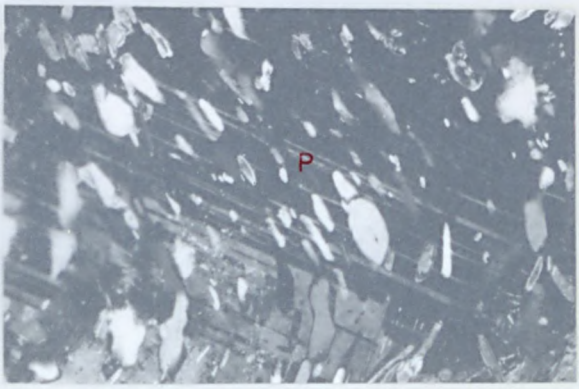

(d)

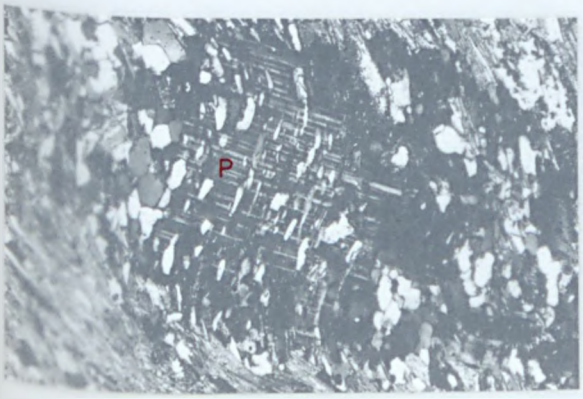

(e)

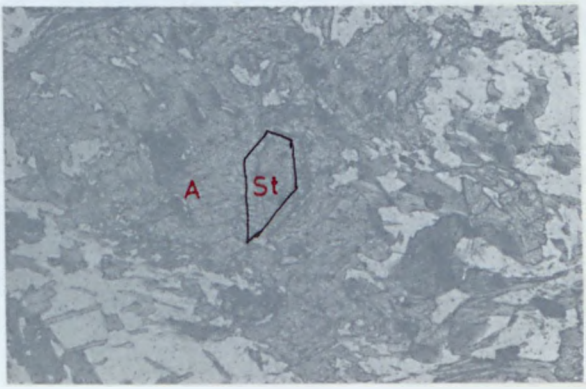

(f)

Plate 4.

(a) Small grains of staurolite dissiminated throughout the rock. (Ardara, x75)

(b) Small grains of staurolite and kyanite dissiminated throughout the rock. (Ardara, x37)

(c) Kyanite crystals growing in and set at different angles to biotite. (Ardara, x75)

(d) Kyanite crystals lying across the biotite. (Ardara, x75)

(e) Kyanite crystals with its terminals merging in the biotite. (Ardara, x75)

(e) Kyanite crystals included in andalusite. (Ardara, x75)

Abbreviations :

A : andalusite
B : biotite
K : kyanite
St : staurolite

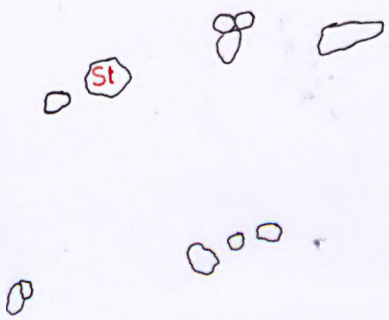

(a)

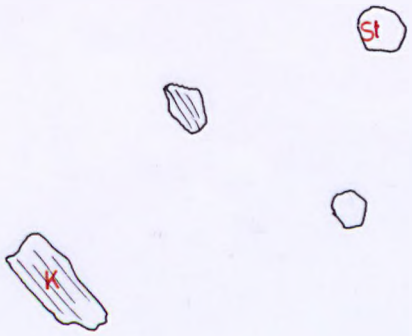

(b)

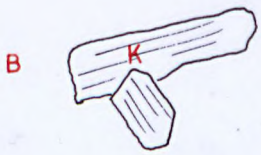

(c)

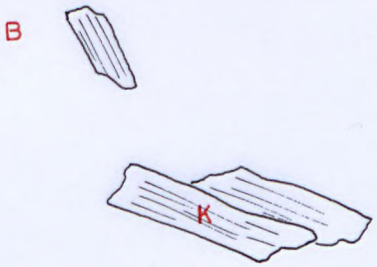

(d)

(e)

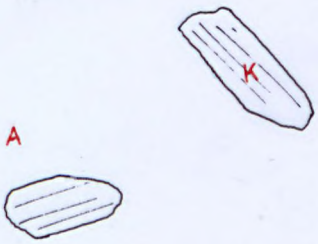

(f)

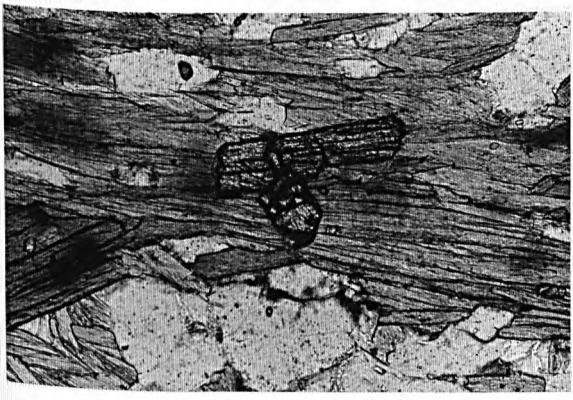

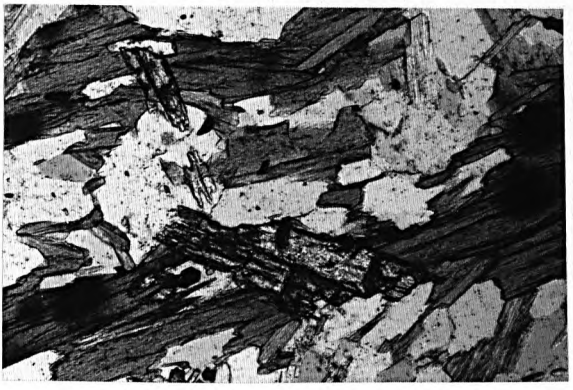

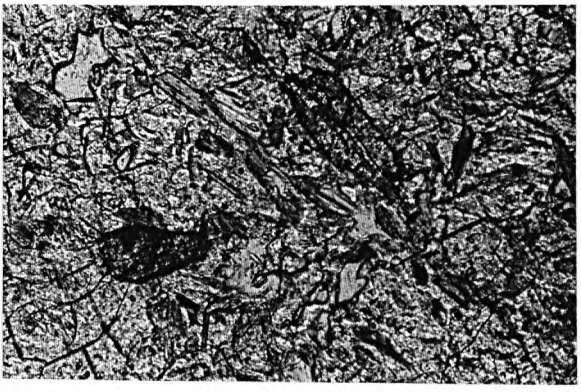

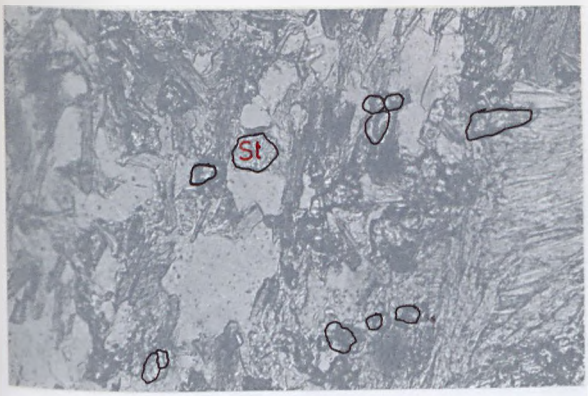

(a)

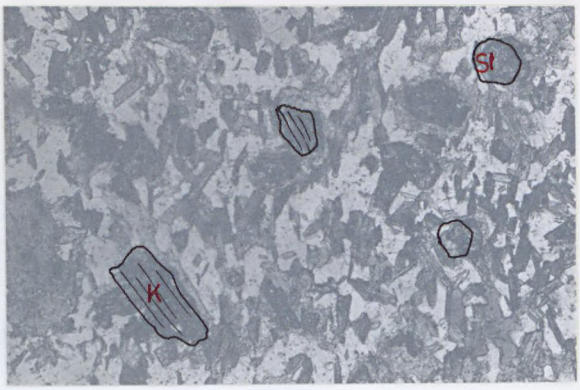

(b)

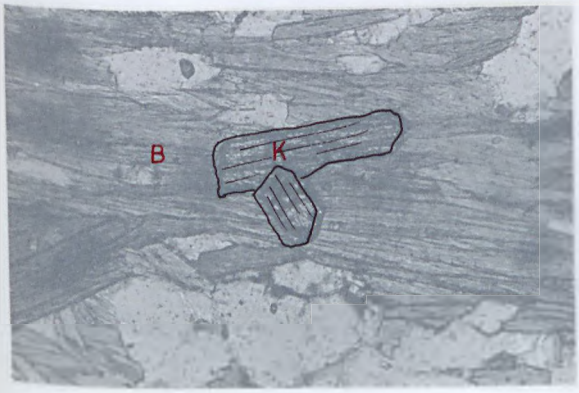

(c)

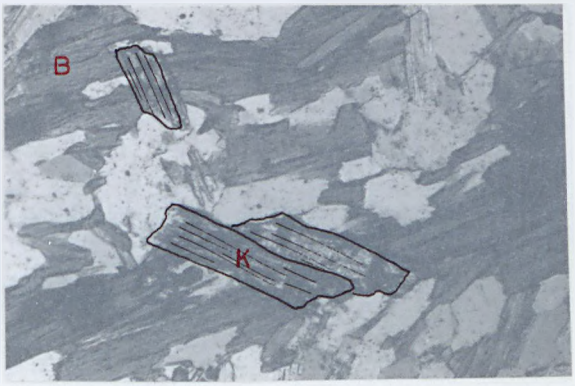

(d)

(e)

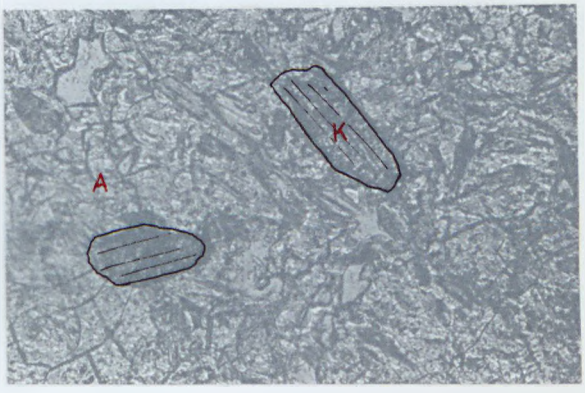

(f)

Plate 5.

(a) Kyanite and staurolite included in andalusite. (Ardara, x75)

(b) Kyanite and staurolite included in a plagioclase augen. The long kyanite prism is lying across and undisturbed by the curved inclusions in the plagioclase. (Ardara, x37)

(c) Kyanite and staurolite in parallel growth. (Ardara, x75)

(d) Fibrolite included in andalusite. (Ardara, x75)

(e) Fibrolite included in andalusite. (Ardara, x75)

(f) Fibrolite included in andalusite. (Ardara, x75)

Abbreviations :

A : andalusite
F : fibrolite
K : kyanite
P : plagioclase
St : staurolite

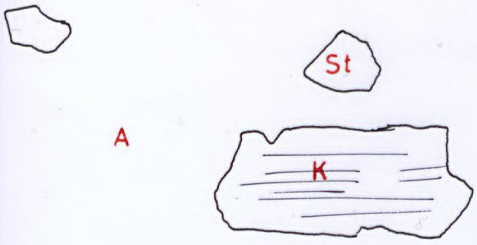

(a)

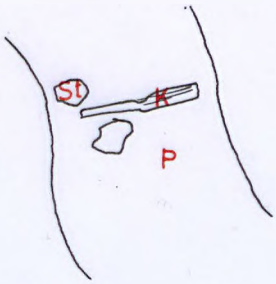

(b)

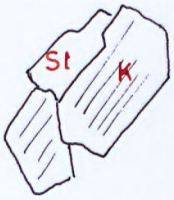

(c)

(d)

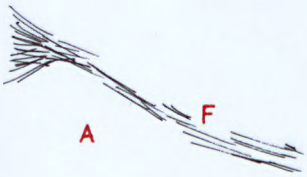

(e)

(f)

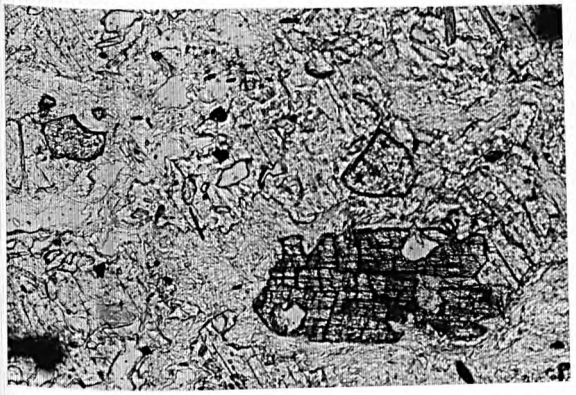

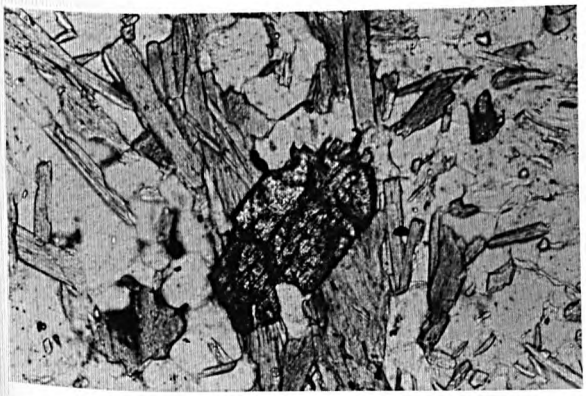

Plate 5.

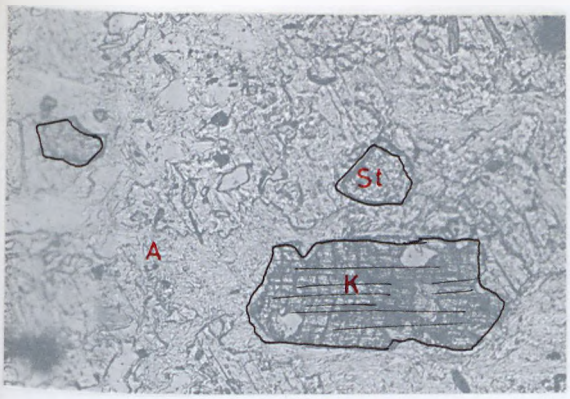

(a)

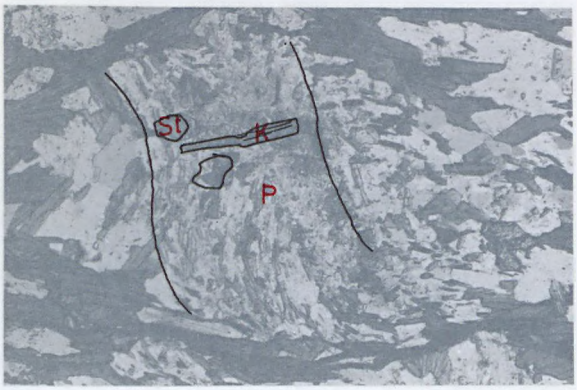

(b)

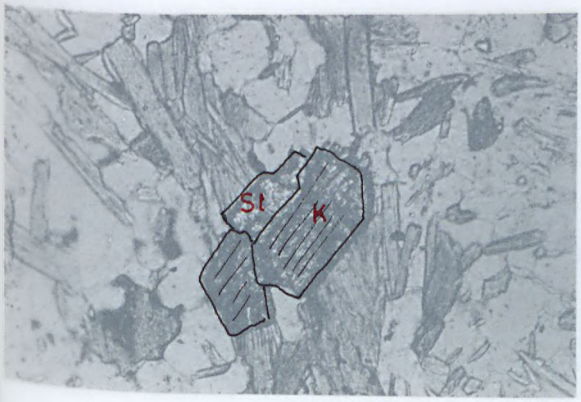

(c)

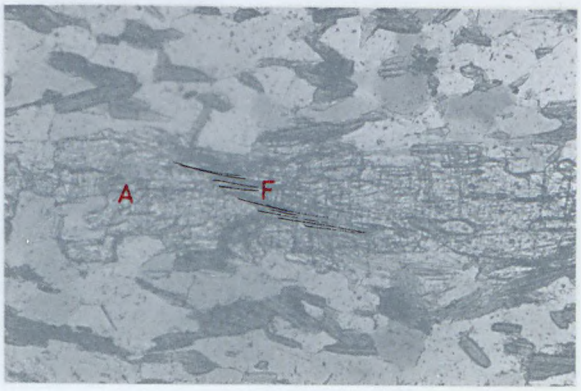

(d)

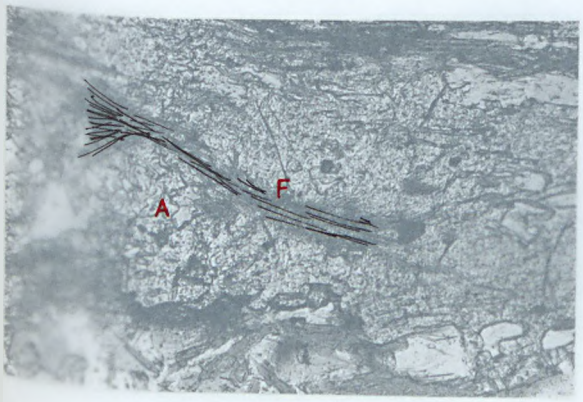

(e)

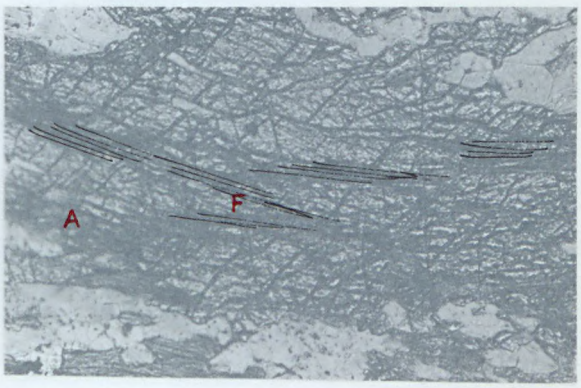

(f)

Plate 6.

(a) Andalusite crystal (chiastolitic) rimmed with graphite and overprinting the foliated groundmass mica. (Fintown, x35)

(b) Andalusite stripes overprinting and intimately following the mica puckers. Although the andalusite is curved, yet it does not show undulose extinction and the cleavage is not curved. (Fintown, x37)

(c) Andalusite crystal containing undeflected inclusions of groundmass material. (Fintown, x37)

(d) Andalusite overprinted on the groundmass with its characteristic puckers. Notice that the groundmass materials pass undeflected through the andalusite. (Fintown, x37)

(e) Remnants of the puckered groundmass materials preserved in the andalusite. (Fintown, x12)

(f) Groundmass schistosity sweeping around andalusite. (Fintown, x37)

Abbreviations :

A : andalusite
B : biotite
M : mica

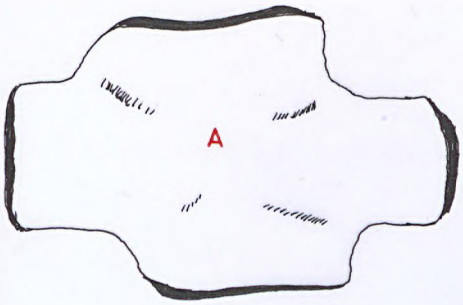

(a)

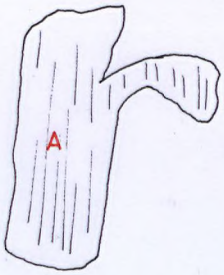

(b)

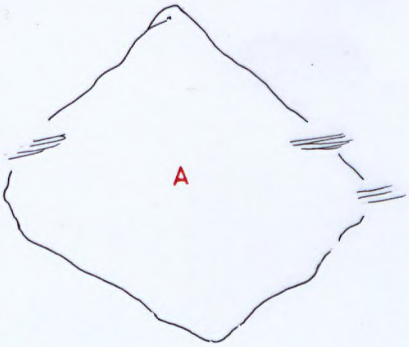

(c)

(d)

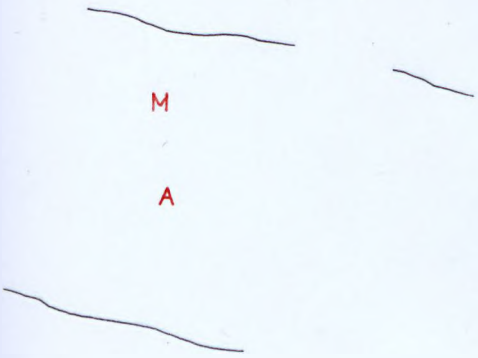

(e)

(f)

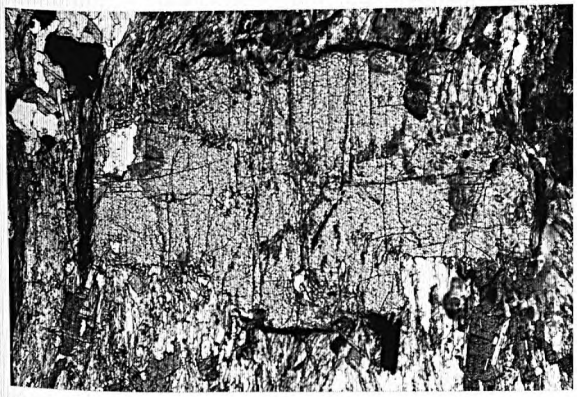

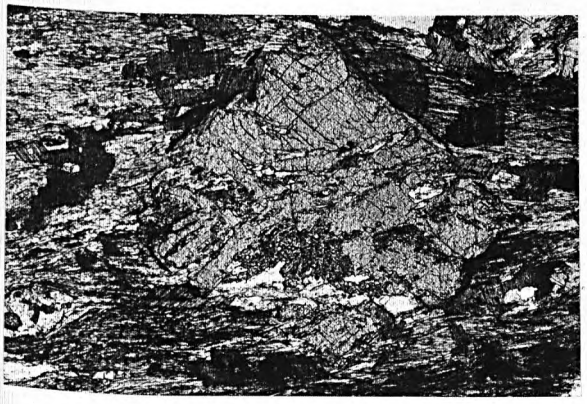

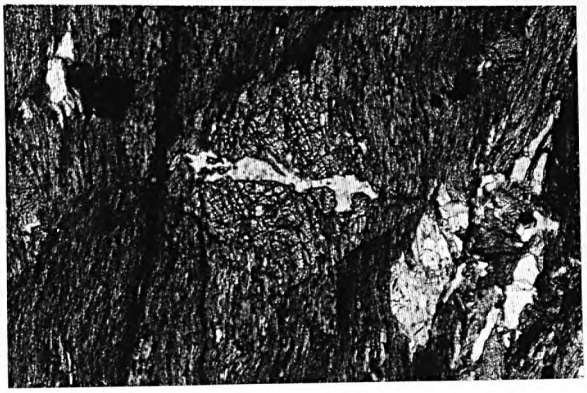

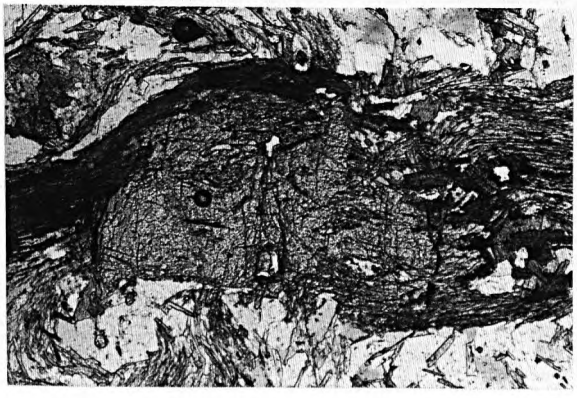

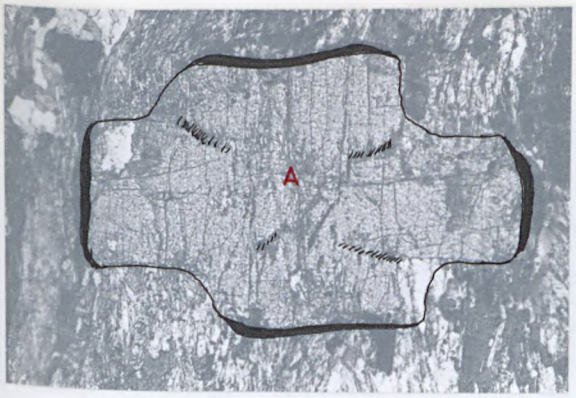

(a)

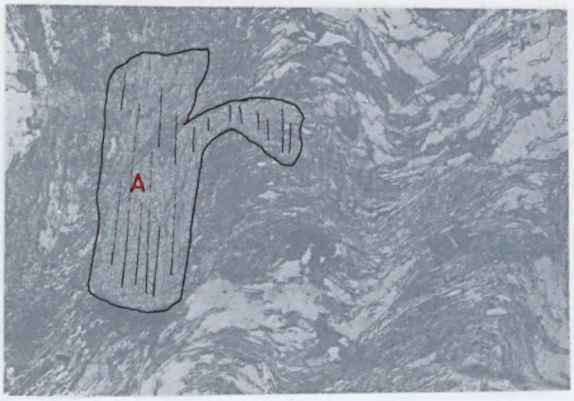

(b)

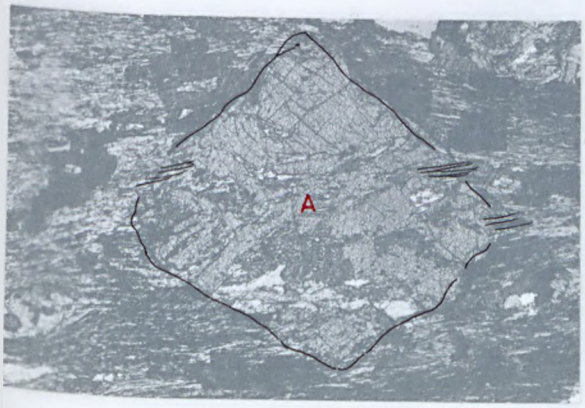

(c)

(d)

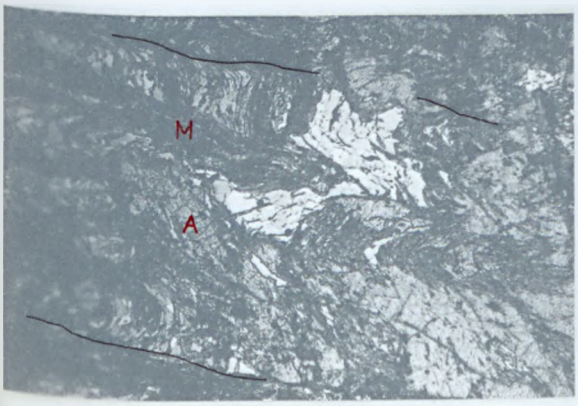

(e)

(f)

Plate 7.

(a) A sketch of a cored andalusite crystal. Notice that the core is relatively inclusion-free compared to the mantle. The irregular outline of the core is due to the fact that the slow-growing core evaded a quartz or a mica grain. (Fintown, x29)

(b) Shimmer aggregates replacing andalusite. Notice the light shimmer patch in the middle of the photo and which may represent the core of the original andalusite. (Fintown, x37)

(c) Euhedral staurolite included in andalusite. (Fintown, x75)

(d) Sites of the regional garnets now represented by biotite knots which sometimes contain ? new regenerated garnets. Notice that the schistosity sweeps around the knots. (Fintown, x37)

(e) Small euhedral to subhedral new aureole garnets growing over the groundmass schistosity. The host schistosity is not deflected around these garnets (cf. photo d). (Fintown, x37)

(f) Small aureole garnets overprinted on the groundmass. (Glenaboghil, x37)

Abbreviations :

A	: andalusite	G	: garnet
B	: biotite	m	: mantle
c	: core	St	: staurolite

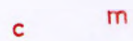

(a)

(b)

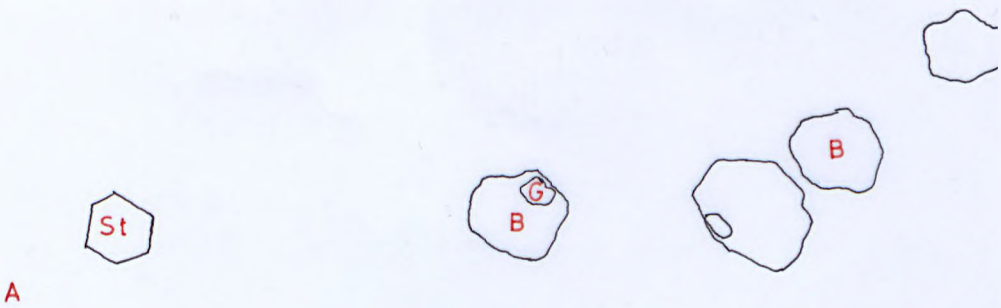

(c)

(d)

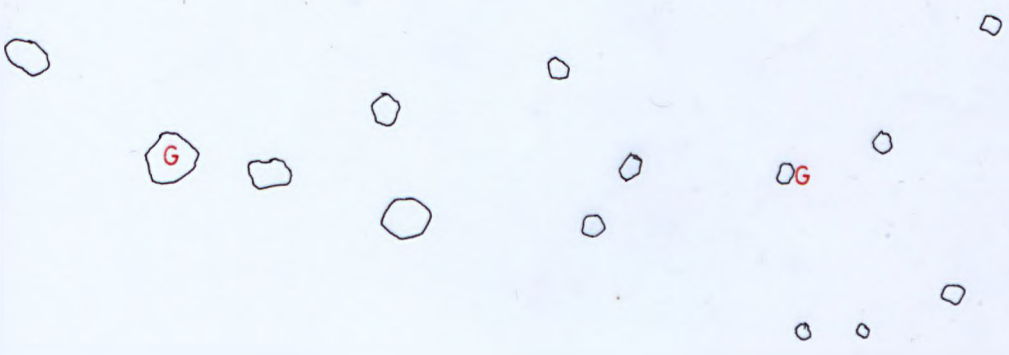

(e)

(f)

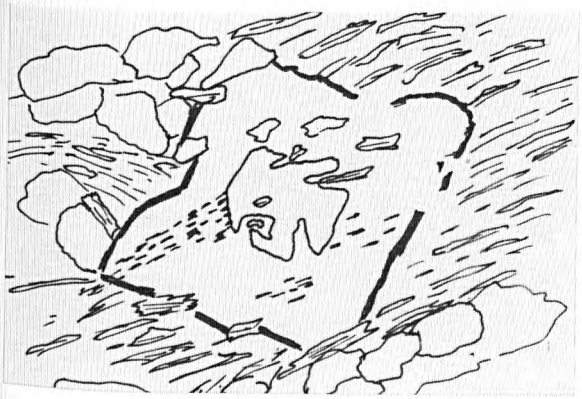

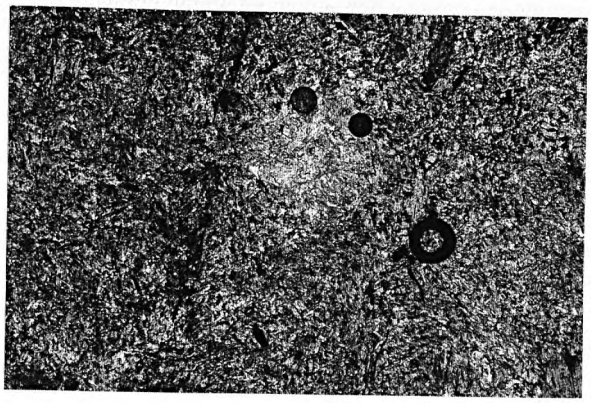

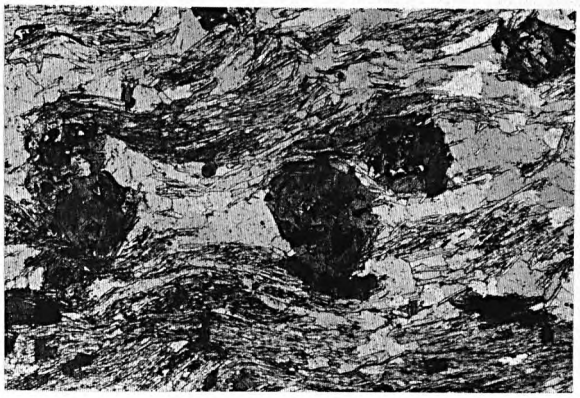

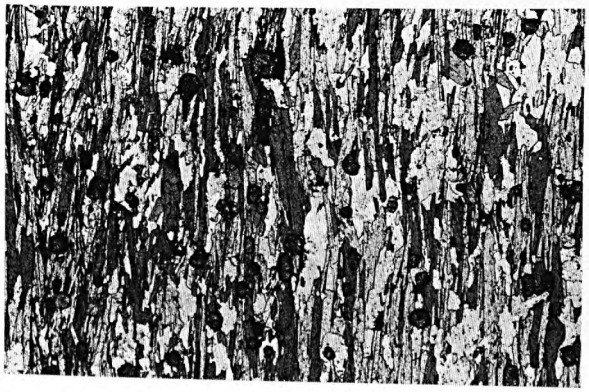

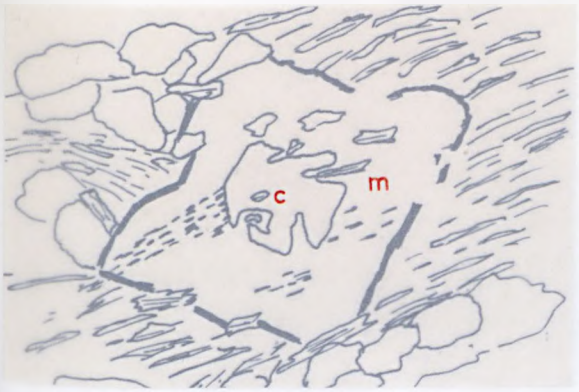

(a)

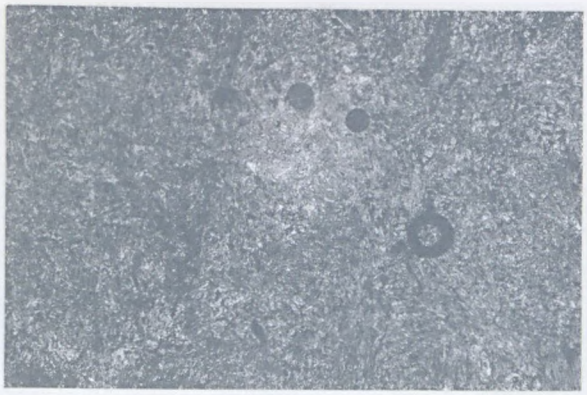

(b)

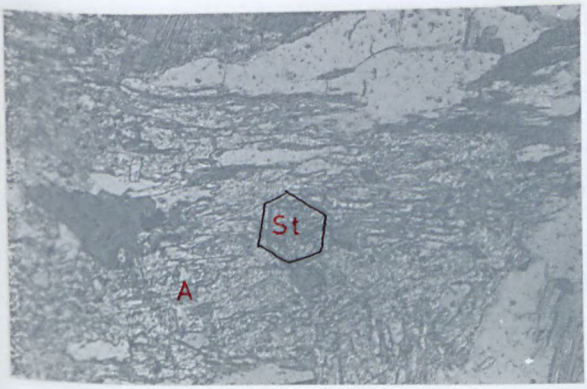

(c)

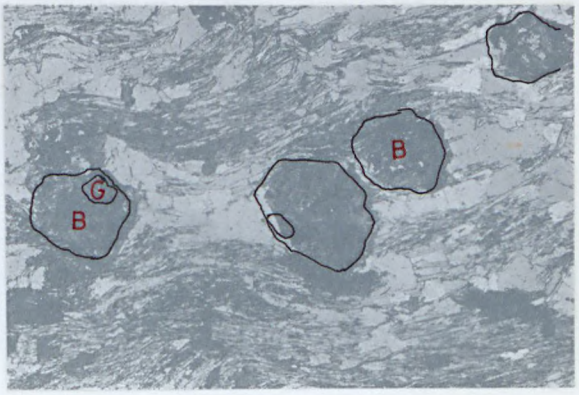

(d)

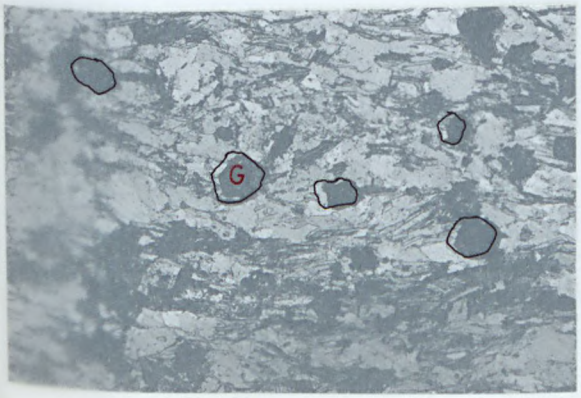

(e)

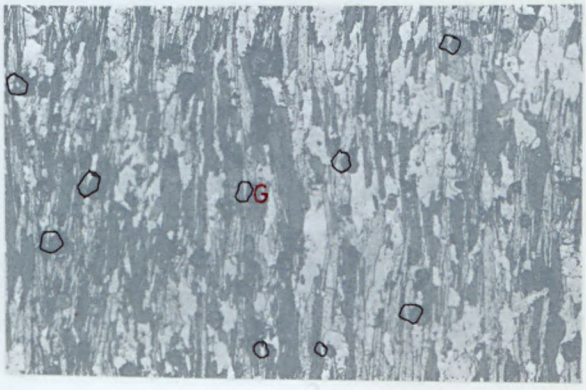

(f)

Plate 8.

(a) Small aureole garnets peppering the rock. (Glenaboghil, x38)

(b) Clusters of aureole garnets. (Glenaboghil, x75)

(c) Aureole garnets overprinted on partly fibrolitized biotite. (Glenaboghil, x75)

(d) Aureole garnets overprinted on partly fibrolitized biotite, the latter sometimes passes unhindered through the garnet. (Glenaboghil, x75)

(e) Aureole garnets overprinted on fibrolite. (Glenaboghil, x75)

(f) Kyanite overgrowing biotite. (Glenaboghil, x75)

Abbreviations :

B : biotite
F : fibrolite
G : garnet
K : kyanite

(a)

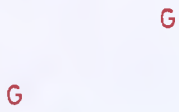

(b)

(c)

(d)

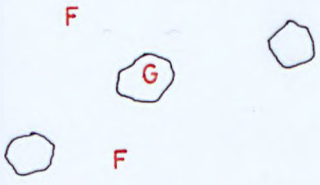

(e)

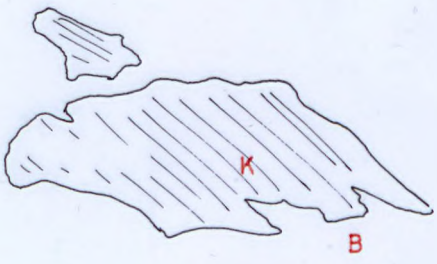

(f)

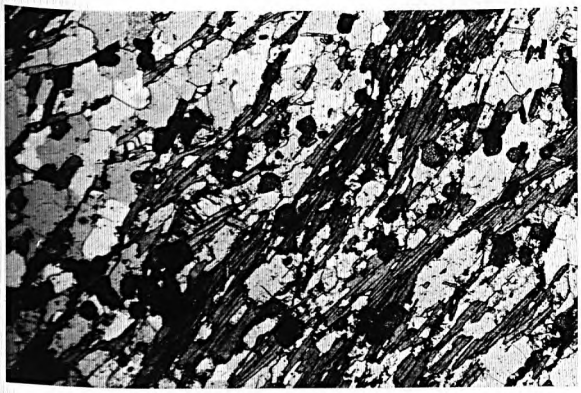

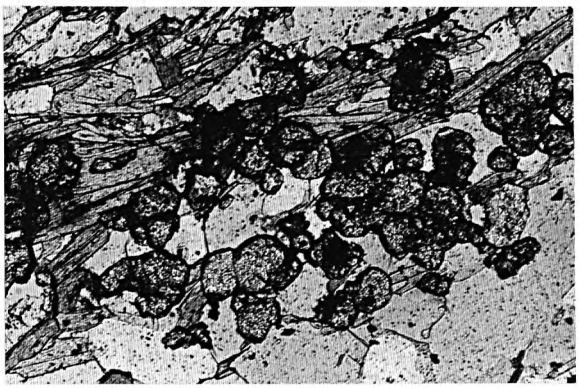

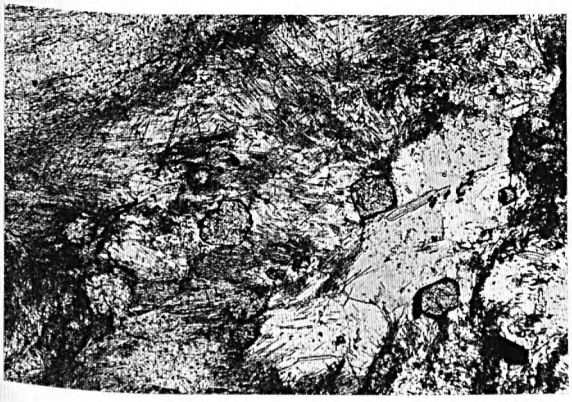

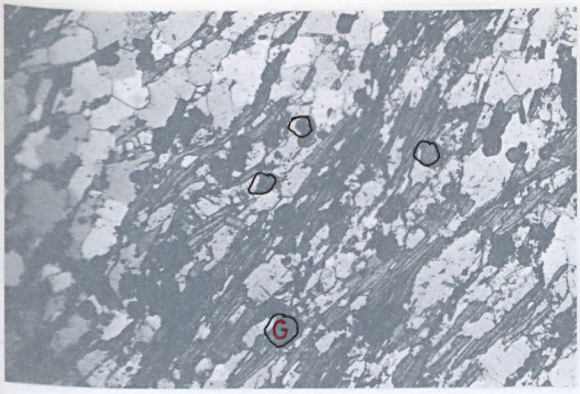

(a)

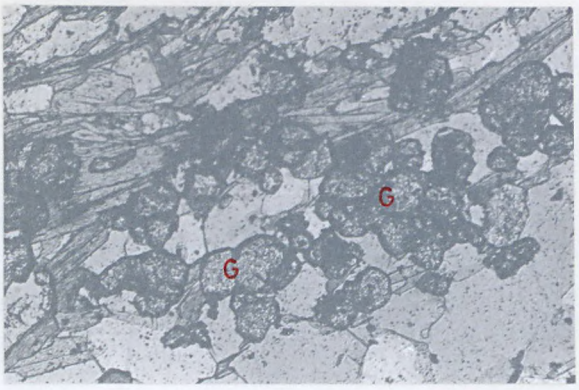

(b)

(c)

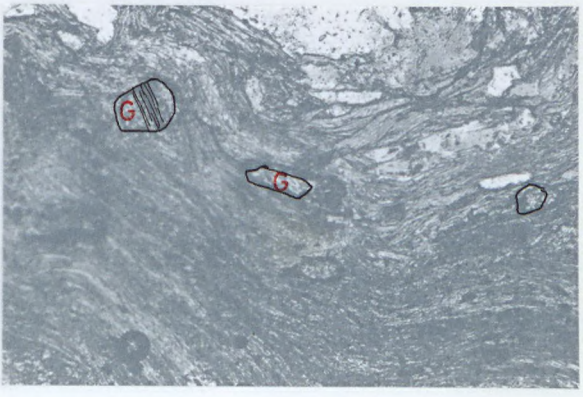

(d)

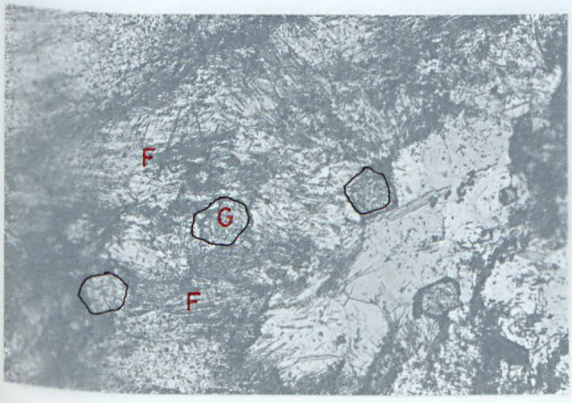

(e)

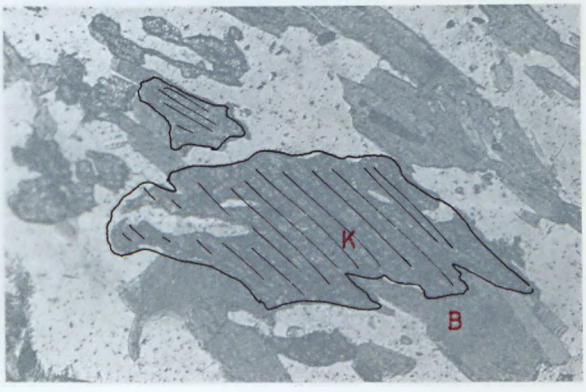

(f)

Plate 9.

(a) Kyanite overprinting biotite. (Glenaboghil, x75)

(b) Kyanite overprinting biotite. Notice that the host schistosity is not deflected around the kyanite. (Glenaboghil, x75)

(c) Aureole garnets included in kyanite. (Glenaboghil, x75)

(d) Aureole garnets included in staurolite. (Glenaboghil, x75)

(e) Kyanite prisms included in feldspar. (Glenaboghil, x75)

(f) Aureole garnets included in feldspar. (Glenaboghil, x75)

Abbreviations :

B : biotite
Fe :feldspar
G : garnet
K : kyanite
St : staurolite

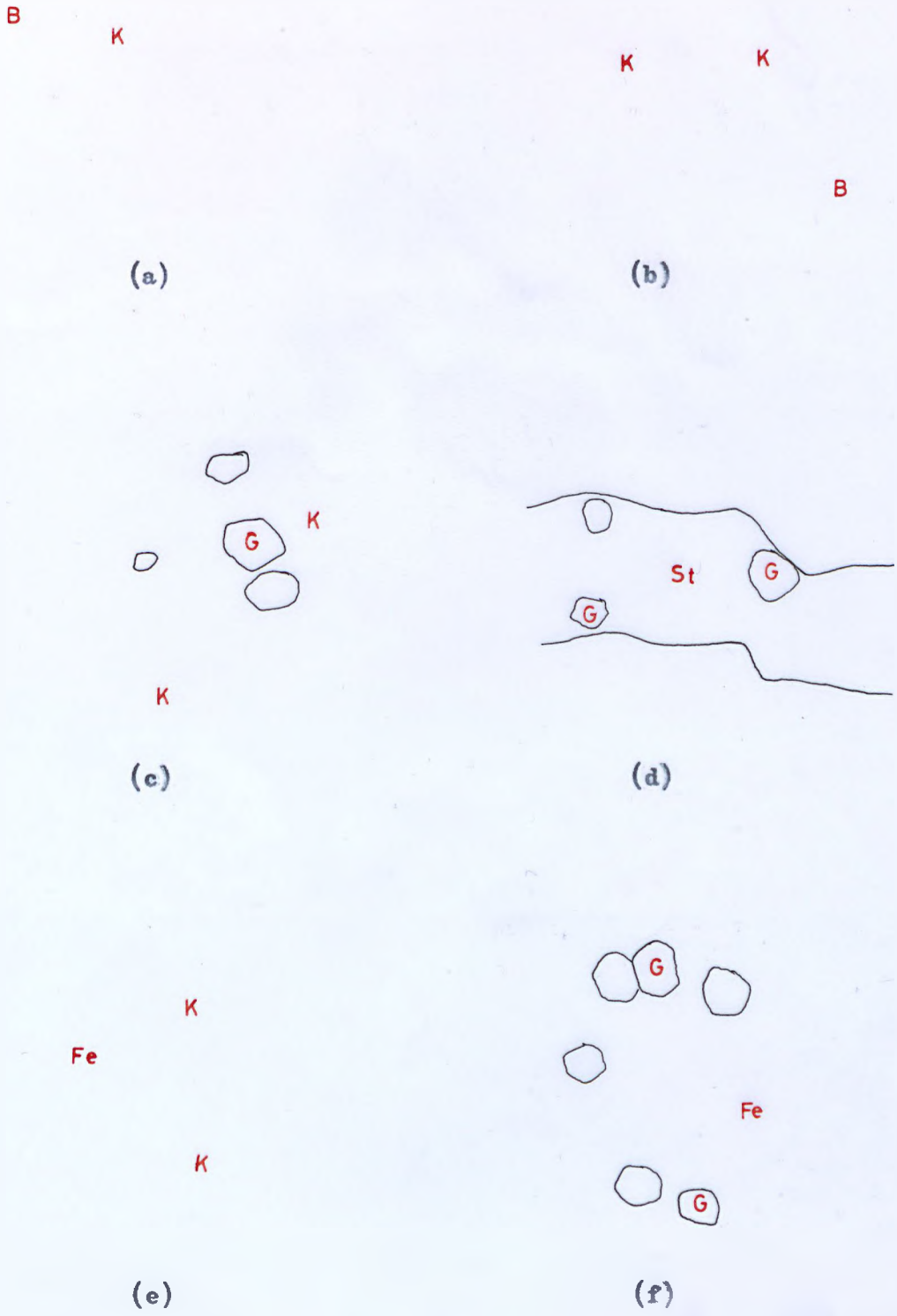
B
K
K
K
B
(a)
(b)
G
K
K
St
G
G
(c)
(d)
K
Fe
K
G
Fe
G
(e)
(f)

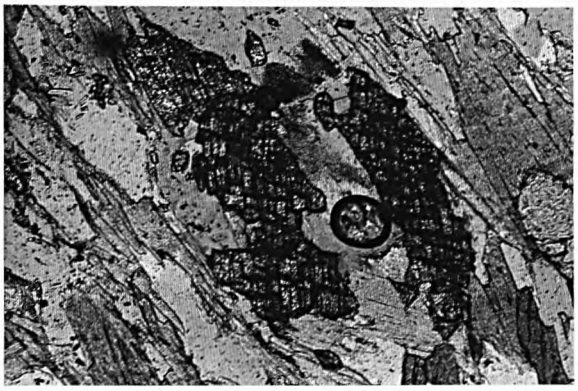

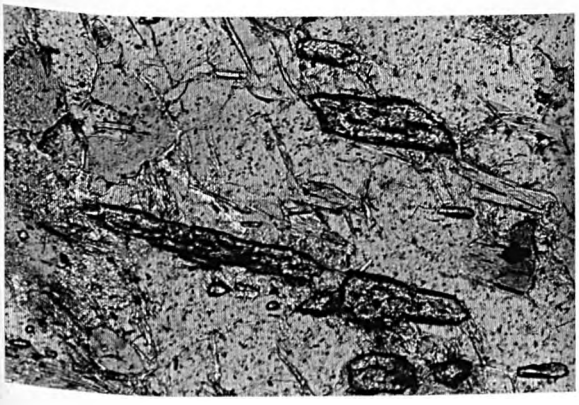

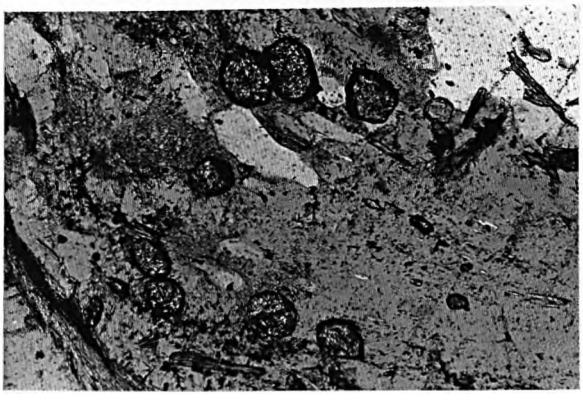

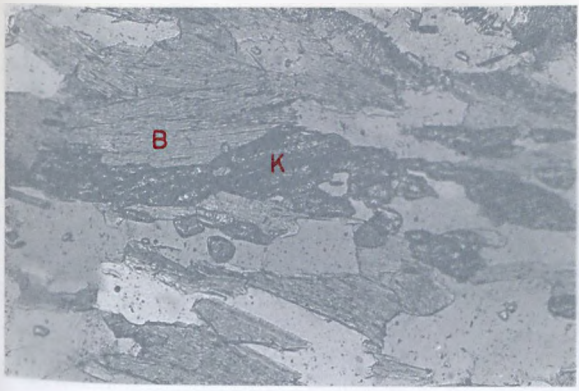

(a)

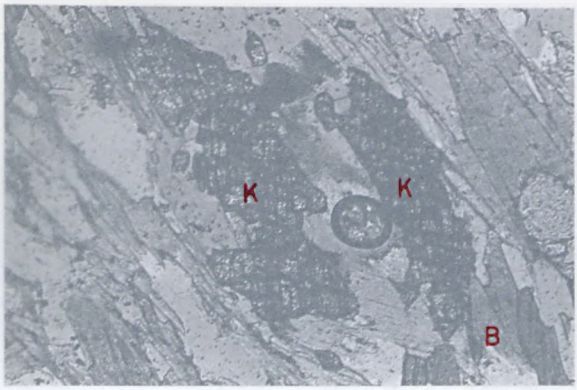

(b)

(c)

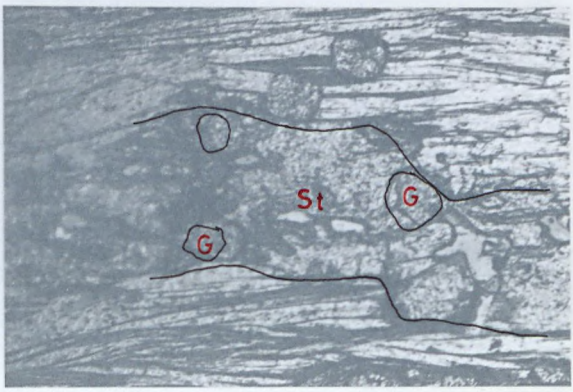

(d)

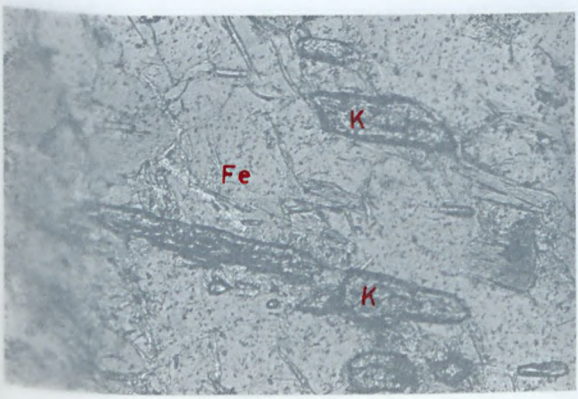

(e)

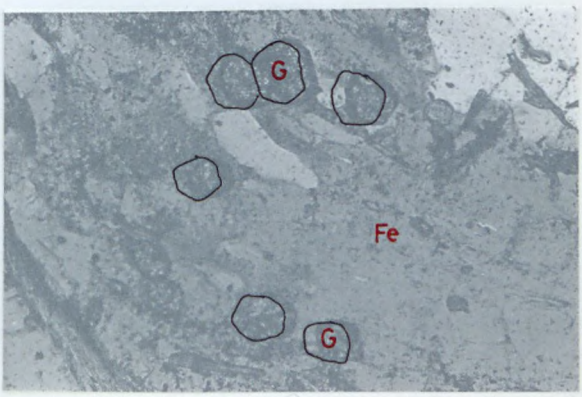

(f)

Plate 10.

(a) Aureole garnets and prisms of kyanite included in plagioclase. (Glenaboghil, x75)

(b) Same as photo (a). Crossed nicols.

(c) Kyanite lying in schistose biotite. Kyanite is not affected by the puckering shown by the biotite. (Lough Reelan, x37)

(d) Kyanite overprinted over biotite and lying at different angles to the schistosity. Notice that the schistosity is not deflected around the kyanite. (Lough Reelan, x75)

(e) Kyanite and staurolite with the groundmass schistosity sweeping around them. (Lough Reelan, x37)

(f) Kyanite and staurolite in parallel growth. Crossed nicols. (Lough Reelan, x75)

Abbreviations :

B : biotite
G : garnet
K : kyanite
P : plagioclase
St : staurolite

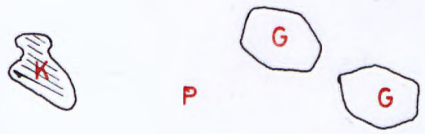

(a)

(b)

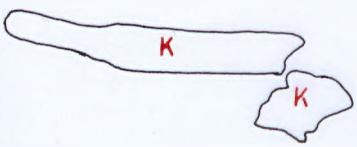

(c)

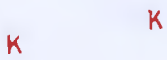

(d)

(e)

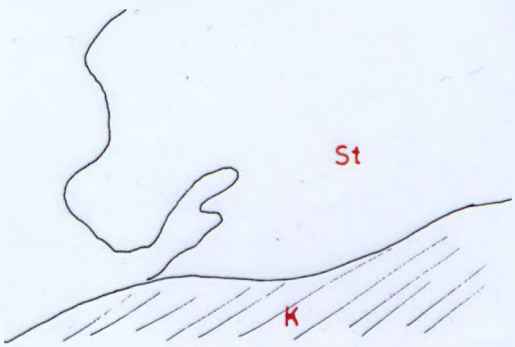

(f)

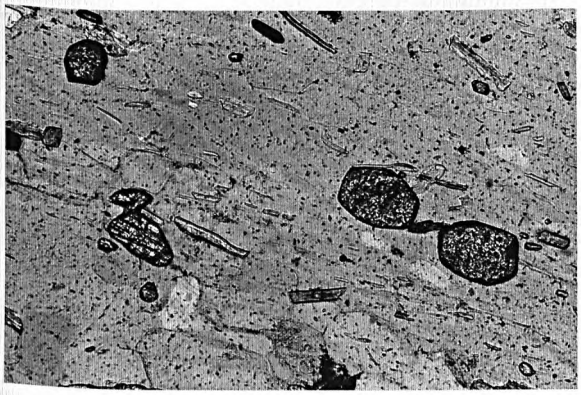

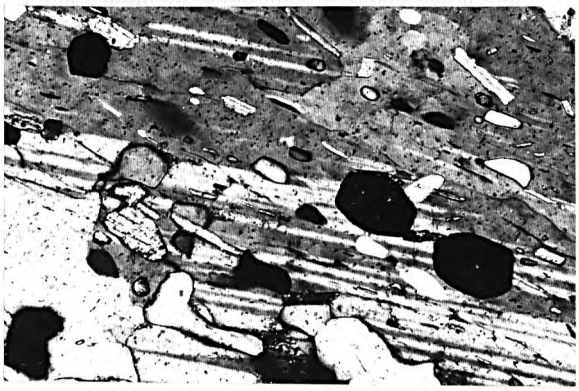

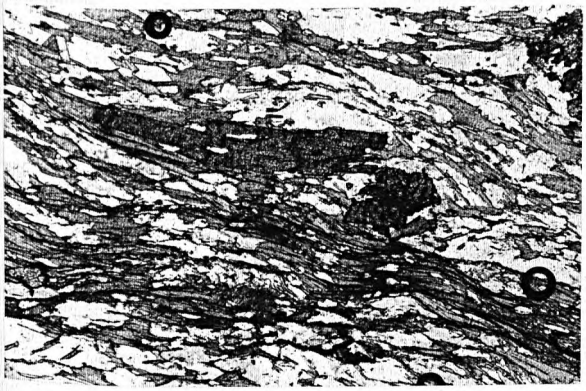

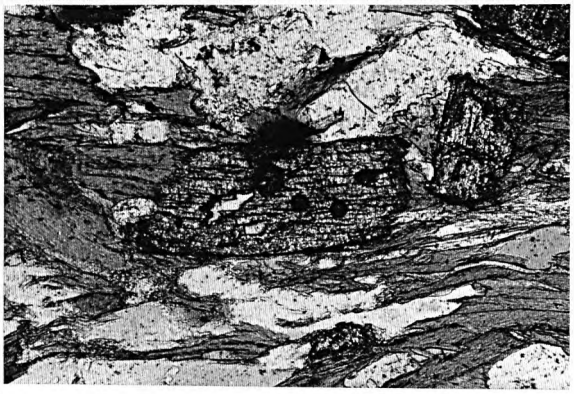

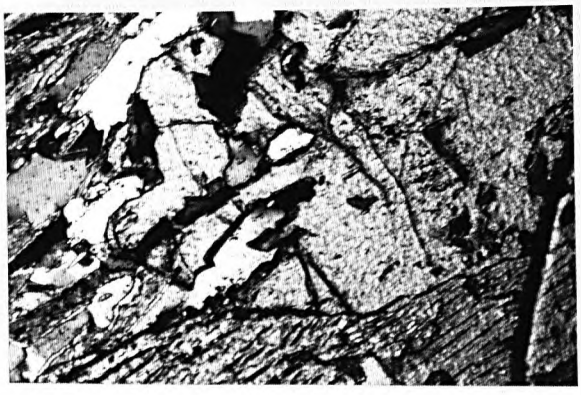

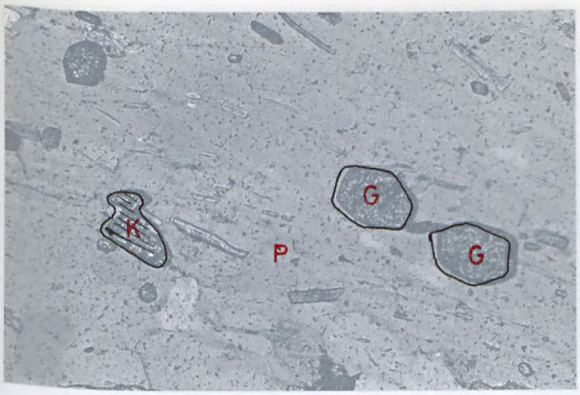

(a)

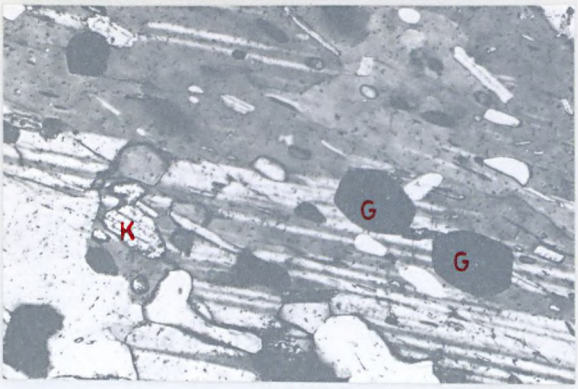

(b)

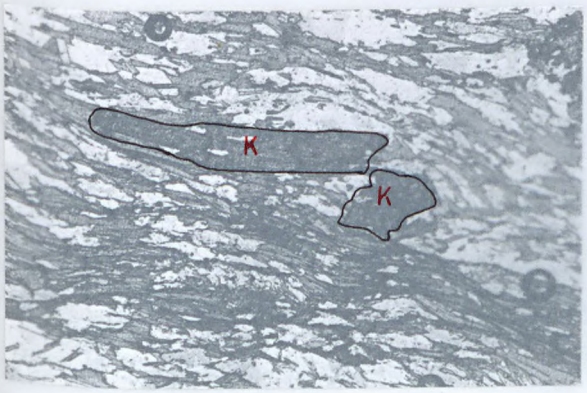

(c)

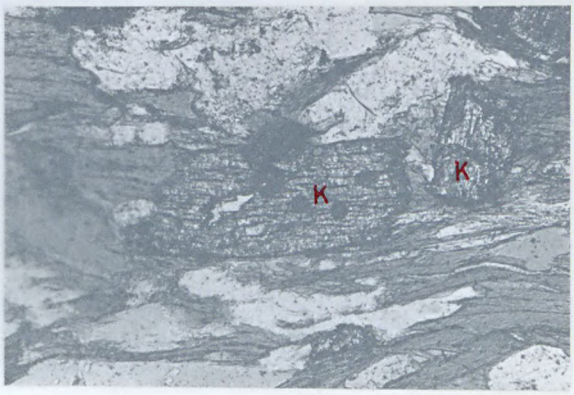

(d)

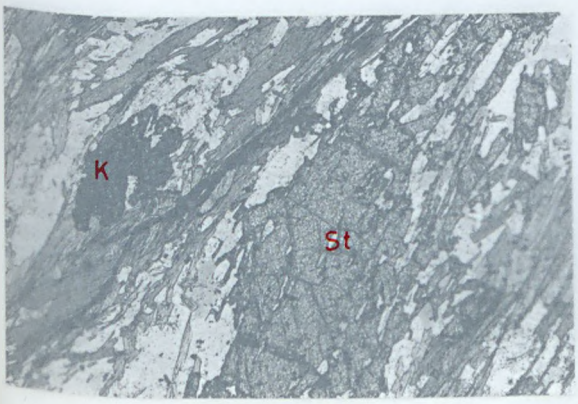

(e)

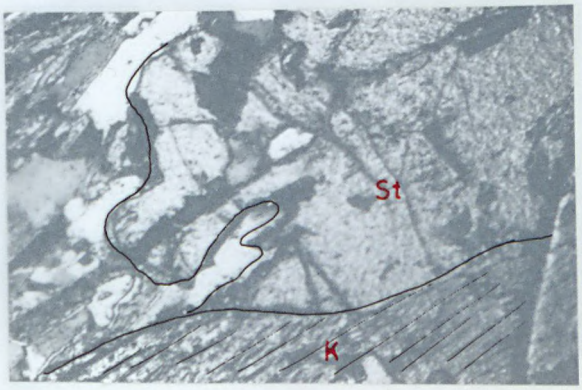

(f)

Plate 11.

(a) Euhedral staurolite included in andalusite. (Lough Reelan, x75)

(b) Kyanite and staurolite included in andalusite. (Lough Reelan, x40)

(c) Kyanite lying at an angle to the biotite. Notice that the host schistosity does not sweep around the kyanite. (Lough Reelan, x37)

(d) Kyanite-feldspar-biotite-quartz augen showing a hornfelsic texture and lying in a schistose rock. (Glenkeo, x10)

(e) Kyanite lying in the schistosity and responding to the strain slip cleavage by zig-zagging. Crossed nicols. (Glenkeo, x37)

(f) Part of the zig-zagged kyanite shown in photo (e) enlarged and seen under polarized light. (Glenkeo, x80)

Abbreviations :

A : andalusite
B : biotite
K : kyanite
St : staurolite

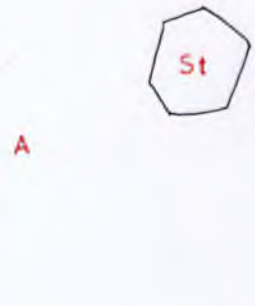

(a)

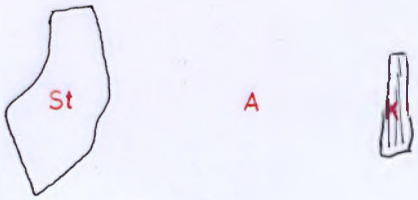

(b)

(c)

(d)

(e)

(f)

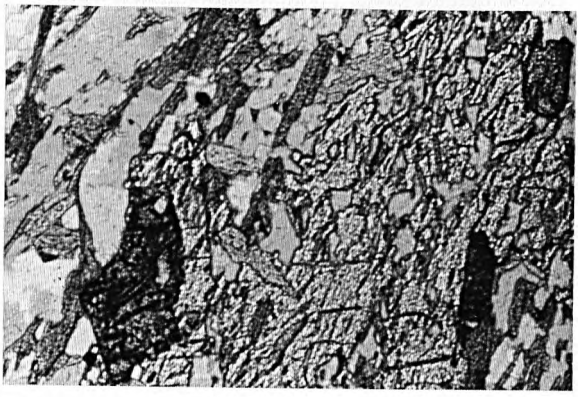

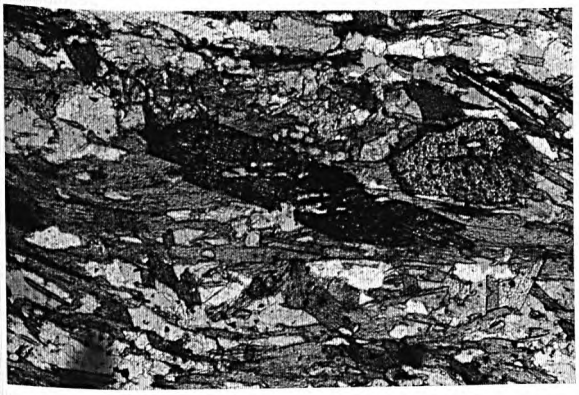

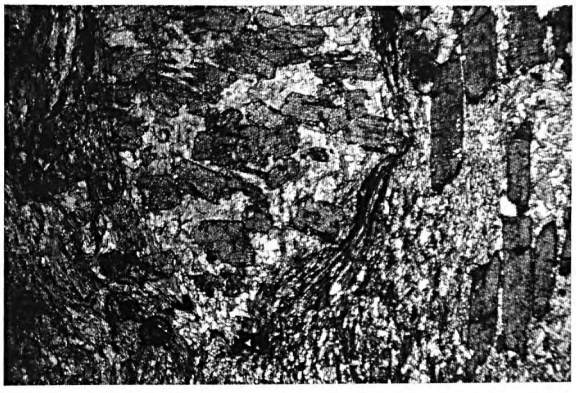

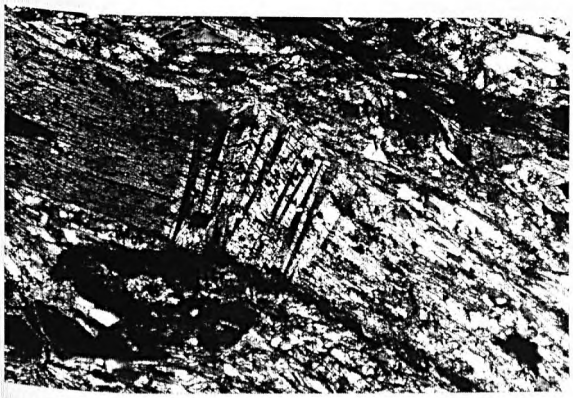

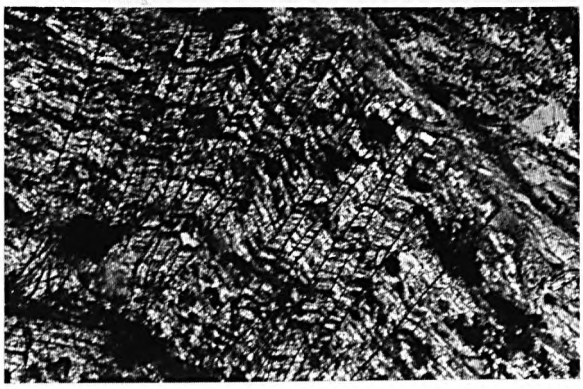

Plate 11.

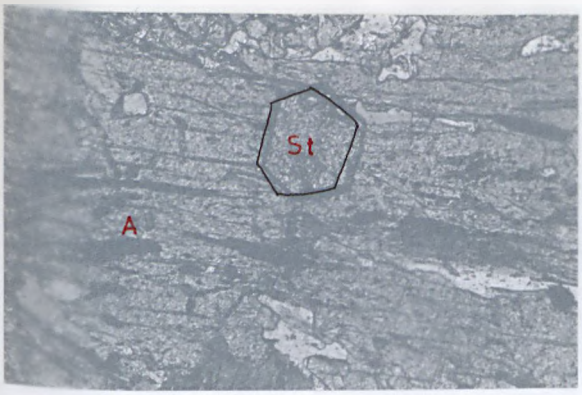

(a)

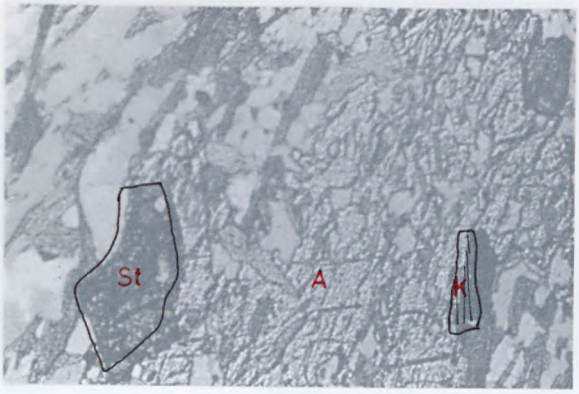

(b)

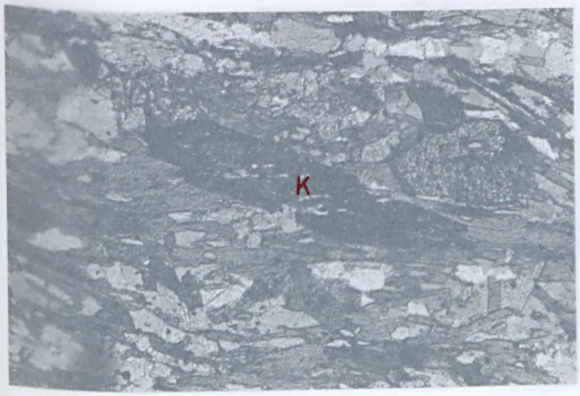

(c)

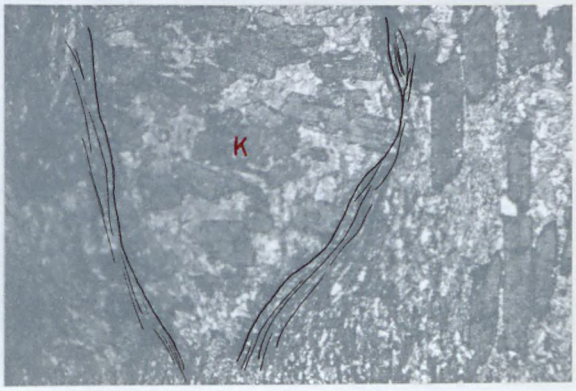

(d)

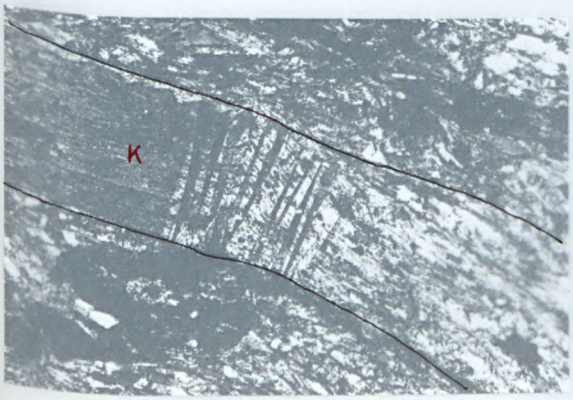

(e)

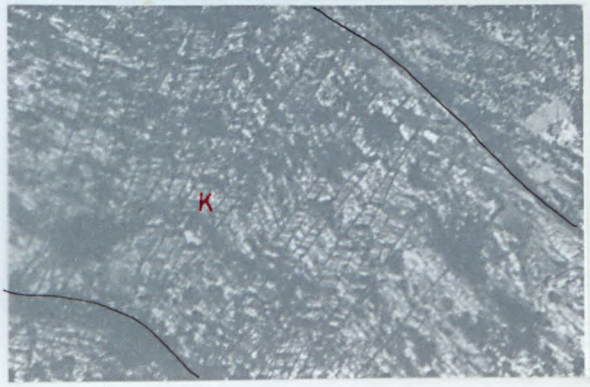

(f)

Plate 12.

(a) Zig-zagged and folded kyanite lying in the schistosity of the rock. (Glenkeo, x37)

(b) Same as (a). Crossed nicols.

(c) Strongly folded and partly snapped kyanite. Notice that from the arrangement of the quartz inclusions, the kyanite before being folded, originally over-printed a synclinal structure. (Glenkeo, x37)

(d) Undeformed kyanite containing folded dark inclusions passing from the groundmass. (Glenkeo, x75)

(e) Undeformed kyanite occurring in the hornfelsic augens. (Glenkeo, x37)

(f) Garnet included in staurolite. Notice the host schistosity sweeping around staurolite. Also kyanite is seen overprinting biotite. (Glenkeo, x37)

Abbreviations :

G : garnet
K : kyanite
St : staurolite

(a)

(b)

(c)

(d)

(e)

(f)

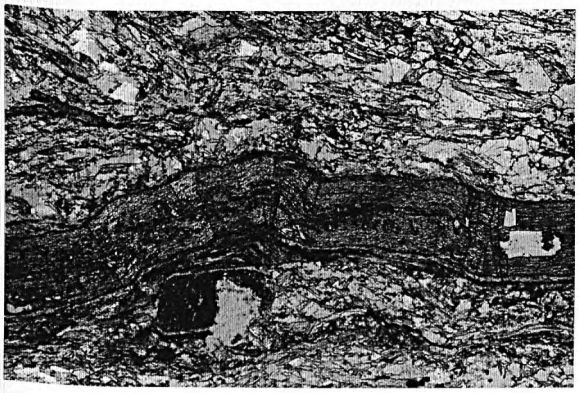

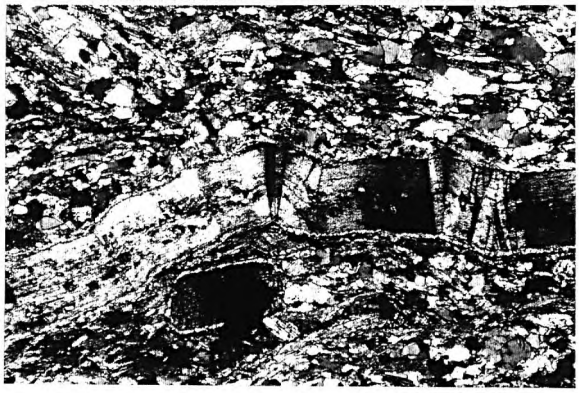

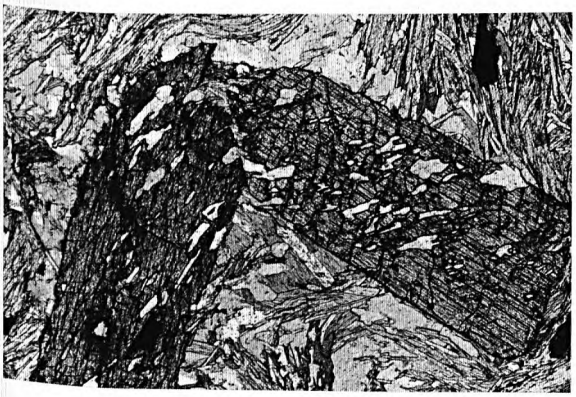

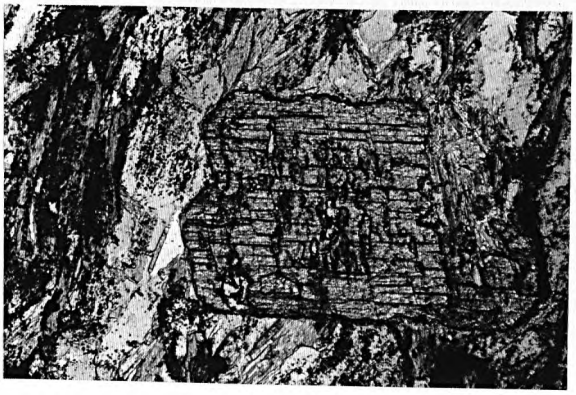

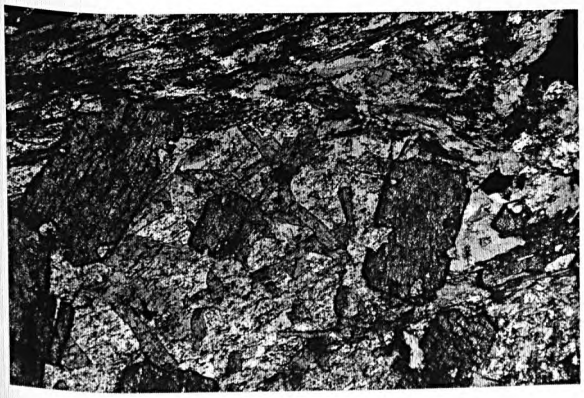

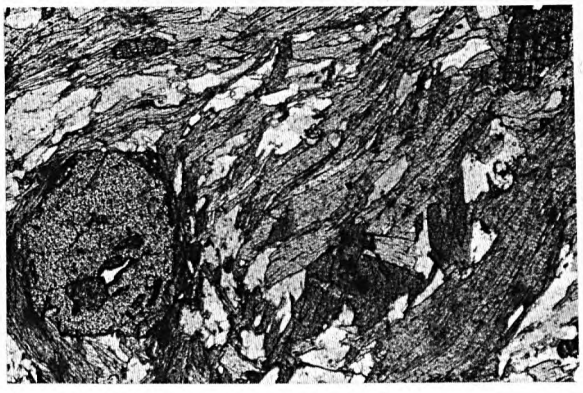

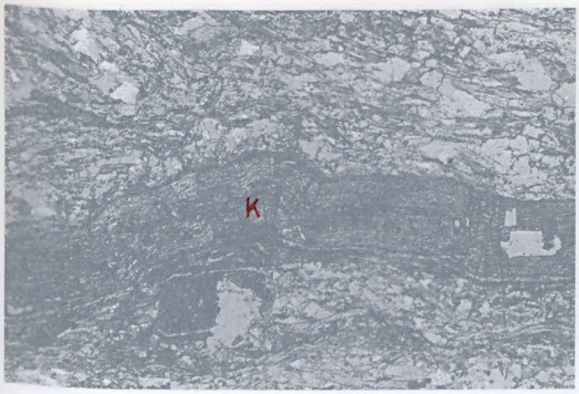

(a)

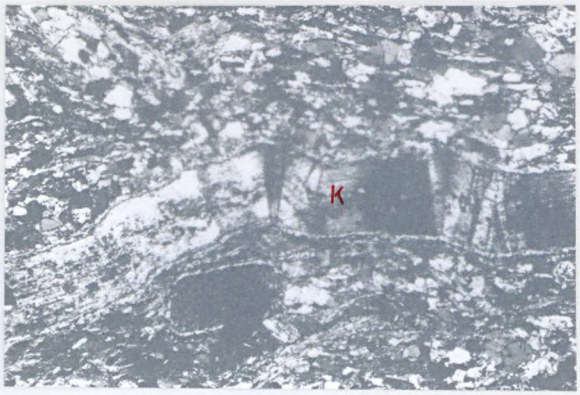

(b)

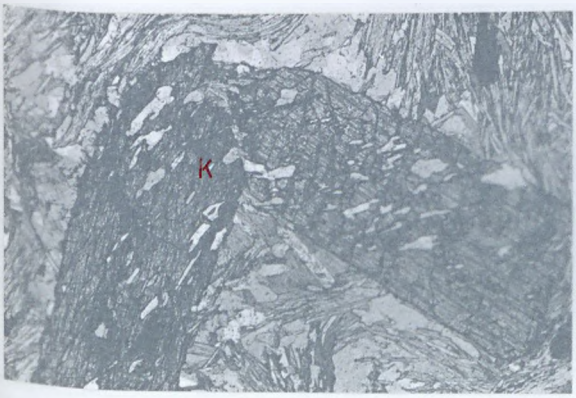

(c)

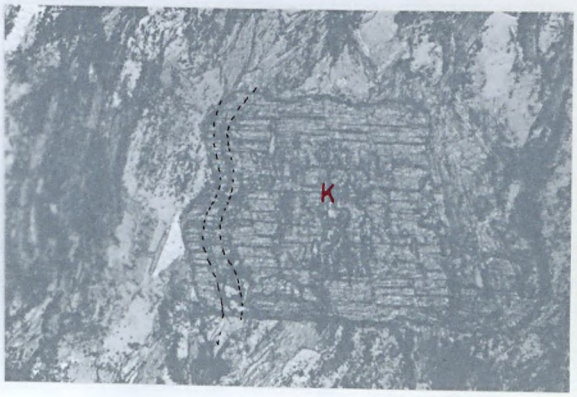

(d)

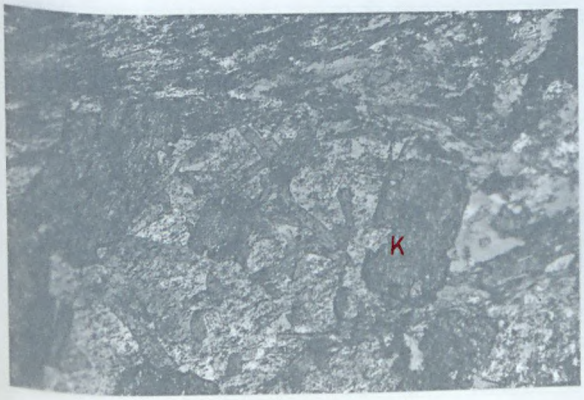

(e)

(f)

Plate 13.

(a) Enlargement of photo (e) in plate 12 showing garnet included in staurolite. (Glenkeo, x82)

(b) Kyanite with graphite inclusions arranged normal to the host schistosity. (Lackagh Bridge, x75)

(c) Host schistosity sweeping around kyanite. (Lackagh Bridge, x39)

Abbreviations :

B : biotite
G : garnet
K : kyanite
St : staurolite

B

St

(a)

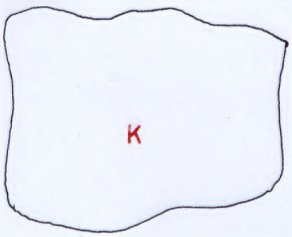

(b)

K

(c)

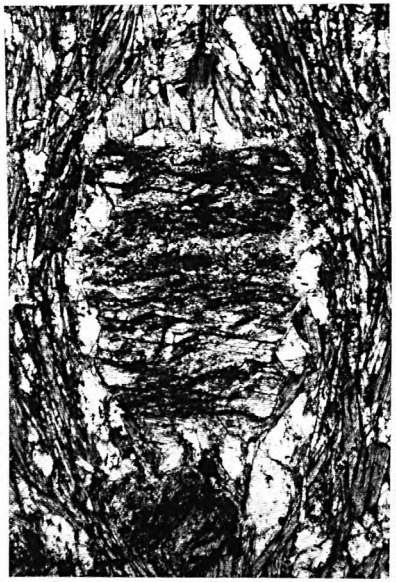

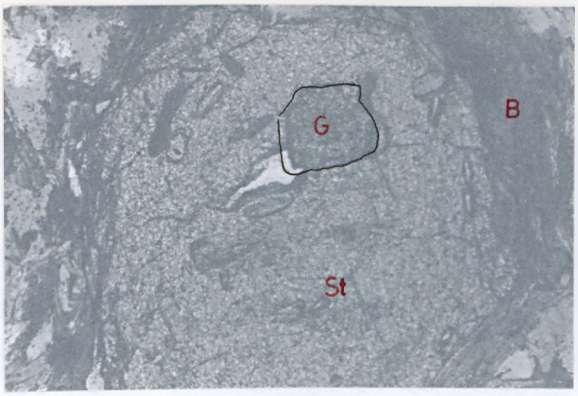

(a)

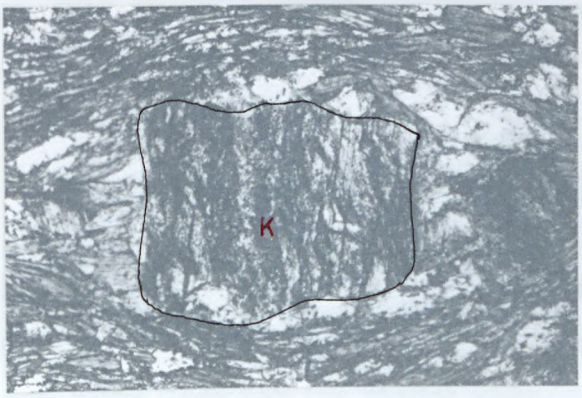

(b)

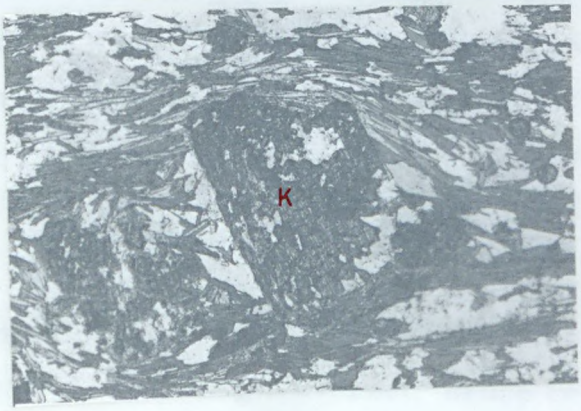

(c)

CHAPTER TWO

FLUORESCENT X-RAY AND MODAL ANALYSES

Eighty rock specimens were used for the fluorescent X-ray and modal analyses. It must be clearly emphasised that for these analyses, the specimens were chosen at random and only on the basis that they are suitably fresh for the analysis and in hand specimen they contain at least one form of the aluminium silicates. Appendix IV is an index for the analysed specimens showing the serial numbering of the specimens as used in the text of this thesis and the corresponding location and field labelling.

I. METHOD OF ROCK ANALYSIS

A rectangular hand specimen was used for each rock. Two parallel slices (normal to the schistosity) were cut from both ends of the specimen and were used for the modal analysis. The part of the specimen between the 2 slices (nearly 2"x 2" x4") were crushed and analysed by X-ray fluorescence as described earlier in Part One. The determination of FeO was carried out chemically by Mr. M. S. Brotherton of Geology Department, Liverpool University, by titration against potassium dichromate solution. By this technique of specimen analysis, it is hoped that the correlation between the chemistry of the rock and its modal composition will be a meaningful one.

For the modal analysis, the Ic number for an average rock was found to be 55 (40 mm. long traverse), hence two slides for each

rock were analysed using a point counter (c. f. Chayes, 1956). For each slide, the area measured ranged between 250-500 mm^2 and the number of counts collected ranged between 800-1600. The analytical results of the two slides were then averaged.

II. METHOD OF BIOTITE ANALYSIS

The biotite was separated from the 100-150 mesh fraction of the rock powder. The asymmetric vibrator was used to separate the platy minerals fraction (including the biotite) from the undesired rounded minerals fraction. The Frantz magnetic separator was then used to separate the biotite from the muscovite and chlorite. Finally, 5 milligrammes of pure biotite were then handpicked.

Partial analysis of 21 biotites was carried out by X-ray fluorescent analysis as described earlier in Part One.

III. CONSTRUCTION OF THE PHASE DIAGRAMS

In the calculation of the phase diagrams components, the oxides are defined in molecular proportion (i. e. $\frac{\text{oxide\%}}{\text{mol. wt.}} \times 1000$) and the corners of the triangles are defined as follows:-

AKF Diagrams :

$A = Al_2O_3 + Fe_2O_3 - (Na_2O + K_2O + CaO)$

$K = K_2O$

$F = FeO + MgO + MnO$

A'KF Diagrams :

$A' = Al_2O_3 - (Na_2O + K_2O + CaO)$

$K = K_2O$

$F = FeO + MgO + MnO + 2Fe_2O_3$

AFM Diagrams : $A = Al_2O_3 + Fe_2O_3 - (Na_2O + K_2O + CaO)$

$F = FeO + MnO$

$M = MgO$

A'FM Diagrams : $A' = Al_2O_3 - (Na_2O + K_2O + CaO)$

$F = FeO + MnO + 2Fe_2O_3$

$M = MgO$

AKFM Diagrams : $A = Al_2O_3 + Fe_2O_3 - (Na_2O + K_2O + CaO)$

$K = K_2O$

$F = FeO + MnO$

$M = MgO$

A'KFM Diagrams : $A' = Al_2O_3 - (Na_2O + K_2O + CaO)$

$K = K_2O$

$F = FeO + MnO + 2Fe_2O_3$

$M = MgO$

Correction for the presence of phosphorus was done as follows:- CaO% (used in the above calculations) = CaO% (in the rock) - 1.33 P_2O_5%.

For the purpose of graphic representation, all the above values were recalculated so that they are expressed as molecular percentages.

The AKFM and A'KFM diagrams are plotted using Philipsborn's (1928) method.

Thompson Phase Diagram for the Rocks:-

Thompson phase diagram (1957) can be applied to rock analyses provided that all mineral phases not appearing in the

projection has first been subtracted from the total bulk composition. Consequently, the amount of oxides contributing to the muscovite present has been calculated and subtracted from the rock analyses. In doing this, 2 approximations were entailed:-

(1) A single muscovite composition was used for all the 80 rocks analysed. This was taken as the average of 6 muscovite analyses (2 from sillimanite zone, one from andalusite zone and one from kyanite zone) given by Lambert (1959) and Albee (1965):- Al_2O_3 35.26%, FeO 0.34%, MgO 0.63% and K_2O 8.83%.

(2) Muscovite content was taken directly as the modal volume per cent. This is justifiable on the basis that the specific gravity of muscovite and that of the average pelite are nearly the same.

The values of the Thompson phase projection are calculated as follows:-

$$A = Al_2O_3 - 3K_2O/(Al_2O_3 - 3K_2O) + MgO + FeO \text{ (moles)}$$

$$M \text{ (or } M/FM) = MgO/MgO + FeO \text{ (moles)}$$

IV. RESULTS

The results of the fluorescent and modal analyses of the rocks are shown in Table 51, the values of their phase diagrams in Table 52. The results of biotite analysis is shown in Table 53.

TABLE 51

Chemical and Modal Analyses of the Aureole Rocks

(1) Fanad Aureole:

Rock Text No.	1	2	3	4	5
SiO_2	64.08	60.00	59.26	54.82	58.64
TiO_2	0.81	1.05	1.19	1.11	1.00
Al_2O_3	18.19	20.41	20.95	24.00	20.40
Fe_2O_3	1.21	0.99	1.00	0.86	1.42
FeO	5.80	6.27	6.69	7.87	7.73
MnO	0.07	0.07	0.06	0.08	0.11
MgO	1.80	1.55	1.63	1.72	1.77
CaO	0.32	0.91	0.27	0.48	0.52
Na_2O	1.38	2.11	1.11	1.98	1.33
K_2O	4.53	4.35	5.06	4.96	4.23
P_2O_5	0.07	0.08	0.07	0.09	0.11
O. R. **	16.5	12.1	11.4	9.3	15.6

** Oxidation ratio = mol. $\frac{2Fe_2O_3}{2Fe_2O_3+FeO}$

TABLE 51 (CONTINUED)

Rock Text No.	1	2	3	4	5
Quartz + Felds.	38.0	48.5*	49.9*	21.4	32.5
Biot- (Green	2.1	-	-	5.3	2.2
ite (Brown	19.7	28.5	29.0	21.0	27.7
Muscovite	34.7	8.3	3.8	36.1	20.8
Chlorite	0.9	-	-	1.6	1.7
Garnet	-	-	-	3.0	-
Ore	2.5	1.1	1.0	4.4	2.3
Graphite	-	-	-	-	-
Cordierite	-	-	-	-	-
Shimmer	0.3	-	3.1	-	-
Andalusite	1.9	13.2	6.8	7.2	12.7
Fibrolite	-	0.2	6.0	-	-
Sillimanite	-	-	0.4	-	-

* Indicates the presence of potash feldspar.

TABLE 51 (CONTINUED)

Rock Text No.	6	7	8	9	10	11
SiO_2	58.76	66.03	58.59	61.09	59.11	63.50
TiO_2	0.88	0.88	0.92	1.06	1.12	0.89
Al_2O_3	19.13	18.62	20.80	19.10	20.66	18.82
Fe_2O_3	0.96	1.34	0.88	0.68	1.14	1.19
FeO	8.21	5.31	7.53	6.00	6.76	6.36
MnO	0.10	0.06	0.06	0.07	0.07	0.06
MgO	2.14	1.50	1.97	1.43	1.67	1.61
CaO	0.86	0.36	0.75	0.60	0.41	0.35
Na_2O	1.74	1.75	1.82	1.71	1.80	1.32
K_2O	4.24	3.72	4.61	5.36	4.67	3.64
P_2O_5	0.14	0.07	0.14	0.06	0.06	0.08
O.R.	9.5	18.5	10.0	8.7	13.6	15.2

TABLE 51 (CONTINUED)

Rock Text No.	6	7	8	9	10	11
Quartz + Felds.	39.9	40.6	38.2	51.0*	39.5	48.1
Biot- (Green	-	-	1.9	-	-	-
ite (Brown	40.9	26.7	22.2	35.4	36.7	22.7
Muscovite	13.1	21.3	22.6	1.3	8.0	19.3
Chlorite	1.3	-	-	-	0.1	0.5
Garnet	0.2	0.7	6.7	-	-	-
Ore	0.9	2.3	1.7	0.8	2.1	1.9
Graphite	-	-	-	-	-	-
Cordierite	-	-	-	-	-	-
Shimmer	0.2	-	1.3	0.3	10.8	1.4
Andalusite	3.5	8.1	5.4	4.3	2.5	6.1
Fibrolite	-	-	-	6.8	0.3	-
Sillimanite	-	-	-	-	-	-

TABLE 51 (CONTINUED)

Rock Text No	12	13	14	15	16	17
SiO_2	58.76	59.18	59.96	61.25	55.61	58.50
TiO_2	1.14	1.19	1.04	1.03	1.17	1.10
Al_2O_3	20.98	20.37	20.99	19.28	22.65	20.06
Fe_2O_3	1.36	0.80	1.60	1.16	1.57	1.27
FeO	7.33	7.30	5.32	6.31	6.94	7.77
MnO	0.10	0.08	0.06	0.06	0.06	0.07
MgO	1.93	1.64	1.73	1.83	1.72	1.68
CaO	0.23	0.59	0.16	0.74	0.46	0.64
Na_2O	0.79	1.53	1.63	1.77	1.66	1.71
K_2O	4.58	4.59	4.60	4.17	4.99	4.04
P_2O_5	0.09	0.08	0.07	0.10	0.08	0.11
O.R.	14.4	8.9	21.2	14.7	16.8	12.9

TABLE 51 (CONTINUED)

Rock Text No.	12	13	14	15	16	17
Quartz + Felds.	38.3	42.9*	36.2	38.4	30.4	43.1
Biot- (Green	-	-	-	-	-	-
ite (Brown	32.7	37.1	14.8	32.0	32.9	26.8
Muscovite	5.4	4.6	10.1	17.6	5.0	9.9
Chlorite	-	-	0.5	-	-	0.7
Garnet	-	-	-	-	0.1	0.2
Ore	1.7	1.3	1.8	0.8	4.1	1.7
Graphite	-	-	-	-	-	-
Cordierite	0.3	-	A	-	0.5	-
Shimmer	8.8	0.1	32.8	-	20.8	8.9
Andalusite	6.0	5.3	2.9	11.3	6.0	6.6
Fibrolite	5.8	8.5	0.7	-	0.3	2.1
Sillimanite	1.0	0.2	0.1	-	-	-

A : altered

TABLE 51 (CONTINUED)

Rock Text No.	18.	19	20	21	22
SiO_2	59.78	57.42	54.79	59.02	59.81
TiO_2	1.09	1.20	1.16	1.10	1.08
Al_2O_3	20.68	21.73	22.03	19.80	19.39
Fe_2O_3	1.25	1.03	1.25	1.39	1.25
FeO	6.88	7.61	7.95	7.49	7.59
MnO	0.07	0.07	0.07	0.09	0.07
MgO	1.76	1.78	2.17	2.00	2.18
CaO	0.37	0.53	0.35	0.72	0.35
Na_2O	1.27	1.41	1.21	1.23	1.08
K_2O	4.17	4.47	4.93	4.07	4.34
P_2O_5	0.09	0.11	0.09	0.10	0.09
O. R.	14.3	10.6	12.6	14.6	13.1

TABLE 51 (CONTINUED)

Rock Text No.	18	19	20	21	22
Quartz + Felds.	35.8	42.9	32.9	37.4	44.0*
Biot- (Green	0.3	0.7	-	-	-
ite (Brown	26.2	25.2	29.5	31.3	39.2
Muscovite	4.5	8.2	16.9	5.2	2.8
Chlorite	0.8	0.5	0.5	0.8	-
Garnet	0.1	0.6	-	0.3	-
Ore	3.1	1.9	1.9	1.5	1.1
Graphite	-	-	-	-	-
Cordierite	-	-	-	A	-
Shimmer	19.4	12.1	8.2	12.5	0.8
Andalusite	6.6	7.3	8.0	9.7	10.5
Fibrolite	3.2	0.4	1.7	1.4	1.3
Sillimanite	-	0.3	0.4	-	0.3

TABLE 51 (CONTINUED)

(2) Ardara Aureole:

Rock Text No.	23	24	25	26	27
SiO_2	61.13	59.53	59.20	58.12	59.92
TiO_2	1.03	1.26	0.88	0.84	0.87
Al_2O_3	19.03	26.10	20.40	20.14	20.05
Fe_2O_3	1.39	1.58	1.82	1.46	1.31
FeO	6.06	3.47	4.69	5.79	6.06
MnO	0.07	0.05	0.07	0.12	0.11
MgO	2.27	1.68	5.25	4.20	2.69
CaO	0.48	0.15	0.19	0.48	0.74
Na_2O	1.84	1.31	0.93	1.28	1.92
K_2O	3.53	3.85	3.07	3.78	3.53
P_2O_5	0.08	0.06	0.07	0.08	0.08
O.R.	17.4	28.8	25.7	18.2	16.1

TABLE 51 (CONTINUED)

Rock Text No.	23	24	25	26	27
Quartz + Felds.	38.4	32.1	34.1	40.3	41.8
Biot- (Green	-	-	-	-	-
ite (Brown	39.4	20.3	22.8	19.6	23.6
Muscovite	5.0	28.4	3.1	5.6	8.7
Chlorite	-	-	7.8	15.7	5.4
Garnet	-	-	-	0.6	1.3
Ore	0.7	3.5	0.3	0.5	1.0
Graphite			-	-	
Cordierite	-	-	-	-	-
Shimmer	-	-	8.2	16.4	14.7
Staurolite	-	0.8	1.3	0.2	0.5
Andalusite	12.7	11.0	14.4	1.2	3.1
Fibrolite	3.9	3.7	-	-	-
Sillimanite	-	-	-	-	-
Kyanite	-	-	1.9	-	-

TABLE 51 (CONTINUED)

Rock Text No.	28	29	30	31	32	33
SiO_2	55.22	50.78	57.81	69.08	60.76	60.81
TiO_2	1.06	1.20	1.17	1.03	0.81	0.84
Al_2O_3	23.91	31.01	23.43	16.64	17.57	18.01
Fe_2O_3	2.01	1.43	1.44	1.77	1.81	2.06
FeO	5.42	3.55	4.88	5.36	4.85	4.48
MnO	0.10	0.05	0.06	0.07	0.08	0.08
MgO	2.39	1.37	2.31	2.55	5.72	5.82
CaO	0.66	0.32	0.88	0.57	0.67	0.58
Na_2O	1.83	1.56	1.92	1.03	1.55	1.52
K_2O	3.97	5.98	2.77	1.57	2.75	2.99
P_2O_5	0.07	0.07	0.10	0.06	0.08	0.09
O.R.	25.6	26.7	21.0	22.8	24.7	29.3

TABLE 51 (CONTINUED)

Rock Text No.	28	29	30	31	32	33
Quartz + Felds.	42.8	17.4	43.6	57.6	48.5	44.8
Biot- (Green	-	-	-	-	-	-
ite (Brown	37.2	2.3	19.3	18.7	32.6	44.0
Muscovite	5.0	39.1	6.7	2.5	5.6	0.7
Chlorite	1.0	6.8	1.1	4.3	5.7	1.5
Garnet	0.2	-	-	3.2	-	-
Ore	1.3	2.2	6.8	5.3	0.7	0.3
Graphite	-			-	-	-
Cordierite	-	-	-	0.4	-	-
Shimmer	8.1	24.5	5.1	-	-	0.2
Staurolite	1.0	tr	-	-	2.3	0.5
Andalusite	3.4	7.6	16.7	1.7	4.1	6.9
Fibrolite	-	-	0.7	5.5	0.2	0.2
Sillimanite	-	-	-	0.7	-	-
Kyanite	-	-	-	-	0.4	0.8

TABLE 51 (CONTINUED)

Rock Text No.	34	35	36	37	38	39
SiO_2	58.03	55.13	58.94	61.82	60.62	60.99
TiO_2	0.97	1.00	0.92	0.83	0.94	0.85
Al_2O_3	18.85	25.27	19.84	18.63	20.64	18.02
Fe_2O_3	1.86	1.64	1.57	1.70	1.49	1.48
FeO	6.38	4.60	4.40	4.29	4.38	4.77
MnO	0.12	0.09	0.11	0.08	0.06	0.08
MgO	4.33	3.16	5.30	5.00	4.66	6.10
CaO	0.75	0.37	1.12	0.68	0.65	0.30
Na_2O	1.36	1.69	1.88	1.27	1.21	0.87
K_2O	3.42	4.36	2.68	2.81	2.97	3.74
P_2O_5	0.08	0.07	0.09	0.08	0.08	0.08
O.R.	20.7	24.5	24.1	26.9	22.8	21.3

TABLE 51 (CONTINUED)

Rock Text No.	34	35	36	37	38	39
Quartz + Felds.	34.8	27.6	42.1	39.8	36.0	39.9
Biot- (Green	-	1.7	-	-	-	-
ite (Brown	43.5	-	40.3	45.2	44.5	41.1
Muscovite	1.8	6.6	1.3	1.7	2.7	1.3
Chlorite	0.8	26.1	3.5	1.4	-	1.8
Garnet	2.4	0.4	-	-	-	-
Ore	1.2	1.4	0.3	0.7	0.9	2.0
Graphite		-	-	-	-	-
Cordierite	-	-	-	-	-	-
Shimmer	-	35.4	1.4	0.1	-	0.2
Staurolite	0.5	-	1.4	1.2	1.7	0.4
Andalusite	14.6	0.8	7.7	8.5	13.4	12.5
Fibrolite	0.5	-	1.0	-	0.3	0.2
Sillimanite	-	-	-	-	-	-
Kyanite	-	-	0.9	1.4	0.6	0.7

TABLE 51 (CONTINUED)

(3) Barnesmore Aureoles:

Rock Text No.	40	41	42
SiO_2	57.17	52.39	56.49
TiO_2	0.90	0.82	0.81
Al_2O_3	20.45	22.44	22.60
Fe_2O_3	2.94	2.23	2.80
FeO	4.34	4.74	4.12
MnO	0.09	0.07	0.09
MgO	2.89	3.03	2.74
CaO	0.46	0.32	0.26
Na_2O	1.61	1.56	1.75
K_2O	6.66	8.52	5.95
P_2O_5	0.11	0.08	0.08
O.R.	37.9	29.9	38.6

TABLE 51 (CONTINUED)

Rock Text No.	40	41	42
Quartz + Felds.	36.4*	35.3*	35.0*
Biotite @	30.2	31.3	12.2
Muscovite	24.0	24.7	47.4
Chlorite	0.9	-	0.8
Ore	1.0	0.7	2.1
Shimmer	5.6	-	0.1
Andalusite	1.6	7.3	2.4
Fibrolite	0.3	0.7	-

@ : Green to brownish green

TABLE 51 (CONTINUED)

(4) Thorr Granodiorite Aureole and Enclaves:

Rock Text No.	43	44	45	46	47
SiO_2	62.95	60.21	65.32	48.55	63.46
TiO_2	0.83	0.92	0.94	1.40	0.97
Al_2O_3	20.04	20.50	18.99	32.16	20.61
Fe_2O_3	1.14	1.70	1.05	1.22	1.53
FeO	5.10	5.68	5.04	6.09	4.60
MnO	0.06	0.07	0.06	0.06	0.09
MgO	2.22	2.50	2.10	2.59	2.28
CaO	0.33	0.23	0.31	0.54	0.15
Na_2O	1.63	1.65	1.08	1.21	0.84
K_2O	4.24	4.41	3.66	4.04	4.25
P_2O_5	0.07	0.04	0.07	0.06	0.06
O.R.	17.2	21.8	15.6	15.8	22.5

TABLE 51 (CONTINUED)

Rock Text No.	43	44	45	46	47
Quartz + Felds.	32.8	36.4	51.1*	25.9*	46.3
Biot- (Green	-	-	-	-	-
ite (Brown	25.9	30.0	10.8	43.7	33.8
Muscovite	35.1	25.2	17.8	1.2	12.7
Chlorite	0.7	2.6	10.1	0.1	-
Garnet	-	-	-	-	-
Ore	1.4	1.4	1.8	1.1	1.7
Shimmer	0.2	0.3	6.8	2.0	3.0
Andalusite	4.0	4.1	-	-	-
Fibrolite	-	-	0.9	-	1.1
Sillimanite	-	-	0.7	26.0	1.5

TABLE 51 (CONTINUED)

Rock Text No.	48	49	50
SiO_2	51.34	59.00	58.21
TiO_2	1.53	1.10	1.22
Al_2O_3	30.41	21.67	22.58
Fe_2O_3	1.29	1.32	1.25
FeO	5.30	6.49	6.82
MnO	0.06	0.07	0.09
MgO	2.63	2.85	3.29
CaO	0.30	0.18	0.28
Na_2O	1.10	0.91	0.72
K_2O	4.57	4.41	3.67
P_2O_5	0.06	0.07	0.06
O. R.	17.8	15.4	14.4

TABLE 51 (CONTINUED)

Rock Text No.	48	49	50
Quartz + Felds.	14.9	61.0*	42.1
Biot- (Green	-	-	0.2
ite (Brown	34.9	26.9	40.1
Muscovite	16.5	0.8	0.8
Chlorite	-	-	0.4
Garnet	-	3.2	-
Ore	3.2	2.1	1.0
Shimmer	-	-	-
Andalusite	-	-	-
Fibrolite	3.9	2.7	2.3
Sillimanite	26.7	3.4	13.0

TABLE 51 (CONTINUED)

(5) The Aureole of the Main Donegal Granite:

Rock Text No.	51	52	53	54	55
SiO_2	63.98	59.51	66.06	60.14	57.07
TiO_2	0.88	0.84	0.82	0.80	1.11
Al_2O_3	20.72	22.99	19.94	19.62	25.47
Fe_2O_3	1.63	1.98	1.93	2.04	1.90
FeO	4.40	4.46	2.89	2.92	3.39
MnO	0.08	0.09	0.08	0.08	0.07
MgO	2.08	1.97	5.79	6.09	2.51
CaO	0.31	0.15	0.15	0.12	0.12
Na_2O	1.43	1.15	2.37	2.26	1.74
K_2O	4.08	4.58	3.09	3.10	5.23
P_2O_5	0.06	0.08	0.05	0.05	0.08
O.R.	25.2	29.2	38.1	39.2	33.0

TABLE 51 (CONTINUED)

Rock Text No.	51	52	53	54	55
Quartz + Felds.	46. 3	33. 2	42. 2	36. 3	26. 4
Biotite	19. 7	3. 9	38. 4	36. 7	16. 6
Muscovite	20. 3	36. 0	0. 9	0. 8	45. 9
Chlorite	0. 9	14. 6	-	-	-
Garnet	0. 8	1. 0	-	-	0. 2
Ore	2. 5	1. 6	5. 9	9. 0	1. 3
Graphite		-			-
Shimmer	1. 9	9. 8	0. 7	1. 1	-
Staurolite	0. 1	-	-	-	9. 1
Andalusite	7. 5	A	-	-	-
Fibrolite	-	-	-	-	-
Kyanite	-	-	11. 8	16. 1	1. 1

A : Andalusite wholly altered to shimmer

TABLE 51 (CONTINUED)

Rock Text No.	56	57	58	59	60	61
SiO_2	57.01	55.81	58.79	55.98	62.43	59.39
TiO_2	1.10	0.62	0.84	0.69	0.76	0.83
Al_2O_3	24.42	14.39	18.41	15.52	18.75	18.24
Fe_2O_3	2.02	2.48	2.68	1.33	2.89	2.86
FeO	4.00	2.48	3.72	3.31	3.12	4.00
MnO	0.15	0.05	0.06	0.05	0.05	0.07
MgO	2.79	11.93	5.01	9.62	3.80	5.07
CaO	0.35	1.99	0.18	2.84	0.09	0.14
Na_2O	1.65	1.90	1.94	2.33	1.52	1.72
K_2O	4.88	4.00	3.43	3.75	3.56	3.47
P_2O_5	0.15	0.09	0.06	0.10	0.05	0.05
O.R.	31.7	47.7	39.2	26.4	45.5	39.1

TABLE 51 (CONTINUED)

Rock Text No.	56	57	58	59	60	61
Quartz + Felds.	27.9	44.0	31.4	47.7	38.3	35.7
Biotite	20.2	50.8	38.1	43.2	35.0	41.5
Muscovite	35.0	-	1.1	-	12.0	3.7
Chlorite	0.5	0.1	0.2	-	0.1	-
Garnet	2.0	-	-	-	-	-
Ore	1.1					
Graphite	-	5.2	6.3	9.1	4.4	4.2
Shimmer	0.2	-	19.0	-	4.2	4.1
Staurolie	11.2	-	-	-	-	-
Andalusite	-	-	-	-	-	-
Fibrolite	-	-	-	-	tr	tr
Kyanite	1.9	-	3.9	-	5.8	10.7
Tourmaline	-	-	-	-	0.2	0.1

TABLE 51 (CONTINUED)

Rock Text No.	62	63	64	65	66	67
SiO_2	59.61	60.61	64.24	64.27	66.19	64.01
TiO_2	0.70	0.80	0.86	0.83	0.75	0.85
Al_2O_3	18.01	21.30	16.32	15.48	14.43	17.03
Fe_2O_3	1.89	2.28	2.62	2.88	1.82	2.00
FeO	4.15	2.95	5.04	5.45	5.22	4.76
MnO	0.07	0.06	0.10	0.11	0.13	0.10
MgO	6.12	3.37	4.18	4.78	4.91	4.44
CaO	0.77	0.14	0.52	0.53	0.62	0.72
Na_2O	1.48	1.32	1.12	1.12	1.04	1.16
K_2O	3.64	4.89	3.18	2.97	2.91	3.26
P_2O_5	0.08	0.06	0.09	0.09	0.10	0.09
O.R.	29.3	40.6	31.5	32.1	23.6	28.2

TABLE 51 (CONTINUED)

Rock Text No.	62	63	64	65	66	67
Quartz + Felds.	38.7	33.7	40.7	41.5	50.3	40.6
Biotite	36.0	29.9	28.2	36.9	37.0	35.7
Muscovite	22.9	23.4	8.9	2.4	2.7	4.7
Chlorite	0.4	-	3.5	1.3	3.3	0.5
Garnet	-	-	1.4	0.3	0.4	0.9
Ore	8.2	9.9	1.5	1.8	1.1	1.3
Graphite			-	-	-	-
Shimmer	-	-	1.8	-	0.4	-
Staurolite	-	2.2	12.7	13.7	3.2	6.8
Andalusite	-	-	-	-	0.3	8.4
Fibrolite	-	-	-	-	tr	-
Kyanite	3.7	0.9	1.0	2.1	1.0	0.9
Tourmaline	-	0.2	0.1	-	0.2	0.1

TABLE 51 (CONTINUED)

Rock Text No.	68	69	70	71	72	73
SiO_2	63.82	63.94	55.75	60.52	60.34	55.97
TiO_2	0.77	0.81	0.88	0.84	0.84	0.85
Al_2O_3	16.26	15.91	19.69	18.20	19.79	19.06
Fe_2O_3	1.12	1.42	0.99	1.32	1.38	1.20
FeO	5.34	5.93	4.44	4.94	4.47	4.40
MnO	0.13	0.14	0.10	0.08	0.10	0.10
MgO	5.27	4.86	4.90	5.05	5.25	5.46
CaO	0.98	1.04	3.59	1.60	0.85	3.16
Na_2O	1.23	1.23	3.14	1.99	1.41	2.70
K_2O	3.11	2.88	3.02	2.99	3.17	3.27
P_2O_5	0.10	0.10	0.13	0.09	0.08	0.10
O.R.	16.2	17.9	16.3	19.2	22.0	20.8

TABLE 51 (CONTINUED)

Rock Text No.	68	69	70	71	72	73
Quartz + Felds.	45.6	36.8	51.0	48.0	40.0	51.4
Biotite	42.1	36.8	37.5	41.3	40.9	43.8
Muscovite	0.8	5.0	-	-	0.9	0.2
Chlorite	0.4	4.5	0.8	0.6	3.9	0.3
Garnet	1.7	1.5	1.0	-	-	0.3
Ore	1.4	1.5	0.6	1.0	1.7	1.3
Graphite	-	-	-	-	-	-
Shimmer	-	-	0.9	0.7	2.4	0.2
Staurolite	1.7	2.0	-	0.4	-	0.1
Andalusite	4.4	11.2	-	2.2	-	-
Fibrolite	0.2	-	0.7	3.1	4.6	-
Kyanite	1.5	0.6	7.2	2.6	5.4	2.3
Tourmaline	0.1	-	0.3	-	0.2	0.3

TABLE 51 (CONTINUED)

Rock Text No.	74	75	76	77	78	79	80
SiO_2	62.06	61.79	58.91	59.65	62.92	60.65	63.59
TiO_2	0.80	0.80	1.00	0.91	0.88	0.92	0.87
Al_2O_3	16.34	17.33	19.73	18.47	17.62	18.52	19.60
Fe_2O_3	1.27	1.23	1.61	1.73	1.94	2.40	1.20
FeO	4.99	4.87	4.77	6.35	6.20	6.31	4.01
MnO	0.10	0.14	0.06	0.14	0.12	0.12	0.05
MgO	5.53	5.63	3.79	4.48	2.48	2.48	1.72
CaO	1.44	1.20	1.75	0.38	0.54	0.55	0.95
Na_2O	1.68	1.48	2.18	0.82	1.48	1.34	2.70
K_2O	2.97	2.62	3.05	3.68	3.24	3.48	3.62
P_2O_5	0.10	0.08	0.10	0.08	0.09	0.11	0.07
O.R.	18.6	19.1	23.3	19.9	22.4	25.4	22.2

TABLE 51 (CONTINUED)

Rock Text No.	74	75	76	77	78	79	80
Quartz + Felds.	50.0	51.3	50.4	42.3	40.3	40.1	45.5
Biotite	41.2	34.0	39.0	21.6	26.8	34.1	28.9
Muscovite	-	0.2	0.9	8.4	21.2	13.2	19.2
Chlorite	1.3	2.0	2.4	14.5	-	0.3	-
Garnet	-	0.4	-	0.8	1.4	1.9	0.4
Ore	3.0	2.4	2.0	0.8	2.0	1.7	2.3
Graphite	-	-	-	-	-	-	-
Shimmer	0.4	0.3	-	-	-	-	-
Staurolite	-	1.4	1.7	-	5.8	6.1	-
Andalusite	-	-	-	-	-	-	-
Fibrolite	1.2	2.4	2.1	11.0	2.4	2.4	3.8
Kyanite	2.7	5.6	1.4	0.5	-	-	-
Tourmaline	0.3	0.1	0.1	0.2	0.1	0.2	-

TABLE 52

Values of Phase Diagrams

(1) Fanad Aureole

Rock Text No.	1	2	3	4	5	6
A	39.0	39.3	42.1	43.8	40.7	33.7
K	16.8	16.2	16.5	15.4	13.5	14.0
F	44.2	44.5	41.3	40.8	45.8	52.4
A'	35.4	36.3	39.4	41.6	37.0	31.2
K	16.4	15.9	16.2	15.2	13.1	13.7
F	48.2	47.8	44.3	43.3	49.8	55.1
A	46.9	46.9	50.5	51.8	47.0	39.1
F	34.3	37.0	34.6	33.5	37.8	41.7
M	18.8	16.1	14.9	14.8	15.2	19.1
A'	42.3	43.1	47.1	49.0	42.6	36.2
F	39.5	41.1	38.4	36.5	42.6	45.1
M	18.2	15.7	14.6	14.5	14.7	18.7
A	39.0	39.3	42.1	43.8	40.7	33.7
K	16.8	16.2	16.5	15.4	13.5	14.0
F	28.6	31.0	28.9	28.3	32.7	35.9
M	15.6	13.5	12.4	12.5	13.2	16.5
A'	35.4	36.3	39.4	41.6	37.0	31.2
K	16.4	15.9	16.2	15.2	13.1	13.7
F	33.0	34.6	32.1	31.0	37.0	38.9
M	15.2	13.2	12.2	12.3	12.8	16.2
Thompson Values						
A	0.089	0.312	0.232	0.273	0.261	0.211
M	0.331	0.300	0.298	0.256	0.276	0.310

TABLE 52 (CONTINUED)

Rock Text No.	7	8	9	10	11	12
A	43.9	37.3	35.6	40.2	43.2	43.0
K	14.6	15.1	20.7	15.9	13.1	13.9
F	41.5	47.6	43.6	43.8	43.7	43.1
A'	39.6	35.0	33.6	37.1	39.7	39.6
K	14.2	14.8	20.4	15.6	12.8	13.5
F	46.3	50.2	46.0	47.3	47.6	46.8
A	51.4	43.9	44.9	47.9	49.7	49.9
F	32.4	38.3	38.8	36.3	34.8	34.2
M	16.1	17.7	16.3	15.8	15.5	15.8
A'	46.1	41.1	42.2	43.9	45.5	45.8
F	38.3	41.5	41.9	40.7	39.4	38.8
M	15.6	17.4	16.0	15.4	15.1	15.4
A	43.9	37.3	35.6	40.2	43.2	43.0
K	14.6	15.1	20.7	15.9	13.1	13.9
F	27.7	32.6	30.7	30.5	30.2	29.5
M	13.8	15.1	12.9	13.3	13.5	13.6
A'	39.6	35.0	33.6	37.1	39.7	39.6
K	14.2	14.8	20.4	15.6	12.8	13.5
F	32.9	35.4	33.3	34.3	34.4	33.5
M	13.4	14.8	12.7	13.0	13.2	13.3
Thompson Values						
A	0.321	0.220	0.116	0.241	0.308	0.257
M	0.317	0.302	0.297	0.292	0.295	0.311

TABLE 52 (CONTINUED)

Rock Text No.	13	14	15	16	17	18
A	39.0	45.6	38.7	43.0	39.3	43.4
K	15.5	16.0	15.2	15.6	13.4	13.6
F	45.6	38.5	46.1	41.3	47.3	43.1
A'	36.8	41.0	35.3	39.0	35.9	40.0
K	15.2	15.4	14.8	15.2	13.1	13.3
F	48.0	43.6	49.8	45.8	51.0	46.7
A	46.1	54.2	45.7	51.0	45.4	50.2
F	38.6	29.1	35.9	34.1	39.5	34.3
M	15.3	16.7	18.4	14.9	15.1	15.5
A'	43.4	48.4	41.5	46.0	41.3	46.1
F	41.6	35.5	40.6	39.6	44.0	38.8
M	15.0	16.1	17.9	14.4	14.7	15.1
A	39.0	45.6	38.7	43.0	39.3	43.4
K	15.5	16.0	15.2	15.6	13.4	13.6
F	32.6	24.5	30.5	28.8	34.2	29.7
M	12.9	14.0	15.6	12.6	13.1	13.4
A'	36.8	41.0	35.3	39.0	35.9	40.0
K	15.2	15.4	14.8	15.2	13.1	13.3
F	35.3	30.0	34.6	33.6	28.2	33.7
M	12.7	13.6	15.2	12.2	12.7	13.1
Thompson Values						
A	0.225	0.227	0.258	0.268	0.277	0.289
M	0.283	0.335	0.329	0.288	0.265	0.297

TABLE 52 (CONTINUED)

Rock Text No.	19	20	21	22
A	41.8	40.4	39.5	38.7
K	13.9	14.3	13.2	13.7
F	44.3	45.2	47.3	47.7
A'	39.2	37.5	35.9	35.5
K	13.7	14.0	12.8	13.4
F	47.2	48.5	51.3	51.1
A	48.6	47.2	45.5	44.8
F	36.4	35.6	37.1	36.6
M	15.0	17.2	17.4	18.6
A'	45.4	43.6	41.1	41.0
F	39.9	39.6	41.9	40.9
M	14.7	16.8	16.9	18.1
A	41.8	40.4	39.5	38.7
K	13.9	14.3	13.2	13.7
F	31.3	30.5	32.2	31.6
M	12.9	14.7	15.1	16.0
A'	39.2	37.5	35.9	35.5
K	13.7	14.0	12.8	13.4
F	34.5	34.1	36.5	35.4
M	12.7	14.4	14.7	15.7
Thompson Values				
A	0.284	0.212	0.262	0.238
M	0.281	0.313	0.312	0.337

TABLE 52 (CONTINUED)

(2) Ardara Aureole

Rock Text No.	23	24	25	26	27	28
A	40.4	60.6	41.4	38.0	39.7	48.1
K	12.5	12.2	8.3	11.0	11.9	12.3
F	47.1	27.1	50.2	51.0	48.4	39.6
A'	36.4	56.0	37.4	34.7	36.1	42.9
K	12.1	11.9	8.1	10.7	11.6	11.8
F	51.4	32.1	54.5	54.6	52.3	45.3
A	46.2	69.1	45.2	42.7	45.0	54.8
F	32.4	16.7	18.5	25.3	30.9	25.5
M	21.4	14.2	36.3	32.0	24.0	19.7
A'	41.5	63.6	40.7	28.8	40.9	48.6
F	37.8	22.7	24.1	30.0	35.8	32.5
M	20.7	13.7	35.2	31.1	23.3	18.9
A	40.4	60.6	41.4	38.0	39.7	48.1
K	12.5	12.2	8.3	11.0	11.9	12.3
F	28.4	14.7	16.9	22.5	27.3	22.4
M	18.7	12.5	33.3	28.5	21.2	17.3
A'	36.4	56.0	37.4	34.7	36.1	42.9
K	12.1	11.9	8.1	10.7	11.6	11.8
F	33.2	20.0	22.1	26.8	31.6	28.6
M	18.2	12.1	32.3	27.8	26.6	16.6
Thompson Values						
A	0.337	0.578	0.330	0.259	0.321	0.430
M	0.398	0.442	0.665	0.559	0.431	0.433

TABLE 52 (CONTINUED)

Rock Text No.	29	30	31	32	33	34
A	59.9	51.5	46.0	33.2	34.2	35.1
K	17.3	9.2	5.8	8.1	8.7	10.1
F	22.9	39.3	48.2	58.6	57.1	54.8
A'	56.1	47.4	40.5	29.2	29.7	30.9
K	16.8	8.9	5.6	7.9	8.4	9.7
F	27.1	43.7	53.9	63.0	62.0	59.4
A	72.4	56.7	48.8	36.2	37.5	39.0
F	16.5	23.6	27.9	20.8	19.0	27.9
M	11.2	19.7	23.3	43.0	43.5	33.1
A'	67.5	52.0	42.9	31.6	32.4	34.2
F	21.7	28.9	34.6	26.8	25.8	33.8
M	10.8	19.1	22.4	41.6	41.9	31.9
A	59.9	51.5	46.0	33.2	34.2	35.1
K	17.3	9.2	5.8	8.1	8.7	10.1
F	13.6	21.5	26.3	19.1	17.4	25.1
M	9.2	17.6	22.0	39.5	39.7	29.8
A'	56.1	47.4	40.5	29.2	29.7	30.9
K	16.8	8.9	5.6	7.9	8.4	9.7
F	18.0	26.3	32.7	24.7	23.6	30.5
M	9.0	17.4	21.2	38.3	38.4	28.8
Thompson Values						
A	0.508	0.522	0.448	0.280	0.287	0.277
M	0.341	0.452	0.458	0.677	0.689	0.547

TABLE 52 (CONTINUED)

Rock Text No.	35	36	37	38	39
A	48.6	36.5	38.2	41.9	33.2
K	12.5	8.1	8.6	8.8	10.3
F	38.9	55.4	53.2	49.3	56.5
A'	44.6	32.7	34.1	38.4	30.1
K	12.2	7.9	8.3	8.5	10.0
F	43.2	59.4	57.6	53.1	59.9
A	55.6	39.7	41.8	46.0	37.0
F	20.2	19.5	19.2	18.8	19.4
M	24.2	40.8	39.1	35.2	43.5
A'	50.8	35.5	37.2	41.9	33.5
F	25.7	24.8	25.0	23.8	24.1
M	23.5	39.6	37.8	34.2	42.4
A	48.6	36.5	38.2	41.9	33.2
K	12.5	8.1	8.6	8.8	10.3
F	17.7	17.9	17.5	17.2	17.4
M	21.2	37.5	35.7	32.1	39.1
A'	44.6	32.7	34.1	38.4	30.1
K	12.2	7.9	8.3	8.5	10.0
F	22.6	22.9	22.9	21.8	21.7
M	20.6	36.5	34.6	31.3	38.2
Thompson Values					
A	0.380	0.359	0.334	0.376	0.207
M	0.337	0.682	0.675	0.654	0.695

TABLE 52 (CONTINUED)

(3) Barnesmore Aureole

Rock Text No.	40	41	42
A	36.4	33.8	43.3
K	22.0	25.2	18.9
F	41.6	40.9	37.8
A'	29.0	28.6	36.2
K	20.9	24.3	17.9
F	50.2	47.1	45.9
A	46.6	45.2	53.4
F	24.7	25.8	21.6
M	28.7	29.0	25.0
A'	36.6	37.8	44.1
F	36.7	34.7	32.4
M	26.7	27.5	23.5
A	36.4	33.8	43.3
K	22.0	25.2	18.9
F	19.2	19.3	17.5
M	22.4	21.7	20.3
A'	29.0	28.6	36.2
K	20.9	24.3	17.9
F	29.0	26.3	26.6
M	21.1	20.8	19.3
Thompson Values			
A	-0.320	-0.974	0.014
M	0.532	0.524	0.523

TABLE 52 (CONTINUED)

(4) Thorr Granodiorite Aureole and Enclaves

Rock Text No.	43	44	45	46	47	48
A	42.7	41.7	45.0	56.7	47.6	55.6
K	15.0	14.5	13.2	9.6	14.2	11.4
F	42.3	43.9	41.8	33.7	38.7	32.9
A'	39.4	37.2	41.9	54.1	43.3	52.7
K	14.7	14.0	12.9	9.5	13.7	11.2
F	46.0	48.8	45.2	36.5	42.9	36.1
A	50.2	48.7	51.9	62.8	55.5	62.8
F	28.2	28.9	27.8	21.3	23.9	19.8
M	21.6	22.4	20.4	16.0	20.7	17.3
A'	46.1	43.2	48.1	59.7	50.2	59.4
F	32.8	35.2	32.1	24.6	29.8	23.6
M	21.0	21.5	19.9	15.7	20.0	17.0
A	42.7	41.7	45.0	56.7	47.6	55.6
K	15.0	14.5	13.2	9.6	14.2	11.4
F	23.9	24.7	24.1	19.2	20.5	17.6
M	18.4	19.1	17.7	14.4	17.7	15.4
A'	39.4	37.2	41.9	54.1	43.3	52.7
K	14.7	14.0	12.9	9.5	13.7	11.2
F	28.0	30.3	27.9	22.3	25.7	21.0
M	17.9	18.5	17.3	14.2	17.2	15.1
Thompson Values						
A	0.246	0.246	0.315	0.555	0.308	0.512
M	0.417	0.427	0.412	0.430	0.461	0.462

TABLE 52 (CONTINUED)

Rock Text No.	49	50
A	43.0	44.7
K	12.8	9.9
F	44.2	45.4
A'	39.9	41.9
K	12.5	9.7
F	47.6	48.4
A	49.3	49.6
F	28.6	27.3
M	22.1	23.1
A'	45.6	46.4
F	32.9	31.0
M	21.6	22.6
A	43.0	44.7
K	12.8	9.9
F	24.9	24.5
M	19.3	20.8
A'	39.9	41.9
K	12.5	9.7
F	28.8	28.0
M	18.9	20.4
Thompson Values		
A	0.308	0.371
M	0.439	0.462

TABLE 52 (CONTINUED)

(5) The Aureole of the Main Donegal Granite

Rock Text No.	51	52	53	54	55	56
A	47.6	51.4	38.4	37.4	51.7	48.9
K	14.4	14.7	9.3	9.1	16.2	14.8
F	38.0	33.9	52.3	53.5	32.1	36.3
A'	42.8	45.9	33.8	32.7	46.6	43.7
K	14.0	14.2	9.0	8.8	15.6	14.3
F	43.3	39.9	57.2	58.5	37.7	42.0
A	55.6	60.2	42.3	41.1	61.7	57.4
F	24.3	22.5	12.9	12.8	16.7	19.4
M	20.1	17.3	44.8	46.1	21.6	23.2
A'	49.7	53.5	37.1	35.8	55.3	51.0
F	31.0	29.9	19.7	19.8	24.0	26.7
M	19.3	16.6	43.2	44.4	20.7	22.3
A	47.6	51.4	38.4	37.4	51.7	48.9
K	14.4	14.7	9.3	9.1	16.2	14.8
F	20.8	19.2	11.7	11.6	14.0	16.5
M	17.2	14.8	40.6	41.9	18.1	19.8
A'	42.8	45.9	33.8	32.7	46.6	43.7
K	14.0	14.2	9.0	8.8	15.6	14.3
F	26.7	25.7	17.9	18.0	20.2	22.9
M	16.6	14.2	39.3	40.5	17.5	19.1
Thompson Values						
A	0.352	0.353	0.344	0.326	0.349	0.343
M	0.444	0.417	0.781	0.788	0.550	0.541

TABLE 52 (CONTINUED)

Rock Text No.	57	58	69	60	61	62
A	11.8	37.5	9.7	44.1	37.4	31.4
K	10.0	10.7	11.1	12.0	10.5	10.6
F	78.1	51.8	79.3	43.9	52.1	58.0
A'	7.9	31.0	7.2	36.3	30.7	27.2
K	9.7	10.2	10.8	11.3	10.0	10.3
F	82.4	58.8	82.0	52.4	59.3	62.5
A	13.2	42.0	10.9	50.1	41.8	35.1
F	9.2	17.3	14.6	15.9	18.1	18.1
M	77.6	40.8	74.5	34.0	40.1	46.8
A'	8.7	34.5	8.1	40.9	34.1	30.4
F	16.7	26.8	19.3	27.2	27.9	24.5
M	74.6	38.6	72.6	31.9	38.0	45.1
A	11.8	37.5	9.7	44.1	37.4	31.4
K	10.0	10.7	11.1	12.0	10.5	10.6
F	8.3	15.4	13.0	14.0	16.2	16.2
M	69.8	36.4	66.3	29.9	35.9	41.8
A'	7.9	31.0	7.2	36.3	30.7	27.2
K	9.7	10.2	10.8	11.3	10.0	10.3
F	15.1	24.1	17.2	24.1	25.1	22.0
M	67.4	34.7	64.8	28.3	34.2	40.5
Thompson Values						
A	0.040	0.254	0.103	0.309	0.261	0.183
M	0.896	0.704	0.838	0.683	0.692	0.723

TABLE 52 (CONTINUED)

Rock Text No.	63	64	65	66	67	68
A	45.6	36.0	33.2	29.8	35.2	29.1
K	15.9	10.3	9.3	9.5	10.6	9.8
F	38.5	53.7	57.6	60.6	54.2	61.1
A'	39.5	29.5	26.5	25.4	30.3	26.5
K	15.2	9.8	8.8	9.2	10.2	9.6
F	45.2	60.7	64.7	65.4	59.6	64.0
A	54.3	40.1	36.6	33.0	39.4	32.3
F	15.3	24.4	25.1	25.4	23.1	24.9
M	30.5	35.4	38.4	41.6	37.5	42.8
A'	46.6	32.7	29.0	28.0	33.7	29.3
F	24.4	33.8	34.7	32.0	30.7	28.9
M	29.0	33.5	36.3	40.0	36.0	41.8
A	45.6	36.0	33.2	29.8	35.2	29.1
K	15.9	10.3	9.3	9.5	10.6	9.8
F	12.8	21.9	22.7	23.0	20.6	22.5
M	25.6	31.8	34.8	37.6	33.6	38.6
A'	39.5	29.5	26.5	25.4	30.3	26.5
K	15.2	9.8	8.8	9.2	10.2	9.6
F	20.7	30.4	31.7	29.0	27.2	26.1
M	24.5	20.2	33.1	26.3	32.3	37.8
Thompson Values						
A	0.241	0.232	0.223	0.195	0.256	0.226
M	0.667	0.594	0.609	0.626	0.624	0.637

TABLE 52 (CONTINUED)

Rock Text No.	69	70	71	72	73	74
A	29.4	20.4	29.8	36.9	21.1	26.7
K	9.2	11.8	9.8	9.3	11.8	9.7
F	61.4	67.8	60.3	53.8	67.2	63.7
A'	26.1	17.8	26.6	33.7	18.1	23.7
K	8.9	11.5	9.6	9.1	11.5	9.4
F	65.0	70.7	63.8	57.2	70.5	66.9
A	32.4	23.2	33.1	40.7	23.9	29.5
F	27.9	26.2	24.0	19.5	24.1	24.0
M	39.7	50.7	42.9	39.8	52.0	46.5
A'	28.6	20.1	29.4	37.1	20.4	26.1
F	32.8	30.5	28.8	24.1	29.0	28.6
M	38.6	49.4	41.8	38.8	50.6	45.3
A	29.4	20.4	29.8	36.9	21.1	26.7
K	9.2	11.8	9.8	9.3	11.8	9.7
F	25.3	23.1	21.6	17.7	21.2	21.7
M	36.1	44.7	38.7	36.1	45.9	42.0
A'	26.1	17.8	26.6	33.7	18.1	23.7
K	8.9	11.5	9.6	9.1	11.5	9.4
F	29.8	27.0	26.1	21.9	25.7	25.9
M	35.2	43.7	37.8	35.3	44.8	41.0
Thompson Values						
A	0.232	0.345	0.299	0.322	0.295	0.243
M	0.593	0.664	0.646	0.676	0.688	0.664

TABLE 52 (CONTINUED)

Rock Text No.	75	76	77	78	79	80
A	31.0	35.6	35.9	39.3	41.0	42.7
K	8.1	10.8	10.4	11.3	11.6	16.0
F	60.9	53.6	53.7	49.3	47.4	41.3
A'	28.1	31.2	32.1	34.0	34.7	38.3
K	7.9	10.4	10.1	10.9	11.1	15.5
F	64.0	58.4	57.8	55.1	54.2	46.1
A	33.7	39.9	40.1	44.4	46.4	50.8
F	22.1	25.1	26.9	32.7	31.8	28.0
M	44.2	35.0	33.1	22.9	21.8	21.2
A'	30.5	34.9	35.7	38.1	39.0	45.4
F	26.3	31.4	32.3	40.0	40.3	34.2
M	43.2	33.8	32.0	21.9	20.7	20.4
A	31.0	35.6	35.9	39.3	41.0	42.7
K	8.1	10.8	10.4	11.3	11.6	16.0
F	20.3	22.4	24.1	29.0	28.1	23.5
M	40.6	31.3	29.6	20.3	19.3	17.8
A'	28.1	31.2	32.1	34.0	34.7	38.3
K	7.9	10.4	10.1	10.9	11.1	15.5
F	24.2	28.1	29.0	35.6	35.8	28.9
M	39.8	30.2	28.8	19.5	18.4	17.2
Thompson Values						
A	0.294	0.374	0.229	0.281	0.298	0.406
M	0.673	0.586	0.555	0.406	0.405	0.419

TABLE 53

X-ray Fluorescent Analysis of Biotites

Rock Text No.	2	7	9	13	15	20
SiO_2	36.54	34.94	34.75	34.38	36.30	35.88
TiO_2	2.57	1.67	2.98	2.70	2.73	2.39
Al_2O_3	20.02	18.42	22.01	21.43	20.50	20.18
Fe_2O_3 (total)	28.09	28.97	25.88	27.25	26.47	24.62
MgO	5.36	6.34	5.18	5.07	5.84	5.73
K_2O	9.30	8.64	9.04	9.13	8.98	8.96
Thompson Values						
A	-0.263	-0.226	-0.187	-0.204	-0.220	-0.242
M	0.273	0.302	0.282	0.269	0.304	0.314

TABLE 53 (CONTINUED)

Rock Text No.	21	22	34	41	43	47
SiO_2	34.33	33.08	35.76	36.03	35.70	36.16
TiO_2	2.70	2.55	1.65	2.12	1.78	2.80
Al_2O_3	20.89	21.08	18.82	18.74	21.68	18.99
Fe_2O_3 (total)	27.93	28.25	21.91	19.89	25.80	23.11
MgO	4.70	4.61	9.81	8.69	7.23	6.49
K_2O	8.82	8.57	8.51	9.59	8.16	9.34
Thompson Values						
A	-0.192	-0.168	-0.200	-0.369	-0.107	-0.336
M	0.251	0.244	0.470	0.463	0.357	0.357

TABLE 53 (CONTINUED)

Rock Text No.	50	56	61	65	66	73
SiO_2	35.69	36.60	35.75	34.70	36.11	38.09
TiO_2	2.64	1.66	1.61	1.45	1.39	1.42
Al_2O_3	20.17	19.05	18.74	19.31	18.68	20.34
Fe_2O_3 (total)	23.30	19.01	12.73	16.83	14.49	16.78
MgO	7.90	10.92	12.96	11.37	10.72	12.75
K_2O	9.23	8.79	8.42	8.72	8.86	9.14
Thompson Values						
A	-0.252	-0.229	-0.214	-0.218	-0.288	-0.217
M	0.402	0.532	0.668	0.572	0.594	0.601

TABLE 53 (CONTINUED)

Rock Text No.	74	75	79
SiO_2	36.16	36.15	35.96
TiO_2	1.31	1.37	1.82
Al_2O_3	18.66	20.10	18.53
Fe_2O_3 (total)	12.49	16.70	21.90
MgO	12.60	13.52	7.98
K_2O	8.48	8.32	8.24
Thompson Values			
A	-0.235	-0.143	-0.211
M	0.666	0.616	0.418

V. COMMENTS ON THE ANALYTICAL DATA OF TABLES 51 - 53

A. Individual Aureoles:

(1) Rocks from the Fanad aureole (specimens 1-22) show a remarkably narrow range of variation in their MgO content. Of the 22 rocks analysed, 18 have values between 1.43 and 1.97% while four rocks have values between 2.00 and 2.18% MgO. The M/Fm ratios of the 22 rocks varies between 0.255 - 0.336. The same observation applies to the results of the analysis of the coexisting biotites. In the 8 biotites analysed, 5 biotites have a range of 5.07 - 5.84% MgO, 2 biotites with 4.61 and 4.70% and only one biotite shows MgO% = 6.34. The iron content of the biotites is high, being 24.62 - 28.97% (total Fe as Fe_2O_3). Yet, the M/FM ratios of the 8 biotites range only between 0.244 and 0.314. These latter values show a similar range to those of the rocks.

(2) The rocks from Ardara aureole (specimens 23-29) show a wide range of variation in the MgO content compared with those of Fanad. For the 17 rocks analysed, the MgO varied between 1.37 - 6.10%. The M/FM ratio of the rocks also varied between 0.337-0.695. This variation can be related to the three zones of the aureole as follows:-

(a) The outermost kyanite-bearing andalusite schist is higher in M/FM ratio than the other two zones.

(b) There is no chemical distinction between the middle kyanite-free andalusite zone and the innermost kyanite-free sillimanite zone.

(3) The three rocks analysed from the Barnesmore aureole

(specimens 40-42) show a narrow range of MgO content, varying between 2.74 and 3.03%, corresponding to M/FM value of 0.523-0.532. The single biotite analysed has an M/FM value of 0.463.

(4) In the Thorr Granodiorite district, rocks from both the aureole and the enclaves (specimens 43-50) also show a narrow range of variation in their MgO content. Of the 8 rocks analysed, 7 have values between 2.10 and 2.85: while only one lies outside this range, being 3.29% MgO. The M/FM values of the 8 rocks are very close, varying between 0.412 and 0.462. For the 3 analysed biotites, MgO varies between 6.49 and 7.90% and their M/FM ratio varies between 0.357 and 0.402. As in Fanad, the iron content of the biotites is high, being 23.11 - 25.80% (total Fe as Fe_2O_3).

(5) Aluminium silicates bearing rocks from the aureole of the Main Donegal granite (specimens 51-80) show a wide MgO variation which is comparable to that of Ardara. For the 30 rocks analysed, the MgO content ranges between 1.72 and 6.12. Similarly, the M/FM ratio of these rocks varies between 0.405 and 0.788. The MgO content of the 8 analysed coexisting biotites also shows a wide range of variation between 7.98 and 13.52%. The M/FM ratios of these biotites range between 0.418 and 0.668 (the biotite of the rock with the highest M/FM value of 0.788 - sample No. 54- was not analysed. The host rock with the highest M/FM biotite value, 0.668, is sample No. 61 and its M/FM value is 0.692. Notice the close agreement between the two values). The group of rocks with the high M/FM ratios are the kyanite $\pm$ andalusite schists whereas the group of those with the low M/FM ratios are the kyanite-free andalusite and/or fibrolite schists.

B. The Relationship between the Biotite Composition and Its Host Rock:-

There is a consistent correlation between the MgO and FeO distribution between the rock and its coexisting biotite. This relationship is demonstrated in Fig. 25 which shows the plots of the M/FM ratio of the rock and that of its biotite (this type of diagram was suggested by Butler 1965). Although the correlation is striking, yet it must be pointed out that the reason why nearly all the points lie just below the 1:1 line is due to the approximation made in the calculation of the M/FM ratio of the biotite. The total iron as Fe_2O_3 in the biotite was divided by 1.11 and the resultant was used as the Fe_2O_3 in the calculation M/FM = MgO + FeO (moles). Had the Fe_2O_3 content of the biotite been subtracted from the total Fe_2O_3 at first, then the M/FM of the biotites would have been fractionally higher (due to a decrease in the denominator of the equation) and the points would lie nearer to or slightly above the 1:1 line more than they do in Fig. 25. Garnet content of these rocks is less than 2.5%, hence the effect of its presence can be ignored.

C. The Relationship between the Type of Aluminium Silicate and the Composition of its Host Rock in all Aureoles:-

(1) From the 80 analyses presented, it can be seen that kyanite occurs only in rocks of high M/FM values whereas andalusite and sillimanite develop in rocks of both high and low M/FM.

(2) The M/FM values of the rocks in the kyanite-free groups from both Ardara and the Main Donegal granite aureoles lie within the M/FM values of the rocks of the other three kyanite-free aureoles, i.e. Fanad, Barnesmore and Thorr.

Fig. 25

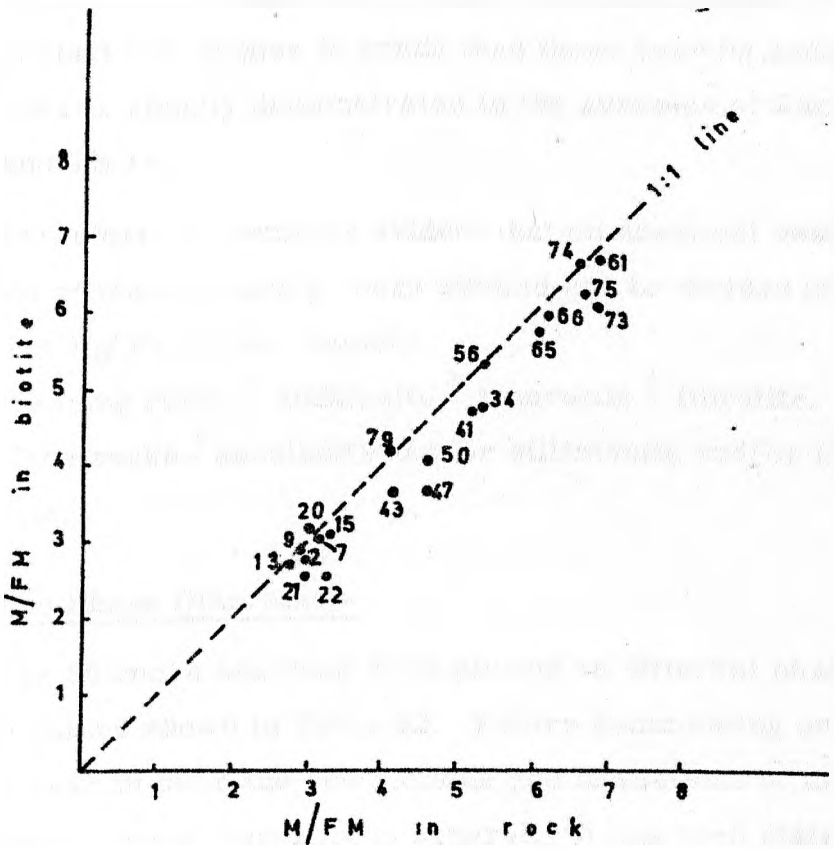

Plot of the M/FM ratios in rocks and their coexisting biotites.

(3) There is no chemical distinction between andalusite-bearing and sillimanite-bearing rocks. The distinction between the two is a spatial one: sillimanite occurs in rocks nearer to the granite contact i.e. higher in grade than those bearing andalusite alone. This is clearly demonstrated in the aureoles of Fanad, Ardara and Thorr.

Therefore, it becomes evident that on chemical basis, the aluminium silicates bearing rocks studied can be divided into 2 groups of different Mg/Fe ratios, namely,
Kyanite-bearing rocks $\pm$ andalusite $\pm$ staurolite $\pm$ fibrolite.
Kyanite-free rocks $\pm$ andalusite and/or sillimanite and/or fibrolite, $\pm$ staurolite.

D. The Phase Diagrams:-

The 80 rocks analysed were plotted on different phase diagrams using the values shown in Table 52. Before commenting on these, one must bear in mind the restrictions and limitations of the use of the triangular phase diagrams in general. It has been stated by Fyfe et al. (1958) regarding the green schist facies (p. 219) "Even the simplest rocks must be treated as systems of many components. The manner in which mineral composition varies regularly with chemical composition of rocks - the very essence of metamorphic facies - cannot adequately be demonstrated by dividing three component diagrams (ACF, AKF, and so on) into triangular fields."

In the AKF and A'KF diagrams (Figs. 26a, 27a, 28a, 29a and 30a) of each aureole, the rocks in their original regional grade lie in the chlorite-muscovite triangle ($\pm$ biotite in some rocks) indicating the probable absence of pyrophyllite. Out of the 80 rocks analysed, the

only exceptions to the last remark are Nos. 24, 29, 30, 31 from Ardara and 46, 48 from Thorr. These 6 rocks lie above the muscovite-chlorite join and might have contained pyrophyllite.

Because FeO and MgO are treated as one component at the F corner of these diagrams, there is no distinction between the kyanite-bearing and the kyanite-free rocks. On the other hand, the distinction between the two groups becomes clear if FeO and MgO are represented separately as in the case of the AFM and A'FM diagrams (Figs. 26b, 27b, 28b, 29b and 30b). The two interesting aureoles are the Ardara and the Main Donegal because both of them contain kyanite-free and kyanite-bearing andalusite and/or fibrolite schists. The phase diagrams of these two aureoles (Fig. 27b, 30b) clearly demonstrate the grouping of the kyanite-bearing schists near the M corner and the kyanite-free rocks near the F corner; a reflection of the difference in the MgO/FeO ratio between the two groups of rocks.

The distinction is better still illustrated on the AKFM and A'KFM diagrams (Figs. 31 to 40). For each aureole, when the rocks are kyanite-free (e. g. Fanad, Thorr aureole and enclaves, Barnesmore) they lie close to each other in one bundle nearer to the F corner. On the other hand, the rocks from each of Ardara and the Main Donegal granite aureoles show a distinct grouping in two bundles; the one near the F corner comprises the kyanite-free rocks whereas the one near the M corner is the kyanite-bearing rocks.

Disregarding the probable difference in the grade of metamorphism, the 80 rocks from all aureoles were plotted on one phase diagram (Figs. 41 to 45). Again the distinction between the two groups of rocks was well shown on the AFM and the A'FM diagrams

and magnificently displayed on the AKFM diagrams. The Thompson phase projection (Thompson, 1957) was then attempted and in spite of all the restrictions and reservations imposed on the application of this phase diagram to rock analysis, yet, the same pattern of group distinction was evident (Fig. 45). Moreover, there is a systematic relation between the type of aluminium silicate and associated minerals and the M/FM values of the 80 rocks, a relation which can be outlined as follows:-

Mineralogy	M x 100/FM
Andalusite and/or sillimanite $\pm$ staurolite	25.5 - 53.6 (on the basis of 45 rocks from all aureoles)
Kyanite + staurolite $\pm$ andalusite $\pm$ fibrolite	54.1 - 69.5 (on the basis of 29 rocks from ardara and the Main Donegal, only 6 rocks are devoid of staurolite but they contain fibrolite)
Kyanite alone	70.4 - 78.8 (on the basis of four rocks from the Main Donegal aureole)
No aluminium silicates	83.8 - 89.6 (on the basis of two rocks from the Main Donegal which also have very low A values)

The M/FM of the coexisting biotites show a similar variation with mineralogy. For the 21 biotites analysed from all aureoles, the

variations in the different assemblages can be outlined as follows:-

Mineralogy	M x 100/FM
Kyanite-free $\pm$ staurolite	24.4 - 47.0 (14 biotites)
Kyanite + staurolite	53.2 - 61.6 (5 biotites)
Kyanite alone	66.6 - 66.8 (2 biotites)

E. Main Conclusions:-

From the foregoing comments, the main conclusions can be outlined as follows:-

(1) The M/FM ratio in the kyanite-bearing rocks is higher than that of the kyanite-free rocks, regardless of the spatial distribution of the two types of rocks relative to the granite contact.

(2) Andalusite and sillimanite develop in the majority of rocks regardless of their M/FM ratio. The distinction between the host rocks carrying the two forms of aluminium silicate is not chemical but is a spatial one, i.e. closeness of the rock to the granite.

(3) There is a close correlation between the M/FM ratio of the rocks and their coexisting biotites.

(4) In the AKF diagrams, the field in which the rocks plot indicates that the original regional rocks were mainly chlorite-muscovite assemblages $\pm$ biotite $\pm$ garnet.

Fig. 26

Fanad Aureole

• Kyanite-free rocks

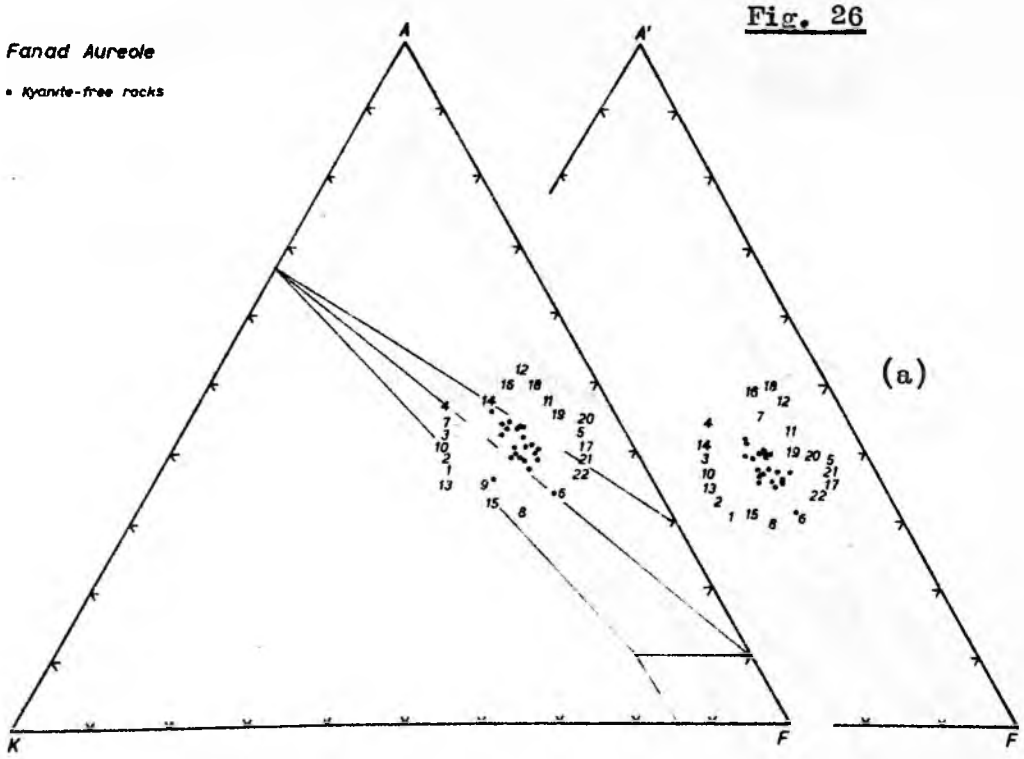

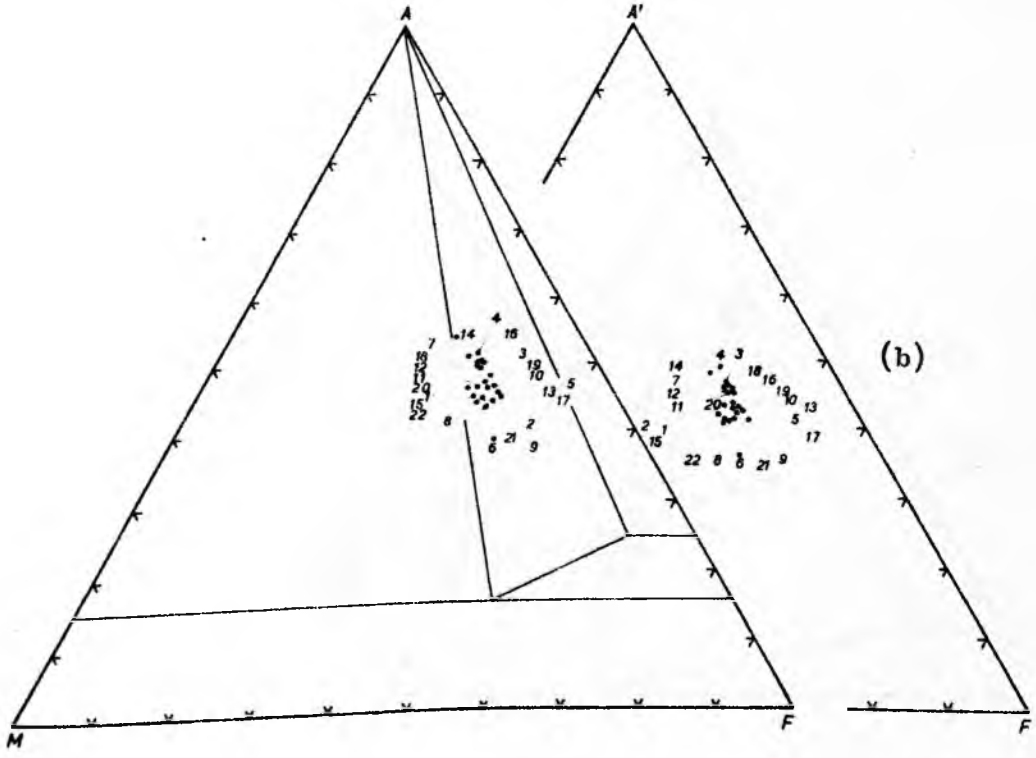

Fig. 27

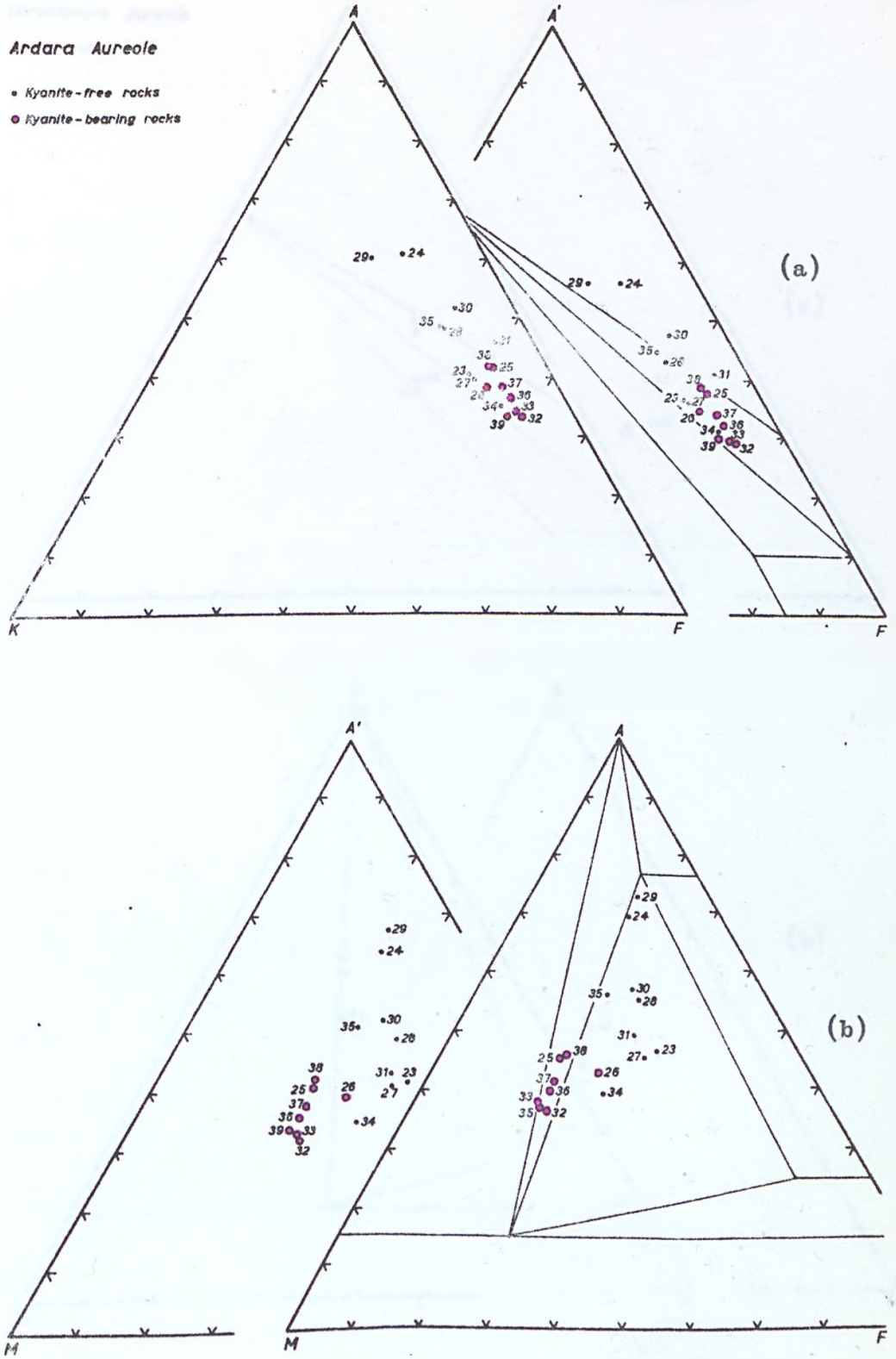
Ardara Aureole
• Kyanite-free rocks
• Kyanite-bearing rocks
A
A'
K
F
F
(a)
A'
A
M
M
F
(b)

Fig. 28

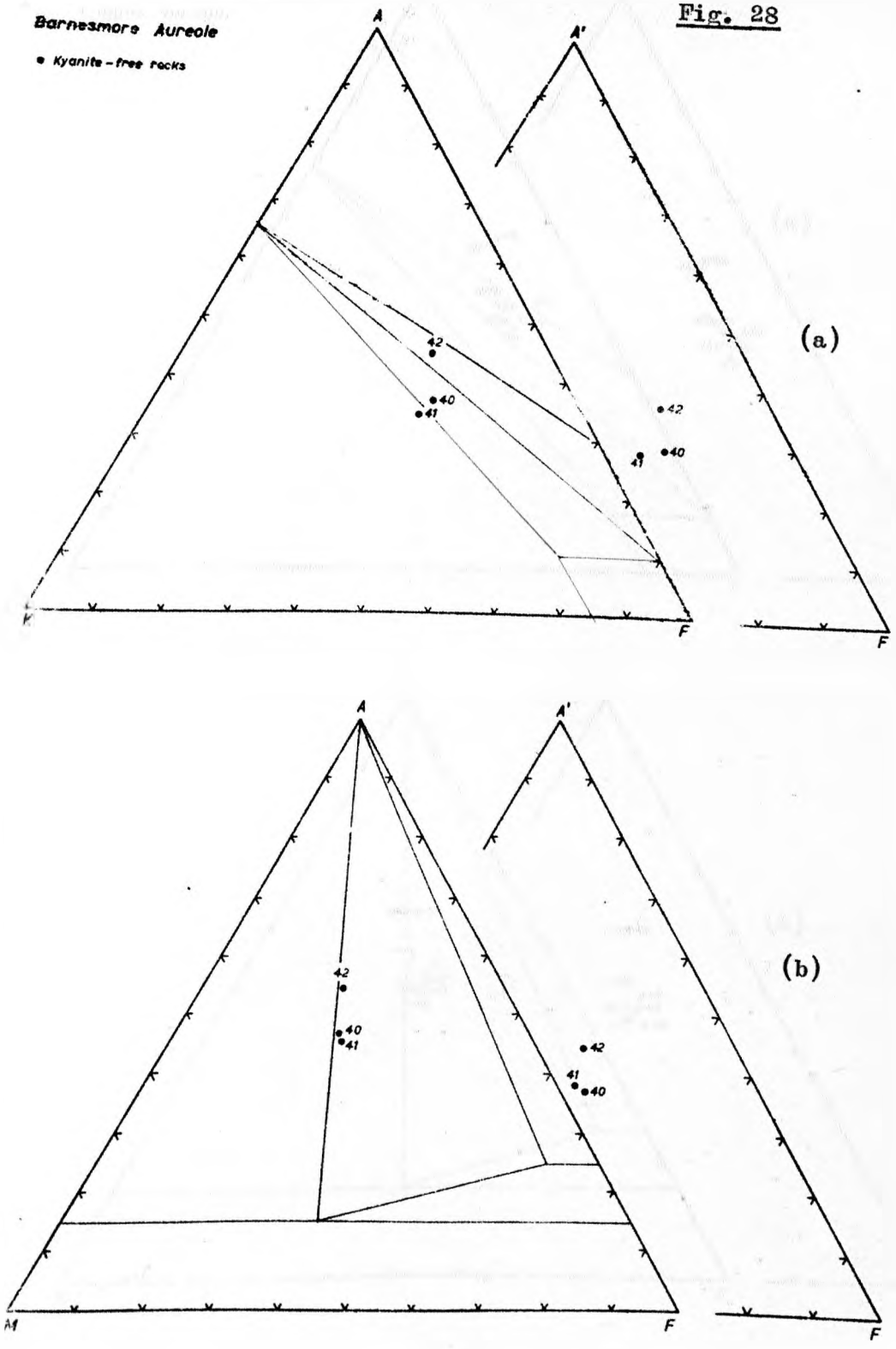

Fig. 29

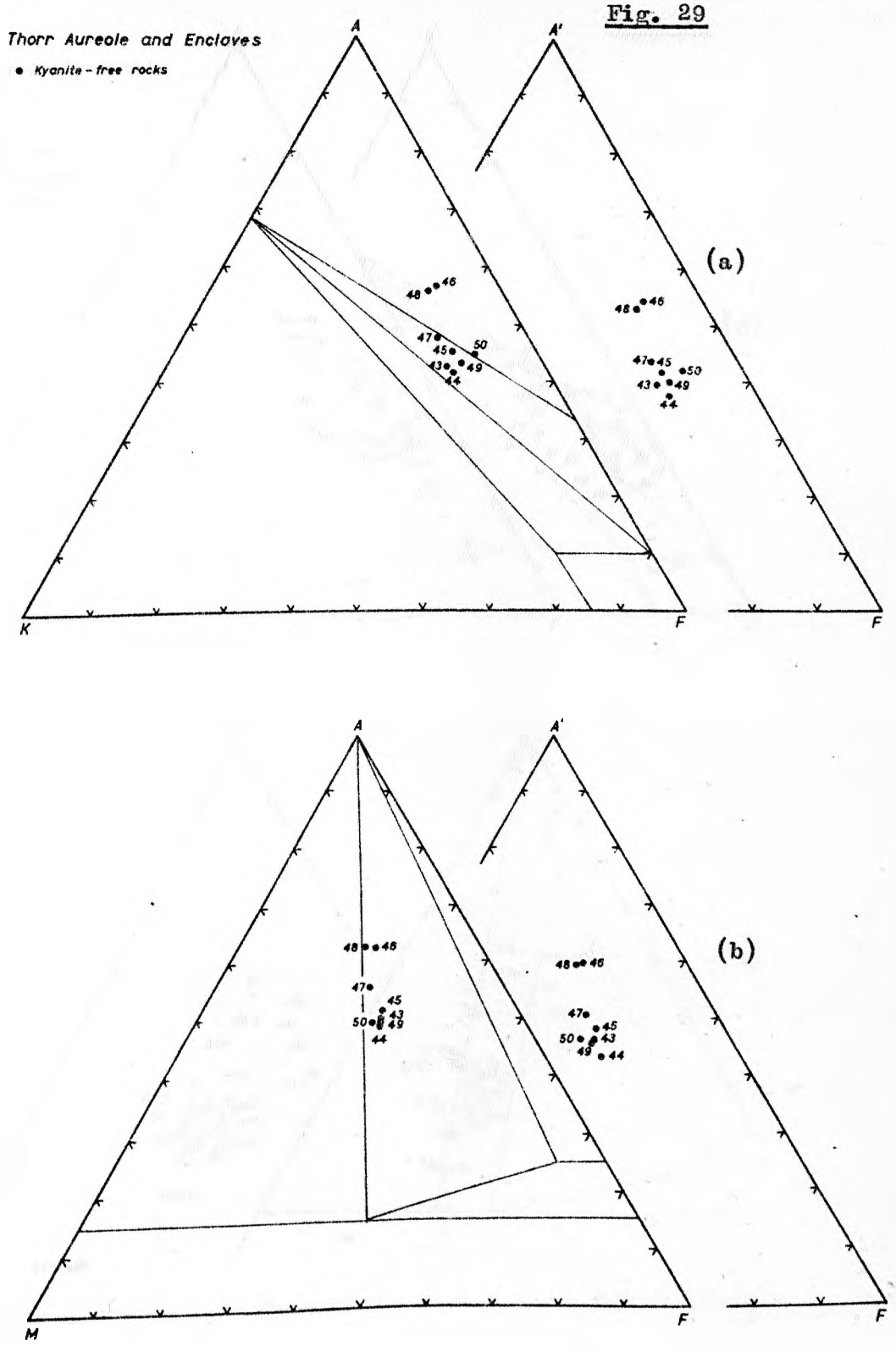
Thorr Aureole and Enclaves
• Kyanite-free rocks
A
A'
K
F
F
(a)
48 46
47 45 50
43 49
44
48 46
47 45 50
43 49
44
A
A'
M
F
F
(b)
48 46
47 45
50 43 49
44
48 46
47 45
50 43
49 44

Fig. 30

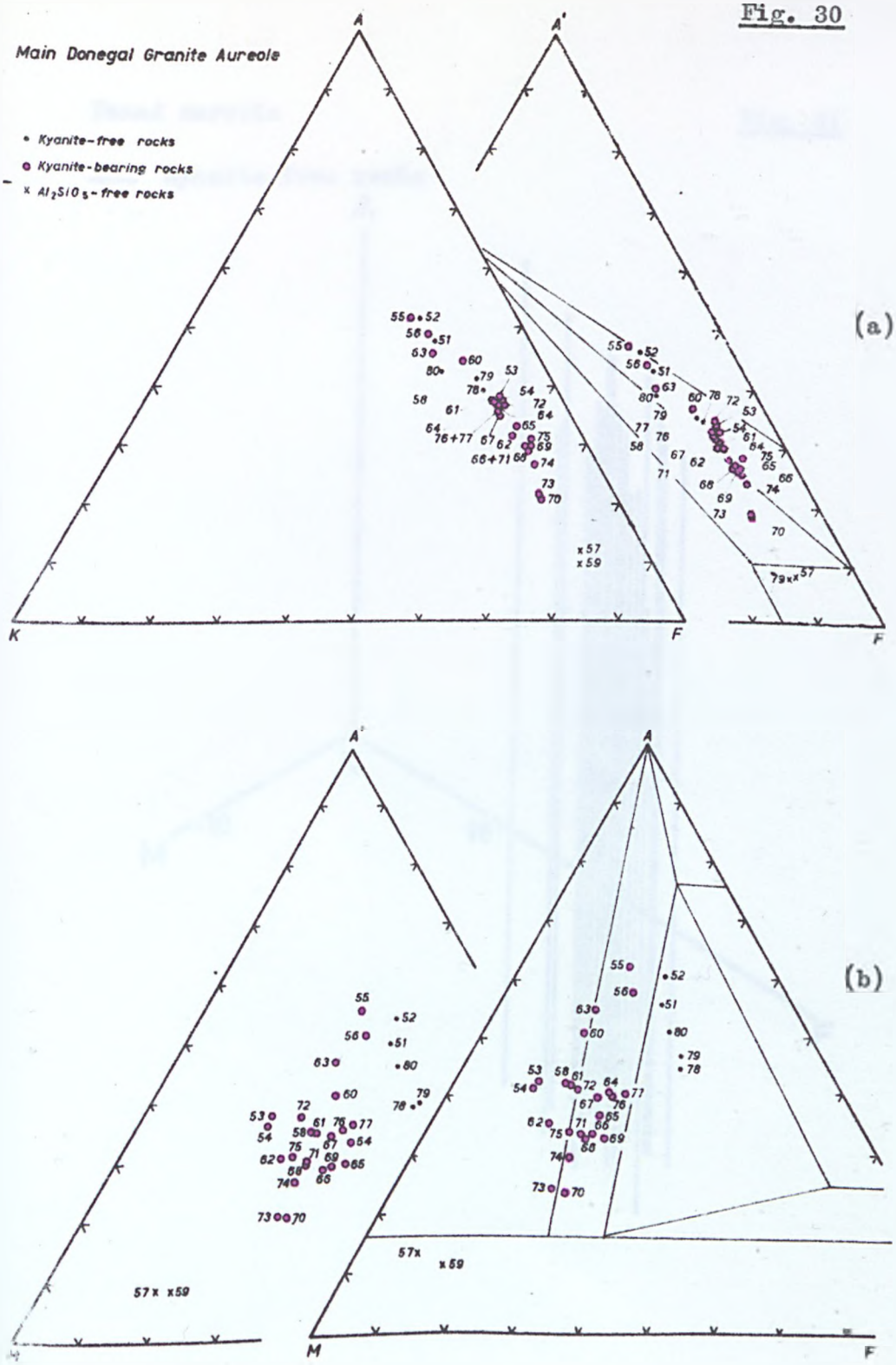
Main Donegal Granite Aureole
• Kyanite-free rocks
o Kyanite-bearing rocks
x Al_2SiO_5-free rocks
A
A'
K
F
F
(a)
A'
A
M
F
(b)

Fanad aureole Fig. 31

—— **kyanite-free rocks**

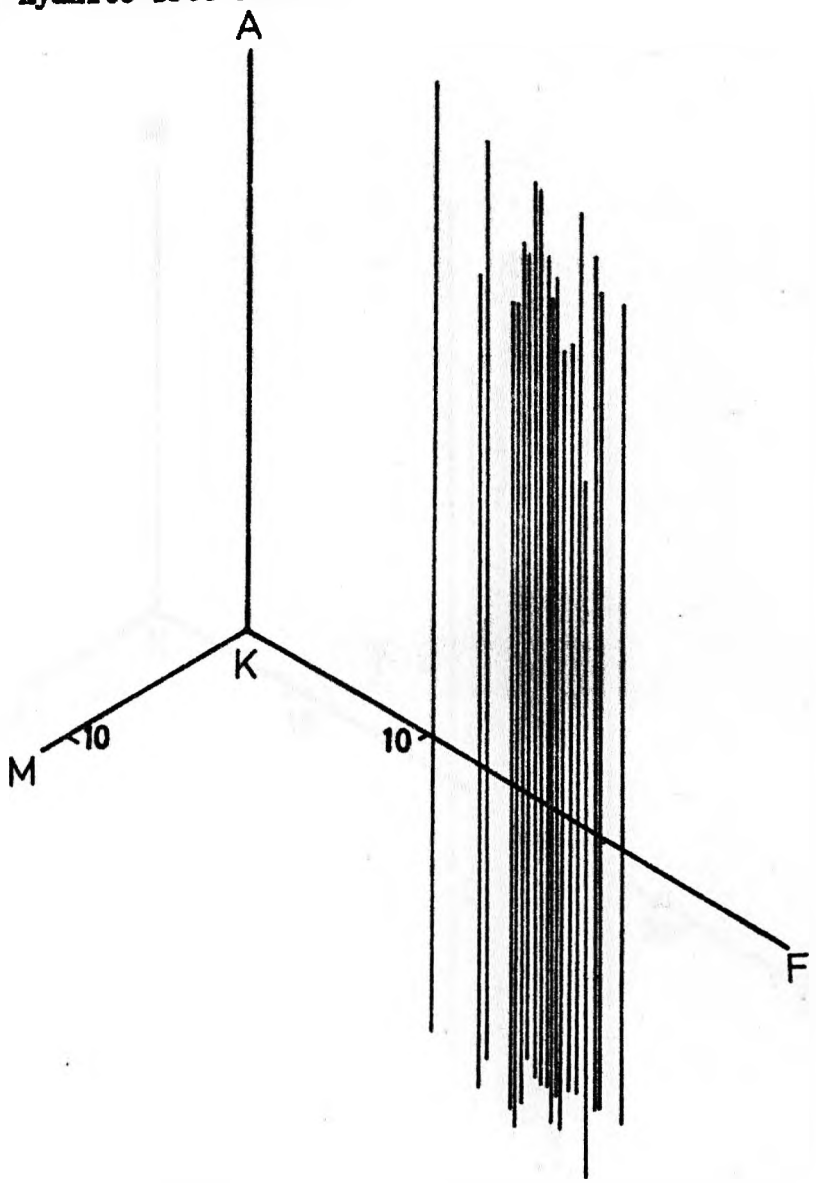

Fig. 32

Fanad aureole

Kyanite-free rocks

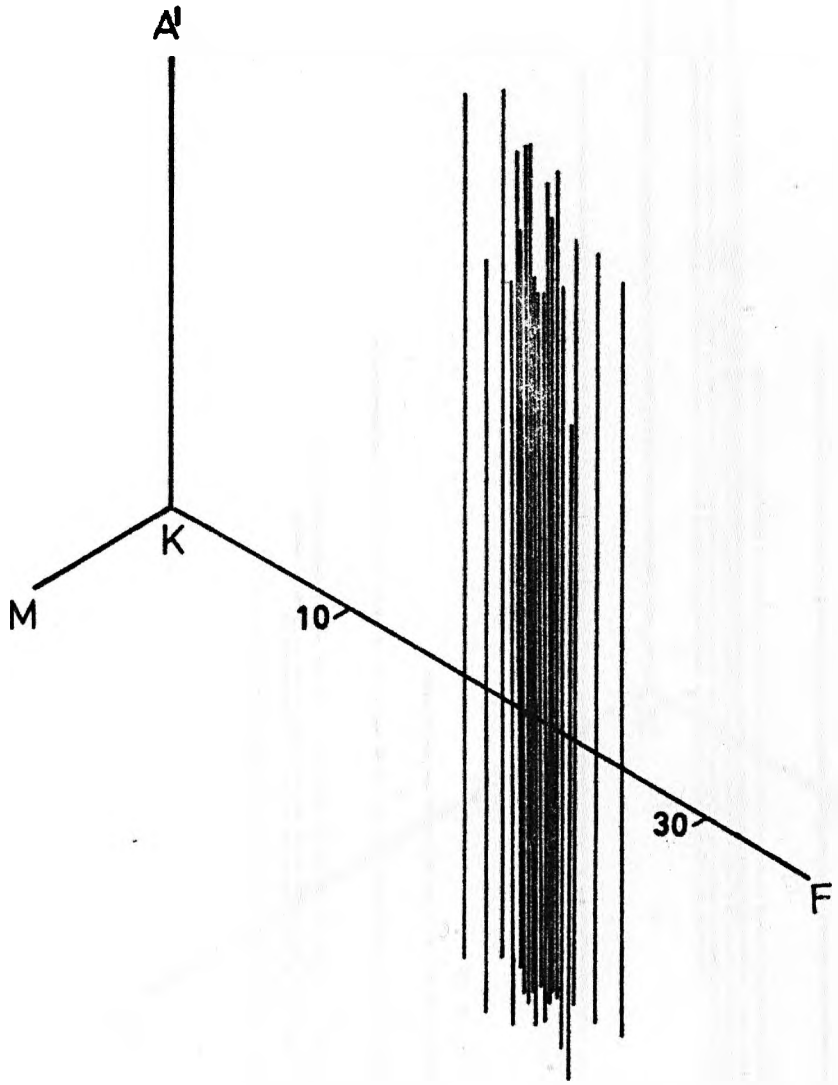

Fig. 33

Ardara aureole

___ kyanite-free rocks

___ kyanite-bearing rocks

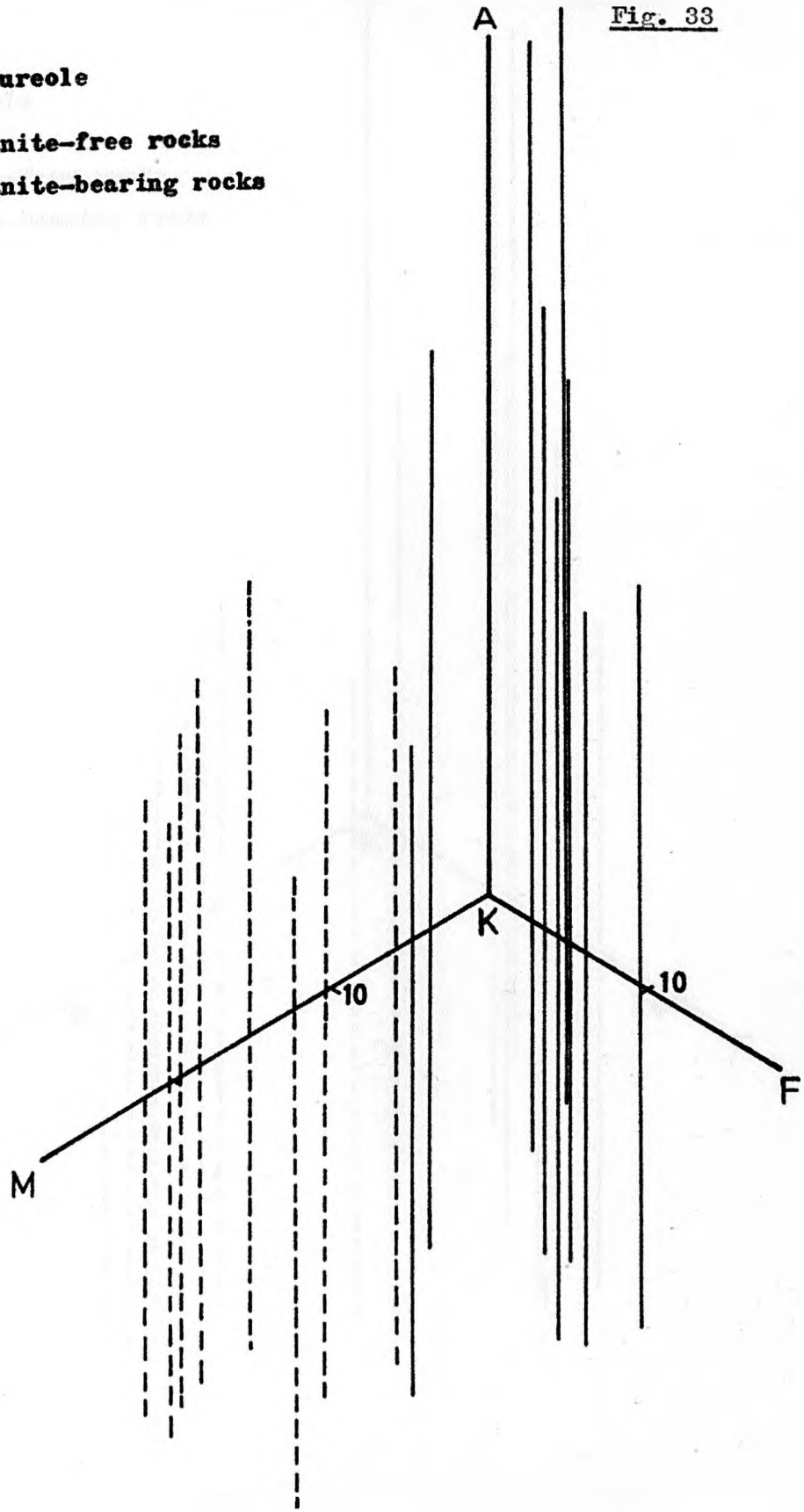

Fig. 34

Ardara aureole

—— kyanite-free rocks

- - - kyanite-bearing rocks

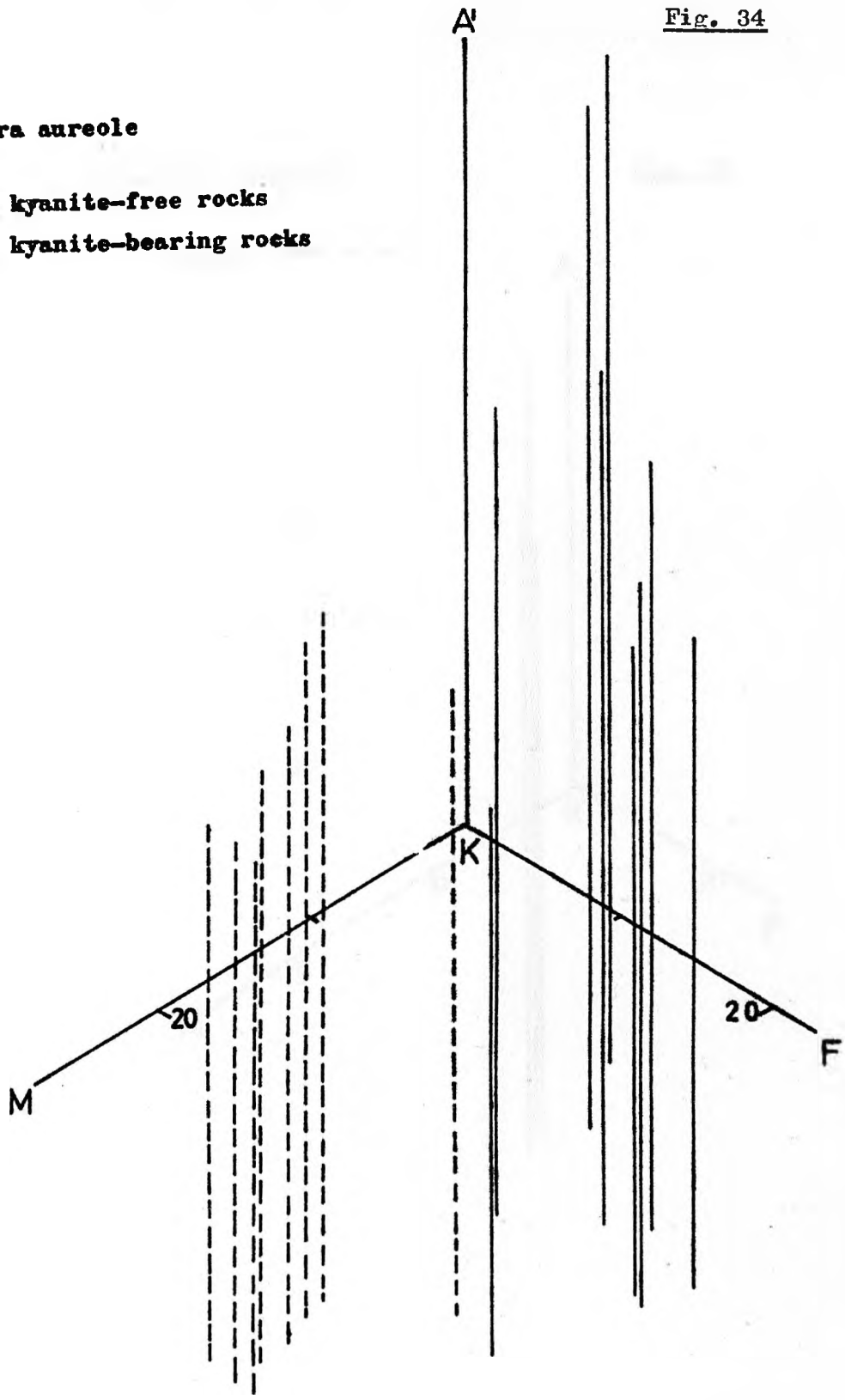

Barnesmore aureole

Fig. 35

—— kyanite-free rocks

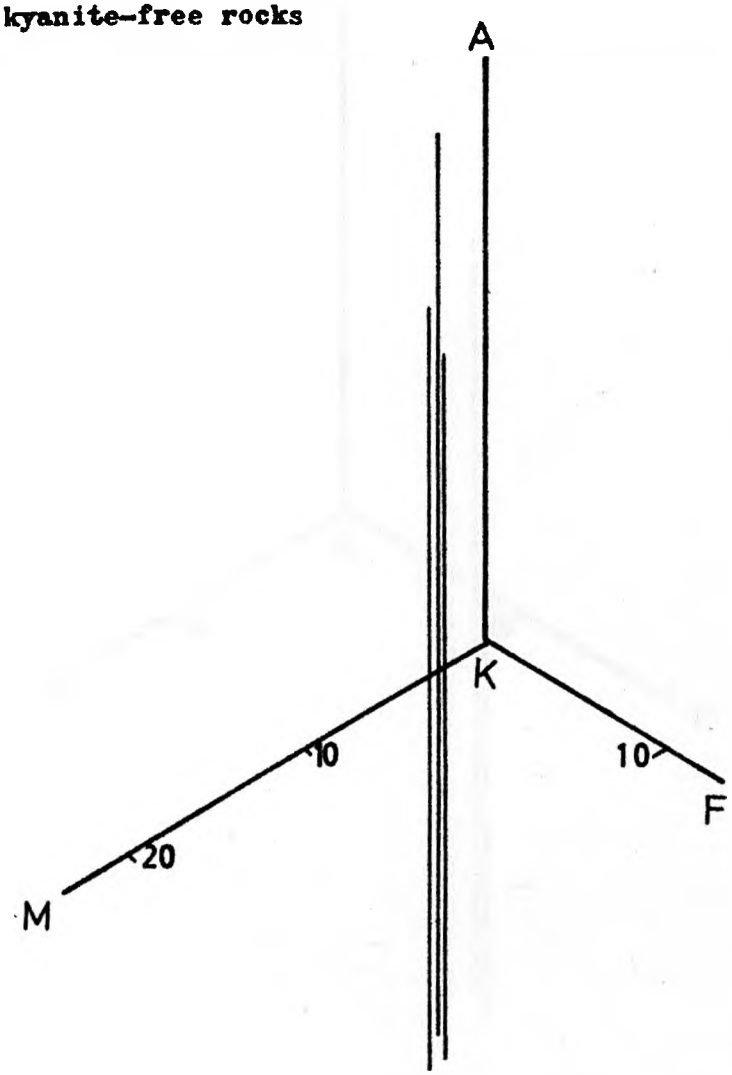

Barnesmore aureole

Fig. 36

—— kyanite-free rocks

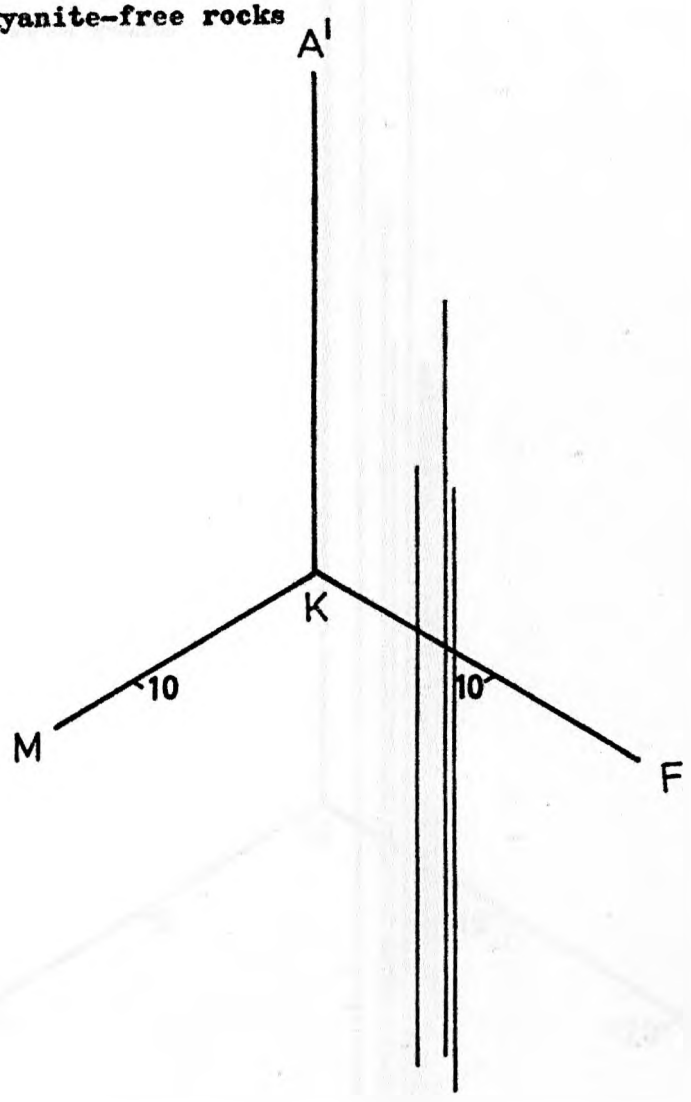

Fig. 37

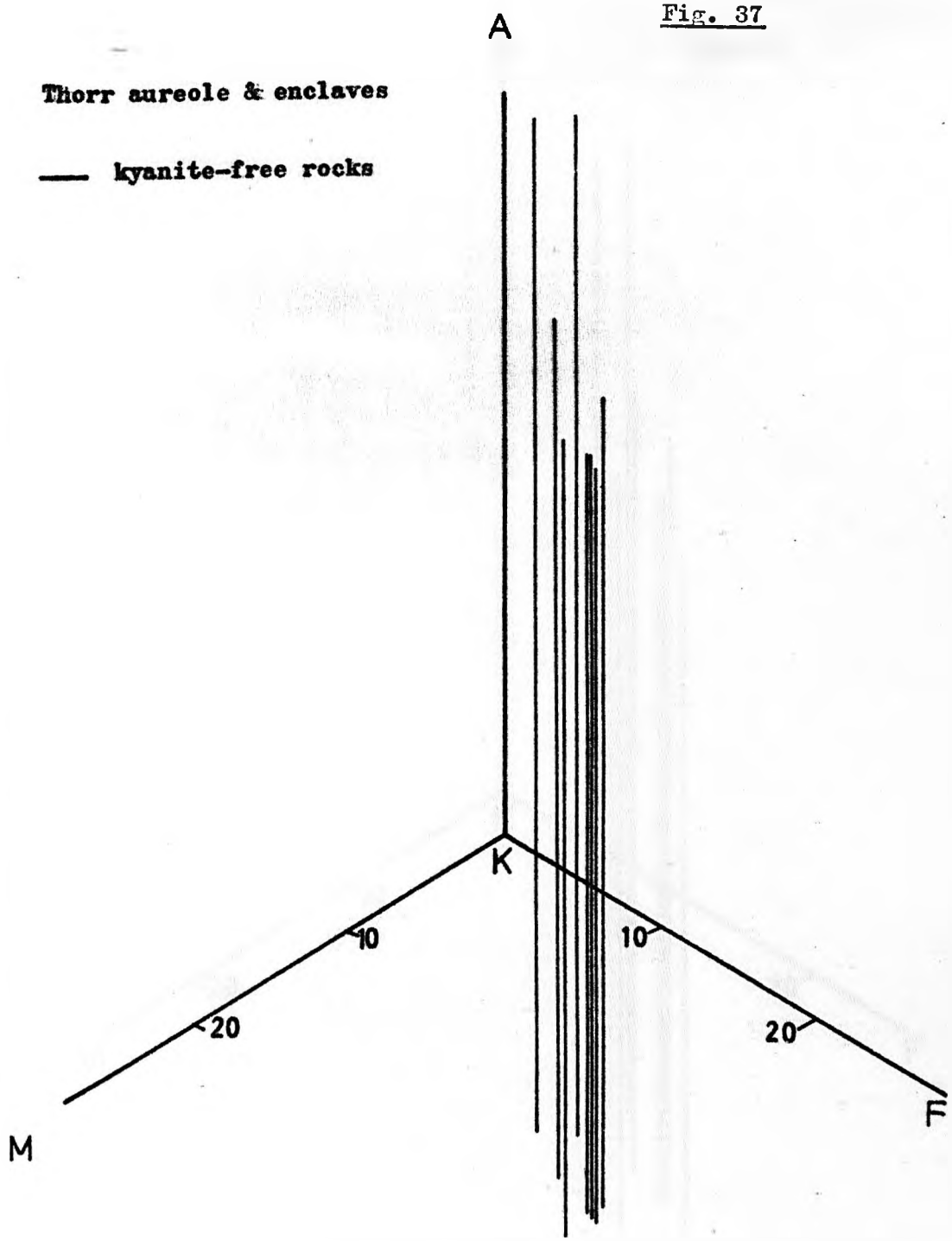

Fig. 38

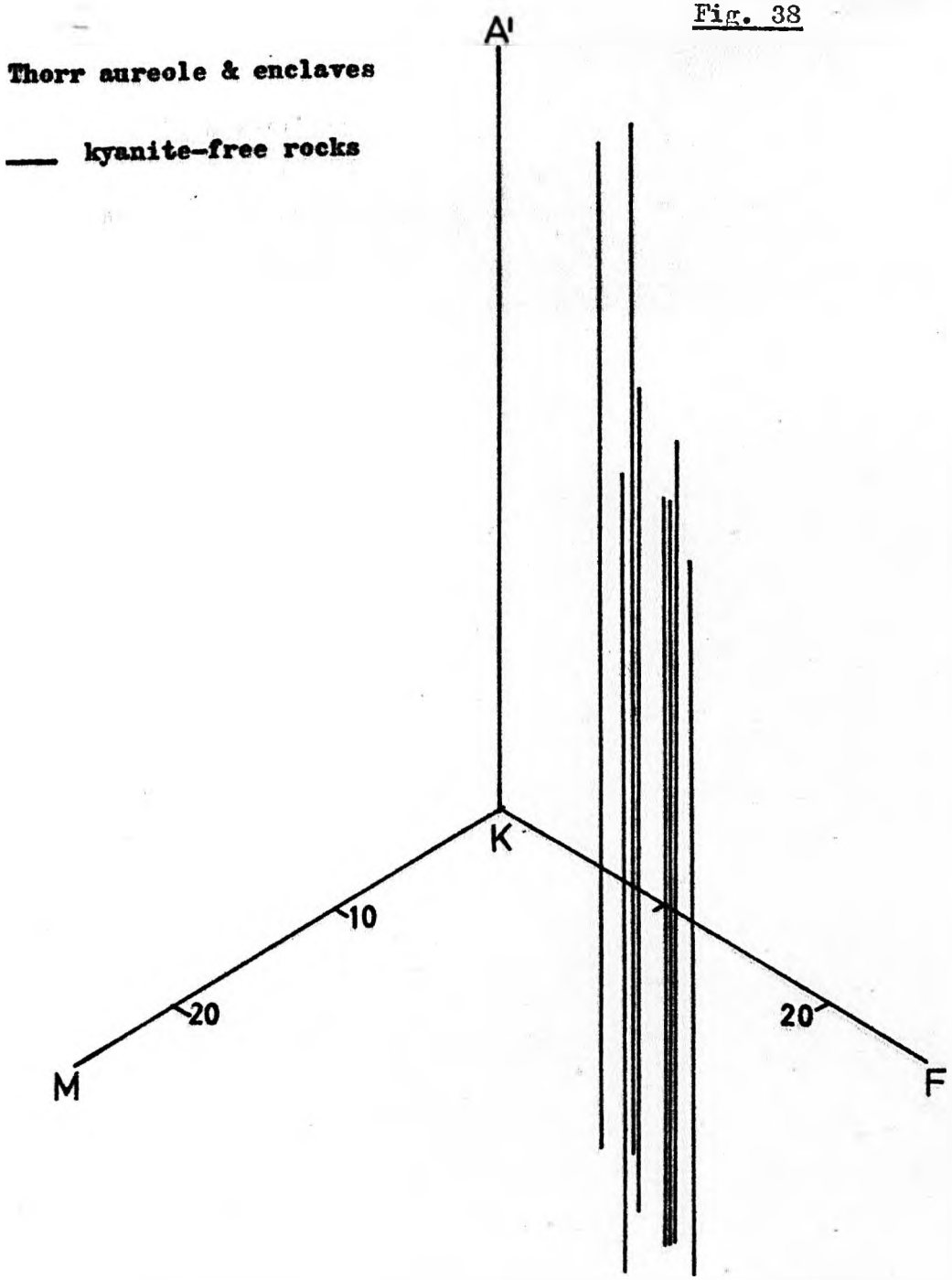

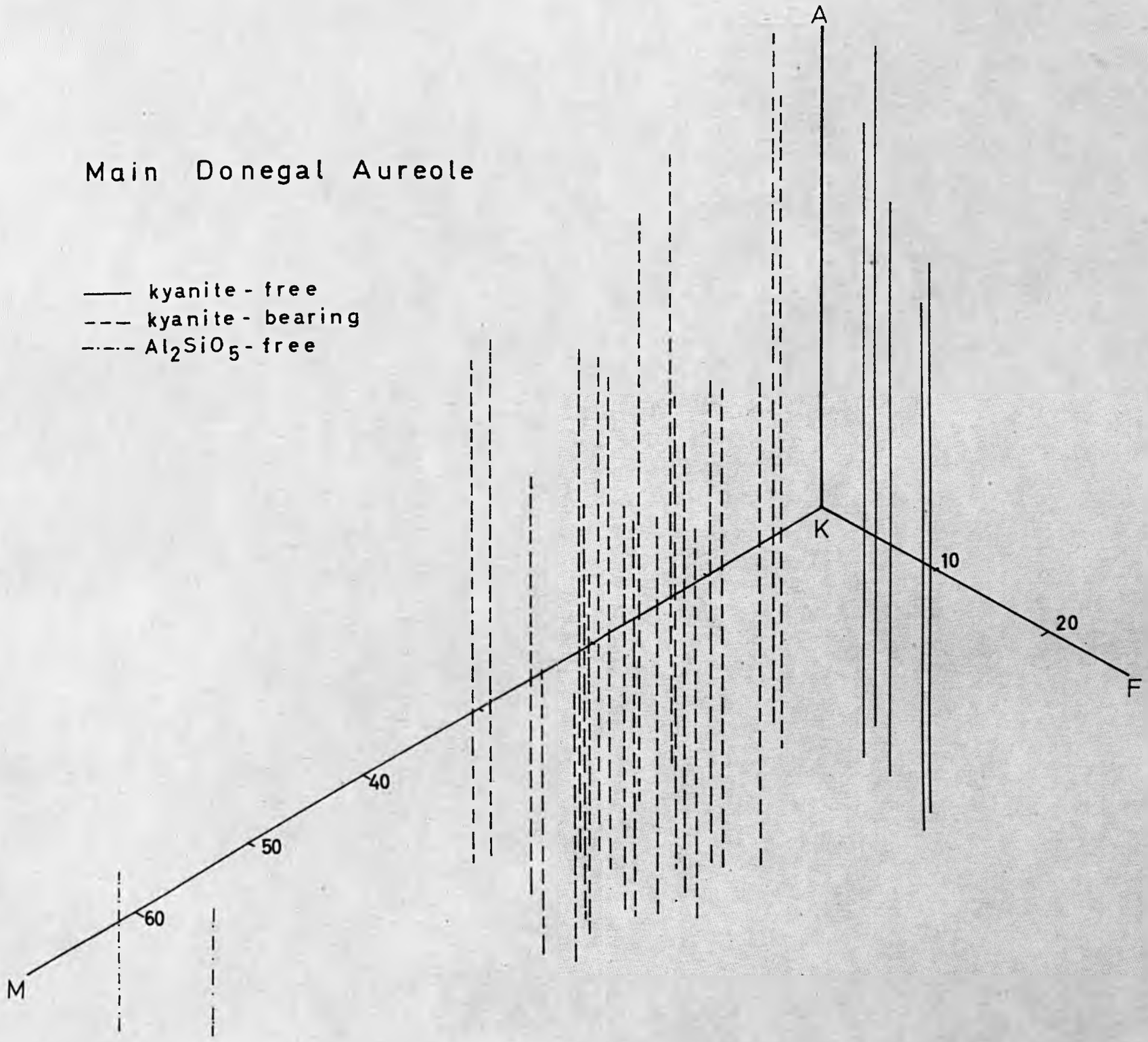
Main Donegal Aureole
kyanite - free
kyanite - bearing
Al_2SiO_5 - free
A
K
F
M
10
20
40
50
60

Fig. 39

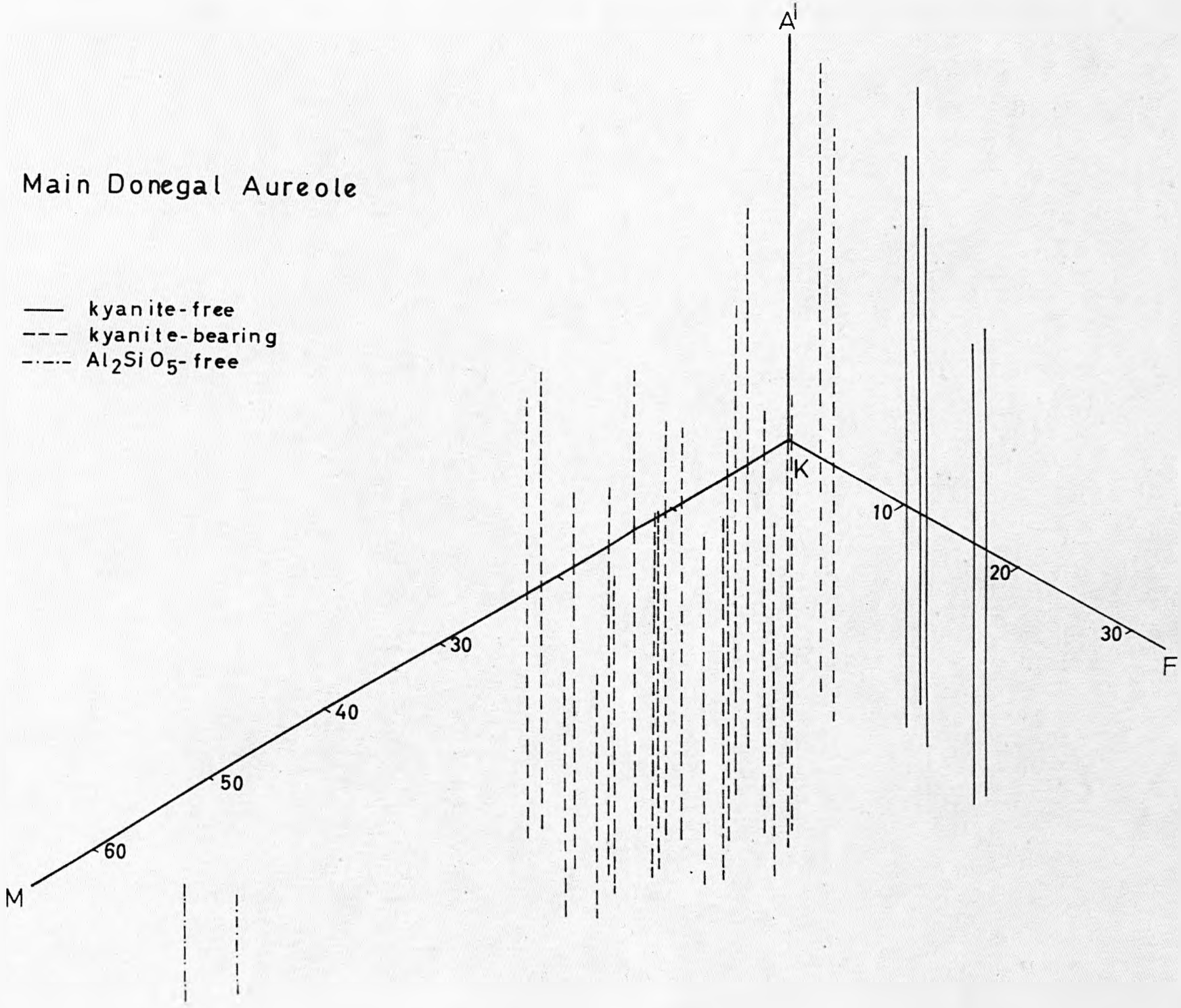
Main Donegal Aureole
kyanite-free
kyanite-bearing
Al_2SiO_5-free
A
K
F
M
10
20
30
30
40
50
60

Fig. 40

Fig. 41

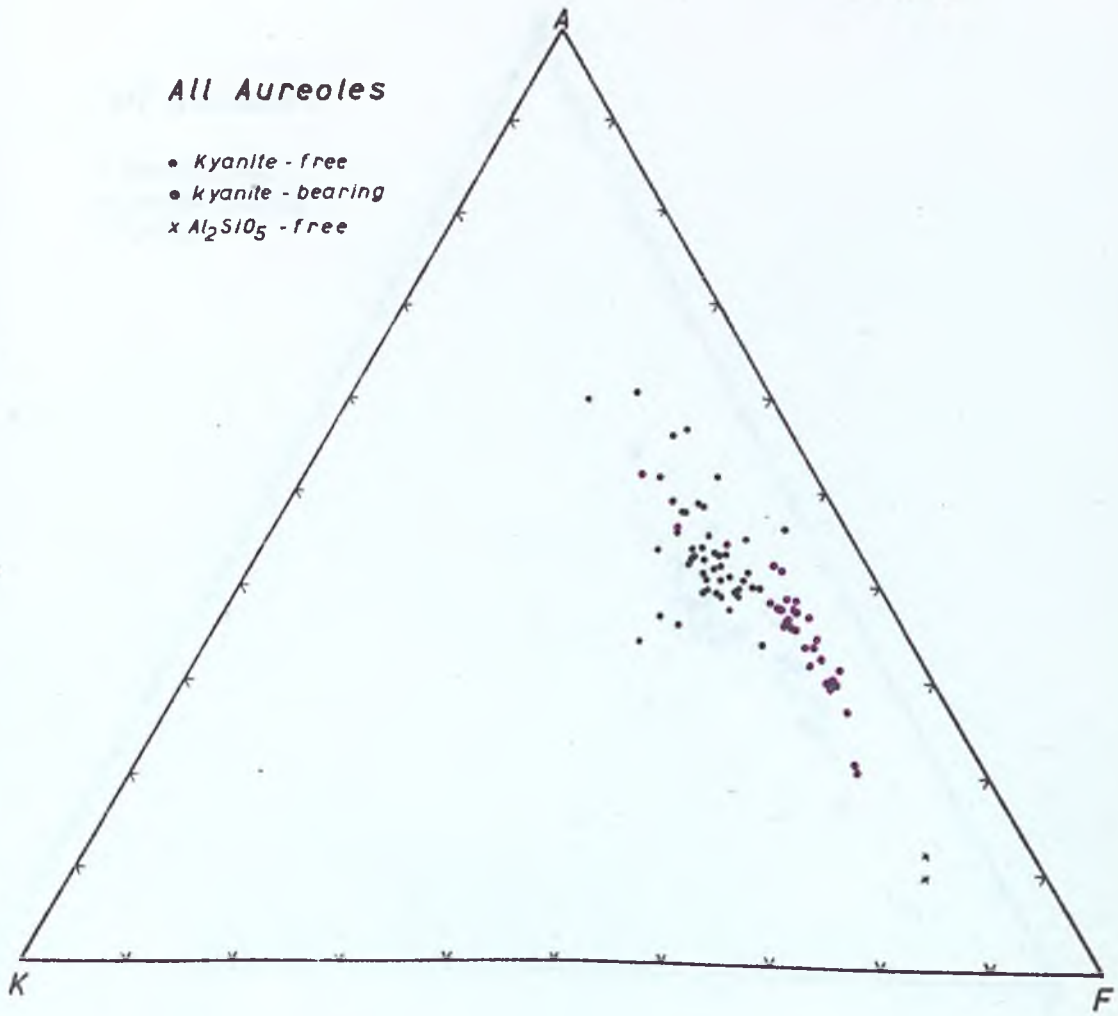
All Aureoles
• Kyanite - free
• kyanite - bearing
x Al_2SiO_5 - free
A
K
F

Fig. 42

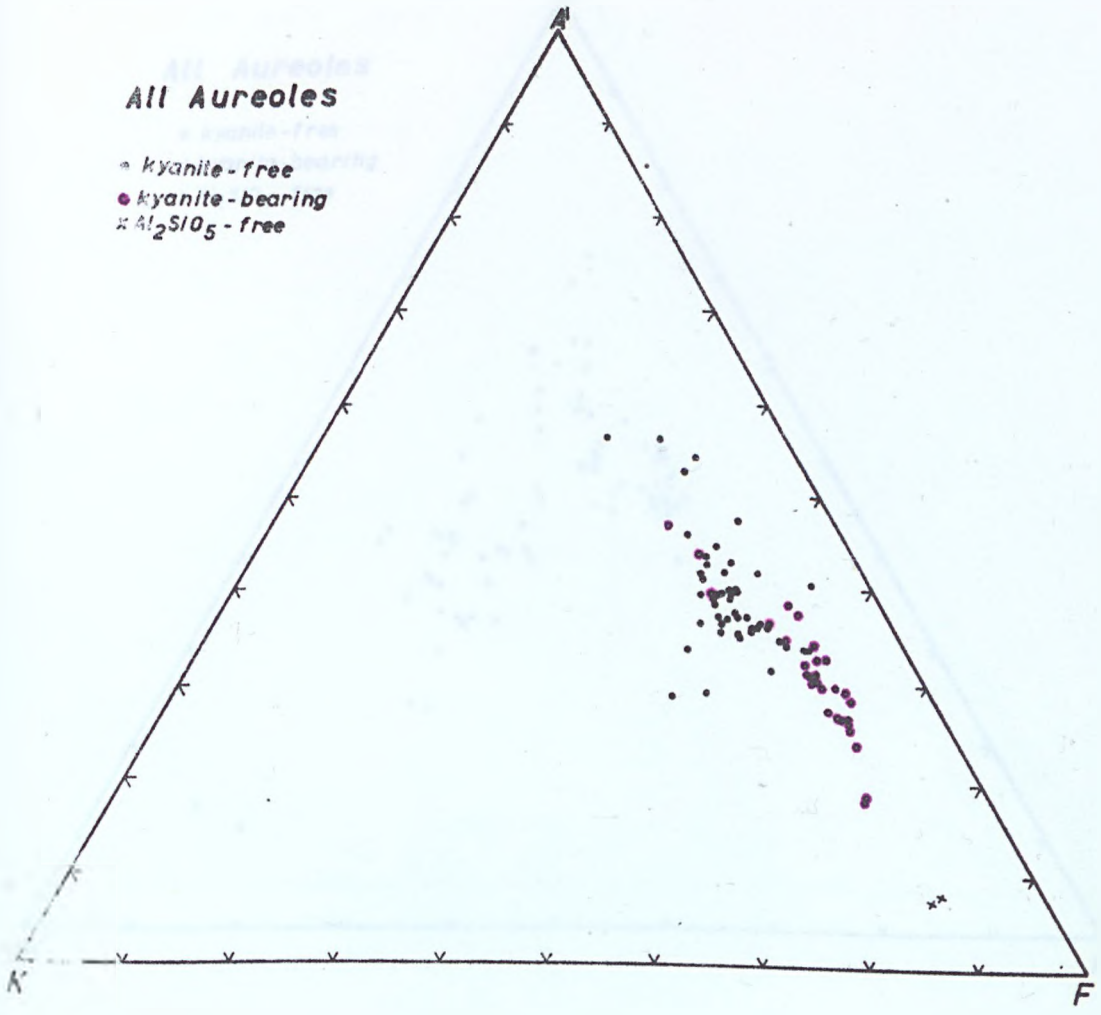
All Aureoles
kyanite-free
kyanite-bearing
Al_2SiO_5-free
A
K
F

Fig. 43


All Aureoles
• kyanite-free
o kyanite-bearing
x Al_2SiO_5-free
A
M
F

Fig. 44

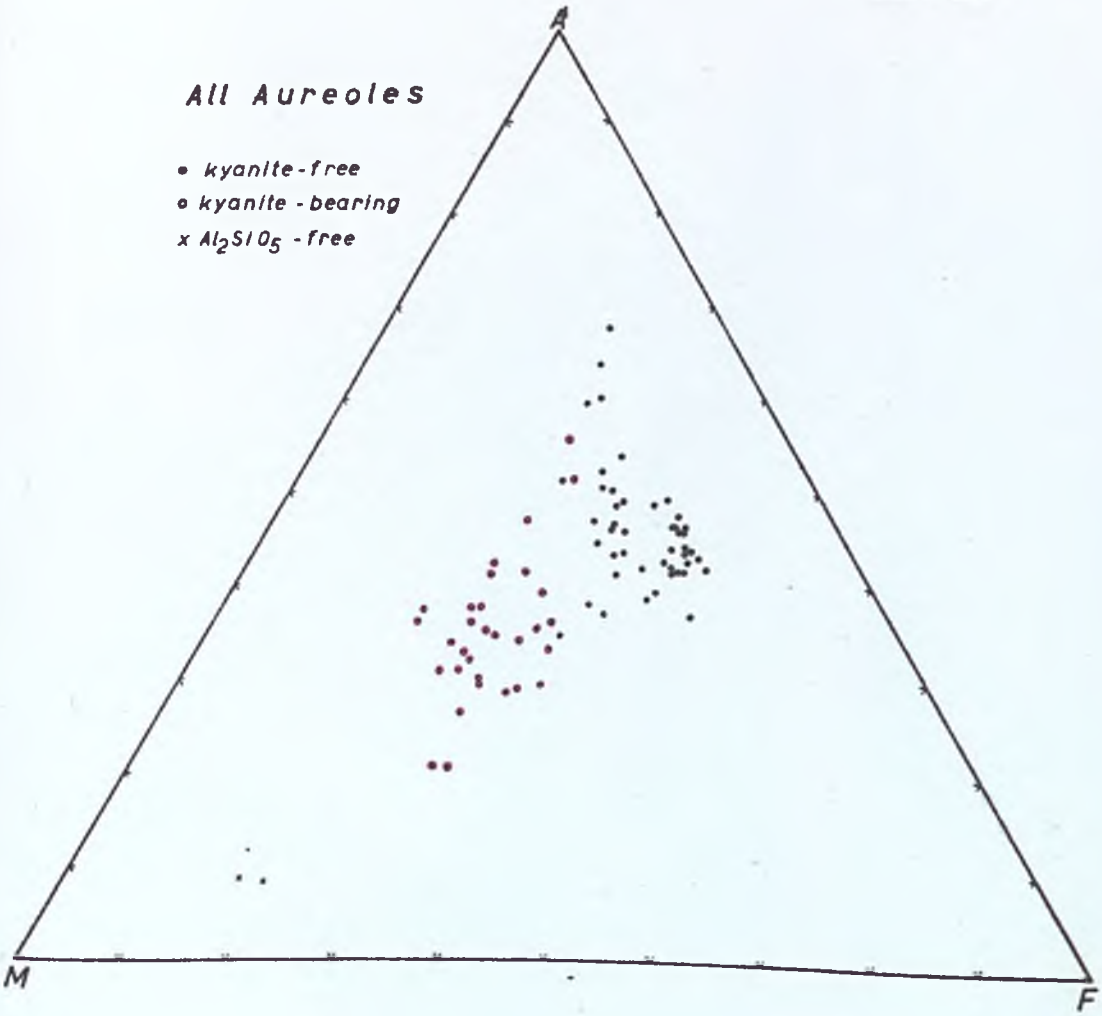
All Aureoles
• kyanite-free
o kyanite-bearing
x Al_2SiO_5-free
A
M
F

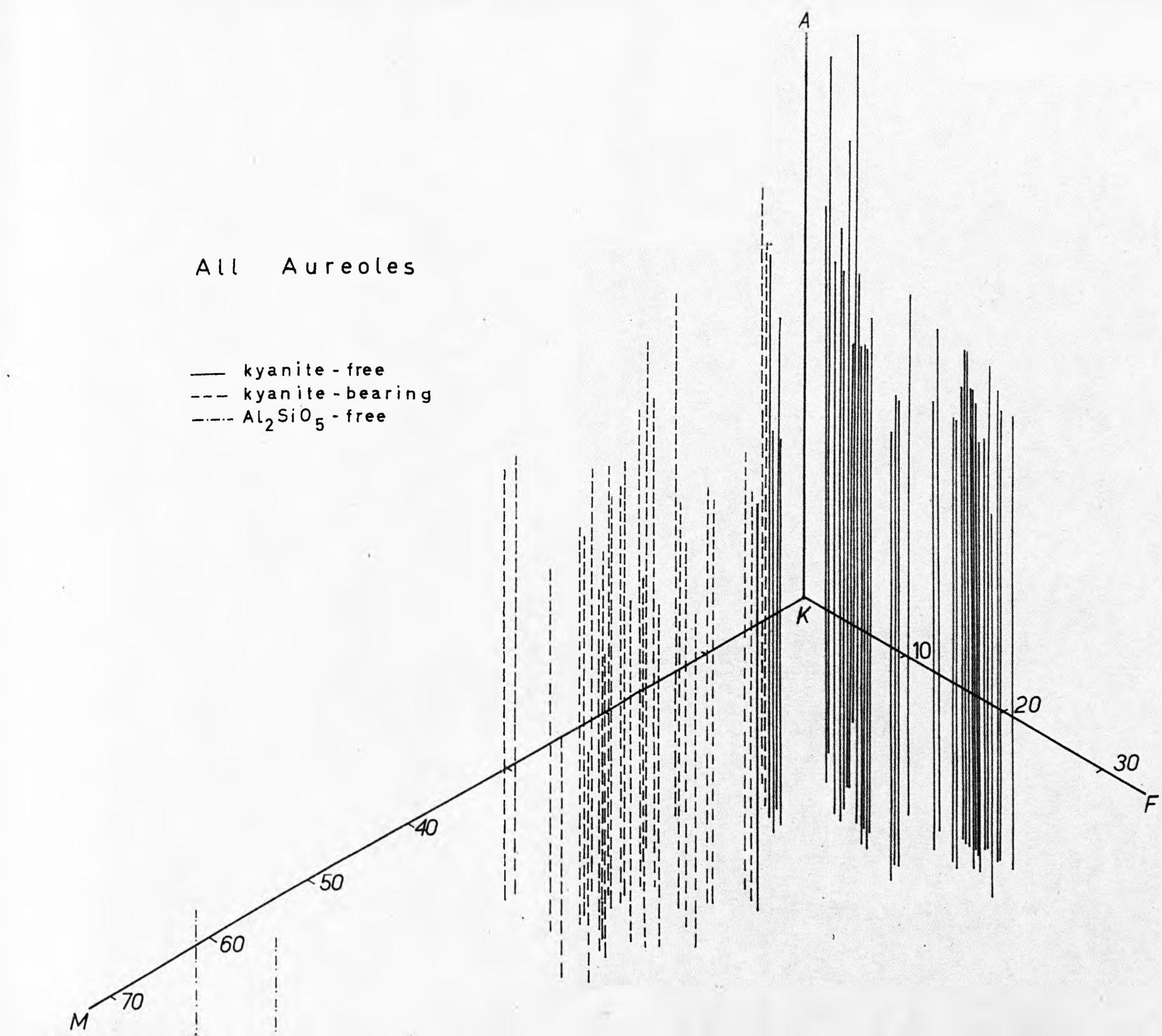
All Aureoles
kyanite - free
kyanite - bearing
Al_2SiO_5 - free
A
K
F
M
10
20
30
40
50
60
70

Fig. 45

Fig. 46

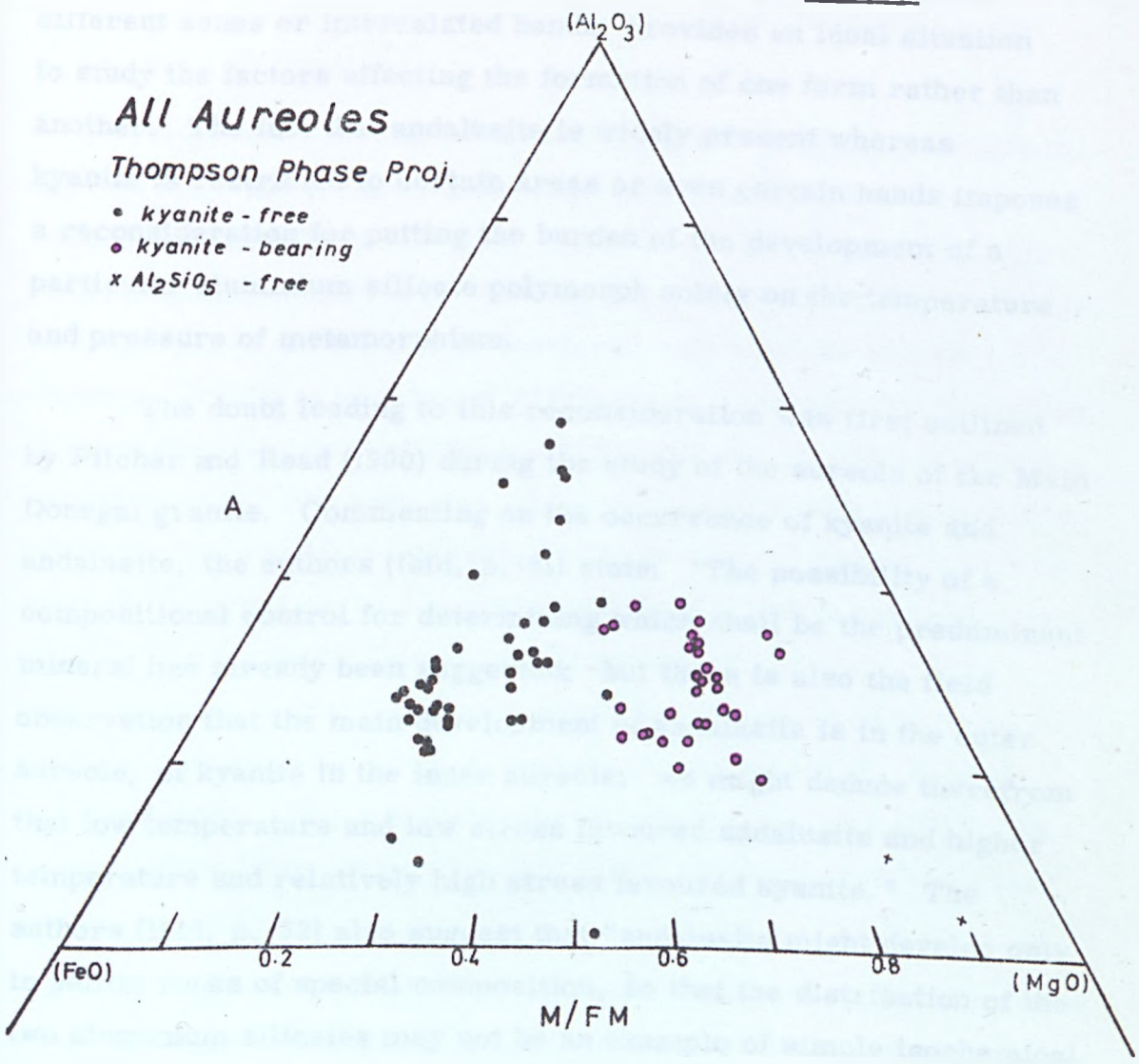
All Aureoles
Thompson Phase Proj.
• kyanite - free
o kyanite - bearing
x Al_2SiO_5 - free
(Al_2O_3)
A
(FeO)
0·2
0·4
0·6
0·8
(MgO)
M/FM

VI. DISCUSSION

The way in which the different forms of aluminium silicates occur in the different aureoles of Co. Donegal granites i. e. in different zones or intercalated bands, provides an ideal situation to study the factors affecting the formation of one form rather than another. The fact that andalusite is widely present whereas kyanite is restricted to certain areas or even certain bands imposes a reconsideration for putting the burden of the development of a particular aluminium silicate polymorph solely on the temperature and pressure of metamorphism.

The doubt leading to this reconsideration was first outlined by Pitcher and Read (1960) during the study of the aureole of the Main Donegal granite. Commenting on the occurrence of kyanite and andalusite, the authors (ibid, p. 31) state: "The possibility of a compositional control for determining which shall be the predominant mineral has already been suggested; but there is also the field observation that the main development of andalusite is in the outer aureole, of kyanite in the inner aureole; we might deduce therefrom that low temperature and low stress favoured andalusite and higher temperature and relatively high stress favoured kyanite." The authors (ibid, p. 32) also suggest that "andalusite might develop only in pelitic rocks of special composition, so that the distribution of the two aluminium silicates may not be an example of simple isochemical zoning. A complete survey of the status of aluminium silicates in aureoles is obviously required."

From the essence of this last comment, the present study was pursued not only on the aureole of the Main Donegal granite, but also

on four of the other main aureoles in Co. Donegal. The outcome of this study in the form of petrological, chemical and modal data makes possible, with a fair degree of certainty, the assessment of the chemical factors, if there are any, affecting the development of a particular aluminium silicate polymorph in the aureole rocks of Co. Donegal Granites.

From the microscopic studies, it has already been concluded that the sequence of mineral development is garnet, staurolite-kyanite, followed by andalusite. Fibrolite develops throughout the metamorphism of the rocks when the physical conditions are suitable, whereas coarse sillimanite is developed only near the granite contacts. There is no textural indication of a polymorphic transition between the aluminium silicates nor there is any resorption of any earlier mineral by a later one. Staurolite occurs only in specimens of the Ardara and Main Donegal granite aureoles. Garnet occurs in most of the rocks of the 5 aureoles and does not show any particular pattern relative to the type of aluminium silicate present. It is worth mentioning that the occurrence of kyanite as an aureole mineral has been recognised earlier in Donegal by McCall (1954), Pitcher and Read (1960, 1963); in north-west Spain by Sergiades (1962); in north-eastern Vermont by Woodland (1963) and south-western Ghana by Lobjoit (1964).

The petrological study of the rocks outside the granite thermal effect as well as the study of the AKF diagrams of the aureole rocks analysed, led to the conclusion that the aureole rocks studied in their original regional grade are principally chlorite-muscovite $\pm$ biotite assemblages, i. e. the lower part of the green schist facies. However, rocks from Fanad aureole probably belong to a higher grade because remnants of regional garnets as well as a great number of large (up to

5 mm. across) chlorite knots-after-garnet are seen in thin sections.

The next step is to relate the chemistry of the rocks with their mineralogy through a closer and detailed study of the AFM diagrams. The main facts to bear in mind are that (a) the development of andalusite is always later than garnet, kyanite and staurolite, and (b) kyanite develops only in rocks of high M/F ratio whereas andalusite occurs in rocks regardless of their M/F ratios. Hence, in the following discussion, an earlier reaction in which kyanite is produced in certain rocks and a later reaction in which andalusite is produced in most of the rocks, are described.

A. The Earlier or First Reaction

(1) Kyanite (+ staurolite) - bearing aureoles:-

These are exemplified by Ardara and the Main Donegal granite aureoles. In the AFM diagram of Ardara aureole (Fig. 27b), two fields are distinguished: the kyanite-staurolite-biotite triangle near the M corner and the biotite $\pm$ staurolite $\pm$ garnet triangle near the F corner. Both the 3-phase triangles have a common point on the line representing the biotite, i. e. invariant point. It is noticed that the kyanite-staurolite rocks analysed (occurring within a span of about 100 yards measured normal to the granite contact) show a narrow range of variation in M/FM values (0. 654 - 0. 695) which is clearly shown in the left hand side triangle of the AFM diagram. In specimen No. 26, no kyanite has been seen in thin sections, but since the rock is highly shimmered and in the field it lies just on the border between the kyanite-bearing and the kyanite-free rocks, it is difficult to state with certainty whether or not it contained kyanite at any time. Therefore, this rock can be ignored.

The kyanite-bearing rocks of Ardara form a zone the inner limit of which coincides in general with a line connecting the points of the abrupt magnesium decrease shown by Pitcher and Sinha (1958). The high magnesium of this zone has been shown by the authors (ibid) to be due to original differences in sedimentary character rather than a magnesium migration in the aureole.

In the aureole of the Main Donegal granite, three fields are recognised on the AFM diagram (Fig. 30b). In decreasing M/F ratio, these fields are: kyanite-biotite, kyanite-staurolite-biotite and staurolite-garnet-biotite. Three characteristic features are seen in this diagram:-

(a) The two fields with kyanite-bearing rocks are nearer to the M corner than the field containing the kyanite-free rocks.

(b) The chemical distinction between the kyanite-biotite and the kyanite-staurolite-biotite fields is remarkable if the samples from Glenkeo area (53-56) and from Owennagreeve River area (62 and 63) are considered. In each of these two areas, kyanite $\pm$ staurolite samples were collected from adjacent bands and hence the same grade of metamorphism. Staurolite-free kyanite schists (53, 54 and 62) plot nearer to the M corner than the staurolite-bearing kyanite schists (55, 56 and 63). Therefore, the absence of staurolite in some of the analysed rocks of the Main Donegal granite aureole is due to a chemical factor rather than a grade effect.

(c) Whereas in Ardara aureole there was a common point between the kyanite-staurolite-biotite and the staurolite-biotite garnet fields representing a single biotite composition for the invariant 3-phase assemblages, a similar point could not be drawn on the AFM diagram of the aureole of the Main Donegal granite.

Instead, there is a range of M/F values for biotite bounded by the biotite-kyanite tie line near the M corner and the staurolite-biotite tie line nearer to the F corner. In fact, the chemical analysis of 5 biotites belonging to this group of rocks shows a variation range of 0.532-0.616 in the M/FM ratio. The reason for the absence of a unique biotite composition could, therefore, be due to the movement of the 3-phase triangle with grade of metamorphism (cf. Chinner, 1965). However, a systematic change in the M/FM ratio in the biotite with grade, i.e. distance from the granite contact could not be detected in the present work; hence the idea of moving the 3-phase triangle with change in temperature and pressure is not evident from the data available. Another alternative explanation is that the rocks may have more variance than is suggested by the phase rule. Additional variances can be effected if the partial pressure of oxygen is considered as an intensive parameter (c.f. Eugester, 1959, Chinner, 1960, Mueller, 1961, Eugester and Wones, 1962, Ganguly, 1968), or if the fluid phase deviated markedly from the system H-O (Wyllie, 1962) or if there is any additional components to the system. It has also been demonstrated earlier than there is a clear correlation between the M/FM ratios of the biotite and their host rocks rather than a change in biotite composition with grade (however, c.f. Barth, 1936, Miyashire, 1953, Engel and Engel, 1958, 1960, Green, 1963, Chinner, 1965). This is suggestive of the presence of an additional variance in which case the composition of biotite will be sensitive to the host rock (Atherton, 1965, Butler, 1965).

A problem of similar nature has been encountered by Chinner, (1965) who found that in Glen Clova, the M/FM of the biotites remains

constant over an interval of 600 meters of the kyanite-staurolite assemblages where Chinner considers that it should decrease as the metamorphic grade increases. Chinner (ibid) explains this discrepancy to be due to undetectable change in biotite or the 600 meters represent disequilibrium or there is greater variance than is suggested. However, in his footnote (p. 140), Chinner states that "M/FM ratios of pelites with sufficient Al/K to develop staurolite and kyanite are surprisingly constant." This constant M/FM values of the rocks may the prime reason for the development of biotites with constant M/FM, thus accounting for the discrepancy mentioned by Chinner.

Finally, as the development of kyanite in the aureoles studied shows a definite relation to the M/FM ratio of the rock rather than to the grade of metamorphism i. e. closeness to the granite, is evident from the following observations:-

(a) The spatial arrangement of the kyanite-bearing rocks and the kyanite- free rocks in Ardara is the reverse of that of the Main Donegal granite. In Ardara, the kyanite-bearing schists occur in the outer-most part of the inner aureole whereas the kyanite-free rocks occur in the middle and innermost parts of the inner aureole. In the Main Donegal granite, andalusite alone occurs in the outer parts of the aureole (Fintown area) whereas kyanite-bearing rocks occur in the inner parts of the aureole.

(b) In the two equigrade parallel traverses taken in the Glenaboghil schists (p. 181), specimens of one traverse (No. 73-77) showed high M/FM ratios and are kyanite-bearing fibrolite schists whereas specimens of the other traverse

(No. 78-80) have a lower M/FM ratios and are kyanite-free fibrolite schists.

(2) Kyanite-free aureoles:-

These are exemplified by Fanad, Barnesmore and Thorr aureole and enclaves. The aureole rocks are all devoid of kyanite and staurolite and have low M/FM values. This low M/FM ratio accounts for the absence of kyanite but the unexpected absence of staurolite will be explained later. If the A corner of the AFM diagram is taken as muscovite, then the muscovite-garnet-biotite field in which the aureole rocks after the first reaction would lie is shown in Figs. 26a, 28a , 29a for each aureole.

(3) Comments on the earlier or first reactions:-

Having discussed the AFM diagrams of all the aureoles, the following comments are relevant to all the rocks studied. The comments will be concerned with, first, the status of staurolite and secondly, the presence or absence of garnet.

(i) The status of staurolite:-

Harker's (1952) ideas about the rarity of the association andalusite-staurolite and the stress-antistress concept of staurolite-cordierite in metamorphic rocks, are becoming less significant in view of the more recent work whether on the basis of geological occurrences or thermodynamic analysis. The validity of these ideas has been discussed in several works and need not be repeated here (c.f. Turner and Verhoogen, Thompson, 1955, Brindley, 1957, Compton, 1960, Pitcher and Read, 1960, 1963). The main conclusions of these works are that staurolite can develop in aureole rocks, the association staurolite-andalusite is not uncommon, and the main

differences between regional and thermal environments are rate of release of dehydration water from a recrystallising rock body as well as the rate of heating.

Ganguly and Newton (1966) synthesised staurolite and concluded that high pressure, probably at least 15 K bar is necessary for the successful synthesis of staurolite. However, Ganguly (1968) considers that the partial pressure of oxygen is an intensive parameter "having very important effects on the phase relations in pelitic assemblages containing iron-bearing phases" (p. 277). The effect is so important that the author (ibid) consider that the isograds defined by the minerals almandine, staurolite and kyanite "lose significance, in the sense that isograds are commonly understood, in the relatively oxidised paragenesis" (p. 294). Moreover, the restricted geological distribution of staurolite can be, according to Ganguly (ibid), due to (i) staurolite is restricted to a limited range of fo_2 and has a narrow range of thermal stability, (ii) the mineral disappears with high pressure (however, this is contrary to the synthesis experiments of Ganguly and Newton, 1966), (iii) additional components admit the possibility of further restriction on the distribution of staurolite due to the bulk composition of the host rock, (iv) the presence of mica quite significantly restrict the Po_2-T limits of staurolite stability. As to the occurrence of kyanite and staurolite, the author (ibid) points out that aluminium silicates (exemplified by kyanite) "are found to be restricted chiefly to the highly oxidised rocks whereas the staurolites are mainly confined to the relatively less oxidised ones" (p. 294).

As to the relation between the host rock and staurolite, some authors advocate that certain chemical abnormalities restrict the formation of staurolite, e. g. the Fe_2O_3 : Al_2O_3 ratio, unusual amount

of Mn compared with Fe^{2+} and Mg or very high MgO content (c. f. Turner and Verhoogen, 1951, Williamson, 1953, Ellitsgaard-Ramussen, 1954, Deer, Howie and Zussman, 1962, Green, 1963). However, Juurinen (1956) showed that although staurolite is high in Al_2O_3, yet the chemical limits of the host rock are not so restrictive as indicated from the analysis of 34 staurolite-bearing rocks having SiO_2 range of 28.12 - 90.44% and Al_2O_3 range of 4.11 - 42.51%.

In the 80 rocks analysed from the 5 aureoles studied, staurolite was recorded in 29 rocks and is not present or seen in the remaining 51 rocks. There is no relation whatsoever between the mineral's presence or absence. and the oxidation ratio of the rock (c. f. Ganguly, 1968). It is recorded in rocks of both low and relatively high oxidation ratios (16. 2 - 40. 6) and is equally absent in rocks having oxidation ratios 8. 7 - 45. 5. However, its absence from some of the rocks studied is thought to be due to any of the following reasons:-

(a) Constrains imposed by the high Mg/Fe ratio of the host rock, (e. g.) the expected absence of staurolite in the 9 rocks from the Main Donegal granite aureole lying to the left hand side of the kyanite-biotite tie line in the AFM diagram (Fig.30b, specimens 53, 54, 57, 58, 59, 60, 61, 62, 72).

(b) High grade effect as seen in 12 rocks from different aureoles, (specimens No. 23, 30, 31, from Ardara, 40-42 from Barnesmore, 46-50 from the enclaves in the Thorr granodiorite).

(c) Simply be cause the rock is completely shimmered as in one specimen (No. 35 from Ardara).

(d) Most important is to explain the absence of staurolite in rocks where it could be expected to form, i. e. where none of the above mentioned 3 restrictions apply (e. g. all the rocks from Fanad except those of the highest grade, specimens No. 43, 44 from Thorr aureole, 52, 70, 74, 77 from the Main Donegal granite aureole). The common feature seen in these staurolite-free rocks is the presence of definite large biotite ($\pm$ chlorite) knots, few millimetres across, formed after regional garnet. Similar knots have never been noticed in the 29 staurolite-bearing rocks from Ardara and the Main Donegal. In the Fanad aureole, these knots are common (constitute up to 15% of the rock - visual estimate) and sometimes the regional garnet is still preserved in them (c. f. Atherton and Edmunds, 1966).

It seems reasonable to conclude that although the whole rock composition may be suitable for the production of staurolite, yet, most of the iron content at the early stages of thermal metamorphism was held in the biotite $\pm$ chlorite $\pm$ garnet knots, thus leaving a groundmass of certain composition not suitable for the formation of staurolite. Similarly, the knots would be enriched in Mn and Ca, thus furthering chemical constrains for the development of staurolite (c. f. Ganguly, 1968). It must be pointed out that this conjecture is based on the unfailing observation of the relation between the presence or absence of either the knots or the staurolite rather than separate chemical analysis of both the knots and the groundmass.

If this was so, the following question arises:- If iron was held in the knots, why then kyanite did not develop in the Mg-rich (or iron-impoverished) groundmass? An attempt to answer this question

was done by subtracting the amount of elements forming the regional garnet from the whole rock analysis. The composition of a regional garnet from Fanad was given by M. W. Edmunds (personal communication) and the amount of garnet was taken as an average of 10% (visual estimate of the amount of the now biotite knots). The result of this calculation would give a rough idea of the groundmass composition. Values of A, K, F and M in the tetrahedral phase diagram was then calculated and the results were represented on a tetrahedral model. The plot of these rocks is shown diagrammatically in Fig. 47. It is clear from this figure that the subtraction of the garnet composition moves the rocks not only away from the F corner but also to sites below the biotite-muscovite plane, a situation in which aluminium silicates or staurolite for that matter, would not be expected to develop.

(ii) The presence or absence of garnet:-

It has been noticed that in some rocks, although the FeO/MgO ratio is appropriate for the development of garnet, yet this mineral does not form. The absence of garnet in rocks where it should be present has been accounted for by Green (1963) to be due to the possibility that "the garnet of this F/Mg ratio actually requires for its formation some minimum amount of Ca and/or Mn that is not available in these particular rocks" (p. 1005). On the other hand, Albee (1965) considers that the Mn-rich garnet in his kyanite rocks to be an additional phase introduced by a high Mn content of the rock. Indeed both explanations may account for the presence or absence of garnets in some rocks of the Donegal aureole studied judging from the available five garnet analyses carried out by M. W. Edmunds (personal communication) where the range of MnO is 0.75-9.30 and that of CaO is 0.17-8.63%.

Fig. 47

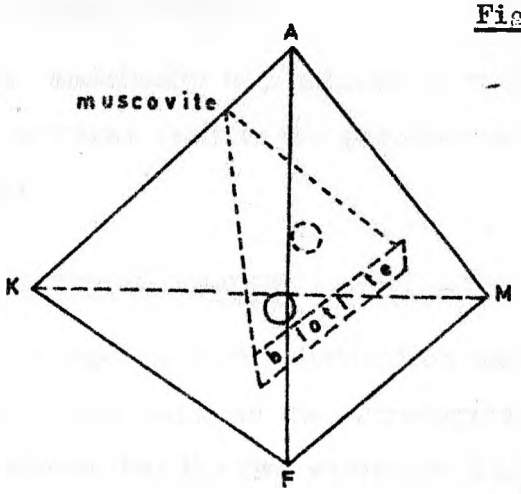

○ rocks lying above the muscovite-biotite plane.

○ rocks lying below the muscovite-biotite plane.

Fig. 48

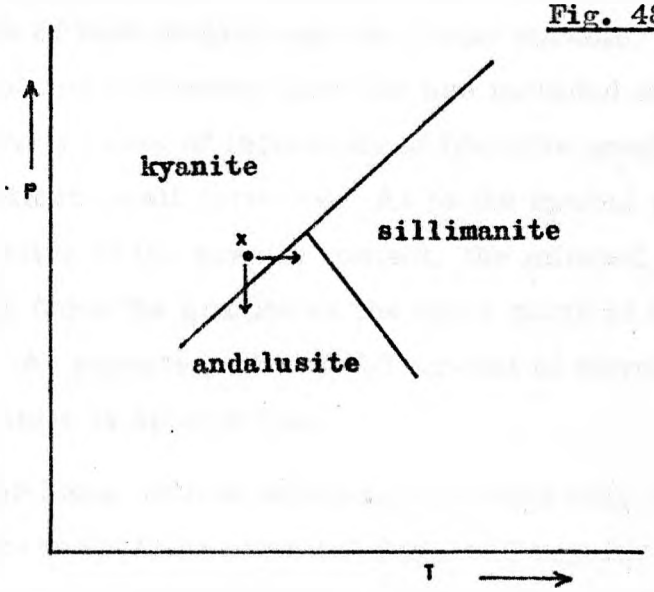

Movement of kyanite-rocks to the stability field of andalusite.

B. The Later or Second Reaction

In this reaction, andalusite is produced in rocks regardless of their M/FM ratios. In rocks near to the granite contact, coarse sillimanite also develops.

C. Fibrolite vs. Coarse Sillimanite

Throughout the foregoing work, distinction was made between fibrolite and coarse sillimanite because the petrological studies of the aureole rocks have shown that the two varieties differ in their genetic significance. Fibrolite has been shown in all the aureoles to replace the mica especially the biotite and occurs as irregular masses or felts meandering throughout the rock. In the Main Donegal granite aureole, the early euhedral aureole garnet occurs within the fibrolite felts, in part apparently replacing fibrolite and in part including it. Fibrolite is also partly included in staurolite and kyanite in the Ardara and in the andalusite of both Ardara and the Fanad aureole. In the Thorr enclaves, isolated patches of fibrolite are included in coarse sillimanite. Numerous cases of inclusions of fibrolite needles in quartz have been noticed in all aureoles. As to the spatial relationship of fibrolite relative to the granite contact, the mineral was found in rocks as far away from the granite as the outer parts of the inner aureole of Ardara. As expected, the modal amount of fibrolite always increases as the granite is approached.

On the other hand, coarse sillimanite occurs only very near to the granite contact in the form of well defined and regular stout prisms. It grows as coarsened fibrolite or independently in the groundmass or sharing the c-axis of pre-existing andalusite crystals.

It is evident that from these textural and spatial differences,

fibrolite development needs less heat than coarse sillimanite. Given this heat, fibrolite is formed earlier than, contemporaneous with and later than the crystallisation or recrystallisation of minerals such as quartz, garnet, staurolite, kyanite and andalusite d ependingon whether these minerals include the fibrolite or else are fringed with it. Although the problem of "piercing minerals" is recognised here to cast some doubt on these assumptions especially when fibrolite is included in another mineral, yet the author finds it difficult to account for the presence of isolated inclusions of fibrolite in andalusite, garnet and sillimanite. It is equally difficult to envisage the remote possibility of alumina metasomatism producing fibrolite needles completly enclosed in some quartz crystals.

The idea of fibrolite development at early stages of metamorphism points to the possibility of a sudden rise in temperature or a surge of heat connected with the earlier phases of granite intrusion. Indeed, this contention is very likely and is to some extent supported by the following two observations:-

(i) In the outer kyanite-bearing schists of Ardara, staurolite and kyanite occur in many slides as very minute individual crystal or clusters of crystals dissiminated all over the rock (pl. 4a, b).

(ii) In the Main Donegal granite aureole, garnets also occur as minute individual crys tals or groups of crystals peppering the rock (pl. 8a, b).

The replacement of biotite by fibrolite has been noticed earlier by Watson (1948), Tozer (1955) and Pitcher and Read (1963). On the other hand, because of the difficulty in determining the fate of displaced elements involved in this replacement (K, Fe, Mg),

Chinner (1961) considers that the role of biotite in the development of fibrolite in Glen Clova appears to have been that of nucleating agent. Fibrolite grew epitaxially on mica and the material for its growth was derived from the unstable kyanite.

Although Chinner's (ibid) epitaxial theory is possible and applies to Glen Clova, it is by no means universal (Rast, 1965). This theory does not account for the undeniable textural evidences of replacement, for the frequent occurrence of knots or spherulitic rosettes of fibrolite, nor for the fact that sometimes fibrolite develops in rocks in which there is no other aluminium silicates present. The possibility of the presence of fluid media to assist in fibrolite development has been discussed by Pitcher and Read (1963). Furthermore, the idea of a late stage, partly independent growth of the mineral has been favoured in recent literature (Watson, 1948, Sanders, 1954, Tozer, 1955, Autran and Guitard, 1957, Brindley, 1957, Zwart, 1958, Schermerhorn, 1959).

As to the fate of displaced elements, it is possible that, according to Francis (1956), the iron molecule of the biotite breaks down first, leaving a biotite enriched in magnesium and precipitating iron as magnetite. As to the fate of potassium, it "is not here retained in potash feldspar but more probably in white mica" (Pitcher and Read, 1963, p. 273).

VII. CONCLUSIONS

From the foregoing discussion and comments, one can proceed to synthesise a general picture of the history of the aluminium silicates in the aureoles of Co. Donegal granites.

The initial thermal effect on the regional muscovite-chlorite $\pm$ biotite $\pm$ regional garnet is the production of biotite on the expense of chlorite and muscovite. Whereas biotite was produced in every rock, other minerals e. g. kyanite, staurolite and garnet were restricted to certain rocks of particular composition. Thus the regional rocks evolved to their present mineralogy through two series of reactions, namely:-

(1) A relatively earlier reaction producing any of the following assemblages depending on the M/FM ratio of the rock:

High M/FM	:	Kyanite-biotite-muscovite $\pm$ garnet (high MnO garnet)
Intermediate M/FM	:	Kyanite-biotite-muscovite-staurolite $\pm$ garnet
Low M/FM	:	Biotite-muscovite $\pm$ staurolite $\pm$ garnet

(2) A relatively later reaction irrespective of the M/FM of the rock and producing andalusite and/or sillimanite depending on the nearness of the rock to the granite contact.

However, it must be emphasized that although an "earlier" kyanite-producing and a "later" andalusite-producing reaction are described, there is no evidence of the presence of a time gap between them nor that the "later" reaction has started only after the cessation of the "earlier" one. In fact, textural evidence (i. e. the smaller and more euhedral character of the kyanite and staurolite

included in andalusite compared to their larger and less euhedral counterparts in the groundmass) suggests that the earlier reaction seems to have continued after the later one has started.

In the earlier or first reaction, the production of the different mineral assemblages can be visualised by the following reactions:-

Chlorite + muscovite = biotite + kyanite + quartz + water
(e. g. Main Donegal aureole)

Chlorite + muscovite + quartz = biotite + staurolite + kyanite + water
(e. g. Main Donegal and Ardara aureoles)

In rocks with low M/F ratio:-

Fe-rich chlorite + muscovite = biotite + staurolite + almandine + water
(e. g. Main Donegal and Ardara aureoles)

Chlorite + muscovite + magnetite + silica = biotite + almandine + water
(e. g. Fanad, Barnesmore, Thorr and Main Donegal aureoles)

Muscovite and quartz are additional phases to the resultants.

In the later or second reaction, andalusite is produced in rocks which now contain biotite $\pm$ kyanite, i. e. rocks which represent mineral assemblages of higher grade than the original regional ones. It develops as large porphyroblasts overprinting the groundmass and including the early formed garnet, staurolite and kyanite. In rocks near to the granite contact, coarse sillimanite is produced with or instead of andalusite. The reactions involved in the production of andalusite can be deduced from the following considerations:-

In Fanad aureole where the effect of thermal metamorphism can be systematically followed, it was noticed that the modal amount

of muscovite decreases as the granite contact is approached and that potash feldspar is absent in the majority of rocks. From these observations coupled with the concurrence of both the earlier and the later reactions, it seems that the reaction involved in the production of andalusite in rocks devoid of K-feldspar was mainly of the following type:

Chlorite + muscovite = andalusite + biotite + quartz + water

However, in the Barnesmore aureole where the regional rocks are mica-schists and the aureole andalusite hornfelses contain potash feldspar, and in Fanad aureole where potash feldspar is present in some sillimanite hornfelses near to the granite contact, the production of andalusite, and for this matter the sillimanite in the Thorr enclaves, could have been accomplished through the breakdown of either muscovite or biotite.

Muscovite + quartz = K-feldspar + andalusite (or sillimanite) + water

For the production of andalusite from biotite, if a similar reaction is invoked, one is faced with the problem of disposing of the iron and magnesium of the reacting biotite. However, it has been shown earlier that the biotite has a similar M/FM ratio to that of the rock and it is evident therefore, that the biotite remaining in the rock adjusts its composition accordingly. The reaction involved can, therefore, be written as follows:-

$$\text{Biotite}_{(1)} + \text{quartz} = \text{K-feldspar} + \text{andalusite} + \text{biotite}_{(2)} + \text{water}$$

Another way of disposing of thedisplaced iron, magnesium and potassium of the breaking biotite has been mentioned by Tozer (1955) who suggests that all the elements have been expelled with the

exception of iron which is precipitated as magnetite. Francis (1956), however, points out that the iron molecule of the biotite breaks down first leaving a biotite enriched in magnesium and precipitating iron as magnetite. In rocks which do not contain K-feldspar, Pitcher and Read (1963) indicate that the potassium resulting from the breakdown of biotite is probably retained in white mica. Grouping all these views together, a reaction of the following type can be deduced:

$$\text{Biotite}_{(1)} + \text{muscovite}_{(1)} = \text{Biotite}_{(2)} + \text{muscovite}_{(2)} + \text{magnetite} + Al_2SiO_5 \text{ (andalusite or sillimanite)} + \text{water}$$

Biotite (2) has a higher M/FM ratio than biotite (1) and muscovite(2) has a higher potassium than muscovite (1). However, it has been maintained in the present work that the M/FM ratio of the biotite is similar to that of its host rock. Therefore, the following variation of this last reaction can be postulated:

$$\text{Biotite}_{(1)} + \text{muscovite}_{(1)} = \text{Biotite}_{(2)} + \text{muscovite}_{(2)} + Al_2SiO_5 \text{ (andalusite or sillimanite)} + \text{water}$$

Each of biotite(1) and (2) has an M/FM ratio depending on the rock composition and the existence of other ferromagnesian phases at the time of the biotite formation; muscovite (2) is higher in potassium than muscovite (1).

The factors governing the production of andalusite can be deduced from a study of its distribution in Ardara and the Main Donegal granite aureoles. Andalusite is invariably present in all the kyanite-bearing and the kyanite-free rocks of Ardara but is not always present in the rocks of the Main Donegal aureole. In the latter

aureole, its presence is restricted to the kyanite-free rocks of Fintown area and the kyanite-bearing rocks of Lough Reelan area, both occurring in the outer parts of the aureole. Andalusite is absent in the kyanite schists of the inner parts of the Main Donegal aureole as well as the kyanite-free fibrolite schists of Glenaboghil (refer to b, p. 253). Contrary to kyanite, andalusite occurs in rocks regardless of their M/F ratios and there is no obvious chemical control governing its occurrence. Therefore, it seems likely that the development of andalusite was physically controlled i. e. changes in pressure and/or temperature according to the inverted-Y phase diagram of aluminium silicate. The manner in which the mineral is distributed gives a clue to the physical changes in the aureoles. Thus, on the phase diagram, the rocks during the earlier reaction would lie in the kyanite stability field at point x for example (Fig. 48). The production of andalusite in the later reaction would be achieved either by an increase in temperature or by decrease in pressure in the direction of arrows indicated on the diagram. In the Main Donegal aureole, the production of andalusite due to an increase in temperature is eliminated judging from the distribution of andalusite in the aureole i. e. its absence from the inner parts and its restriction to the outer parts of the aureole. The other alternative i. e. a decrease in pressure seems likely to be the factor involved in the production of andalusite in the Main Donegal aureole. This decrease or rather relaxation in pressure was apparently felt only in the outer parts of the aureole, hence the development of andalusite and the continuous growth of kyanite in the inner parts. On the other hand in the rocks of the Ardara aureole, all of which contains andalusite $\pm$ kyanite, either a rise in temperature or a drop in pressure or both may have effected the production of andalusite.

In conclusion, it is evident that in the 5 aureoles studied, the production of kyanite was controlled by the chemical composition of the rock, andalusite by changes in physical conditions (either an increase in temperature or a decrease in pressure or both) and coarse sillimanite by high temperature.

REFERENCES

AKAAD, M.K.
(1954). Ph.D. thesis, London University.

AKAAD, M.K.
(1956a). The Ardara Granitic Diapir of Co. Donegal, Ireland. Geol. Soc. London Quart. Jour., v. 112, p. 263-288.

AKAAD, M.K.
(1956b). The northern aureole of the Ardara Pluton of Co. Donegal. Geol. Mag., v. 93, p. 377-392.

ALBEE, A.L.
(1965). Phase equilibria in three assemblages of kyanite zone pelitic schists, Lincoln Mountain Quadrange, Central Vermont. J. Petrol., v. 6, p. 246-301.

ANDREW, G.
(1928). The contact relations of the Donegal Granite. Mem. Proc. Manchester Lit. Phil. Soc., v. 72, p. 210-219.

ARAMAKI, S. and ROY, R.
(1958). Further equilibrium studies in the system Al_2O_3-SiO_2-H_2O under hydrostatic and uniaxial pressure. Bull. Geol. Soc. Amer., v. 69, p. 1530.

ARAMAKI, S. and ROY, R.
(1959). Revised equilibrium diagram for the system Al_2O_3-SiO_2. Nature, v. 184, p. 631-632.

ARAMAKI, S. and ROY, R.
(1963). A new polymorph of Al_2SiO_5 and further studies in the system Al_2O_3-SiO_2-H_2O. Amer. Mineral., v. 48, p. 1322-1347.

ATHERTON, M. P.
(1965). The chemical significance of isograds. In W. S. Pitcher and D. Flinn (editors) Controls of Metamorphism. Oliver and Boyd, Edinburgh, p. 169-202.

ATHERTON, M. P. and EDMUNDS, W. M.
(1966). An electron microprobe study of some zoned garnets from metamorphic rocks. Earth and Planetary Science Letters, v. 1, p. 185-193.

AUTRAN, A. and GUITARD, G.
(1957). Sur la signification de la sillimanite dans les Pyrenees. Soc. Geol. de France Compte Rendu Sommaire des Seances, p. 141-143.

BAIRD, A. K., McCOLL, R. S. and McINTYRE, D. B.
(1961). A test of the precision and sources of error in quantitative analysis of light major elements in granitic rocks by X-ray spectrography. Advances in X-Ray Analysis, v. 5, p. 412-422.

BAIRD, A. K., McINTYRE, D. B. and WELDAY, E. E.
(1962). Sodium and magnesium fluorescence analysis-II. Application to silicates. Advances in X-Ray Analysis, v. 6, p. 377-388.

BALCONI, N.
(1941). Sentesi della sillimanite. Rend. Soc. Min. Ital., 1, p. 30.

BANNERJEE, N. N. and COLLIS, B. A.
(1955). Rapid analysis of ash from coal and oil shale by colorimetric methods. Fuel, v. 34, p. S71-S83.

BARTH, T. F. W.
(1936). Structural and petrologic studies in Dutchess County, New York. Part II. Petrology and metamorphism of Palaeozoic rocks. Bull. Geol. Soc. Am., v. 47, p. 775-850.

BELL, P. M.
(1963). Aluminium silicate system : experimental determination of the triple point. Science, v. 139, p. 1055-1056.

BERGER, A. R.
(1967). The Main Donegal Granite and its regional setting : A study of its fabric and structural relationships. Ph. D. thesis (2 vols) University of Liverpool.

BIRKS, L. S. and BROWN, D. M.
(1962). Precision in X-ray spectrochemical analysis - Fixed time versus fixed count. Anal. Chem., v. 34, p. 240.

BRINDLEY, J. C.
(1957). The aureole rocks of the Leinster granite in south Dublin, Ireland. Proc. Roy. Ir. Acad., v. 59, Section B, p. 1-18.

BUTLER, B. C. M.
(1965). Compositions of micas in metamorphic rocks. In W. S. Pitcher and D. Flinn (Editors) Controls of metamorphism, Oliver and Boyd, Edinburgh, p. 291-298.

CARD, K. D.
(1964). Metamorphism in the Agnew Lake Area, Sudbury District, Ontario, Canada. Bull. Geol. Soc. Am., v. 75, p. 1011-1030.

CARR, R. M. and FYFE, W. S.
(1960). Synthesis fields of some aluminium silicates. Geochim. et Cosmochim. Acta, v. 21, p. 99-109.

CHAYES, F.
(1956). Petrographic modal analysis. Wiley, New York.

CHINNER, G. A.
(1960). Pelitic gneisses with varying ferrous/ferric ratios from Glen Clova, Angus, Scotland. J. Petrol., v. 1, p. 178-217.

CHINNER, G. A.
(1961). The origin of sillimanite in Glen Clova, Angus. J. Petrol., v. 2, p. 312-323.
(1965). The kyanite isograd in Glen Clova, Angus, Scotland. Min. Mag., v. 34, p. 132-143.

CHINNER, G. A.
(1966). The significance of aluminium silicates in metamorphism. Earth Sci. Rev., v. 2, p. 111-126.

CHODOS, A. A. and ENGEL, C.
(1961). Fluorescent X-ray spectrographic analysis of amphibolite rocks. Am. Mineral, v. 46, p. 120-133.

CLAISSE, F.
(1956). Accurate X-ray fluorescence analysis without internal standard. Norelco Reporter, P. R. 327, Quebec Department of Mines, p. 1-16.

CLAISSE, F. and SAMSON, C.
(1961). Heterogeneity effects in X-ray analysis. Advances in X-ray Analysis, v. 5, p. 335-354.

CLARK, S. P.
(1961). A redetermination of equilibrium relations between kyanite and sillimanite. Amer. J. Sci., v. 259, p. 641-650.

CLARK, S. P., ROBERTSON, E. C. and BIRCH, F.
(1957). Experimental determination of kyanite-sillimanite equilibrium relations at high temperatures and pressures. Amer. J. Sci., v. 255, p. 628-640.

COES, L. Jr.
(1955). High pressure minerals. J. Amer. Ceram. Soc., v. 38, p. 298.

COMPTON, A. R.
(1960). Contact metamorphism in the Santa Rosa Range, Nevada. Bull. Geol. Soc. Amer, v. 71, p. 1383-1416.

COREY, R. B. and JACKSON, M. L.
(1953). Silicate analysis by a rapid semi-microchemical system. Anal. Chemistry, v. 25, p. 624.

DEER, W. A., HOWIE, R. A. and ZUSSMAN, J.
(1962). Rock-forming minerals. Longmans.

ELLITSGAARD-RASMUSSEN, K.
(1954). On the geology of a metamorphic complex in west Greenland. Medd. om Gronland, v. 136, No. 6.

ENGEL, A. E. J. and ENGEL, C. G.
(1958). Progressive metamorphism and granitization of the major paragneiss, Northwest Adironac Mountains, New York, Part 1: Total rock. Bull. Geol. Soc. Amer., v. 69, p. 1369-1414.

ENGEL, A. E. J. and ENGEL, C. G.
(1960). Progressive metamorphism and granitization of the major paragneiss, Northwest Adironac Mountains, New York. Part II: Mineralogy. Bull. Geol. Soc. Amer. v. 71, p. 1-58.

EUGSTER, H. P.
(1959). Reduction and oxidation in metamorphism. In Abelson P. H. (Editor) Researches in Geochemistry, John Wiley and Sons, New York, p. 397-426.

EUGSTER, H. P. and WONES, D. R.
(1962). Stability relations of ferrugenous biotite, annite. J. Petrol., v. 3, p. 82-125.

EVANS, B. W.
(1965). Application of reaction rate method to the breakdown equilibria of Muscovite and muscovite plus quartz. Amer. J. Sci., v. 263, p. 647-667.

FAIRBAIRN, H. W.
(1953). Precision and accuracy of chemical analysis of silicate rocks. Geochim. et Cosmochim. Acta, v. 4, p. 143-156.

FAIRBAIRN, H. W. and OTHERS
(1951). A cooperative investigation of precision and accuracy in chemical, spectrochemical and modal analysis of silicate rocks. U. S. Geol. Survey Bull. 980, 71p.

FAIRBAIRN, H. W. and SCHAIRER, J. F.
(1952). A test of accuracy of chemical analysis of silicate rocks. Am. Mineral., v. 37, p. 744-754.

FRANCIS, G. H.
(1956). Facies boundaries in pelites at the middle grades of regional metamorphism. Geol. Mag., v. 93, p. 353-368.

FYFE, W. S.
(1967). Stability of Al_2SiO_5 polymorphs. Chem. Geol., v. 2, p. 67-76.

FYFE, W. S., TURNER, F. J. and VERHOOGEN, J.
(1958). Metamorphic reactions and metamorphic facies. Geol. Soc. Amer. Mem. 73, 259p.

GANGULY, J.
(1968). Analysis of the stabilities of chloritoid and staurolite and some equilibria in the system $FeO-Al_2O_3-SiO_2-H_2O-O_2$. Amer. J. Sci., v. 266, p. 277-298.

GANGULY, J. and NEWTON, R. C.
(1966). Synthesis and stability of staurolite. Geol. Soc. Amer., Special Paper 87, p. 63.

GAYLOR, D. W.
(1962). Precision of fixed-time vs. fixed-count measurements. Anal. Chemistry, v. 34, p. 1670.

GREEN, J. C.
(1963). High level metamorphism of pelitic rocks in northern Hampshire. Am. Mineral., v. 48, p. 991-1023.

HARKER, A.
(1952). Metamorphism. Methuen and Co. London, 362p.

HEINRICH, K. F. J.
(1959). Count dis tribution and precision in X-ray fluorescence analysis. Advances in X-Ray Analysis, v. 3, p. 95-109.

HEINRICH, K. F. J.
(1960). Pulse height selection in X-ray fluorescence. Advances in X-ray Analysis, v. 4, p. 370-381.

HENKE, B. L.
(1961). Microanalysis with ultrasoft X-radiations. Advances in X-Ray analysis, v. 5, p. 285-305.

HENKE, B. L.
(1962). Sodium and magnesium fluorescence analysis - Part I: Method. Advances in X-Ray Analysis, v. 6, p. 361-376.

HENRIQUES, A.
(1957). The alkali content of kyanite. Arkiv. Min. Geol., v. 2, p. 271.

HIETANEN, A.
(1956). Kyanite, andalusite and sillimanite in the schist in Boehl Butte quadrangle, Idaho. Am. Mineral., v. 41, p. 1-27.

HOLM, J. L. and KLEPPA, O. J.
(1966). The thermodynamic properties of the aluminium silicates. Am. Mineral., v. 51, p. 1608-1622.

HOOPER, P. R.
(1964). Rapid analysis of rocks by X-ray fluorescence. Anal. Chem., v. 36, p. 1271-1276.

HORNUNG, G.
(-). Major and trace element analysis using the Siemens Halske Krystalloflex-4. Dept. of Geology, Univ. of Leeds, 12p., 5 figs.

HORNUNG, G.
(1963). The analysis of Basalts and granites by X-ray spectrography. 7th. Annual Report on Scientific Results, Univ. of Leeds, Session 1961-62, p. 59-63.

HULL, E. and OTHERS.
(1891). Northwest and Central Donegal. Geol. Survey of Ireland Mem., 274p.

JAKOB, J.
(1937). Uber den Alkaligenhalt der Disthene. Schweizer. Min. Petr. Mitt., v. 17, p. 214-219.

JAKOB, J.
(1940). Uber der Chemiscus des Andalusits, Schweizer. Min. Petr. Mitt., v. 20, p. 810.

JAKOB, J.
(1941). Chemische und strukturelle Untersuchungen am Disthene. Schweizer Min. Petr. Mitt., v. 21, p. 131-135.

JONES, K. A. and GALWEY, A. K.
(1964). A study of possible factors concerning garnet formation in rocks from Ardara, Co. Donegal, Ireland. Geol. Mag., v. 101, p. 76-93.

JUURINEN, A.
(1956). Composition and properties of staurolite. Acad. Sci. Fennicae Annales, ser. AIII, Geol.-Geog., v. 47, 53p.

KARPOV, I. K.
(1967). A thermodynamically calculated P-T diagram for the polymorphs of Al_2SiO_5 and mullite. Dok. Acad. Sci. U. S. S. R., Earth Science Section, v. 174, p. 143-145.

KHITAROV, N. I. and OTHERS.
(1963). Relations between andalusite, kyanite and sillimanite in the field of moderate temperatures and pressures. (In Russian) Geokhimiya, v. 3, p. 219-228.

KNILL, D. C. and KNILL, J. L.
(1961). Time relations between folding, metamorphism and emplacement of granite in Rosguill, Co. Donegal. Geol. Soc. London Quart. Jour., v. 117, p. 273-302.

KUMAGAI, N. and ITO, H.
(1959). The P-T diagrams of the trimorphic minerals of Al_2SiO_5 with a special reference to andalusite and cyanite as a geological thermometer or a geological piezometer. Mem. Coll. Sci. Kyoto, Ser. B, v. 26, p. 215-223.

LIEBHAFSKY, H. A. and OTHERS.
(1960). X-Ray absorption and emission in analytical chemistry. John Wiley and Sons Inc., New York.

LOBJOIT, W. M.
(1964). Kyanite produced in a granite aureole. Min. Mag., v. 33, p. 804-808.

MACDONALD, G. L.
(1964). Counting statistics in X-ray spectrometry. 4th Conference on X-Ray Analytical Methods,Sheffield Symposium. Scientific Equipment Department, Philips, Netherlands, p. 1-10.

McCALL, G. J. H.
(1954). The Dalradian geology of Cresslough area, Co. Donegal. Geol. Soc. London Quart. Jour., v. 110, p. 153-175.

MERCY, E. L. P.
(1956). The accuracy and precision of "rapid methods" of silicate analysis. Geochim. et Cosmochim. Acta, v. 9, p. 161-173.

MERCY, E. L. P.
(1960). The geochemistry of the Older Granodiorite and of the Rosses Granite Ring Complex, Co. Donegal, Ireland, Roy. Soc. Edin. Trans., v. 64, p. 101-138.

MICHEL-LEVY, M. C.
(1950). Reproduction artificielle de la sillimanite Acad. Sci. Paris Comptes rendus, v. 230, p. 2213-2214.

MITHAL, R. S.
(1952). Geology of Portnoo District of Co. Donegal. Ph. D. thesis, London University.

MIYASHIRO, A.
(1949). The stability relations of kyanite, sillimanite and andalusite and the physical conditions of metamorphic processes. J. Geol. Soc. Japan, v. 55, p. 218.

MIYASHIRO, A.
(1953). Calcium poor garnet in relation to metamorphism. Geochim. et Cosmochim Acta, v. 4, p. 179-208.

MUELLER, R. F.
(1961). Oxidation in high temperature paragenesis. Amer. J. Sci., v. 259, p. 460-480.

NEWTON, R. C.
(1966a). Kyanite-sillimanite equilibrium at 750°C. Science, v 151, p. 1222-1225.

NEWTON, R. C.
(1966b). Kyanite-andalusite equilibrium from 700-800°C. Science, v. 153, p. 170-172.

ORREL, E. W. and GIDLEY, P. J.
(1964). The analysis of alumino-silicates by X-ray fluorescence. Trans. Brit. Ceram. Soc., v. 63, p. 19-30.

PANKRATZ, L. B. and KELLEY, K. K.
(1964). High temperature heat contents and entropies of andalusite, kyanite and sillimanite. U. S. Bureau of Mines, Rept. Invest., 6370.

PARISH, W. and KOHLER, T. R.
(1956). Use of counter tubes in X-ray analysis. Rev. Sci. Instruments, v. 27, p. 795-808.

PEARSON, G. R. and SHAW, D. M.
(1960). Trace elements in kyanite-andalusite-sillimanite. Amer. Mineral., v. 45, p. 808-817.

PHILIPSBORN, H. V.
(1928). Zur graphischen Behandlung quarternarer Systeme. N. Jahrb. f. Min. Beil.-Bd. 57, p. 973-1012.

PITCHER, W. S.
(1953). The migmatitic Older Granodiorite of Thorr District, Co. Donegal, Geol. Soc. London Quart. Jour., v. 108, p. 413-446.

PITCHER, W. S.
(1965). The aluminium silicate polymorphs. In W. S. Pitcher and D. Flinn (Editors) Controls of metamorphism, Oliver and Boyd, Edinburgh, p. 327-341.

PITCHER, W. S. and READ, H. H.
(1959). The Main Donegal Granite. Geol. Soc. London Quart. Jour., v. 114, p. 259-305.

PITCHER, W. S. and READ, H. H.
(1960). The aureole of the main Donegal Granite. Geol. Soc. London Quart. Jour., v. 116, p. 1-36.

PITCHER, W. S. and READ, H. H.
(1963). Contact metamorphism in relation to manner of emplacement of the granites of Donegal, Ireland. J. Geology, v. 71, p. 261-296.

PITCHER, W. S. and SINHA, R. C.
(1958). The petrochemistry of the Ardara aureole. Geol. Soc. London Quart. Jour., v. 113, p. 393-408.

RAST, N.
(1965). Nucleation and growth of metamorphic minerals. In W. S. Pitcher and D. Flinn (Editors) Controls of Metamorphism, Oliver and Boyd, Edinburgh, p. 73-96.

READ, H. H.
(1958). Donegal Granite. Sci. Progress, 46, p. 225-240.

READ, H. H.
(1961). Aspects of Caledonian magmatism in Britain. Liverpool and Manchester Geol. Jour., v. 2, p. 653-683.

RICHARDSON, S. W., BELL, P. M. and GILBERT, M. C.
(1965). Kyanite-sillimanite relations. Annual Report of the Director, Geophysical Laboratory Carnegie Inst. Year Book 1965, p. 247-248.

RICKARD, M. J.
(1957). Ph. D. thesis, London University.

RILEY, J. P.
(1958). The rapid analysis of silicate rocks and minerals. Analytica Chimica Acta, v. 19, p. 413-428.

ROSE, H. J., ADLER, I. and FLANAGAN, F. J.
(1962). Use of La_2O_3 as a heavy absorber in the X-ray fluorescence analysis of silicate rocks. Art 31 in U. S. Geol. Survey Prof. Paper 450-B, p. 80-82.

ROSE, H. J., CUTTITTA, F., CARRON, M. K. and BROWN, R.
(1964). Semimicro X-ray fluorescence analysis of tektites using 50-milligram samples. Art. U. S. Geol. Survey Prof. Paper 475-D, p. 171-173.

ROSE, H. J., CUTTITTA, F. and LARSON, R. R.
(1965). Use of X-ray fluorescence in determination of selected major constituents in silicates. Art in U. S. Geol. Survey Prof. Paper 525-B, p. 155-159.

ROY, D. M.
(1954). Hydrothermal synthesis of andalusite. Amer. Mineral., v. 39, p. 140-143.

ROY, D. M. and ROY, R.
(1955). Synthesis and stability of minerals in the system $MgO-Al_2O_3-SiO_2-H_2O$. Amer. Mineral., v. 40, p. 147-148.

ROY, R. and OSBORN, E. F.
(1954). The system $Al_2O_3-SiO_2-H_2O$. Amer. Mineral., v. 39, p. 853-885.

RUTLAND, R. W. R.
(1965). Tectonic overpressures. In W. S. Pitcher and D. Flinn (Editors) Controls of Metamorphism, Oliver and Boyd, Edinburgh, p. 119-139.

SANDERS, L. D.
(1954). The status of sillimanite as an index of metamorphism in the Kenya Basement System. Geol. Mag., v. 91, p. 144-151.

SCHERMERHORN, L. J. G.
(1959). Igneous, metamorphic and ore geology of the Castro Daire-Sao Pedro do Sul Santo Region (Northern Portugal). Ser. Geol. Portugal Com., v. 37, 617p.

SCHUILING, R. D.
(1957). A geo-experimental phase-diagram of Al_2SiO_5 (sillimanite, kyanite, andalusite). Proc. Kon. Akad. Wetensch. Series B60, p. 220-226.

SCHUILING, R. D.
(1962). Die Petrogenetische Bedeulung der drei Modificationen von Al_2Si0_5. N. Jb. Miner., v. 9, p. 200-214.

SERGIADES, D. A.
(1962). Geology of Palas de Rey (Provincia de Lugo, N. W. Spain). Ph. D. thesis, University of Liverpool.

SHAPIRO, L. and BRANNOCK, W. W.
(1952). Rapid analysis of silicate rocks. U. S. Geol. Survey Circ. 165, 17p.

SHAPIRO, L. and BRANNOCK, W. W.
(1956). Rapid analysis of silicate rocks. U. S. Geol. survey Bull. 1036-C. 56p.

SKINNER, B. J., CLARK, S. P., and APPLEMAN, D. E.
(1961). Molar volumes and thermal expansions of andalusite, kyanite and sillimanite. Amer. J. Sci., v. 259, p. 651-668.

SMART, T.
(1962). The aureole of the Barnesmore Granite, Co. Donegal. Irish Nat. Jour., v. 14, p. 55-59.

SOBOLEV, V. S.
(1960). Role of high pressure in metamorphism. Int. Geol. Congress, 21 st. Session, 14, Copenhagen, p. 72-82.

STEVENS, R. E. and OTHERS.
(1960). Second report on a cooperative investigation of the composition of two silicate rocks. U. S. Geol. Survey Bull. 1113, 126p.

THOMPSON, J. B.
(1955). The thermodynamic basis for the mineral facies concept. Amer. J. Sci., v. 253, p. 65-103.

THOMPSON, J. B.
(1957). The graphical analysis of mineral assemblages in pelitic schists. Amer. Mineral., v. 42, p. 842-858.

TOZER, C. F.
(1955). The mode of occurrence of sillimanite in the Glen District, Co. Donegal. Geol. Mag., v. 92, p. 310-320.

TURNER, F. J. and VERHOOGEN, J.
(1951). Igneous and metamorphic petrology. McGraw Hill Book Co., 602p.

VOLBORTH, A.
(1963). Total instrumental analysis of rocks. Nevada Bur. Mines Rept. 6, p. 1-72.

VOLBORTH, A.
(1964). Biotite mica effect in X-ray spectrographic analysis of pressed rock powders. Amer. Mineral., v. 49, p. 634-643.

WALDBAUM, D. R.
(1965). Thermodynamic properties of mullite, andalusite, kyanite and sillimanite. Amer. Mineral., v. 50, p. 186-195.

WALKER, G. P. L. and LEEDAL, G. P.
(1954). The Barnesmore granite Complex, Co. Donegal. Roy. Soc. Dublin Sci. Proc., v. 26 (N. S.), p. 207-243.

WATSON, J.
(1948). Late sillimanite of Kildonan, Sutherland. Geol. Mag., v. 85, p. 149-162.

WEILL, D. F.
(1963). Hydrothermal synthesis of andalusite from kyanite. Amer. Mineral., v. 48, p. 944-947.

WEILL, D. F.
(1966). Stability relations in the Al_2O_3-SiO_2 system calculated from solubilities in the Al_2O_3-SiO_2-Na_3AlF_6 system. Geochim. et Cosmochim. Acta, v. 30, p. 223-237.

WHITTEN, E. H. T.
(1955). The metasediments of Bunbeg (County Donegal) and their relationship to the surrounding granite. Geol. Assoc. London Proc., v. 66, p. 51-67.

WILLIAMSON, D. H.
(1953). Petrology of chloritoid and staurolite rocks N. of Stonehaven, Kincardineshire. Geol. Mag., v. 90, p. 353-361.

WINKLER, H. G. F.
(1965), (1967). Petrogenesis of metamorphic rocks. Springer-Verlag, Berlin.
1st edition, 1965, 220p.
2nd edition, 1967, 237p.

WOODLAND, B. G.
(1963). A petrographic study of thermally metamorphosed pelitic rocks in the Burke Area, Northeastern Vermont. Amer. J. Sci., v. 261, p. 354-375.

WYLLIE, P. J.
(1962). The effect of "impure" pore fluids on metamorphic dissociation reactions. Mineral. Mag., v. 33, p. 9-25.

ZWART, J. H.
(1958). Regional metamorphism and related granitisation in the Valle de Aran (Central Pyrenees). Geologie en Mijnbouw, v. 20, p. 18-30.

APPENDIX I

An Index to the Rock Specimens used in the X-ray Spectrographic Determination

Text No.	Specimen Marking*	Text No.	Specimen Marking
1	J. M. 28892	18	EDM. AG-3
2	J. M. 30698	19	EDM. GL-16
3	EDM. V-552	20	EDM. LM-18
4	EDM. V-551+3	21	EDM. GL-11
5, 5a	EDM, AG-6	22	EDM. A-1
6	EDM. GL-40	23	M. A. 22779
7	EDM. GL-20	24	M. A. 22777
8	EDM. GL-7	25	M. A. 22771
9	EDM. GL-47	26	M. B. A-25
10	J. M. 29133	27	M. B. A-27
11, 11a	EDM. B-5	28	M. B. GL-45
12	M. B. GL-10 (std)	29	M. B. A-14
13	Std. Tonalite T-1	30	M. B. A-29
14	EDM. LM-17	31	J. M. 28893
15	EDM. V-54	32	EDM. B-8a
16	J. M. 30694	33	M. B. GL-31
17	EDM. GL-10		

*Marking as present in Geology Dept. of Liverpool University.
The samples were chemically analysed by:
J.M. : Dr. J. Mather, EDM : Mr. M. Edmunds,
M.A. : Dr. M.P. Atherton, M.B. : Mr. M. Brotherton.

APPENDIX II

An Index to the Minerals Specimens used in the X-ray Spectrographic Analysis

Text No.	Specimen Marking*	Text No.	Specimen Marking*
	Biotites		
1	EDM. LM-18	8	M. A. Sc-27
2	EDM. GL-2	9	EDM. AG-6
3	EDM. GL-47	10	EDM. AG-3
4	EDM. GL-16	11	EDM. V-561+3
5	EDM. V-562	12	Biotite Standard
6	EDM. A-1	13	M. A. Sc-39
7	EDM. GL-7	14	M. A. P-5
	Garnets		
1	EDM. A-1	4	EDM. LM-18
2	EDM. LM-17	5	EDM. B-8a
3	EDM. GL-2		

* Marking as present in Geology Department of Liverpool University. The specimens were chemically analysed by:
EDM: Mr. M. Edmunds, M. A. : Dr. M. P. Atherton.

APPENDIX III

An Algol KDF9 Programme for Calculating the Calibration Equation (y = ax + b) and the Composition of the Unknowns

(A) Preparation of the Data Tape

The data tape is prepared with the data written in the following order:-

Carriage return

n;	where n is the number of observations or the number of rocks used in constructing the calibration graph.
x1; y1; x2; y2; ⋮ ⋮ xn yn	where x's are the X-ray intensity ratios of the rocks used in constructing the calibration graph and y's are the corresponding chemical analyses of the element under consideration.
l;	where l is the number of the unknown rocks to be analysed.
m;	where m is the number of pellets for each rock. This m should be kept constant for one program.
x1; x2; .. etc;	where x is the X-ray intensity ratio of the unknown rocks to be analysed.

(B) The Computer Programme

```
begin integer f, i, j, n, m, l; real xl, yl, s, sl, s2, s3, a, b;
      open (20); open (30);
      f:=format ( [sss-ddd. dddddd]);
      writetext (30, [[c3s] x-ray*fluorescence*analysis*of [c]] );
      n:=read (20);
begin array x, y [1:n] ;
            for i: = 1 step 1 until n do
                begin
                      x [i] :=read (20);
                      y [i] :=read (20)
                end;
      s:=s1:=s2:=s3:=0;
                for i:= 1 step 1 until n do
                begin
                    s:= s + x [i] ;
                    s1: = s1 + y [i];
                    s2: = s2 + x [i] X y [i] ;
                    s3: = s3 + x [i] ↑ 2
                end;
      b: = (s X s1 - n X s2)/(s↑2 - n Xs3);
      a: = (s1 - b Xs)/n;
      writetext (30, [[c3s] y [s]=]); write (30, f, b);
      writetext (30,[[s] x [s] +] ); write (30, f, a);
      writetext (30, [[2c8s] x [17s] y [c]] ); l:= read (20);
                                               m:=read (20);
```

```
        for  j: = 1  step 1  until  1 do
        begin
                writetext (30, [[2c]]);
                for  i:  =  1  step  1  until  1   do
                begin
                     xl:= read (20);
                     yl:= b X xl + a;
                     write(30, f, xl);  write (30, f, yl);
                     writetext (30, [[c]])
                end
           end
end;
   close (20);  close (30)
end →
```

APPENDIX IV

Index for the Analysed Specimens

Text No.	Specimen No. and Location
	FANAD AUREOLE
1	GL 7
2	11
3	12
4	18
5	19
6	20
7	21
8	25
9	29
10	30
11	31
12	35
13	36
14	38
15	40
16	41
17	43
18	44
19	45
20	46
21	51
22	56
	ARDARA AUREOLE
23	A 7
24	9
25	14
26	17
27	22
	BARNESMORE AUREOLE
40	B 1
41	2
42	3
	THORR GRANODIORITE
	(a) S. Gortahork
43	Th 1
44	2
	(b) Lough Agher
45	Ag 2
46	3
47	5
	(c) Ardveen Raft
48	Ad 1
49	2
50	3
	MAIN DONEGAL GRANITE
	(a) Fintown
51	F 2
52	3
	(b) Glenkeo
53	Z 2
54	3
55	4
56	5
	(c) Lackagh Bridge
57	LB 2
58	3

Text No.	Specimen No. and Location	Text No.	Specimen No. and Location
	ARDARA AUREOLE		MAIN DONEGAL GRANITE
28	26	59	4
29	27	60	5
30	29	61	6
31	32		(d) Owennagreeve R.
32	34	62	R 9
33	35	63	10
34	37		(e) Lough Reelan
35	38	64	LR 14
36	50	65	15
37	51	66	19
38	52	67	20
39	55	68	26
	(f) Glenaboghil	69	31
70	Bo 1	75	7
71	2	76	8
72	4	77	9
73	5	78	11
74	6	79	12
		80	14